PETROGENESIS, U-Pb ZIRCON GEOCHRONOLOGY AND TECTONIC EVOLUTION OF THE MALAYSIAN GRANITE PROVINCES IN THE SOUTHEAST ASIAN TIN BELT

Samuel Wai-Pan Ng (Hong Kong)

St. Anne's College and

Department of Earth Sciences

Thesis submitted for the degree of Doctor of Philosophy at the University of Oxford

Trinity Term 2014

PETROGENESIS, U-Pb ZIRCON GEOCHRONOLOGY AND TECTONIC EVOLUTION OF THE MALAYSIAN GRANITE PROVINCES IN THE SOUTHEAST ASIAN TIN BELT

Samuel Wai-Pan Ng (Hong Kong)

St. Anne's College and

Department of Earth Sciences

Thesis submitted for the degree of Doctor of Philosophy at the University of Oxford

Trinity Term 2014

Abstract

The Malaysian granitoids form the backbone of the Malay Peninsula and have long been recognized as composed of two distinct granitic provinces separated by the Bentong-Raub suture zone:

1. Early Permian to Late Triassic Eastern Province (Indochina – East Malaya) with mainly "I-type" hornblende-bearing granitoids, associated with Cu-Au deposits, and subordinate hornblende-free pluton roof-zones hosting limited Sn-W deposits; and
2. Late Triassic Main Range Province, western Malaysia (Sibumasu) with mainly "S-type" hornblende-free granitoids, associated with Sn-W deposits, and subordinate hornblende-bearing granitoids.

Field observations and new geochemical data suggested that the division of the Eastern Province and Main Range granitoids using Chappell and White's (1974) I-S

classification could be problematic, as there is a large degree of overlap between the two granitic provinces in terms of lithology, mineralogy and metallogenic affinity. The Main Range granitoids are more fractionated than the hornblende-bearing Eastern Province. Although the two granitic provinces were emplaced into different continental terranes, both granitic provinces exhibit common trace element geochemistry in the enrichment of high field strength elements (HFSE) and rare earth elements (REE) compared to typical Cordilleran I-S granites. Such enrichment is interpreted as an inheritance signature from the protoliths. The Kontum massif (an analogue of Indochina lower continental crust) comprises intraplate ortho-amphibolites and para-gneisses, which could serve as two hypothetical source end-members for the Malaysian granitoids. The model suggests that the geneses of the parental magmas of the Eastern Province and the Main Range Province were related to hybridization of melts derived from protoliths, geochemically and isotopically similar to these two source end-members, but in differing proportions. The fact that the granites from the two granitic provinces are so similar compositionally and metallogenically, suggests that similar protoliths were involved in their source. The incorporation of sedimentary-sourced melt makes the Main Range granitoids transitional I/S-type in nature, but this is unlikely to be true for the less evolved Eastern Province fractionated I-type granitoids. The hybridization of igneous- and sedimentary-sourced melts, and granite fractionation promotes Sn metallogenesis in the Main Range granitic province.

Previous ages were obtained using whole rock Rb-Sr and biotite K-Ar geochronology in the 1970s and 1980s, dating methods that almost certainly do not accurately represent the crystallization age of granites. New ion microprobe U-Pb zircon ages are presented that provide new temporal constraints for the Malaysian granitic magmatism. Eastern

Province granitoids have U-Pb zircon ages that range from 289 to 220 Ma, while Main Range Province magmatism is constrained between 227 and 201 Ma. A progressive westward younging trend is apparent across the Eastern Province, but becomes less obvious in the Main Range Province. In addition, the U-Pb zircon analysis of the Malaysian granitoids suggests that both granitic provinces have Cambro-Ordovician and Mesoproterozoic inheritance signatures, which match the ages of the Kontum intraplate ortho-amphibolites and para-gneisses, the two source end-members of the suspected Indochina basement.

Two different tectonic models have been suggested to explain the formation and the emplacement of the Malaysian granitoids. Both models involve an east-dipping subduction zone during the Early and Mid-Triassic with Palaeo-Tethys lithosphere rolling back along the Bentong-Raub suture zone to produce westward younging ages in the Eastern Province granitoids. The first model (modified after Searle *et al.* 2012) suggests the younger Main Range granitoids were produced by another Late Triassic – Cretaceous east-dipping (Neo-Tethyan) subduction to the west of Sibumasu, after the Sibumasu – East Malaya collision. The transitional I/S-type geochemistry of the Main Range granitoids was caused by the partial melting of the more heterogeneous Sibumasu basement. The second model (Oliver *et al.* 2014) suggests the younger Main Range granitoids were produced by the westward underthrusting of Indochina crust of East Malaya beneath Sibumasu along the Bentong-Raub suture zone after the continental collision. In this model, the source of the Main Range granitoids was the pre-collision I-type Eastern Province granitoids. The second model is less likely, as no geological evidence for such underthrust is found in the Malay Peninsula.

PETROGENESIS, U-Pb ZIRCON GEOCHRONOLOGY AND TECTONIC EVOLUTION OF THE MALAYSIAN GRANITE PROVINCES IN THE SOUTHEAST ASIAN TIN BELT

Samuel Wai-Pan Ng (Hong Kong)

St. Anne's College and

Department of Earth Sciences

Thesis submitted for the degree of Doctor of Philosophy at the University of Oxford

Trinity Term 2014

Extended abstract

The Malaysian granitoids were formed in response to the re-assembly of Precambrian continental terranes, namely the Indochina – East Malaya terrane and the Sibumasu terrane, along the Eurasian margin, which were rifted off from Gondwana since Devonian. The Malaysian granitoids form the backbone of the Malay Peninsula, and they have been long recognized with two distinct granitic provinces separated by the Bentong-Raub suture zone:

1. Early Permian to Late Triassic "I-type" Eastern Province hosted by Indochina – East Malaya; and
2. Late Triassic "S-type" Main Range Province hosted by Sibumasu.

Field observations suggest the Eastern Province granitoids are composed of predominantly hornblende-bearing granitoids hosting Cu-Au deposits, with hornblende-free phase developed at the pluton roof-zones hosting Sn-W deposits. The Main Range

Province granitoids are mainly hornblende-free, lithologically similar to the pluton roof-zones in the Eastern Province. These hornblende-free granitoids are usually altered by hydrothermal activity and characterized by Sn and W mineralization. The Main Range Province is one of the most productive Sn-W metallogenic provinces in the world. The Bintang Batholith hosts the only hornblende-bearing granite in the Main Range Province.

New geochemical data suggested that the division of the Eastern Province and Main Range granitoids using Chappell and White's (1974) I-S classification could be problematic, as there is large degree of overlap between the two granitic provinces in terms of granite type and texture, mineralogy, metallogenic affinity and compositional attributes. All the Malaysian granitoids can be defined in terms of a single continuous liquid-line-of-descent (LLOD), in which they are all fractionated with Main Range granitoids, or the hornblende-free biotite granites more fractionated than the hornblende-bearing Eastern Province. Although the two granitic provinces were emplaced into different continental terranes, both granitic provinces exhibit common trace element geochemistry in the enrichment of high field strength elements (HFSE) and rare earth elements (REE) compared to typical Cordilleran I-S granites. Such enrichment is interpreted as an inheritance signature from the protoliths. The Kontum massif (an analogue of Indochina lower continental crust) comprises intraplate ortho-amphibolites and para-gneisses, which could serve as two hypothetical source end-members for the Malaysian granitoids. The model suggests that the geneses of the parental magmas of the Eastern Province and the Main Range Province were related to hybridization of melts derived from protoliths, geochemically and isotopically similar to these two source end-members, but in differing proportions. The fact that the granites

from the two granitic provinces are so similar compositionally, suggests that similar protoliths were involved in their source. The incorporation of sedimentary-sourced melt makes the Main Range granitoids transitional I/S-type in nature, but this is insufficient in the Eastern Province, leaving fractionated I-type granitoids in the province. The hybridization of igneous- and sedimentary-sourced melts, and granite fractionation promotes Sn metallogenesis in both granitic provinces.

Previous ages were obtained by whole rock Rb-Sr and biotite K-Ar geochronology in the 1970s and 1980s, dating methods that may not accurately represent the crystallization age of granites. New ion microprobe U-Pb zircon ages are presented that provide new temporal constraints for the Malaysian granitic magmatism. Eastern Province granitoids have U-Pb zircon ages ranging from 289 to 220 Ma, while the Main Range Province magmatism is constrained between 227 and 201 Ma. A progressive westward younging trend is apparent across the Eastern Province, but becomes less obvious in the Main Range Province. In addition, the U-Pb zircon analysis of the Malaysian granitoids suggests that both granitic provinces have Cambro-Ordovician and Mesoproterozoic inheritance signatures, which match the ages of the Kontum intraplate ortho-amphibolites and para-gneisses, the two source end-members of the suspected Indochina basement.

Cretaceous granitoids were found in the Stong region (~76–84 Ma) and on Tioman Island (~80 Ma). These granitoids generally have slightly lower Y/Nb ratios than the Permo-Triassic Malaysian granitoids. The extracted zircons from these Cretaceous granitoids are also characterized by higher Th/U ratios up to 2.5. It is speculated that the

Cretaceous granitoids were formed from different sources from the Permo-Triassic granitoids, but further field and laboratory investigations are required.

Two different tectonic models have been suggested to explain the formation and the emplacement of the Malaysian granitoids. Both models involve an east-dipping subduction zone, with subducting Palaeo-Tethys lithosphere rolling back along the Bentong-Raub suture zone to produce westward younging Eastern Province granitoids. The first model (modified after Searle *et al.* 2012) suggests the younger Main Range granitoids were produced by another Late Triassic east-dipping (Neo-Tethyan) subduction zone to the west of Sibumasu, after the Sibumasu – East Malaya collision. The transitional I/S-type geochemistry of the Main Range granitoids was caused by the partial melting of the more heterogeneous Sibumasu basement. The second model (Oliver *et al.* 2014) suggests the younger Main Range granitoids were produced by the westward underthrusting of Indochina - East Malaya crust beneath Sibumasu along the Bentong-Raub suture zone after the continental collision. In this model, the source of the Main Range granitoids was the pre-collision I-type Eastern Province granitoids. The second model is less likely, as no geological evidence for such underthrusting has been found in the Malay Peninsula and the Eastern Province granitoids are unlikely to be the source of melting for the Western Province Main Range granitoids.

Acknowledgements

This thesis could not be completed without the help of my supervisors, collaborators and friends, who deserve recognition. I wish to thank my supervisors in Oxford, Mike Searle and Laurence Robb, for offering me such a challenging project. I may not be able to overcome all the obstacles without their guidance and encouragement. They are patience and can always give me timely advices. I have not only gained in geology from my supervisors, but also been nurtured as a professional geologist and scientist. Also, I deeply appreciate the freedom they gave me during the study, so that I could pursue and explore my own research interest. Here, I also need to thank our local collaborator, Azman Ghani, Masatoshi Sone, Grahame Oliver and Muhammad Roselee, who showed me the geology, culture and natural beauty of the Malay Peninsula, and for the logistics being arranged.

Technical staff from various institutes kindly offered support in the laboratory works conducted in this study. I am very grateful to have professional technicians like Owen Green and Steve Wyatt who offered support in sample handling and preparation. Norman Charnley and Jeremy Hyde are also acknowledged here for operating the SEM and making thin sections respectively. High-quality geochronological and geochemical data were yielded in NordSIM of the Swedish Museum of Natural History and the Department of Geosciences in the National Taiwan University (NTU) respectively. I am particularly thankful to have Martin Whitehouse and Sun-Lin Chung being my on-site supervisors. I have to thank them for all the academic advices and logistical supports. However, without the professional preparation works and instrument maintenance by the following workers, the quality of data presented in this thesis could not be that

satisfactory. Here, Kerstin Lindén and Lev Ilyinsky in NordSIM, and Hao-Yang Lee, Chiu-Hong Chu and Chien-Hui Hung in NTU are specially acknowledged.

The journey towards a DPhil is long and tough. It is my pleasure to have it gone through with the company of my friends in Oxford. I wish to take this chance to thank Petrina Lau, Hayley Chan, Terry Wong, Maira Seeley and Tony Chan in particular. I also wish to thank my old buddies in the Department of Earth Sciences in the University of Hong Kong. George Ma, Stephen Ng, Jean Wong and Debbie Tsang, who always stand with me in the journey.

Last but not least, I would like to express my gratitude to my mentor, John Malpas, who recommended me and encouraged me to come to Oxford. He is the one who brought me into the world of geologists.

I would also like to express my love and gratitude to my family, who always encourage me to chase my dream.

The WYNG Foundation (Hong Kong) and Raphael Martin of Dark Capital Group are gratefully acknowledged for funding support. Much of the fieldwork was covered by the High Impact research grant of the University of Malaya (UMC/HIR/MOHE/SC/27). The Penjom Gold Mine (J. Resources) is also acknowledged for the permission of sample collection in the mine. The NordSIM facility is operated under an agreement between the research funding agencies of Denmark, Iceland, Norway and Sweden, the Geological Survey of Finaland and the Swedish Museum of Natural History.

Table of Contents

Chapter 1 – Introduction and Background

1.1 Introduction: granite petrogenesis

In contrast to the denser basaltic oceanic crust, continental crust is much lighter and comprises greater variety of rock types. The bulk composition of continental crust is close to that of andesite, found commonly in orogenic belts along active continental margins (Taylor and McLennan, 1985). The formation of calc-alkaline andesite is usually associated with regional-scale intrusion of granitic batholiths. This process has been recognized as the major mechanism of continental growth (Taylor, 1967). Hence, studying granite petrogenesis and emplacement allows a better understanding of the origin and the evolution of continental crust.

The origin of granites has been a hotly debate topic between the transformists (e.g. H. H. Read), who suggested that granites are ultrahigh grade metamorphic rocks, and the magmatists (e.g. N. L. Bowen), who suggested that granites are purely igneous, being differentiated from basalts (Pitcher, 1997). It was not until geophysical models and experimental data became available that the multi-origin of granites was revealed. The composition of granites is mainly controlled by the melting sources, whether the melts were derived from igneous or sedimentary protolith or even both, and how the melts were hybridized. In addition, varied geological processes, such as crustal assimilation and fractional crystallization, could alter the chemical composition of granitic parental magma once it was derived. These lead to complexity in studying the magmatic evolution of granites. The complexity is usually reflected by the subtle difference in accessory mineral assemblages and mineral geochemistry, which are not easily observed. Therefore, petrologists and geochemists need to use various techniques to

discriminate granites from different tectonic origins effectively and model their magmatic evolution. These techniques include careful field relationships and petrographic observations, as well as geochemistry and isotope chemistry. Various granite classification schemes have been proposed, namely by Chappell and White (1974), Ishihara (1977), Whalen *et al.* (1987), Maniar and Piccoli (1989) and Frost *et al.* (2001). Trace element geochemical classifications of granites formed in different tectonic settings have also been reported by Pearce *et al.* (1984) and Harris *et al.* (1986). All these classification/discrimination schemes require high quality major and trace element analyses on granites. Nevertheless, these schemes may not be universally applicable due to the complex nature of granites. Hence, petrologists and geochemists seldom rely on single system to study granitic rocks. More recently, owing to the advance of instrumental analytical geochemistry, which allowed rapid and precise analyses of mineral and rock samples, isotopic analyses (e.g. Sr, Nd and Hf) play an important role in revealing the source region of the granitic melts. The isotopic compositions of certain robust accessory minerals, such as zircon, may be able to record the environment in which the primary melts were derived. In this chapter, landmark theories of granite petrogenesis, from the formation of the first granitic melt, through the segregation and transportation of the melt, to the final emplacement of granite will be reviewed. The classification schemes of granite will be discussed and various granite discrimination schemes will be introduced in the following section, with their applications to classic granitic terranes.

1.2 The granite origin controversy

In the mid-20th century, the conflicts between the transformists and magmatists reflected the broad difference between laboratory studies and field observations. As a

representative of transformists and a field geologist, H. H. Read (1948) suggested that granites are closely related to migmatites, and hence related to the end-product of regional metamorphism. He named the formation process of granite as "granitization", which is a kind of ultrahigh grade metamorphism of various protoliths to form granites without going through any "true" magmatic stage. At the same time, representative of magmatists and an experimental petrologist, N. L. Bowen (1948), suggested that granites are differentiation products of basalts based on his physiochemical experimental results.

Apparently, these two hypotheses were contradictory, while neither side could agree with the model proposed by the opposite camp. Read's (1948) argument is simple: if granites were differentiation products of basalts, enormous amount of basaltic material would be required, yet mafic rocks are not commonly seen in the field associating with granites. For example, the synkinematic granite referred by Eskola (1932), such as those purely sedimentary-sourced syn-collisional leucogranites in the Himalayan region, seldom occur naturally with mafic rocks. Bowen's (1948) fractional crystallization and magmatic differentiation model may be able to explain the generation of oceanic plagiogranites in ophiolitic suites (Pedersen and Malpas, 1984). However, whereas this can easily explain the simple derivation of granitic melts as the end-member of oceanic basaltic fractionation, many other processes are operative in the formation of large-scale continental crustal granitic batholiths. Furthermore, the granites produced by fractionation of basalts are essentially more sodic, i.e. dacitic or trondhjemitic (Figure 1.3) (Green and Ringwood, 1968; Clarke, 1992; Chappell *et al.*, 2012).

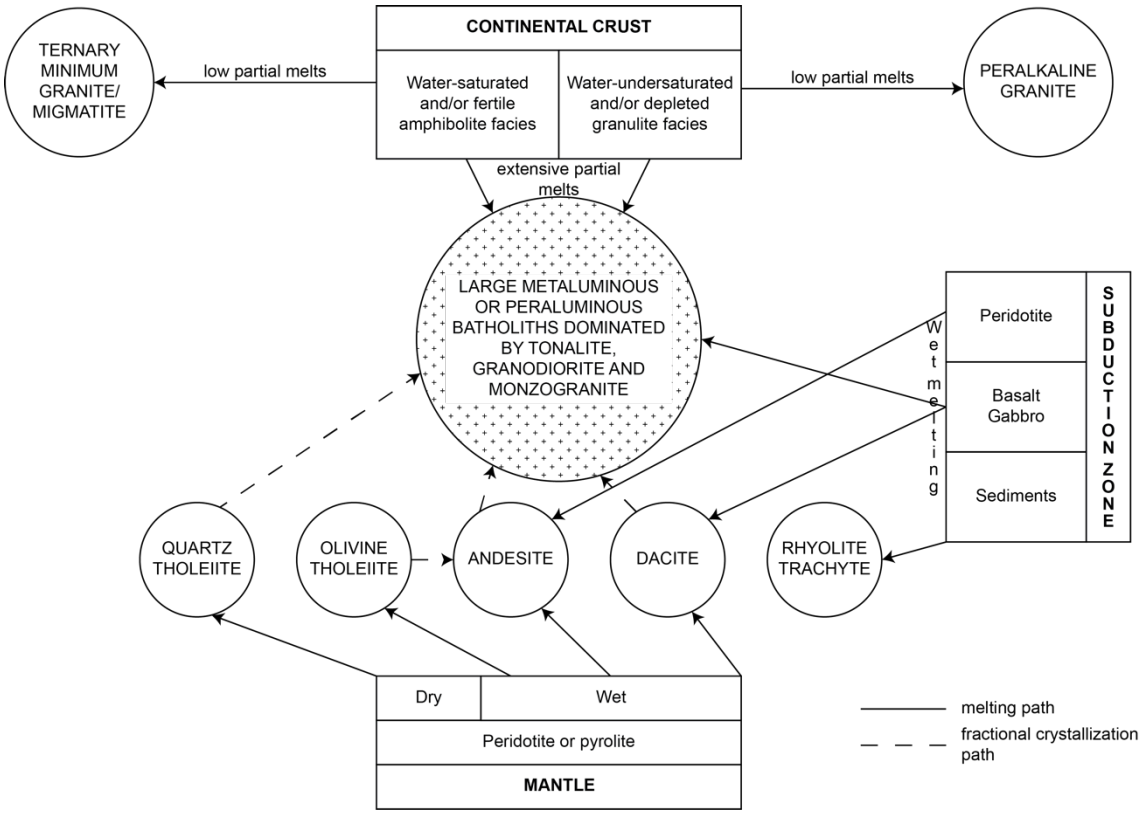

Figure 1.1 Simplified diagram drawn by Clarke (1992), showing the petrogenesis of granites.

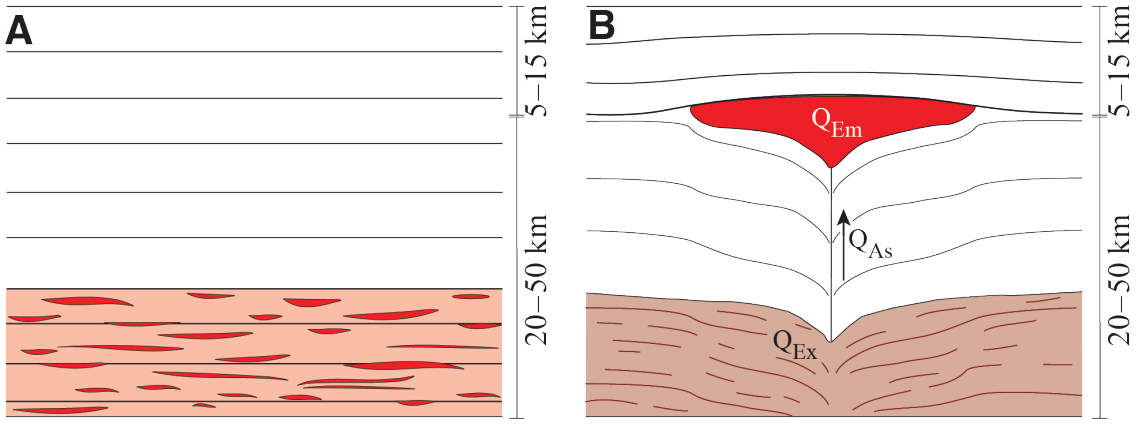

Figure 1.2 Brown's (2010, 2013) schematic diagram showing granitic melt extraction, ascent, and emplacement along active continental margins, based on the model proposed by Cruden (1998). (A) Melt was segregated in the source region, marked as red seams, parallel to the fabric of the source. (B) The melt ascent as a dyke, injecting melt to the ductile-brittle transition zone of the crust. Assuming the rate of melt production, extraction (Q_{Ex}), ascent (Q_{As}) and emplacement (Q_{Em}) are balanced, the volume of melt extracted from the source should equal to the volume of the pluton formed.

In the meantime, Bowen (1948) also criticized Read's (1948) "granitization" for being purely hypothetical, and not supported by any available physiochemical data. He pointed out that "granitization" might only be feasible in local scale, as enormous energy would be required for solid-state diffusion of elements and ions to take place at high-level crust and replace completely any protolith by voluminous granitic batholiths. In fact, many of the intrusive relationship between granites and country rocks cannot be explained by "granitization". Although the igneous origin of granites were later demonstrated experimentally by Tuttle and Bowen (1958), in which they defined the granitic magmatic system. The granite origin controversy carried on for decades. It was not widely accepted until Whitney (1975) confirmed that the cotectic composition of granites could not be produced by metasomatism. Metasomatic processes, although important, are related to retrograde lower temperature fluids rather than prograde magmatic melting processes.

1.2.1 Middle to lower crust as possible source of granite

Although granites were recognized as igneous rocks, the constraints limiting Bowen's (1948) model still existed. The formation of granitic batholiths by inefficient fractionation of basalts is unlikely. Hence, workers have to seek another source for granitic melts. The formation of granitic melts by partial melting of crustal meta-sedimentary rocks was recognized and demonstrated by Winkler (1965). Presnall and Bateman (1973) later used phase equilibria to propose that the Sierra Nevada batholith could have originated from partial melting of the lower crust, given that enormous amount of heat was required, as these lower crustal materials (granulite facies) are essentially dry. They suggested that such heat could be obtained conductively from the mantle and from radioactive decay in the crust. They also recognized that additional

heat might be provided by subduction-related magmatism. This kind of lower-crustal melting can be facilitated with the presence of water in the system. Although the importance of water in the granitic system has already been addressed by Tuttle and Bowen (1958), the role and the source of water in petrogenesis had not been thoroughly discussed until Whitney (1988) published his landmark paper. It is now widely accepted that felsic igneous rocks could not be produced without the presence of water. This is to account for the hydrated minerals present in the felsic rocks, and more importantly, to facilitate the melting process (Whitney, 1988).

1.2.2 Mantle vs crust as sources

Apart from identifying the lower crust as a possible source of granites, Presnall and Bateman's (1973) work also recognized the role played by mantle in granite petrogenesis in providing heat for lower-crustal melting. However, it was controversial whether mantle is a potential source for the genesis of granites. In the late 1980s to 2000s, Sr and Nd isotopic data, and numerical modelling suggested that granites are products of hybridization of melts with mantle signature and melts with crustal signature (Gray, 1984; Keay *et al.*, 1997; Kemp *et al.*, 2007; Kemp *et al.*, 2009; Brown, 2013). This is supported by the Hf and O isotopic compositions of the I-type granites in the Australian Lachlan Fold Belt, which appear to be derived from hybridizing mantle melt and crustal meta-sedimentary melt (Kemp *et al.*, 2007), and experimental results (Patiño Douce, 1999).

Clemens *et al.* (2011), on the contrary, proposed that the mantle isotopic signature was inherited from the meta-igneous precursors in the crust by **P**eritectic **A**ssemblage **E**ntrainment (PAE). This mechanism involves small crystals of peritectic phases being

carried by the melt out of the source, and passed on the mixed mantle and crustal isotopic signature to the resulting I-type granites. It is also viable in generating the sedimentary-sourced granites (S-type) in the Cape Granite Suite (Western Cape, South Africa) with heterogeneous source region (Villaros *et al.*, 2012). Clemens and Stevens (2012) compared various mechanisms to explain the chemical variation among granites. They recognized that such variations depend primarily on protolith chemistry, in which PAE in varying degrees could account for most of the primary compositional variation in granites with support of geochemical and isotopic data.

1.3 Generation of granitic melts

As the composition of granites is largely determined by the composition of source rocks, it is important to understand the melting processes that could occur. In the previous section, we have seen that the source region of granites is restricted to the middle to lower crust. If partial melting of these crustal materials form the granitic magma, heat and water have to be provided into the melting system.

1.3.1 Heat and Water

In Presnall and Bateman's (1973) model, heat is released from radioactive decay, directly from the mantle, or by dissipation in mechanical and chemical processes, such as shear heating and latent heat. The latter two could be significant, particularly in subduction systems where thrusting and crystallization of basaltic magma occur. Water involvement in the granitic melt generation occurs in two aspects. Firstly, water could suppress the solidus of the mantle wedge, such that basaltic underplating could be formed along the base of the crust (van Keken, 2003). Secondly, the crystallization of this basaltic underplating would leave an H_2O-rich fluid residual. It is thought that this

residual would again provide water and heat for crustal melting at the **D**eep **C**rustal **H**ot **Z**one (DCHZ) (Huppert and Sparks, 1988; Annen *et al.*, 2006). The DCHZ is the location, where **M**elting, **A**ssimilation, **S**torage, and **H**omogenization (MASH) take place (Hildreth and Moorbath, 1988). In this zone, meta-sedimentary rocks started to melt at around 650 - 700 °C when fluid is present (Brown and Korhonen, 2009; Sawyer, 2010; Brown, 2013). Water could also be provided by hydrate-breakdown melting of meta-igneous protoliths, for mica-bearing rocks at temperature above 750 °C and amphibole-bearing rocks above 850 °C (Clemens, 2006). These melting reactions will be discussed in the following sections. Base-level isotopic and trace element signature is given to the melt by the source (PAE) and crustal assimilation in the DCHZ, where the melts derived from different sources are stored temporarily and homogenized.

1.3.2 Fluid-present melting of middle to lower crust

Partial melting of protoliths could be easily achieved with the presence of fluid. Aqueous fluid could be introduced into the middle to lower crust by fluids driven off a subducted lithospheric slab. Fluids could be brought into the melting system by the structural weaknesses along subduction zones or fracture systems to facilitate the melting process (Whitney, 1988). In sedimentary-sourced granites (S-type granites), the fluid-present melting of sedimentary precursors can be achieved from the muscovite dehydration reaction at lower temperatures (Brown, 2010a):

$$Ms + Bt + Pl + Qtz + H_2O = Melt \quad [1]$$

or by the biotite dehydration reaction at slightly higher temperatures (Brown, 2010a):

$$Bt + Pl + Qtz + H_2O = Grt + Crd + Melt \quad [2]$$

Melting of igneous sourced (I-type) trondhjemite, tonalite and granodiorite can be achieved by the following reactions (Sawyer, 2010):

$$Kfs + Pl + Qtz + H_2O = Melt \quad [3]$$

$$Bt + Pl + Qtz + H_2O = Melt + Am + Pl \pm Sp \quad [4]$$

$$Bt + Pl + Qtz + H_2O = Melt + Sp \quad [5]$$

However, these aqueous fluids are limited. In fact, partial melting of middle to lower crustal materials occurs usually in fluid-undersaturated environment by hydrate-breakdown melting reactions (Brown, 2010a).

1.3.3 Fluid-absent melting of middle to lower crust

Large amounts of hot H_2O-undersaturated granitic melt (10 – 50 vol%) could be generated by fluid-absent hydrate-breakdown melting reactions (Stevens and Clemens, 1993; Brown, 2010a). These hydrates include muscovite, biotite and hornblende. If such melting reactions occur within shallower crust, water could also be introduced to deeper rocks for further melting when there is an inverted pressure gradient at depth, which is less than the hydrostatic gradient of the fluid (Stüwe *et al.*, 1993; Stüwe and Sandiford, 1994). Clemens (2006) suggested that the partial melting of meta-pelites (S-type) could be achieved by breaking down of muscovite at lower temperature:

$$Ms \pm Bt + Pl + Qtz = Als \pm Grt \pm Kfs + Melt \quad [6]$$

or by breaking down of biotite at slightly higher temperature:

$$Bt + Pl + Als + Qtz = Grt \pm Crd \pm Kfs + Melt \quad [7]$$

In the meantime, the partial melting of metaluminous quartzo-feldspathic rocks (I-type) could be achieved by breaking down of biotite as well (Clemens, 2006):

$$Bt + Pl + Qtz = Hbl + Cpx \pm Kfs + Melt \quad [8]$$

If the temperature increases, breakdown of hornblende is also possible:

$$Bt \pm Hbl + Pl + Qtz = Opx + Cpx \pm Grt \pm Kfs + Melt \quad [9]$$

These reactions taken to completion make amphibolite/granulite rocks into migmatites. Hydrous phases would be segregated preferentially into the melt and evidence is preserved as the leucosome (Stevens and Clemens, 1993; Sawyer, 2001; Brown, 2010a). However, the residual or restite may not be completely anhydrous or restitic, as biotite and hornblende may still be present in the melanocratic part.

1.3.4 Role of water in metallogenesis

Water content of the melt is also important for mineral ore formation. The amount of water released from hydrous minerals determines the formation of different porphyry ores. Robb (2005) suggested that the formation of porphyry Cu–(Mo) is related to oxidized shallow granitic magma with low water content (2 vol%), initiated by fluid-absent melting of an amphibolite protolith. Higher initial water content could be achieved if the granite was emplaced at deeper levels with melt derived from biotite-bearing protolith (3 vol%). In such case, porphyry Mo–(Cu) would be formed. The difference is caused by the lack of early-phase crystallization in water-saturated melt in shallower magma (Robb, 2005). Finally, in reduced hydrous granitic magma (8 vol% H_2O), the formation of porphyry W–(Mo) is more favoured.

1.4 Migmatite: evidence of melt segregation

Once the first granitic melt was produced by partial melting of the source rocks, the melt has to be segregated and extracted from the residue. This process has been discussed by Sawyer (1991, 1994, 1998, 2001), Brown (1994, 2010b, 2013) and Brown *et al.* (1995). The weakening of the melt-bearing crust would happen when the volume of melt increased to form an inter-connected grain-boundary network during the "melt connectivity transition" after around 7 vol% of melt has been formed (Rosenberg and

Handy, 2005; Brown, 2013). Rosenberg and Handy (2005) suggested that after this point, the strength of the melt-bearing crust would drop dramatically. They also suggested that melts were extracted from the source by compaction and they were drained into a network of veins within the weakened crust. The deformation of melt-bearing crust would depend on the amount and the distribution of the melts (Dell'Angelo and Tullis, 1988). The melt-network and the residual are segregated in the form of leucosome and melanosome in migmatite respectively. The leucosomes transport the melt and volatiles to the upper crust, while the melanosomes are sometimes restitic. Migmatites separate usually the lower-level granulite residues from higher-level granites and mark the location of melting in the crust (Brown, 2001b). They are therefore, recognized as the products of this melt-producing reaction (Brown, 2001a).

1.5 Transport of granitic magma

In migmatites, granitic melt is transported from in situ leucosomes via a network of veins, dykes and sills to higher level sheets or diapirs. Sawyer (2001) suggested that the geometry of leucosomes and melanosomes could indicate the region of melting and magma stoping in the crust. For example, melting regions are usually characterized by arrays of thin leucosomes with little melanosomes, while the magma stoping regions are the migmatite zones with high melanosome to leucosome ratio. According to Brown (2010a, 2013), melts are formed in triple junctions of grain boundaries, eventually forming melt seams along foliation or lineation as temperatures increase. As the melt volume increases granitic melts accumulate in veins and then sills/dykes. Grain-boundary sliding and granular flow weaken the melt-bearing crust and decrease the effective mean stress. This allows the injection of melts into the fractures, shear zones,

and strain-controlled conduits. These conduits are controlled by melt-pressure gradients between the source and the pluton emplacement. Dykes (discordant) and sills (concordant) represent the transportation paths of the granitic melts. Dykes are formed by brittle fracturing in the middle to lower crust, followed by brittle-elastic fracturing in more viscous subsolidus crust, while sheets are formed by meso-scale pervasive migration of melt (Brown and Solar, 1998; Brown, 2004, 2010b, 2013). Magma ascent is controlled mainly by buoyancy, but the ascent style is also controlled by the wall-rock rheology (Brown, 2013). Transport by diapirism has been proposed by Paterson and Miller (1998). However, Brown (2010a) suggested that diapirs may be only effective in lower crustal levels, or in hotter but thinner Archaean crust.

1.6 Assimilation and Fractional Crystallization (AFC)

Assimilation of country rocks by magma was proposed by Taylor (1980), but quantified by the governing equations provided by DePaolo (1981). Taylor (1980) recognized that igneous rocks in various magmatic suites usually have positive correlation between the initial $^{87}Sr/^{86}Sr$ ratios and $\delta^{18}O$ values. He suggested that this resulted from mixing of mantle-derived rocks and crustal-derived rocks. It was later realized that the low initial $^{87}Sr/^{86}Sr$ ratios and $\delta^{18}O$ values (mantle signature) were inherited from the meta-igneous precursors in the middle to lower crust (Clemens *et al.*, 2011). Nevertheless, mixing of melts derived from different sources takes place at the DCHZ, where the melts are stored temporarily and homogenized (Hildreth and Moorbath, 1988; Annen *et al.*, 2006). In the DCHZ, the melts would assimilate the wall rock of the hosting crust, and this would continue as the melts ascend and are emplaced. This melt – wall rock interaction exchange elements between the hosting crust and the emplaced magma through the wall rock. Incompatible elements such as Rb and K tend to stay in the melt, while compatible

elements like transition elements would stay in the solid phases. Moreover, within the melt body, fractional crystallization takes place, which may be caused by the density difference of different phases, crystal settling or floatation, and convection effect. Hence, these processes (AFC) had modified the composition of the granitic melt since their derivation from the sources until their complete crystallization. These processes are particularly important to ore formation, as they facilitate the exchange and fractionation of elements among different phases in the melt system.

1.7 Emplacement of granitoids

It is generally believed that granitic plutons are built incrementally (Daniel *et al.*, 1987). It has been suggested that the size-frequency and the spacing of pluton emplacements obey power-law distributions and magmatic systems are self-organized (Bons and Elburg, 2001; Cruden and McCaffrey, 2001; Brown, 2010a, 2013). Assuming the rate of melt production, extraction (Q_{Ex}), ascent (Q_{As}) and emplacement (Q_{Em}) are balanced, along an active continental margin, the distance between plutons and their corresponding sources are usually less than 30 km, whereas the thickness of the source region is usually less than 20 km (Figure 1.2) (Cruden, 1998; Brown, 2010a, 2013). The volume of the plutons formed should also equal the volume of melt being extracted from the source. Emplacement of granitic plutons occurs when the intrusion reaches the ductile-to-brittle transition zone, where there is an inversion of mean stress gradient. This leads to back freezing in the ascent conduit (Brown and Solar, 1999). In order to accommodate the melt in the middle to upper crust, the floor of the intrusive body could be depressed while the roof is lifted for inflation (Cruden, 1998). According to the dimensional data of granitic emplacement, such as sills, laccoliths, plutons and composite batholiths, collected by McCaffrey and Petford (1997) and McCaffrey and

Cruden (2002) (Figure 1.3), it is suggested that sills are formed by a change of direction in minimum principle stress from horizontal to vertical in the local stress regime (Vigneresse *et al.*, 1999; Brown, 2013). As the melt pressure increases, sills will change eventually to laccoliths by roof lifting. However, if this continues, the emplacement floor will start to depress and the emplacement will become a pluton. In deeper crust, this could be caused by the weaker strength of the materials beneath the emplacement than that of the roof, or by subsidence of the melt (Brown, 2013).

1.8 Variety of granites and their geochemical classification

Granite is defined as a coarse-grained plutonic rock, which has 20-60% of the sum of **Q**uartz, **A**lkali feldspar and **P**lagioclase (QAP) in volume percentage, while the plagioclase should make up 10-65% of the total feldspar in the rock (Streckeisen, 1976; Clarke, 1992). However, as described by Read (1948, 1957), "there are granites and granites". As the controversy in origin of granites carried on and more granites studied, workers started to realize that subtle difference in accessory mineral assemblages and mineral chemistry among granites may reflect the difference in their formation, source and tectonic setting. For example, granites associated with continental arc settings may have less silica contents, and may be named as adamellites (quartz monzonite) or even granodiorites (Harpum, 1963; Streckeisen, 1976). Hence, workers usually termed the granite family as granitoids.

1.8.1 Aluminium saturation index (ASI or A/CNK)

Petrologists are interested in discrimination or categorization of different granites using geochemical analyses for quantifying granitoid composition. The geochemical results obtained can be easily converted back to normative mineralogy by calculating the

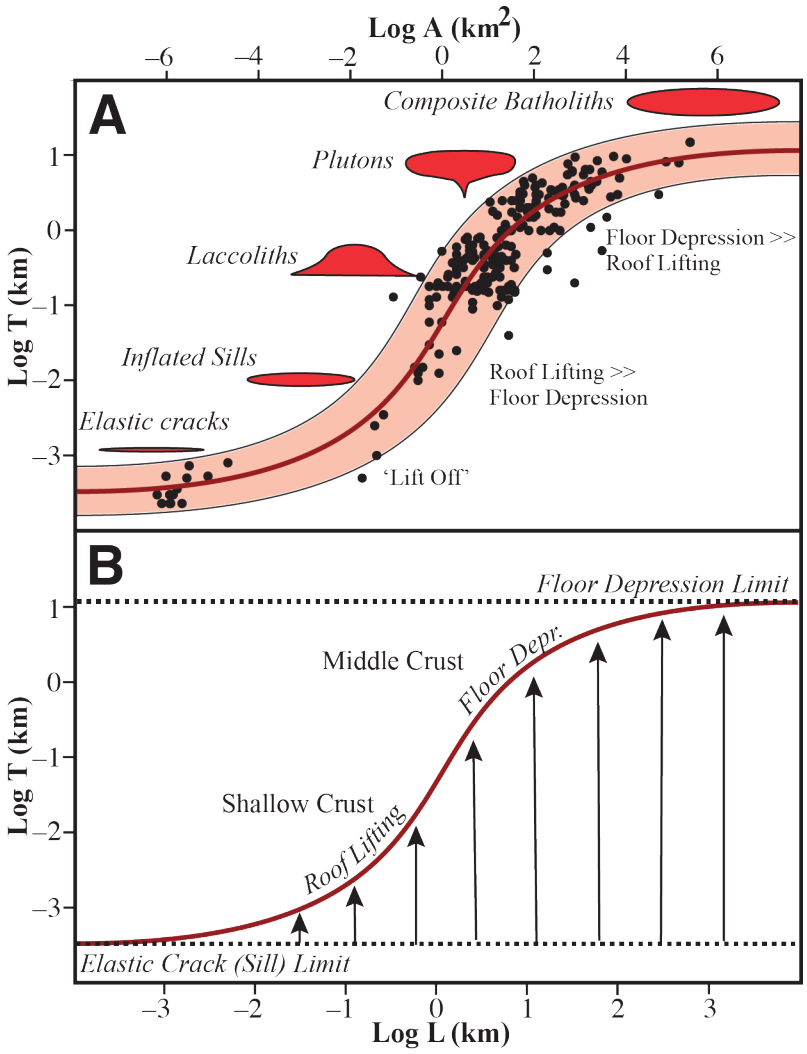

Figure 1.3 Relationship between granite emplacement thickness (*T*), width (*L*) and horizontal area (*A*) shown by McCaffrey and Cruden (2002). S-curve and shaded area were drawn by Brown (2007) to illustrate the relationship between the dominant emplacement mechanism and emplacement depth (Cruden and McCaffrey, 2002) in terms of minimum and maximum growth limit.

CIPW norm (Cross *et al.*, 1903), Barth-Niggli norm (Niggli, 1936; Barth, 1952) or mesonorm (Mielke and Winkler, 1979). Quartz, alkali feldspar and plagioclase are the three essential minerals found in granites, while calcium, sodium, potassium and aluminium are the most dominant oxides, except silica. Shand (1943) defined the A/CNK or **A**luminium **S**aturation **I**ndex (ASI) as the molar ratio of aluminium oxide to the sum of these oxide of eruptive rocks. The ratio is defined as

$$\frac{A}{CNK} = molar\ [\frac{Al_2O_3}{(CaO-1.67P_2O_5)+Na_2O+K_2O}][10]$$

The CaO content is corrected with P_2O_5 to account for the presence of apatite. This ratio is always 1.0 when there are only quartz, alkali feldspar and plagioclase in granite (haplogranite). Any minor or accessory mineral present could affect the balance. Normally, if the ratio is above unity, the granite is described as peraluminous. Otherwise, the granite is metaluminous (Shand, 1943). The A/CNK of hornblende ranges from 0.3 to 0.5 (Zen, 1986). For example, if the granite contains hornblende, the A/CNK of the whole rock will be dragged below the unity and therefore, it is described as metaluminous. The presence of peraluminous minerals such as muscovite (A/CNK value ranges from 2.0 to 2.5) and tourmaline (A/CNK value is roughly 6) would on the contrary makes the granite peraluminous. If the ratio is below unity and the Al_2O_3 content is smaller than the sum of K_2O and Na_2O, the granite is described as peralkaline (Shand, 1943). In such case, the alkalis are in excess such that hornblende, or even sodic amphiboles and pyroxenes, may form. Since the A/CNK value is closely related to the major and accessory minerals forming the rock, it reflects the composition of the source (Frost *et al.*, 2001). Maniar and Piccoli (1989) correlated the granites from different tectonic settings using Shand's (1943) granitoids classification (Figure 1.4). They showed that continental collision granites are always peraluminous, while oceanic and island arc granites are usually, but not exclusively metaluminous. Peralkaline granites

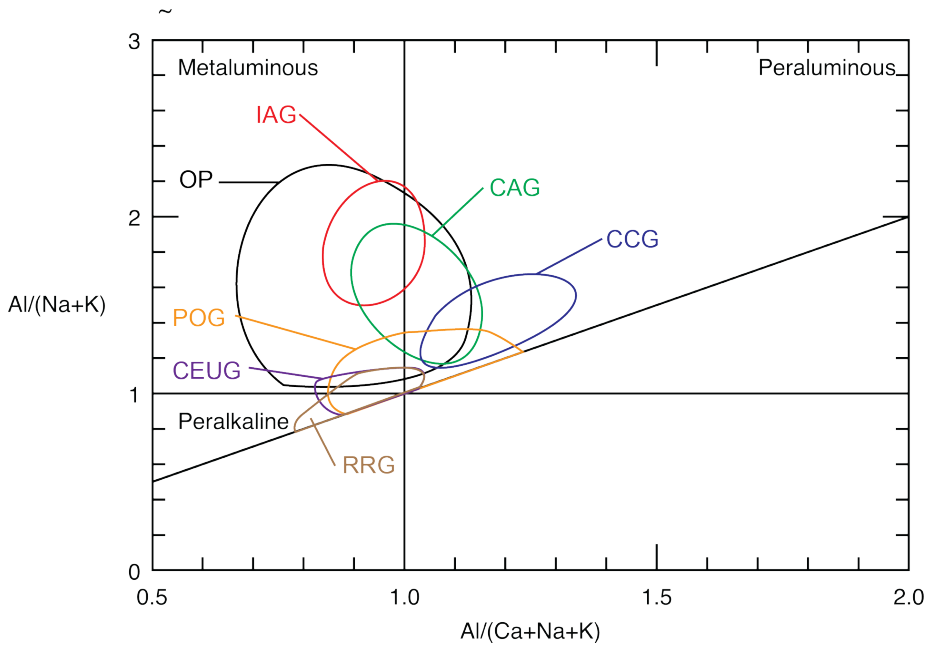

Figure 1.4 Maniar and Piccoli (1989) correlated granites formed from different tectonic setting with Shand's (1943) granite classification in aluminium saturation index (IAG = island arc granitoids, CAG = continental arc granitoids, CCG = continental collision granitoids, POG = post-orogenic granitoids, RRG = rift-related granitoids, CEUG = continental epeirogenic uplift granitoids, OP = oceanic plagiogranite).

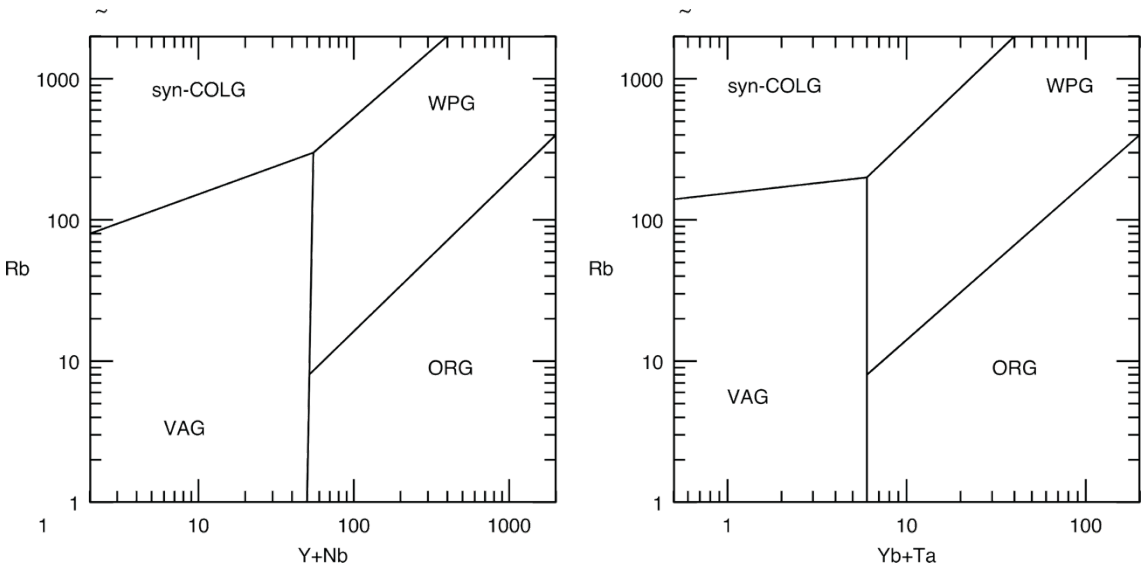

Figure 1.5 Pearce *et al.*'s (1984) granite discrimination using Rb–Y–Nb and Rb–Yb–Ta systems. Granites formed in different tectonic settings have different trace element geochemistry. This is because WPG are formed from enriched mantle source. In contrast, the generation of ORG involves loss of Rb during magmatic evolution. Amphibole fractionation occurred when VAG is formed, while volatile-induced enrichment in Rb and Ta is common when forming syn-COLG.

are generally related to anorogenic environment. The concept of A/CNK was introduced by Chappell and White (1974) to separate the two contrasting granitic belts they have encountered in the Australian Lachlan Fold Belt, one originated from igneous precursor (I-type) and the other from sedimentary precursor (S-type).

1.8.2 Chappell and White's (1974) classification of granites by source rock (I- and S-type granites)

Chappell and White (1974) determined that the melt source was the primary control of the composition of granites. They identified two contrasting granitic belts in the Berridale-Kosciuszko region of the Australian Lachlan Fold Belt. Based on mineralogy and geochemistry, they recognized a belt of hornblende-bearing granites and a belt of cordierite–muscovite-bearing granites. The former is also characterized by the presence of sphene, magnetite and occasionally clinopyroxene. These granites are metaluminous to weakly peraluminous (A/CNK < 1.1). They termed them the I-type granites as these rocks were formed by melt derived from an igneous source. Apart from cordierite and muscovite, the latter is also characterized by the presence of monazite and occasionally garnet and andalusite. These granites are peraluminous (A/CNK > 1.1). Chappell and White (1974) named them S-type for having sedimentary precursor as their melting source. The comparison between the I- and S-type granites are summarized in Table 1.1. This landmark paper inspired the generic classification of granites. Later White (1979) further divided metaluminous granites (A/CNK < 1.0) as M-type. He argued that these granites were formed from mantle-derived source. However, the designation of M-type granites is not popular, as their mantle-origin is still controversial (Frost *et al.*, 2001). They are usually regarded as primitive I-type. Other petrologists also noticed that some of these I-, S- and M-type granites are relatively potassic, while having relatively high

TABLE 1.1 COMPARISON BETWEEN CHAPPELL AND WHITE'S (1974) I- AND S-TYPE GRANITES (CHAPPELL AND WHITE, 1974; MCCULLOCH AND CHAPPELL, 1982; CHAPPELL AND WHITE, 1992; CLARKE, 1992; COBBING *ET AL.*, 1992; PITCHER, 1997; GHANI *ET AL.*, 2013)

Characteristics	I-type granitoids	S-type granitoids
Indicative minerals	Hornblende, biotite, sphene, magnetite	Muscovite, biotite, sillimanite, ilmenite, garnet
Enclaves	Mafic to dioritic microgranular enclave	Metasediments
SiO_2	53-76 wt%	65-79 wt%
Na_2O	> 3.2 wt%	> 2.2 wt% but < 3.2 wt% at 5 wt% K_2O
P_2O_5	Decrease with increasing SiO_2	Increase with increasing SiO_2
A/CNK	< 1.1, increase with increasing SiO_2	> 1.1, decrease with increasing SiO_2
CIPW corundum	< 1 mol%	> 1 mol%
$(^{87}Sr/^{86}Sr)_i$	< 0.708	> 0.708
εNd(*t*)	+0.4 to -8.9	-4 to -17

TABLE 1.2 PEARCE *ET AL.*'S (1984) TECTONIC CLASSIFICATION FOR GRANITES.

Ocean **R**idge **G**ranites (ORG)

- Normal ocean ridges
- Anomalous ocean ridges
- Supra-subduction zone

Volcanic **A**rc **G**ranites (VAG)

- Tholeiitic
- Calc-alkaline
- Shoshonitic

Within **P**late **G**ranites (WPG)

- Intraoceanic
- Intracontinental
- Attenuated continental lithosphere

COLlision **G**ranites (COLG)

- **Syn-COL**lision **G**ranites (syn-COLG)
- **Post-COL**lision **G**ranites (post-COLG)

Fe/Mg ratio, Ta, Nb, Zr, **R**are **E**arth **E**lements (REE) and F concentration (Loiselle and Wones, 1979; Eby, 1992). These granites are commonly found in anorogenic environments and were named as A-type granitoids, later further divided into plume-related (A_1-type) and post-collision-related (A_2-type) (Eby, 1992). Clarke (1992) criticized this classification as "A-type" is a pure geochemical designation and not defined by the nature of the source rock like the I- and S-type granites. More recently, charnockitic granitoids were termed as "C-type" by Kilpatrick and Ellis (1992). These rocks are defined by the presence of orthopyroxene (e.g. hypersthene), pigeonite or olivine (fayalite). It is believed that the C-type melts are derived from a hornblende-poor, **L**arge **I**on **L**ithophile **E**lements (LILE)-rich fertile granulitic source by partial melting at very high temperature (950-1050°C) and subsequent fractionation. However, the formation of charnockites is mainly controlled by fluid activity, especially when water activity is restricted (Frost *et al.*, 2000, 2001). Therefore, in contrast to the I- and S-type, the definition of "C-type" granites is imprecise. In general, the I-, S- and A-type granites are the most widely applied designations.

Further elaborating from their igneous/sedimentary generic model of granite origin, White and Chappell (1977) proposed the derivation of granitic magma would leave a residual product called "restite". They suggested that fragments of restite are incorporated into the granitic melt causing a higher mafic content in the granites than experimental values. Hence, the degree of "restite unmixing" would control the composition of granites (Chappell *et al.*, 1987). However, later workers realized that the actual situation is even more complex than they thought, as experimental results could hardly replicate the "restite unmixing" model. They suggested that incorporated material in the granitoids should include restite and the source materials that did not

take part in the melting process, while some of these entrained materials were dissolved during the magmatic evolution (Clemens *et al.*, 2011; Clemens and Stevens, 2012). This "restite unmixing" model was eventually replaced by Clemens *et al.*'s (2011) PAE model discussed in previous section. Nevertheless, Chappell and White's (1974) model and classification remain widely accepted.

1.8.3 Ishihara's (1977) magnetite-series and ilmenite-series granites

Ishihara (1977) also recognized the existence of contrasting granitic belts along the active continental margins in the circum-Pacific region, based on their magnetite contents and mineralization. He defined the granites containing 0.2 to 1.5 modal percent of magnetite as the magnetite-series. In contrast, those with less than 0.2 modal percent of magnetite are defined as the ilmenite-series. Hence, this classification divides granites according to their oxygen fugacity. In other words, magnetite-series granites are more oxidized than the ilmenite-series granites. In this classic work, he found that the more oxidized magnetite-series granites are usually associated with sulphide deposits notably Cu, Pb, Zn and Mo, while the more reduced ilmenite-series granites contain Sn and W oxide deposits. Ishihara's magnetite-series and ilmenite-series granites are usually compared with Chappell and White's (1974) I-S granites (Table 1.3). In general, S-type granites belong essentially to ilmenite-series, but I-type granites can belong to magnetite-series or ilmenite-series.

1.8.4 Trace element behaviour of granitoids by tectonic setting

Trace element discrimination diagrams have been useful tools to trace the tectonic setting that forms mafic volcanic rock (Pearce and Cann, 1973). Trace element compositions are controlled by the partition coefficients of elements that depend on

temperature and composition of the system (Henderson, 1982). An igneous rock may contain just a few, up to ten, major elements but may have up to eighty trace elements available for comparison. Pearce *et al.* (1984) realized that although Chappell and White's (1974) I-S generic system gives clues to the source region of granites, there is no well-defined boundaries between each designated granite type, hindering the correlations with the corresponding tectonic settings. Moreover, Chappell and White's (1974) system classified granites is largely based on major element geochemistry. This is not ideal because this system can only work well only if the granites are significantly different in mineralogy.

Pearce *et al.* (1984) adopted a different approach comparing trace element geochemistry to tectonic setting. They analyzed the geochemistry of granitoids derived from different tectonic settings, and divided them into **O**cean **R**idge **G**ranites (ORG), **V**olcanic **A**rc **G**ranites (VAG), **W**ithin **P**late **G**ranites (WPG) and **COL**lision **G**ranites (COLG). Each granite category was further subdivided into small categories (Table 1.2). They summarized the trace element characteristics of different granitoids and found that the ocean ridge granites and the within plate granites are usually enriched in Y and **H**eavy **R**are **E**arth **E**lements (HREE), in which within plate granites tend to have higher Nb and Ta concentration. In contrast **syn-**tectonic **COL**lision **G**ranites (syn-COLG) are usually characterized by high Rb content. These granites can be easily discriminated from each other by plotting bivariate diagrams with these elements. Pearce *et al.* (1984) proposed that the best distinction between syn-COLG, VAG, WPG and (non-SSZ) ORG could be seen on Rb vs (Y + Nb) and Rb vs (Yb + Ta) diagrams (Figure 1.5). However, no diagram could be made to separate post-tectonic **COL**lision **G**ranites (post-COLG) and oceanic plagiogranites from supra-subduction zone satisfactorily. All

these granite classification/discrimination systems being discussed are compared in Table 1.3.

1.9 Distribution of granites and classic granitic belts in the world

Granites are found in various tectonic environments, and their geochemical signatures have been summarized by Pearce *et al.* (1984). Granites differentiated directly from the crystallization of mantle-derived basaltic melts, termed usually as plagiogranite, are found within the plutonic sequence of oceanic crust. They are not significant in volume, and are usually exposed on land in ophiolitic suites (Pedersen and Malpas, 1984). Archaean granitoids are also different from those formed in Proterozoic and Phanerozoic time because of the thicker crust at the time they were emplaced (Foley *et al.*, 2003). Similar to plagiogranite, these "ancient granitoids" are correlated to mantle source (M-type). They are essentially **T**onalite, **T**rondhjemite and **G**ranodiorite, which are usually referred as TTG series. TTG are well exposed in all Precambrian cratonic areas. In Phanerozoic time, continental scale batholithic granitic belts are usually found along orogenic belts, both Cordilleran-type subduction-related (I-type) and Himalaya, continental collision related (S-type) and within-plate environment (A-type). In the following sections, famous granitic belts, which have been extensively studied, will be reviewed.

1.9.1 Himalaya-Tibet collision zone

The Indus-Tsangpo suture zone separating the Indian and Asian plates represents the site of closure of the Neo-Tethys Ocean along the Himalayan region. The youngest marine rocks along the suture are Early Eocene in age and the age of collision with Asia is thought to be *ca.* 50 Ma (Figure 1.6) (Green *et al.*, 2008; Searle *et al.*, 2010, 2011).

TABLE 1.3 COMPARISONS OF GRANITE CLASSIFICATION/DISCRIMINATION SYSTEMS.

<table>
<tr><td colspan="2">Classification basis</td><td colspan="9">Origin</td></tr>
<tr><td colspan="2"></td><td colspan="3">Crustal</td><td colspan="3">Mixed</td><td colspan="3">Mantle</td></tr>
<tr><td>First chemical nomenclatures</td><td>Shand (1943)</td><td colspan="3">Peraluminous rocks</td><td colspan="5">Metaluminous rocks</td><td>Peralkaline rocks</td></tr>
<tr><td>Opaque oxides</td><td>Ishihara (1977)</td><td colspan="4">Ilmenite series</td><td colspan="4">Magnetite series</td><td></td></tr>
<tr><td rowspan="2">Geochemistry (major elements)</td><td>Chappell and White (1974)
White (1979)
Loiselle and Wones (1979)</td><td></td><td colspan="2">S-type</td><td colspan="3">I-type</td><td colspan="2">M-type</td><td colspan="2">A-type</td></tr>
<tr><td>Maniar and Piccoli (1989)*</td><td colspan="2">CCG</td><td colspan="3">POG</td><td>CAG</td><td>IAG</td><td>OP</td><td>RRG</td><td>CEUG</td></tr>
<tr><td>Geochemistry (trace elements)</td><td>Pearce et al. (1984)*</td><td colspan="5">(syn-tectonic) COLG (post-tectonic)</td><td colspan="2">VAG</td><td>ORG</td><td colspan="2">WPG</td></tr>
<tr><td colspan="12">Note:
Maniar and Piccoli’s system (1989) and Pearce et al.’s system (1984) were not designed to classify granitoids. These works show the trace element behaviour of granitoids from different tectonic settings.
IAG = island arc granitoids, CAG = continental arc granitoids, CCG = continental collision granitoids, POG = post-orogenic granitoids, RRG = rift-related granitoids, CEUG = continental epeirogenic uplift granitoids,
OP = oceanic plagiogranite, COLG = collision granites, VAG = volcanic arc granites, ORG = oceanic ridge granites, WPG = within-plate granites.</td></tr>
</table>

To the north of the suture, along the Asian plate margin Early Jurassic to Early Eocene hornblende-biotite bearing Gangdese-Ladakh granites and granodiorites have been interpreted as the product of Andean I-type magmatism during the subduction of Tethyan oceanic lithosphere (Chu *et al.*, 2006; Searle *et al.*, 2010). These granites are also associated with contemporaneous calc-alkaline Linzizong volcanics (Chiu *et al.*, 2009). The Gangdese I-type granites have initial $^{87}Sr/^{86}Sr$ ratios ranging from 0.7044 to 0.7048 and εNd(*t*) values ranging from +3.2 to +0.9 (Wen *et al.*, 2008). South of the suture, the Indian plate Greater Himalaya Sequence hosts the Early Miocene tourmaline + garnet ± cordierite bearing two-mica leucogranites, interpreted as collisional S-type granites, derived from 100% crustal meta-sedimentary protolith (Searle *et al.*, 2010; 2011). The initial $^{87}Sr/^{86}Sr$ ratios of these leucogranites range from 0.7240 to 0.7973 and the εNd(*t*) values range from -13.92 to -17.91 (Guo and Wilson, 2012). These two contrasting granitic belts reflect the extreme end-members of Chappell and White's (1974) I-S granite classification.

1.9.2 Cordilleran Belt granites – Famatinian magmatic arc, northwestern Argentina

Although parallel granitic belts are observed along the active continental margin in the circum-Pacific region (Ishihara, 1977), the geochemical difference between two belts are not always as distinctive as those in the Himalaya-Tibet collision zone. The Famatinian magmatic arc in the Cordilleran Belt was formed in response to the eastward subduction of the Palaeo-Pacific Ocean in Early Ordovician (Figure 1.7) (Pankhurst *et al.*, 2000): According to Grosse *et al.* (2011), the outer western belt consists of hornblende-bearing I-type granites, which are metaluminous to weakly peraluminous (A/CNK = 0.94 to 1.05) with εNd(*t*) values range from -3.9 to -4.9. The inner eastern belt consists of muscovite–biotite granitoids and cordierite–biotite granitoids. These S-

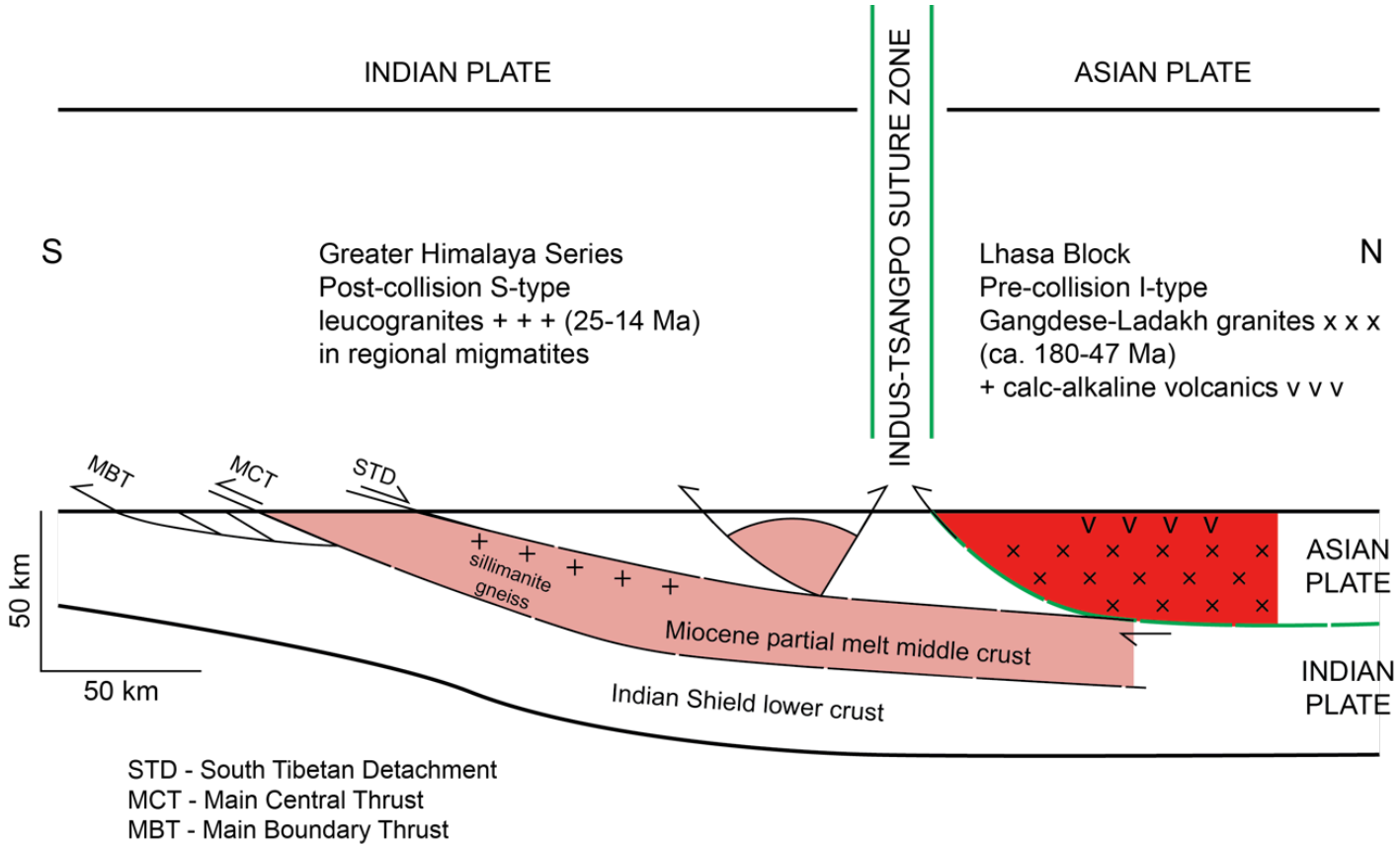

Figure 1.6 Schematic cross-section shows the Indo-Asian collision in the Miocene and the spatial relationship between the pre-collision Andean I-type Gangdese-Ladakh granites and the post-collision S-type Greater Himalayan leucogranites, edited after Searle *et al.* (2010, 2011). Ages were provided by Chiu *et al.* (2009) and Chu *et al.* (2006).

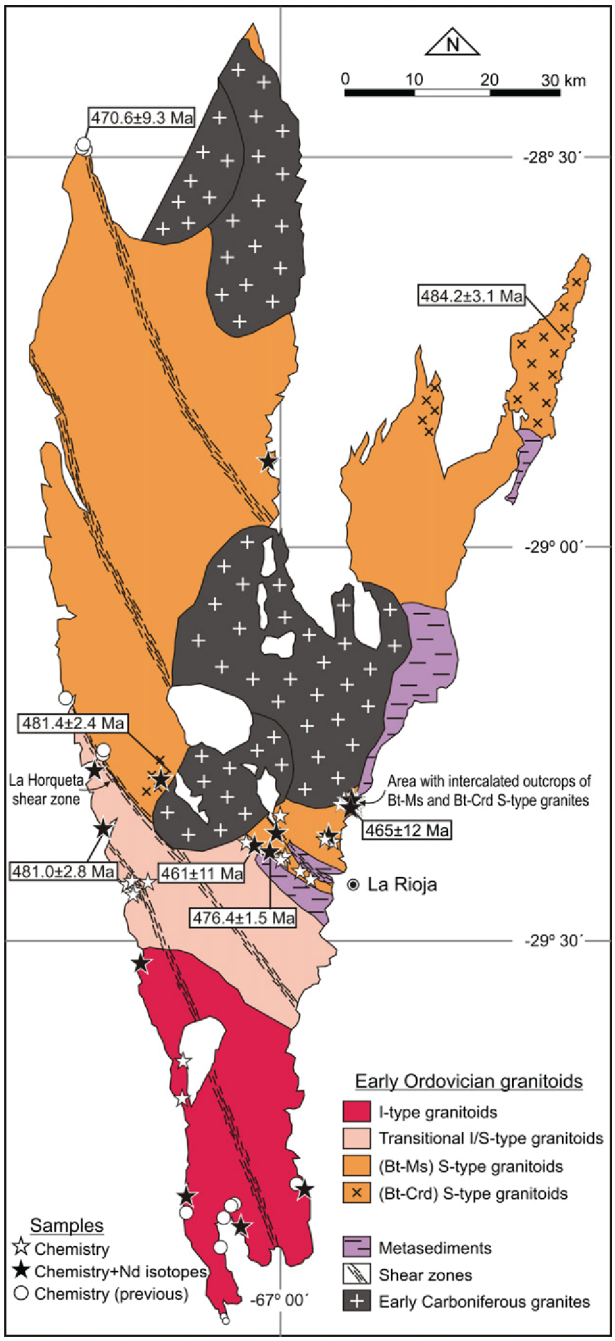

Figure 1.7 Simplified geological map of Sierra de Velasco in the northwestern Argentina, showing the distribution of I-type, transitional I/S-type and S-type granites (Grosse *et al.*, 2011).

type granites are peraluminous (A/CNK = 1.13 to 1.63) with εNd(*t*) values range from -4.4 to -8.2. In between these two belts, transitional I/S-type granite was identified, where biotite granite is dominant with rare muscovite–biotite granitoids. Hornblende has never been reported in this transition zone (Grosse *et al.*, 2011). Both meta-igneous and meta-sedimentary enclaves can be observed in these transitional granitoids. They are normally weakly to moderately peraluminous (A/CNK = 1.03 to 1.24) with εNd values range from -4.1 to -6.2. It has been suggested that these transitional granitoids were formed by hybridization of melts derived from meta-igneous and meta-sedimentary precursors (Grosse *et al.*, 2011).

1.9.3 Northeastern China A-type granites

The Northeastern China A-type granites were emplaced during the amalgamation of microcontinental terranes in Late Palaeozoic to Mesozoic time (Figure 1.8). These A-type granites were emplaced in three episodes (Permian, late Triassic to early Jurassic, and early Cretaceous), with the two older A-type granitic provinces formed during post-collisional slab break-off or lithospheric delamination, while the Cretaceous granitoids were formed during anorogenic rifting (Wu *et al.*, 2002). According to Wu *et al.* (2002), the northeastern China A-type granites are generally leucocractic, feldspar-rich granitoids, with Na-rich amphibole and pyroxene present as accessory minerals. Both magnetite and ilmenite could co-exist in the granitoids. Geochemically, these granitoids are peralkaline and characterized by high Rb, Ga and **R**are **E**arth **E**lement (REE) contents. It is also found that the Permian and late Triassic to early Jurassic granitoids are A_2-type, suggesting a post-collisional setting, while the early Cretaceous granitoids are A_1-type, suggesting a plume origin (Wu *et al.*, 2002). The northeastern China A-

Figure 1.8 Distribution of A-type granites in northeastern China (Wu *et al.*, 2002). The numbers in bracket are the emplacement ages of the plutons.

type granites have rather restricted initial $^{87}Sr/^{86}Sr$ ratios ranging from 0.704 to 0.705 and positive εNd(*t*) values, similar to those measured in the I-type granitoids nearby (Wu *et al.*, 2000).

1.10 Aim of research and thesis structure

The formation of granite melts involves a complete spectrum from mantle-derived melts to wholly crustal melts associated with regional metamorphic terranes. Emplacement of granite can vary from dyking and large-scale plutonism to in situ melting and emplacement along sill complexes. The composition of granites is mainly source-controlled by peritectic assemblage entrainment (PAE) processes. However, later fluid-rock interaction between the melt and the host crust, and crystal fractionation within the melt can cause variations in granite composition. Therefore, although the source-type generic system (alphabet system) has been widely adopted by workers studying granites, e.g. Cordilleran granitoids (Hervé *et al.*, 2007; Grosse *et al.*, 2011), Himalayan granitoids (Searle *et al.*, 2010, 2011), it does not always work perfectly well in many cases. For example, in the Famatinian Arc of the Cordilleran Belt, transitional I/S-type pure biotite granite is found in between the hornblende-bearing I-type granites and muscovite/cordierite S-type granites across the arc (Figure 1.7) (Grosse *et al.*, 2011). This suggests that granite compositions exhibit a spectral variation in which without definite mineralogical indicator of the source region, the origin of transitional granites could be difficult to interpret. This is exactly the case for the Malaysian granitoids in the Southeast Asian Tin Belt. In spite of being divided into an I-type Eastern Province and S-type Main Range Province in the traditional geological model of the Malay Peninsula (Beckinsale, 1979; Cobbing *et al.*, 1986), the mineralogical difference between two granitic provinces are not as distinctive as has been previously suggested. As will be

seen in the later chapters, there is large degree of overlap between the two granitic provinces in terms of lithology, mineralogy and even metallogenic affinity. Clearly, the petrogenesis of the Malaysian granitoids are more complicated than previous workers thought, while the compositional variation cannot be simply explained by Chappell and White's (1974) I-S generic system.

This thesis aims to study the petrogenesis of the Malaysian granitoids by re-interpreting the whole-rock geochemistry and their Sr-Nd isotopic compositions. A petrogenetic model for these granitoids will be proposed. Time constraints of granitic magmatism are provided by ion microprobe U-Pb zircon geochronology. All these data and models are used to reconstruct the magmatic and tectonic setting of the Malay Peninsula during Permian and Mesozoic time. Finally, the various tectonic models presented will be discussed.

Chapter 2 – The Geology of the Malay Peninsula

2.1 Introduction

The Southeast Asian Tin Belt is the most important and largest tin producing metallogenic province in the world. Since 1800, over half of tin production has come from the countries lying within the Belt (Schwartz *et al.*, 1995). It comprises scattered tin-bearing granitic outcrops running from Myanmar (Burma), Thailand and Malaysia to Indonesia (Figure 2.1). Despite the tin production nowadays being dominated by alluvial placer deposits derived from the tin granites, primary tin ores were once significant in the Southeast Asian Tin Belt (Taylor, 1979). Other important mineral resources such as tungsten, copper and gold are also mined from the granitoids and their host rocks (Scrivenor, 1928; Hutchison and Taylor, 1978; Taylor, 1979; Mitchell and Garson, 1981; Schwartz *et al.*, 1995). Traditionally, three granitic and mineralization provinces have been defined, based on the age, the geochemistry of granitoids and the stratigraphy of the hosting country rocks (Figure 2.1). These include:

1) Middle Permian to Late Triassic Eastern Province dominated by Cu-Au bearing I-type granitoids, with subordinate Permo-Triassic alkali granitoids and Late Cretaceous granitoids,
2) Late Triassic to Early Jurassic Main Range Province dominated by Sn bearing S-type granitoids, and
3) Cretaceous Western Province with Sn bearing S-type granitoids mixed with Cu-Au bearing I-type granitoids.

Chappell and White's (1974) source-type generic classification (I-S granite system) was introduced and applied directly to explain the origin and emplacement of the Malaysian

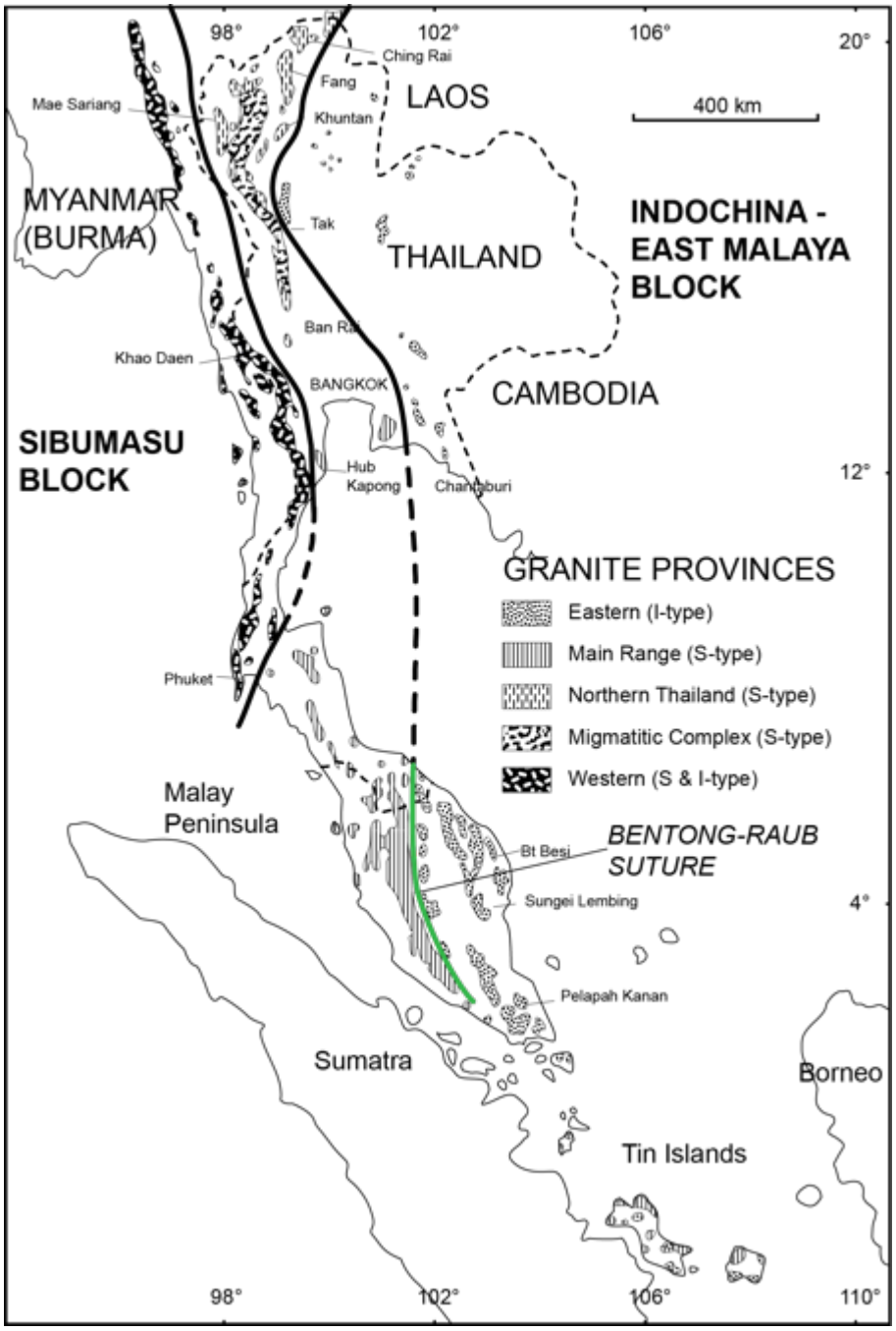

Figure 2.1 Simplified geological map showing the distribution of granitoids in the Southeast Asian Tin Belt (Cobbing *et al.*, 1986). The green line represents the Palaeotethyan suture recognized in Malaysia, the Bentong-Raub Line.

granitoids by Beckinsale (1979) and Cobbing *et al.* (1986). However, the direct application of the I-S granite system has oversimplified the petrogenetic complexity of the Malaysian granitoids. It has also been noted that the existing ages were mainly obtained by Rb-Sr whole-rock dating and K-Ar mica dating, which do not represent the crystallization ages of granites. Furthermore, the relationship of the tin metallogenesis and the hosting granitoids is still unclear. Although it is widely accepted that tin granites are usually S-type (Hutchison and Taylor, 1978; Taylor, 1979; Yeap, 1993; Blevin and Chappell, 1995), the I-type dominated Eastern Province is also tin producing, but not as productive as the Main Range Province. These uncertainties leave a research opportunity to revisit the petrology and geochemistry of the granites in the Southeast Asian Tin Belt.

In addition, this study (Chapter 4) presents new **S**econdary **I**on **M**ass **S**pectrometer (SIMS) U-Pb zircon geochronology that provides reliable temporal constraints for the timing of granitic magmatism and tin metallogenesis. Compared to other parts of the Southeast Asian Tin Belt, the Malaysian granitoids are relatively well studied since the early 1930s because of the tin mining, and previous geochemical and isotopic data are available for comparison and as reference (Cobbing *et al.*, 1986, 1992; Schwartz *et al.*, 1995; Hutchison and Tan, 2009).

Rock samples were collected on two separate field trips and were analyzed at National Taiwan Univeristy, Taipei (geochemistry) and NordSIM, Stockholm (U-Pb zircon geochronology). The localities of the samples collected are shown on Figure 2.2, while their mineral assemblages are presented in Table 2.1. The new geochemical and geochronological data will be presented in the following chapters. Interpretation of

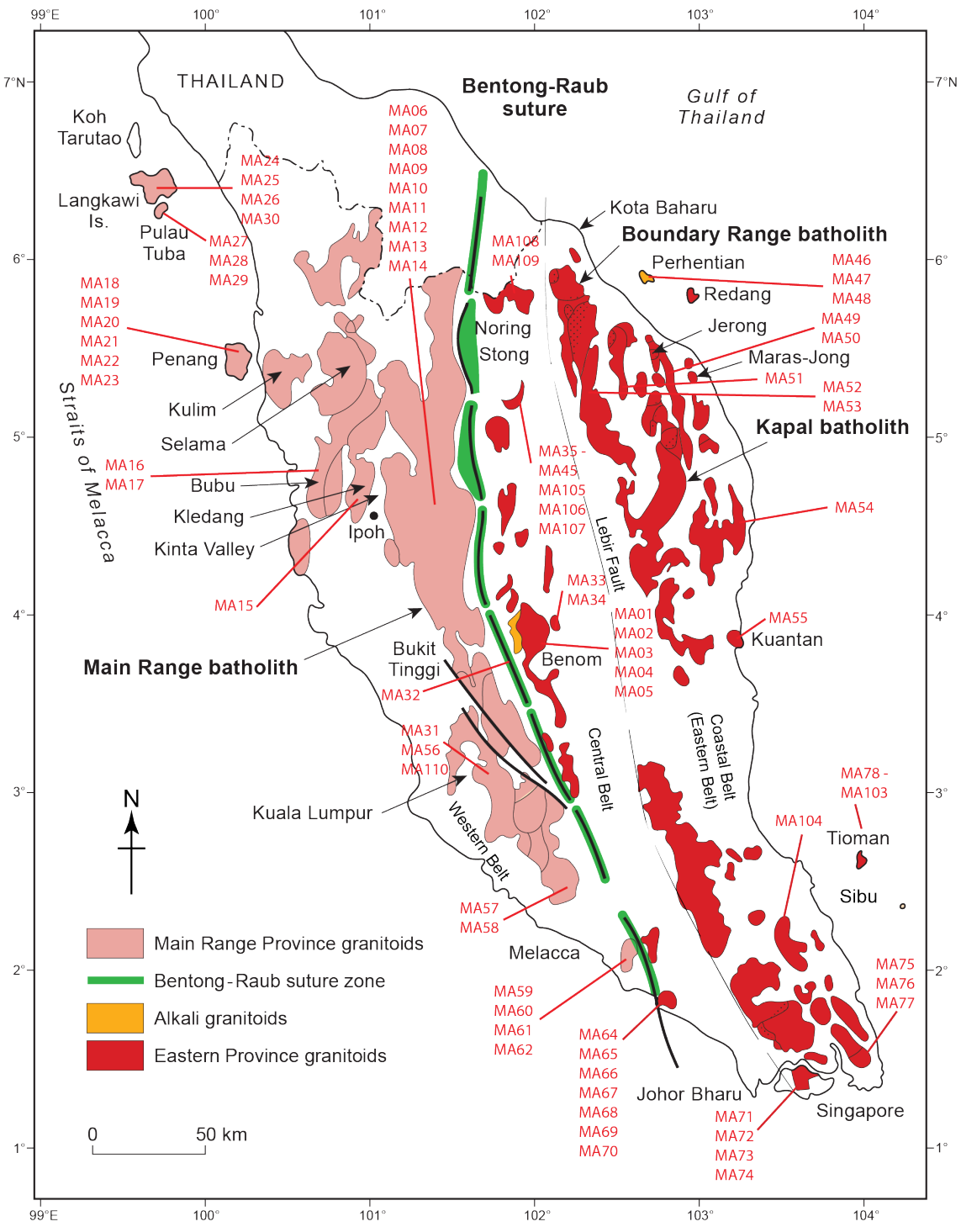

Figure 2.2 The Malaysian granitoids are divided into the Eastern Province and the Main Range Province by the Bentong-Raub Line. The sample localities are shown in this map, modified after Searle *et al.* (2012).

TABLE 2.1A. I-S INDICATIVE FEATURES PRESENT IN THE EASTERN PROVINCE GRANITOIDS (Y = PRESENT, P = PRIMARY, S = SECONDARY).

Sample No.	Lithology	Location	Enclave	Hbl	Px	Ms	Sph	Aln	Ap	Mag	Ilm	Other
MA03	Syenite	Benom	Mafic	Y	Cpx		Y		Y	Y	Y	
MA33	Felsite dyke	Penjom Gold Mine		Y			Y	Y	Y	Y	Y	
MA36	Kfs phyric Hbl-Bt tonalite	Berengkat – Kampong Jerek	Dioritic	Y			Y	Y	Y	Y	Y	
MA39	Grt-Hbl-Bt migmatite	Kenerong		Y			Y	Y	Y	Y	Y	
MA42	Migmatitic tonalite	Renyok River		Y			Y	Y	Y		Y	
MA43	Leucogranitic dyke						Y	Y	Y		Y	
MA45	Kfs phyric Hbl-Bt granite	Noring		Y			Y	Y	Y	Y	Y	
MA47	Bt granite	Perhentian Island						Y		Y	Y	Py
MA48	Syenite		Mafic	Y	Cpx		Y		Y	Y	Y	
MA50	Kfs phyric (Hbl)-Bt granite w/ Qtz-Tour miarolitic cavities	Maras-Jong		Y		S			Y		Y	Grt, Tour
MA52	Hbl-Bt granite	Boundary Range		Y				Y	Y	Y	Y	
MA55	Hbl-Bt granite	Kuantan		Y				Y	Y		Y	
MA57	Kfs phyric (Hbl)-Bt granite	Gunung Ledang		Y		S	Y		Y		Y	
MA58	Leuco- Kfs phyric (Hbl)-Bt granite			Y		S	Y		Y		Y	

Sample No.	Lithology	Location	Enclave	Hbl	Px	Ms	Sph	Aln	Ap	Mag	Ilm	Other
MA64	Kfs phyric Hbl-Bt granite	Batu Pahat		Y					Y	Y	Y	
MA66	Cpx-Hbl-Bt granite	Minyak Beku		Y	Cpx				Y	Y	Y	
MA69	Kfs phyric Bt granite w/ Qtz-Tour veins	Batu Pahat – Hanson Quarry				S			Y		Y	
MA73	Migmatitic granite	Ubin Island		Y		S	Y		Y		Y	
MA77	Kfs phyric Hbl-Bt granite	Bukit Batupejal Quarry		Y			Y	Y	Y	Y	Y	
MA78	Cpx-Hbl-Bt granite	Tioman Island	Hornfels	Y	Cpx		Y	Y	Y	Y	Y	
MA81	Bt granite						Y		Y	Y	Y	
MA83	(Hbl)-Bt granite		Hornfels	Y		S				Y	Y	
MA87	(Hbl)-Bt granite			Y				Y	Y	Y	Y	
MA90	Microgranitic dyke			Y		S				Y	Y	
MA97	Ms-Tour granite		Mafic			S				Y	Y	Tour
MA100	Migmatitic granite						Y	Y	Y	Y	Y	
MA104	Kfs phyric Hbl-Bt granite	Jemaluane – Kluang		Y				Y	Y		Y	
MA109	Kfs phyric Bt granite	Jeli – Blunero Quarry					Y	Y	Y		Y	

TABLE 2.1B. I-S INDICATIVE FEATURES PRESENT IN THE MAIN RANGE PROVINCE GRANITOIDS (Y = PRESENT, P = PRIMARY, S = SECONDARY).

Sample No.	Lithology	Location	Enclave	Hbl	Px	Ms	Sph	Aln	Ap	Mag	Ilm	Other
MA06	Kfs phyric Crd-Bt granite	Bentong				S		Y	Y		Y	Crd
MA07	Fe-stainning Bt granite							Y	Y		Y	
MA09	Kfs phyric Crd-Bt granite	Cameron Highlands				S					Y	Crd
MA11	Tour-Bt granite		Qtz-Tur				Y	Y	Y		Y	Tour
MA13	Kfs phyric Ms-Bt granite		MS			S	Y		Y		Y	
MA14	Kfs phyric Ms-Bt microgranite						Y		Y		Y	Fl
MA15	Kfs phyric Ms-Bt granite	Ipoh				S	Y		Y		Y	Py
MA16	Kfs phyric Hbl-Bt granite	Taiping	Qtz-Tur	Y			Y	Y	Y	Y	Y	
MA19	Kfs phyric Bt granite	Penang Island	Qtz-Tur			S		Y	Y		Y	
MA20	Kfs phyric microgranite					S			Y		Y	
MA23	Kfs phyric Bt granite					S		Y	Y		Y	Py
MA26	Kfs phyric Bt granite	Langkawi Island	Qtz-Tur			S					Y	
MA30	Kfs phyric Ms-Bt microgranite		Qtz-Tur			S					Y	
MA29	Ms-Bt microgranite	Tuba Island				P + S			Y		Y	
MA31	Kfs phyric Bt granite	Kuala Lumpur							Y		Y	
MA62	Kfs phyric Bt granite	Bukit Mor							Y		Y	

these data allows a better understanding of the petrogenesis and tectonic evolution of the Malaysian granitoids. This study also provides new insights to the Indosinian orogeny and the amalgamation of the Southeast Asian micro-continental terranes during Permo-Triassic time.

2.2 Research background and geological framework

Geological studies in the Malay Peninsula were initiated by the tin mining industry in the late nineteenth-century. Scrivenor laid the foundation of geological research in Malaysia with two important publications, *The Geology of Malayan Ore-deposits* (1928), and *The Geology of Malaya* (1931). The first set of Rb-Sr and K-Ar radiometric ages of the granitoids were published by Snelling (1965) and Bignell (1977), which range between 300 – 200 Ma with several Late Cretaceous plutons (*ca.* 80 Ma). However, it was not until the 1970s when Hutchison (1973a, 1977) and Mitchell (1977) summarized all this information and proposed the tectonic framework of Southeast Asia with three granitic belts. The three granitic belts were emplaced onto Precambrian micro-continental terranes, which rifted off from Gondwana, since the Early Devonian, when the Palaeo-Tethys Ocean started opening (Metcalfe, 2011). These terranes were re-assembled again along sutures on the Eurasian plate, forming a biogeographical terrane referred as Sundaland in some literature (Figure 2.3) (Asama, 1984; Bird *et al.*, 2005; Metcalfe, 2011). The tectonic evolution of Sundaland can be constrained temporally and spatially by both the fossil record and by palaeomagnetic data from various terranes. Cathaysian related Upper Permian *Gigantopteris* flora is found in Indochina – East Malaya and Northern Thailand East of the Nan-Uttaradit suture (Fontaine and Workman, 1978; Asama, 1984; Hutchison, 2007). Gondwana-related Permian *Glossopteris* flora is found to the west of the Uttaradit suture in the Sibumasu

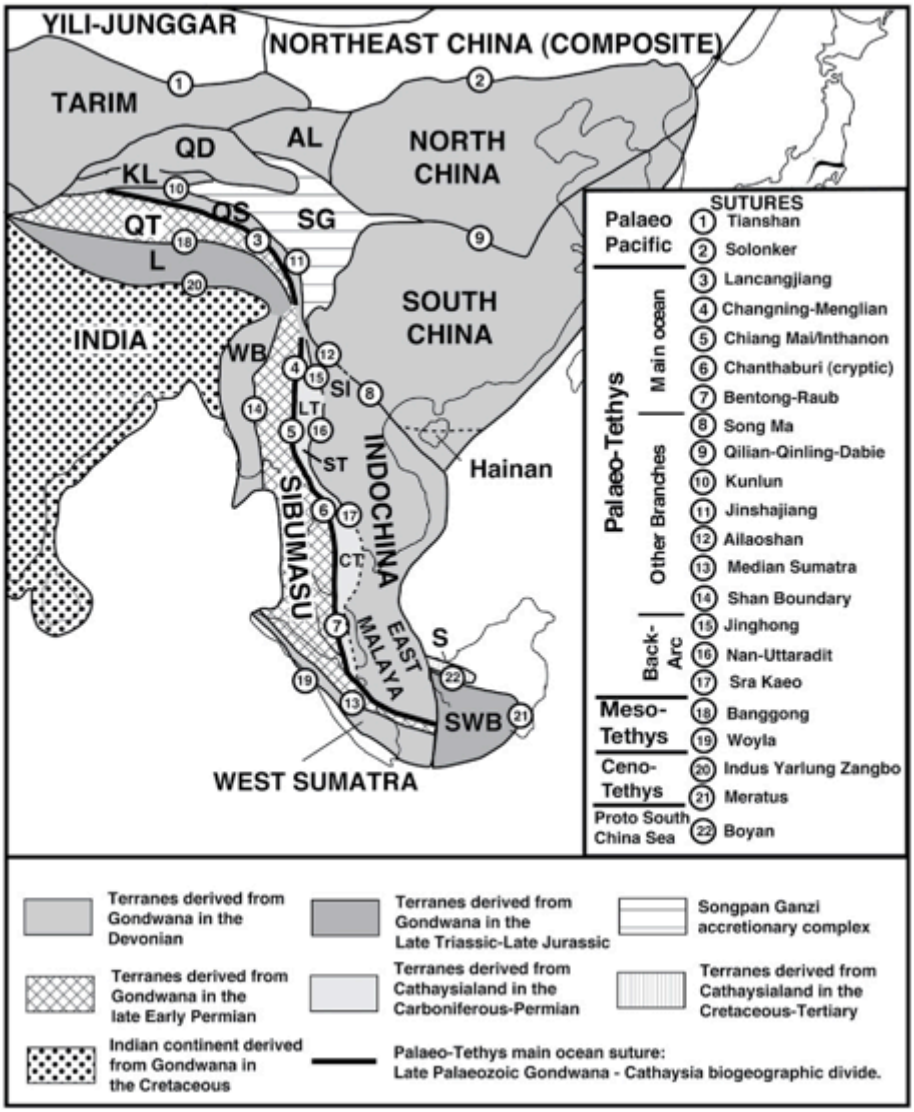

Figure 2.3 Distribution of continental blocks, arc terranes and sutures in East Asia, modified after Metcalfe (2011). WB = West Burma Block, SWB = Southwest Borneo Block, S = Semitau Block, L = Lhasa Block, QT = Qiangtang Block, QS = Qamdo-Simao Block, SI = Simaoi Block, SG = Songpan Ganzi Accretionary Complex, KL = Kunlun Block, QD = Qaidam Block, AL = Ala Shan Block, LT = Linchang Arc Terrane, ST = Sukhothai Arc Terrane, CT = Chanthaburi Arc Terrane.

terrane, which was not separated from Gondwana until Early Permian (Hutchison, 2007; Metcalfe, 2011). The division between these two floral provinces lies on both the Nan-Uttaradit suture and the Bentong-Raub suture (Figure 2.1 and 2.3) (Hutchison, 2007). It was traditionally believed that these divisions marked the location of the Palaeo-Tethys Ocean, however, the nature of the Nan-Uttaradit line as a major suture has been recently challenged by Sone and Metcalfe (2008). These authors suggested on the contrary that the Nan-Uttaradit line should be regarded as a parallel suture, which was responsible for the closure of the supra-subduction back-arc basin created between the Sukhothai arc terrane and the Indochina terrane (Sone and Metcalfe, 2008). Metcalfe (2013) later suggested that this island arc could be extended to the Malay Peninsula and was responsible for the I-type magmatism in the Eastern Province. Although further investigation is still required to support the existence of such parallel subduction systems in Malaysia, the Bentong-Raub suture running along the Malay Peninsula remains as the most widely accepted main suture of the Palaeo-Tethys Ocean (Hutchison, 1977; Mitchell, 1977; Sone and Metcalfe, 2008).

Beckinsale (1979) applied the I-S granite system originally proposed by Chappell and White (1974) to discriminate the granitoids in the Southeast Asian Tin Belt. This system discriminates the hornblende-bearing granitoids, which are usually found to the east of the Bentong-Raub suture, into I-type, and the muscovite-bearing granitoids, which formed the Main Range on the west, into S-type. His observations support Mitchell's tectonic model (1977) and proposed that an eastward subduction along the Bentong-Raub suture would produce these I-type granites on the overriding slab associated with volcanic activities, while the S-type granites were produced during the subsequent continental collision of the Sibumasu terrane and the Indochina – East Malaya terrane.

The Western Belt in Burma is made up of both I-type and S-type granitoids owing to another eastward subduction of Indian subcontinent beneath Southeast Asia (Beckinsale, 1979). Since then, the geological framework of Southeast Asia has been constructed.

This model is generally accepted, and supported by the field observations and geochemical data obtained by Cobbing *et al.* (1986, 1992). Throughout the Southeast Asian Tin Belt, the ages of the granitic provinces were mainly dated by whole-rock Rb-Sr isochron method and K-Ar mica dating, e.g. Bignell and Snelling (1977), Darbyshire (1988a, c, b), Darbyshire and Swainbank (1988), Putthapibian and Gray (1983), and Krähenbuhl (1991). However, both methods are unreliable as the parent and daughter isotopes in the Rb-Sr system are extremely mobile in magmatic-hydrothermal systems and readily reset, while the K-Ar age only represents the cooling age of the rock through the closure temperatures of muscovite and biotite (350-300 °C). More accurate U-Pb zircon ages are provided by Liew (1983), Liew and Page (1985), Liew and McCulloch (1985), Barley *et al.* (2003), Searle *et al.* (2012), and Oliver *et al.* (2014), in which the U-Pb ages presented in the recent papers were obtained by ion microprobe, while the results published in the 1980s were obtained by **I**sotope **D**ilution – **T**hermal **I**onization **M**ass **S**pectrometry (ID-TIMS). Before this work, these zircon ages were the only ones available, mainly on the granitoids exposed on the western and eastern coast of the Malay Peninsula, Northern Thailand, Phuket, Myanmar and Singapore.

Cobbing *et al.* (1992) produced a report on the lithology, geochemistry and Rb-Sr/K-Ar geochronology of the Southeast Asian Tin Belt. They also correlated the texture of granites with mineralization, suggesting granitoids with homogeneous texture are generally unmineralized, while those with varying textures (two-phase variant) are

usually correlated with mineralization, especially for Sn-W deposits. Our field observations suggest that the "two-phase variants" are the granites with textural and mineralogical variation. They may probably represent the roof-zone boundary of the plutons, where the granite is severely altered by fluid. This is characterized by evidence of fluid activities, such as the extensive development of quartz–tourmaline veins and secondary minerals, like pyrite and fluorite. Another group of workers compiled a review paper of *The Southeast Asian Tin Belt* (Schwartz *et al.*, 1995). They summarized all the geological, geochemical and geochronological data available since 1960s and provided both tectonic and metallogenic models to explain the tin mineralization in the Malaysian granitoids.

Schwartz *et al.* (1995) generally followed Cobbing *et al.*'s (1986; 1992) grouping of granitic provinces, but they further separated the migmatitic complex in Northern Thailand as the Northern Province from the Main Range Province. The Indonesian Tin Islands were also studied separately where the I- and S-type boundary is not well defined in the field.

More recently, Ghani (2000, 2001; 2002; 2003b, a, 2005a, b, 2006, 2009a) focused on the petrology and geochemistry of the Malaysian granitoids. He argued that the granitoids in the Main Range Province exhibit mixed I- and S-type features, some of the Main Range S-type granitoids reported by Cobbing *et al.* (1986, 1992) are actually closer to the I-type granites in the Lachlan Fold Belt in Australia (Ghani, 2000). This showed that the mineralogical and geochemical differences between the Eastern Province and Main Range Province might not be as distinctive as previous workers suggested.

2.3 The Bentong-Raub suture

The Bentong-Raub suture zone was recognized as a zone of oceanic rocks mainly radiolarian cherts and mélanges separating zones with different stratigraphy. This suture zone was mapped along the eastern margin of the Main Range, a 20 km wide zone characterized by the presence of meta-sediments with deep-sea radiolarian chert, uncommon serpentinite and metabasite (Haile, 1973; Hutchison, 1973b, 2009). Radiolarian extracted from the cherts were dated at between Middle Devonian to Middle Permian, while the age of tectonic mélange including chert and limestone clasts ranged from Early Carboniferous to Early Permian (Metcalfe, 2000). This coincides with the timing of opening of the Palaeo-Tethys Ocean, which initially rifted in the Devonian when the Indochina – East Malaya terrane was separated from Gondwana and closed in the Late Triassic (Metcalfe, 1984, 1988, 1996, 2002, 2005). Hence, Metcalfe (2000) suggested that this Bentong-Raub suture represented the Palaeo-Tethyan suture in the Malay Peninsula, and connected north with the Changning-Menglian suture and Chiang Mai/Inthanon suture in Thailand (Figure 2.3). It has been generally accepted that the Bentong-Raub subduction was east-dipping, because of the older volcanic-arc-related Eastern Province granitoids were emplaced to the east. Post-collision slab breakoff has been proposed by Ghani *et al.* (2013) to explain the regional-scale intrusion of younger doleritic dykes on the overriding Indochina – East Malaya terrane, and by Oliver *et al.* (2014) with subsequent change of subduction direction to explain the Main Range magmatism. However, this is not supported by any field evidence, as there is no ultrahigh potassic complex, such as adakites, lamprophyres and shoshonites, being observed in the Malay Peninsula. These rocks represent the magmatic "flare-ups" during the slab breakoff in southern Tibet (Chung *et al.*, 2003; Lee *et al.*, 2009; Searle *et al.*, 2011).

2.4 Palaeozoic and Mesozoic Stratigraphy of Malay Peninsula

The Malay Peninsula has been divided into three belts based on stratigraphy (Figure 2.4) (Lee, 2009; Tate *et al.*, 2009; Metcalfe, 2013). The Coastal (Eastern) and Central Belts are defined as the East Malaya terrane, while the Western Belt is defined as the Sibumasu terrane. The oldest rocks exposed in the Malay Peninsula are found in the Northwestern Domain, they can be dated as Late Cambrian. Representative stratigraphic columns presented by Lee (2009) and Metcalfe (2000, 2013) are shown in Figure 2.5. The stratigraphy of each Belt will be described separately.

2.4.1 East Malaya terrane

The East Malaya terrane comprises the Coastal Belt (Eastern Belt) and the Central Belt. The Eastern Belt in previous literature is renamed as Coastal Belt here to avoid any confusion with the Eastern Province. In the Malay Peninsula, it is bounded to the west by the Bentong-Raub suture and to the south by the Lalang Line and Sumatran Fault Zone (Metcalfe, 1988). The location of the eastern boundary is still unclear. It has been argued that the East Malaya terrane could be a natural extension of the Sukhothai arc terrane defined in Thailand, while a postulated cryptic suture line may be found offshore against the Indochina terrane (Metcalfe, 2013). However, this is still controversial because half of the granitoids in the Eastern Province are weakly peraluminous as shown in next chapter, and this is generally not the case for island arc granites (Maniar and Piccoli, 1989). The East Malaya terrane has similar stratigraphy and igneous suites, which are also found in the Indochina terrane across the Gulf of

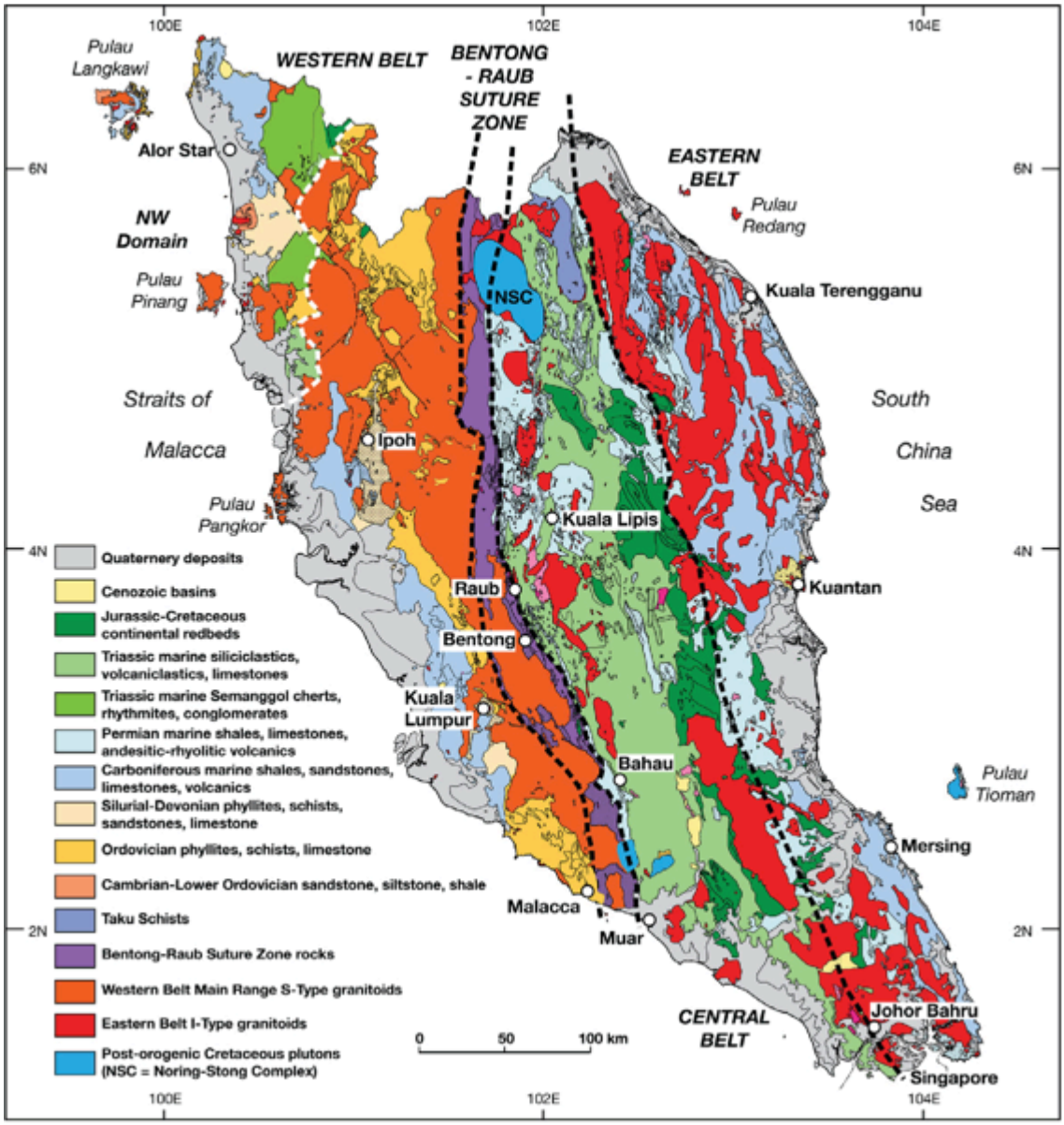

Figure 2.4 Simplified geological map of the Malay Peninsula, modified after Tate *et al.* (2009) and Metcalfe (2013). Three stratigraphic belts were defined in the Malay Peninsula, while the oldest Upper Cambrian rocks are exposed in the Northwest Domain (Lee, 2009).

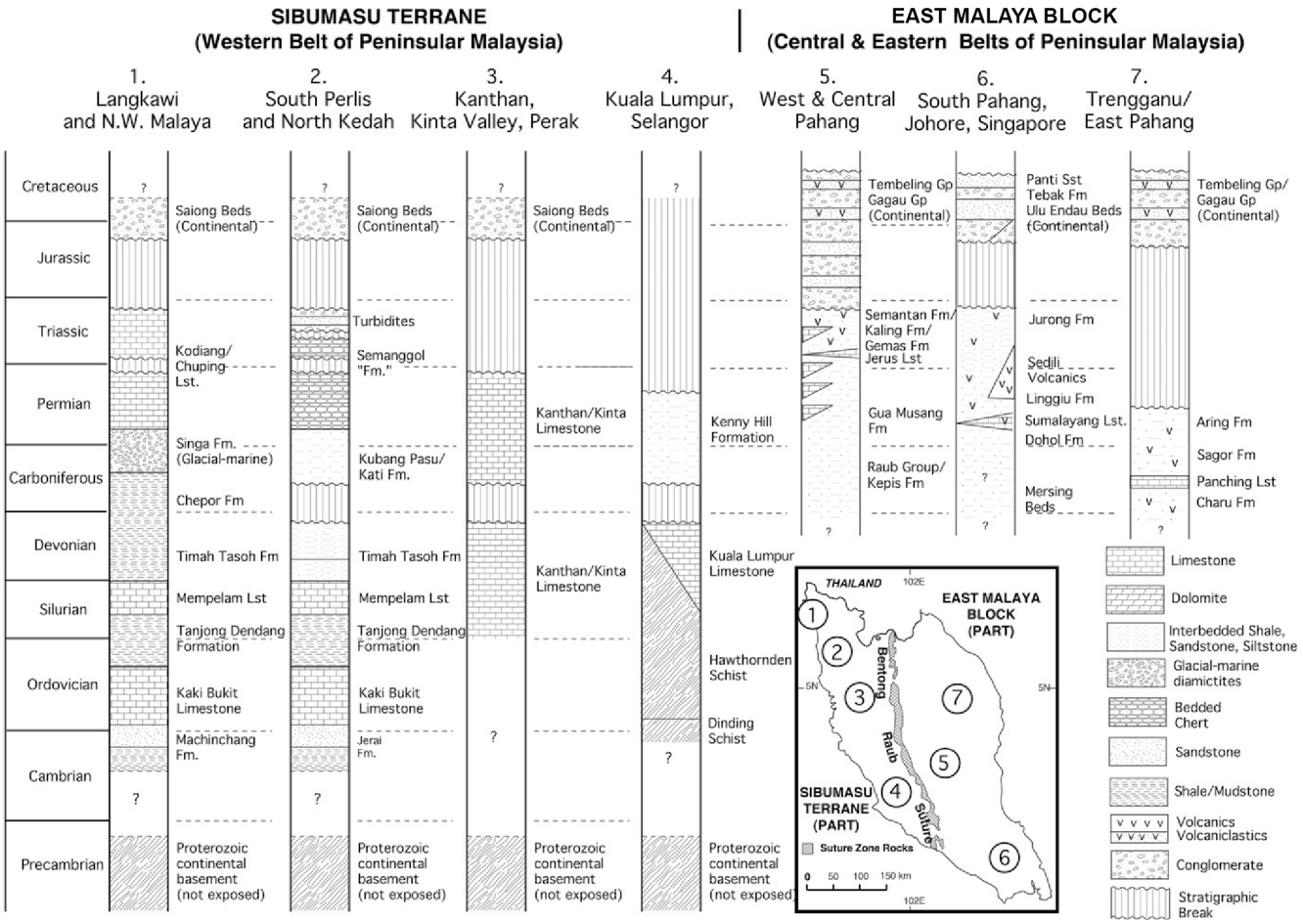

Figure 2.5 Representative stratigraphic columns for the East Malaya Block, modified after Lee (2009) and Metcalfe (2000, 2013).

Thailand. They belong to a single continuous continental terrane before rifting during the Palaeogene (Metcalfe, 1988; Hutchison, 2007).

Coastal Belt (Eastern Belt): The Coastal Belt (Eastern Belt) runs from the eastern Kelantan, Terengganu, and eastern Pahang to eastern Johor. The oldest rocks can be dated as Late Carboniferous, and they are grouped as the Kuantan Group, which includes the Charu volcanics, the Panching limestone and the Sagor volcanics in eastern Pahang (Lee, 2009; Metcalfe, 2013). The Sungai Perlis beds in Terengganu could be a northern extension of the Kuantan Group, while the Seri Jaya and Kambing beds are interpreted as the southern extension (Lee, 2009). These beds are highly deformed continental margin carbonates of the East Malaya terrane (Charkraborty and Metcalfe, 1985; Shuib, 2009b). Alternating flora and warm-water fauna are found in the Carboniferous sandstones and shales, suggesting sediment deposition in a marginal marine setting (Lee, 2009). The sedimentary succession is continuous up to Permian time in Terengganu and Eastern Pahang, and may be up to the Triassic time in southern Pahang, Johor and Singapore, which are followed by a disconformity (Figure 2.5). This disconformity might be related to the uplift of the East Malaya terrane (Lee, 2009). On top of the disconformity, continental sediments such as fluvial conglomerate and red sandstone intercalated with siltstones/mudstones are found. Volcanic components are significantly reduced higher in the stratigraphic column; this may imply the cease of magmatic activity in the Coastal Belt (Lee, 2009).

Central Belt: The boundary between the Eastern Belt and the Central Belt runs along the Lebir Fault in the north and the western boundary of the Dohol Formation in the south (Lee, 2009). To the west, it is bounded by the Bentong-Raub suture. As in the

Eastern Belt, the oldest rocks are dated as Late Carboniferous. However, in contrast to the marginal marine sediments associated with andesitic volcanics in the Eastern Belt, the Palaeozoic strata are mainly shallow marine carbonates (limestones and calcareous sediments) and arenaceous sediments (Lee, 2009). Volcanic rocks are occasionally found within the sedimentary strata and have been interpreted as products of submarine volcanism (Lee, 2009). A disconformity is again located above the Upper Triassic strata. On top of the disconformity, the Central Belt is characterized by the alternate deposition of continental sediments and volcaniclastics, such as the Tembeling redbeds (Figure 2.5) (Metcalfe, 2013). This shows that the magmatic activity migrated from the Eastern Belt in the Mesozoic time.

2.4.2 Sibumasu terrane

The Sibumasu terrane is a north-south striking narrow continental strip, which runs from the Shan Plateau of Myanmar, across north and west Thailand, western part of the Malay Peninsula to the eastern part of Sumatra (Metcalfe, 2013). Along the east, the Sibumasu terrane is bounded by the Changning-Menglian suture and Chiang Mai/Inthanon suture in Thailand, and Bentong-Raub suture in Malay Peninsula (Figure 2.3) (Sone and Metcalfe, 2008; Metcalfe, 2011, 2013). To the north, it is sutured against the South China terrane; while to the west, it is separated from the West Burma terrane by the Sagaing Fault (Metcalfe, 2011, 2013). Sengör (1984) suggested that the Sibumasu terrane was the eastern part of the Cimmerian continent, and suggested that it had close tectonic affinity with the Baoshan – Tengchong terrane in western China, and Qiangtang terrane in Tibet. Its Gondwana-affinity is supported by fossil records, detrital zircon provenance, and palaeomagnetic data, which suggest a northwestern Australian origin (Stauffer and Mantajit, 1981; Archbold *et al.*, 1982; Metcalfe, 1988, 1994, 2002,

2013; Shi and Archbold, 1995). In the Malay Peninsula, it contains the Western Belt, which has the oldest rocks being in the Northwestern Domain in Kedah, Penang, Perlis and Langkawi. The Western Belt is separated from the Central Belt by the Bentong-Raub suture, and is characterized by the emplacement of batholithic tin-bearing granites.

Western Belt: The Palaeozoic succession in the Western Belt is exposed along the western foothills of the Main Range. The oldest rocks exposed in the Malay Peninsula are found in the Northwestern Domain in the Western Belt. They are the Middle Cambrian to Lower Ordovician Machinchang and Jerai Formation clastics and metapelites (Lee, 2009). These strata form part of the Palaeozoic shallow-marine continental shelf sediments. In contrast to the Eastern and Central Belt, volcanic rocks are not commonly observed in the Western Belt, but carbonates are well developed here, including the Kaki Bukit limestone, the Mempelam limestone and the Kodiang/Chuping limestones (Figure 2.5). The deposition of the Semanggol Formation (shallow marine sediments and turbidites) in the Northwestern Domain during Triassic may represent the foredeep basin sediments deposited during the Sibumasu – East Malaya collision (Metcalfe, 2000). This is followed by a disconformity in the Jurassic time, and subsequent deposition of continental Saiong redbeds.

2.5 Eastern Province granitoids

Granitoids of the Eastern Province of Malaysia were emplaced into the Indochina (Sukhothai Arc) – East Malaya terrane, which is made up of Lower Carboniferous to Cretaceous marine-fluvial sediments and volcanics, underlain by postulated Mesoproterozoic continental basement (Hutchison, 2007; Metcalfe, 2013). However, this continental basement is not exposed in the Malay Peninsula, but the evidence of its

existence is supported by the 1100-1300 Ma inherited zircon ages extracted from the Eastern Belt granitoids on the eastern coast of the Malay Peninsula (Liew, 1983; Liew and McCulloch, 1985). This is also shown in the Nd depleted mantle model ages and in the new U-Pb inherited zircon ages presented in the following chapters. Although local workers further divided the Eastern Province into Coastal Belt (Eastern Belt) and Central Belt according to the stratigraphy of the host rocks (Hutchison and Tan, 2009; Metcalfe, 2013; Oliver *et al.*, 2014), no significant geochemical difference is found between the Eastern Belt and the Central Belt granitoids (Cobbing *et al.*, 1992). This will be further discussed in Chapter 3.

The Eastern Province has a wide spectrum of lithologies ranging from K-feldspar–hornblende dacite (e.g. Kerteh, MA54 in Figure 2.2) to K-feldspar phyric (hornblende)–muscovite–biotite granite (e.g. Maras-Jong, MA49 and MA50 in Figure 2.2), in which the latter only has insignificant hornblende and is mineralogically similar to S-type granitoids. Accessory minerals include apatite, secondary epidote, zircon, allanite, sphene and iron oxide (Table 2.1), are commonly observed in the Eastern Province granitoids. In the Eastern Province granitoids, both magnetite-series and ilmenite-series granitoids are found (Ishihara *et al.*, 1979; Yeap, 1993). This implies that some of the I-type Eastern Province granitoids are less oxidized than the Cordilleran I-type granites, which are primarily magnetite-series.

Two-thirds of the Eastern Province exposure are hornblende-bearing granitoids; while the remaining one-third are hornblende-free pure biotite granitoids (Cobbing *et al.*, 1986, 1992). The hornblende-bearing granitoids formed the main body of the plutons, leaving the more fractionated hornblende-free phase at the roof-zone. Roof-zone boundaries are

characterized by gradual textural and mineralogical variation. In addition, these two phases are usually formed contemporaneously (Chapter 4). These suggest that both the hornblende-bearing granitoids and the hornblende-free phases belong to the same plutonic body. Indications of hydrothermal activity, such as greisenization (chloritization and sericitization of minerals, Plate 2.1) and vein development, are usually associated in the roof-zone. These greisenized granitoids host the tin deposits of the Malaysian granitoids.

The Eastern Province comprises small batholithic granitic bodies up to 1000 km^2 in size, occasionally cut by mafic doleritic. These dykes are significantly younger than the granitoids, and ranging from 79 ± 2 Ma to 179 ± 2 Ma (Ghani *et al.*, 2013). Clearly, they are not related to the Permo-Triassic Eastern Province magmatism. The I-type Eastern Province granitoids are also associated with acidic to intermediate calc-alkaline Andean-type volcanics, tuff, rhyolite, andesite and ignimbrite, as seen for example in the Andean Cordillera and south Tibet provinces. They form volcanic complexes, such as those outcropping in Eastern Pahang, Southern Johor and off southeastern Malay Peninsula. Extraordinary volcanic suprastructures are associated with the Cretaceous granitoids on some Eastern offshore islands such as the Tioman Island volcanic complex (MA78-MA103 in Figure 2.2).

In the following sections, the Eastern Province granitoids will be discussed according to their geographical position.

2.5.1 *Boundary Range and Kapal Range batholiths* (MA51-MA53 in Figure 2.2 and 2.6)

Major mountain ranges such as the Boundary Range and Kapal Range are uplifted granitic batholiths. Among these, the Boundary Range Composite Batholith is the largest in the region; its size could be over 1000 km^2. However, because of intense weathering and dense tropical vegetation, samples were collected mainly from roadcuts and quarries. The composition of these granitoids ranges from diorite to monzogranite. According to Cobbing *et al.* (1992), biotite granites are often found at the centre of the batholiths (Figure 2.6, e.g. the Nal granite of the Boundary Range Batholith, the Peda granite of the Lawit Batholith and the Kenyir Granite of the Kapal Batholith), they are surrounded by outcrops of K-feldspar megacrystic hornblende– biotite meso- to microgranites. Hornblende–biotite enclaves are found occasionally in the granitoids but not abundantly (Plate 2.2). The field relationships between the hornblende-bearing phase and hornblende-free phase are not clear. SIMS U-Pb zircon ages of these granitoids (Chapter 4) suggest that the two phases are contemporaneous. It is likely that the pure biotite granites are fractionated from the hornblende-bearing phase, forming the roof-zones of the batholith.

2.5.2 *Eastern coast (MA46-MA50, MA55 in Figure 2.2 and 2.6)*

In contrast to massive composite batholiths forming the mountain ranges, the granitoids found along the coast are normally exhibited as individual small plutons. The granitoids exposed on the Perhentian Island (MA46-MA48) were thought to be a natural extension of the Kapal Range (Figure 2.2 and 2.6) (Cobbing and Mallick, 1987; Ghani, 2001). However, the ages of Perhentian granitoids obtained in this study (Chapter 4) is significantly older than the Kapal Range, which does not support this hypothesis. The

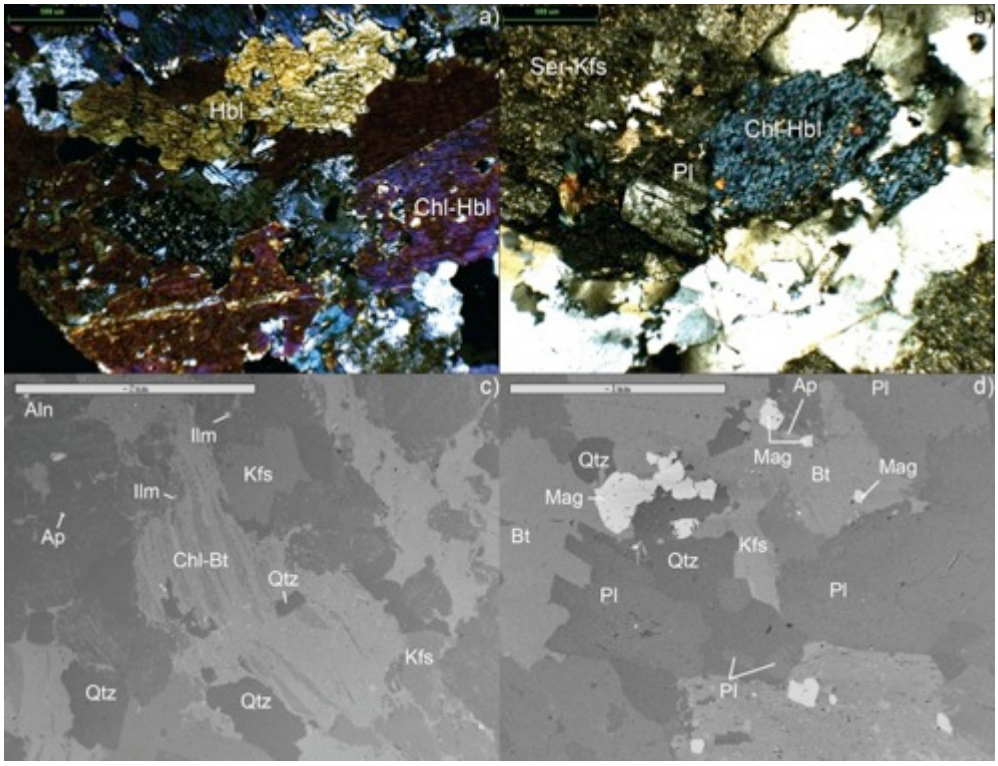

Plate 2.1 a) Perhentian syenite (MA47) contains significant amount of hornblende, some of them are chloritized (40x, cpl); b) Hornblende-bearing granite is typical in the Eastern Province. Hornblende is chloritized by post-magmatic hydrothermal alteration (MA52 Boundary Range granite, 40x, cpl); c) and d) Scanning electron microscope images of MA52 and MA74 show the common accessory minerals found in the Eastern Province granitoids, including allanite, apatite, magnetite and ilmenite.

Plate 2.2 Mafic hornblende-biotite enclave found in the Kapal granite (MA51).

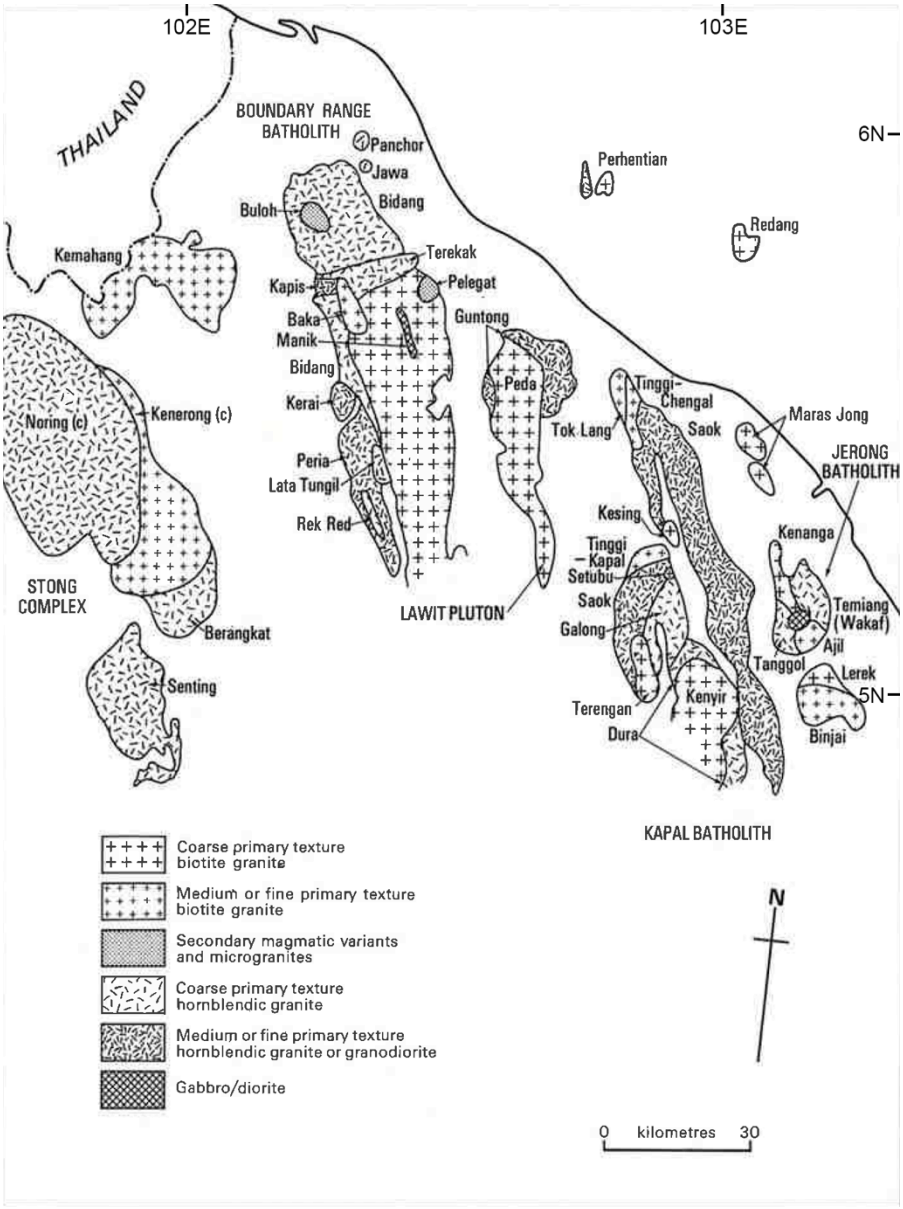

Figure 2.6 Distribution of the Eastern Province granitoids in Terengganu area (Cobbing *et al.*, 1992).

roof-zone of the Perhentian granite is medium to coarse grained and hornblende-free. Hornblende-bearing microgranite can be found near the contact with the Perhentian syenite, which is exposed on the southern part of Perhentian Kecil. The syenite contains K-feldspar, plagioclase, hornblende, pyroxene, quartz and biotite in decreasing abundance, which is interpreted as the fractional product of alkali basalt (Ghani, 2001). It is cut by the Perhentian granite, and in turn cut by doleritic dykes (Plate 2.3a and b). Mafic enclaves were found in the Perhentian syenite (Plate 2.3c).

The Maras-Jong granite (MA49 and MA50) is a small granitic body outcropping at Bukit Maras and Bukit Jong (Figure 2.2 and 2.6). It has been considered as an anomaly in the Eastern Province, as in contrast to other I-type granites, the Maras-Jong granite is garnet- and muscovite-bearing, lithologically similar to S-type granite. Tourmaline–quartz veins and miarolitic cavities are commonly found on the Maras-Jong granite resulting from later hydrothermal activity (Plate 2.4a). It was interpreted as S-type granite formed from meta-sedimentary precursors to account for its aluminous mineral assemblage (Cobbing *et al.*, 1986, 1992). However, the geochemistry of the Maras-Jong granite on the contrary, suggested an I-type origin (Ghani, 2003b). The low A/CNK but high $\varepsilon Nd(t)$ values obtained from the fresh Maras-Jong granite in this study, which are presented in Chapter 3, also support Ghani's (2003b) argument. The parental magma of the granite could be formed from hybridization of igneous-sourced melt and sedimentary-sourced melt. It is suggested that the "S-type" lithology is given by the sedimentary protolith, then intensified by hornblende fractionation and fluid activities (muscovitization). This is supported by the fact that most of the muscovite grains observed in the Maras-Jong granite are secondary, while tiny and insignificant amount of hornblende grains are also found in the granite (Plate 2.4b).

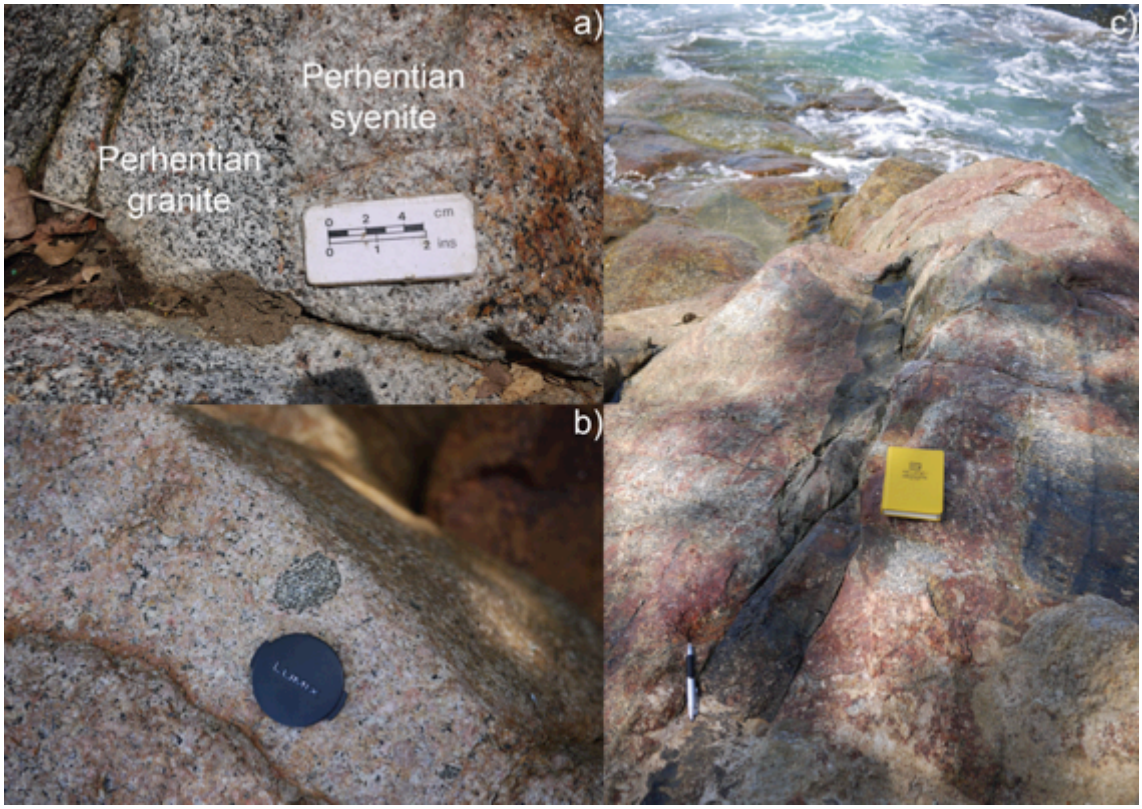

Plate 2.3 a) Intrusion of Perhentian granite (MA47) into older syenite (MA48), the grain size of the Perhentian granite is finer in the chill margin; b) Mafic hornblende-biotite enclave observed in the Perhentian syenite (MA48); c) Mafic doleritic dyke cutting through Perhentian syenite.

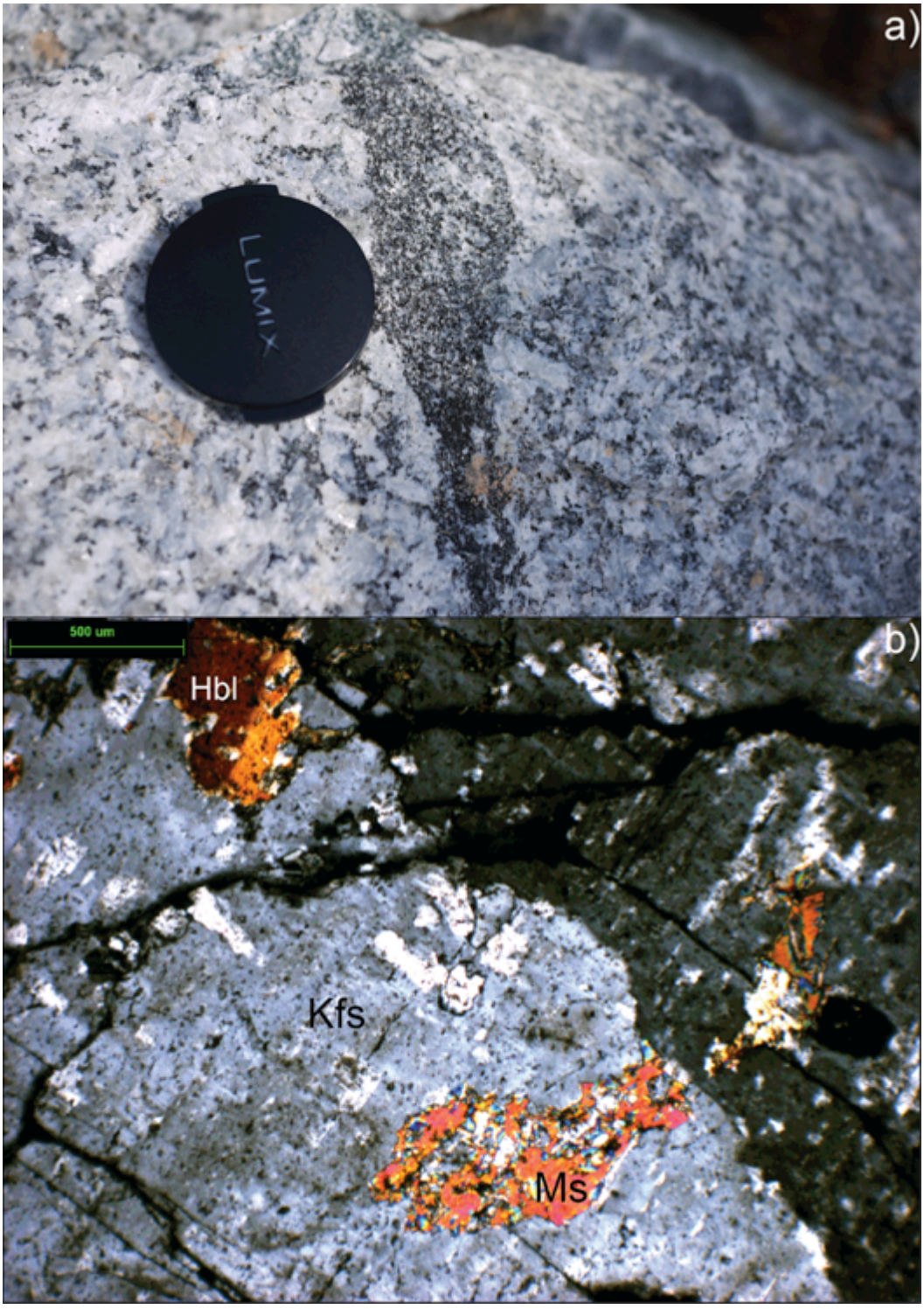

Plate 2.4 a) Toumaline-quartz vein observed in the Maras-Jong granite (MA50); b) Secondary muscovite from alteration of feldspar is common in Maras-Jong granite, which may simulate S-type texture. However, tiny hornblende grains are also found in the sample under petrographic microscope. This shows that the Maras-Jong granite is I-type in nature (40x, cpl).

The Kuantan granite (MA55) is another isolated small pluton on the eastern coast. It is exposed as an equigranular hornblende–biotite granite in a quarry near to the city of Kuantan (Plate 2.5). The granite exposed is pristine and has insignificant alteration induced by fluid activity. Cobbing *et al.* (1992) suggested that its lithology and texture are similar to the Lunchoo granite in South Johor.

2.5.3 South Johor and Singapore (MA64-MA104 in Figure 2.2 and 2.7)

Singapore is a natural extension of Johor. The island itself lies on the boundary of the Eastern Belt and the Central Belt (Figure 2.2). Granites exposed in Johor and Singapore are dominantly emplaced into the Eastern Belt (Oliver *et al.*, 2014).

Samples were collected from the abandoned Hindhede Quarry in Singapore (MA72) and from the coast of Ubin Island near Singapore (MA74). These granitoids are equigranular hornblende–biotite mesogranite. A lithologically similar sample was also collected at a roadcut connecting Jemaluane and Kluang in South Johor (MA104). Migmatitic granite is exposed on the coast of Ubin Island (Plate 2.6). Unlike the equigranular Singaporean granitoids, the sample collected from the Bukit Batupejal Quarry in southeastern Johor (MA77) is a microgranite with hornblende-bearing matrix and megacrystic K-feldspar phenocrysts.

Granitoids on Tioman Island (MA78-MA103) are much younger in age (*ca.* 80 Ma), and will be discussed in Chapter 4. They are associated with andalusite-hornfels aureole (Plate 2.7a) and acidic volcanics (Plate 2.7b). Hornblende-bearing granite is mainly found on the western coast of the island, while the remainder is hornblende-free. Clinopyroxene is observed in these granites, representing high temperature magmatism,

Plate 2.5 Equigranular hornblende-biotite granite is exposed near Kuantan (MA55). This individual pluton has been correlated with those exposed in South Johore by Cobbing *et al*. (1992).

Plate 2.6 Migmatitic granite (MA73) exposed on the shore of Ubin Island in Singapore may represent the restite of the Luchoo and Singapore granite.

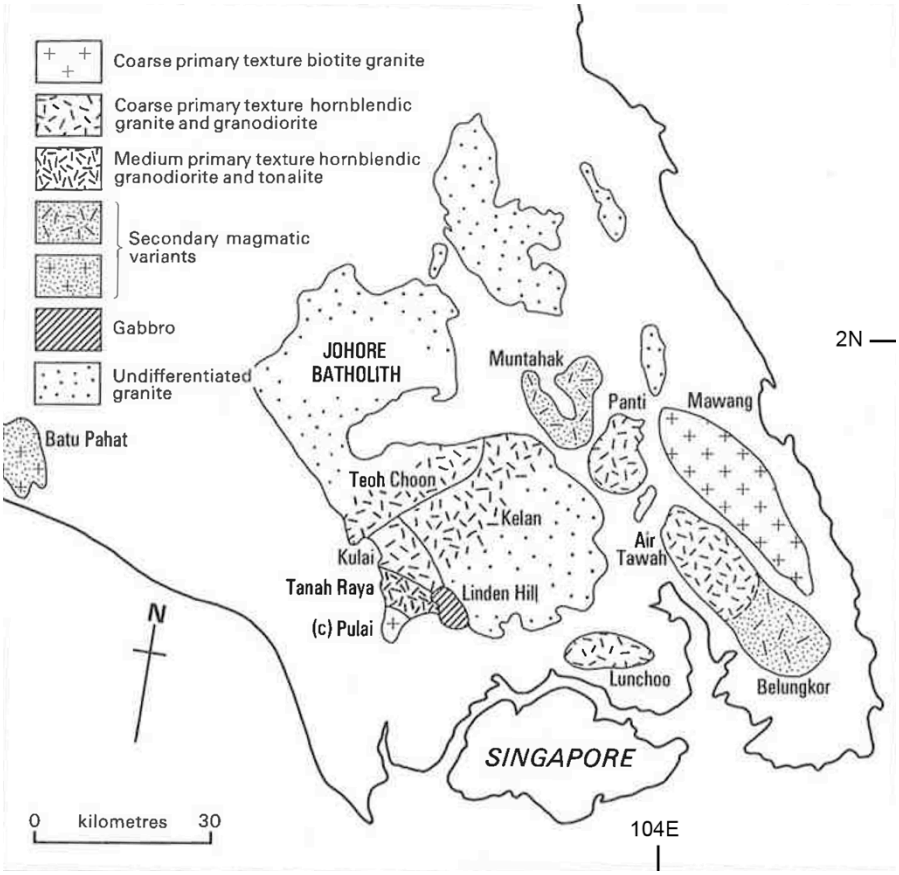

Figure 2.7 Distribution of the Eastern Province granitoids in Johor area (Cobbing *et al.*, 1992).

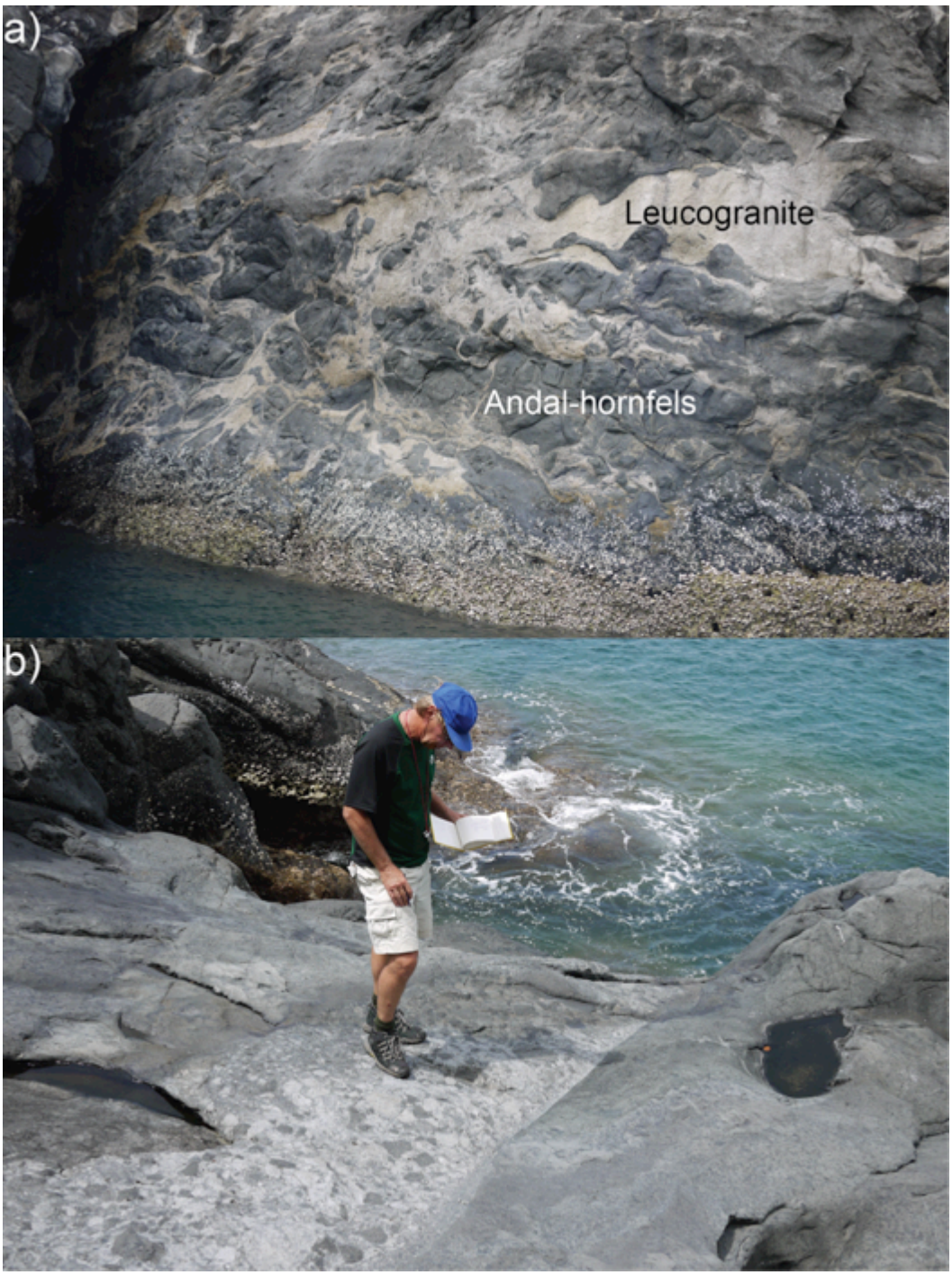

Plate 2.7 a) Andalusite-bearing hornfels (MA101) formed the metamorphic aureole of the Tioman granite; b) Gabbroic, dioritic and granitic xenoliths brought up by volcanic gas pipe on Tioman Island, it is one of the volcanic feature associated with the Tioman magmatism.

this is supported by zircon saturation thermometry presented in Table 3.1. Biotite granite is found mainly on the eastern coast associating with the rhyolitic volcanic succession.

2.5.4 Central Belt granitoids (MA01-05, MA35-MA45, MA57-MA70 in Figure 2.2 and 2.8)

The Benom alkali suite (MA01-05) comprises calc-alkaline syenites, monzonites and gabbros (Hutchison, 1971; Ahmad, 1979; Ghani, 2009a). The syenite is made up of megacrystic K-feldspar phenocrysts in a matrix of hornblende, quartz, plagioclase and epidote, while the gabbro contains plagioclase phenocrysts with hornblende, clinopyroxene, quartz and biotite in the matrix. The monzonite contains the same minerals as found in the syenite and gabbro (Ghani, 2009a). Inclusions of syenite are observed in the gabbro, and vice versa, suggesting they were cogenetic immiscible liquids (Plate 2.8) (Ghani, 2006; Searle *et al.*, 2012). Ghani *et al.* (2006) again interpreted the syenite as a fractionated product of alkali basaltic intrusion.

Large-scale migmatitic bodies are found in the Stong region in the Central Belt (Hutchison, 2007; Searle *et al.*, 2012). The Stong Complex comprises three unrelated components, the Berangkat tonalite (MA35 and 36), Kenerong leucogranite (MA37-44) and Noring granite (MA45), and except for the Upper Triassic Berangkat tonalite; the latter two have Late Cretaceous ages as shown in Chapter 4. Although these three granitic suites are in close proximity to each other, owing to the limited exposure the spatial relationships are not clear. The U-Pb zircon age suggest that the highly deformed Berangkat tonalite (MA35 and MA36) has been intruded by the Kenerong and Renyok leucogranite (MA37-MA44), which are in turn cut by the Noring granite (MA45). Both

Berangkat tonalite and Noring granite are hornblende bearing. However, the former is highly deformed. Migmatitic tonalite is observed along the Kenerong River and Renyok River (Plate 2.9a). In contrast, the Noring granite is undeformed, and is characterized by the presence of pink rounded K-feldspar grains (Plate 2.9b).

The Central Belt granitoids exposed in the Malacca region are different from the exposure in Benom and Stong. They are hornblende–biotite granites similar to those found in the Eastern Belt. The Minyak Beku granitoids (MA66 and MA67) contain microgranite and mesogranite, which probably represent the roof-zone boundary of the pluton. In the outcrop being visited, the mesogranite (MA66) contains clinopyroxene-bearing enclaves in megacrystic quartz–K-feldspar vein (Plate 2.10a), which may have been entrained in the residual liquid. The granite sample collected from Batu Pahat is a coarse-grained hornblende-bearing granite (MA64). It is associated with gabbro (MA65), but the field relationship between them is unclear. Similar to the Minyak Beku granitoids, the Batu Pahat granitoids can be finer-grained in some parts, containing K-feldspar megacrystic phenocrysts. Extensive tourmaline–quartz veins are found intruding the granite in the Hanson Quarry (MA68 and MA69) (Plate 2.10b). This may represent the roof-zone region of the granitic body, which was influenced by the later hydrothermal activity. Unlike the heterogeneous Minyak Beku granitoids and the Batu Pahat granitoids, the Gunung Ledang granite (MA57 and MA58) is homogeneously fine-grained and hornblende-bearing.

2.6 Main Range Province granitoids

The Main Range Province granitoids were emplaced into the Sibumasu crust composed of Upper Cambrian to Upper Permian metasediments and shallow-marine shelf

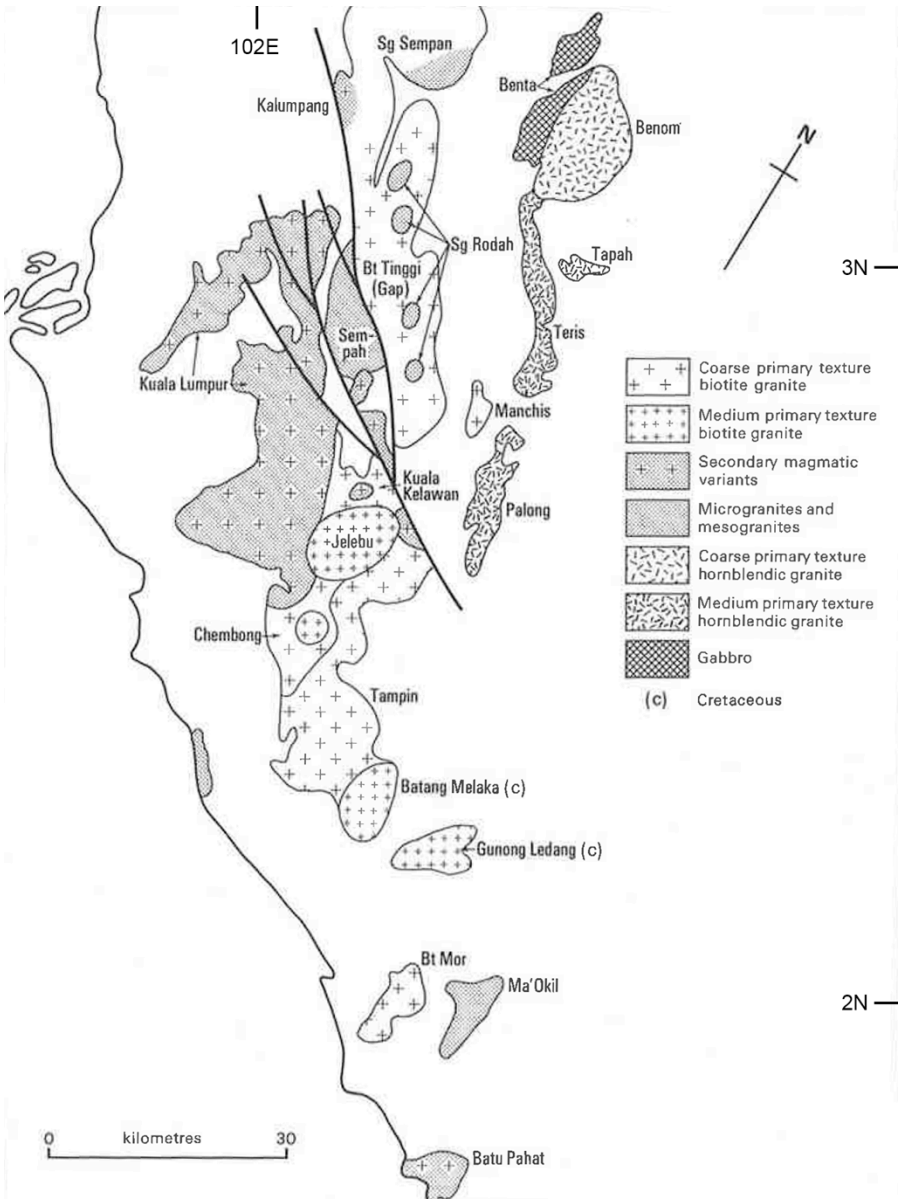

Figure 2.8 Distribution of the southern Main Range Province granitoids and the Eastern Province Central Belt granitoids (Cobbing *et al.*, 1992).

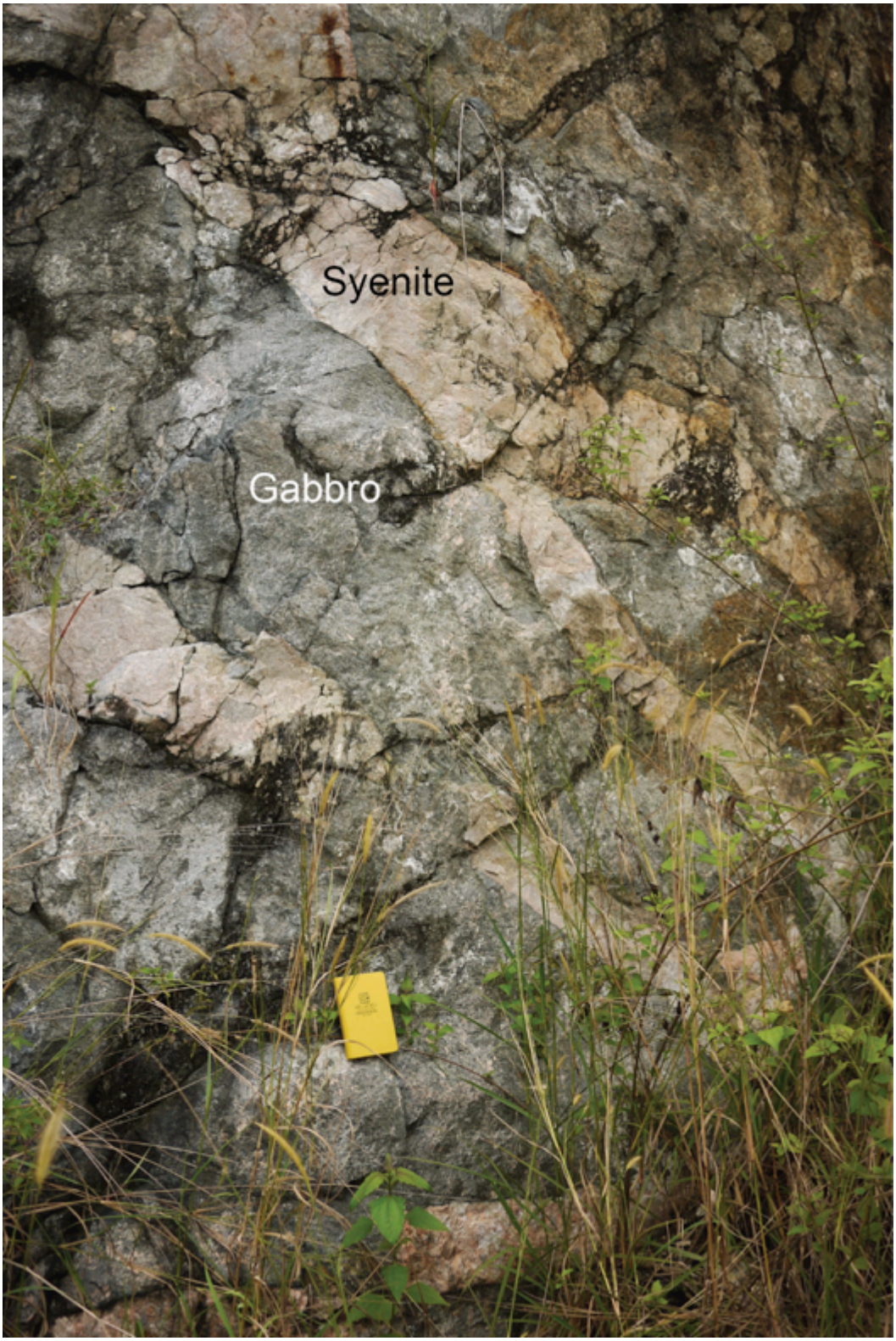

Plate 2.8 Syenite (MA03) cuts the gabbro (MA02) in the Benom Complex. However, gabbro also cuts syenite in some localities of Benom Complex. Hence, it is suggested that they were cogenetic immiscible liquids (Searle *et al.*, 2012).

Plate 2.9 a) Upper Triassic Berangkat migmatitic gneiss of tonalitic composition (MA35 and MA36) is cut by Upper Cretaceous Kenerong leucogranite (MA42) at Renyok River; b) Pink rounded K-feldspar grains are commonly observed in Noring granite (MA45).

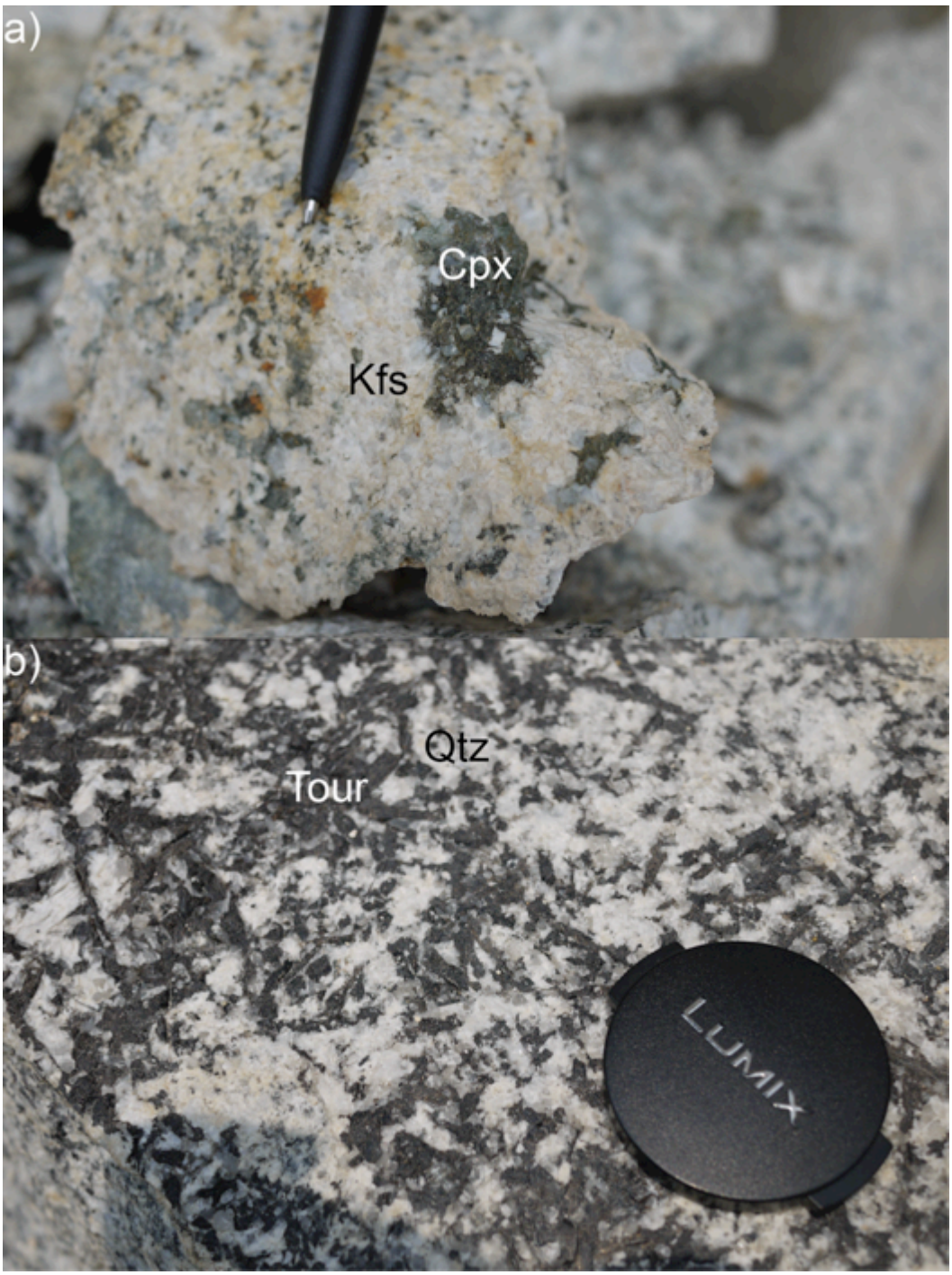

Plate 2.10 a) Clinopyroxene grains are developed within Quartz–K-feldspar vein in Minyak Beku granite (MA66 and MA67); b) Tourmaline-quartz veins (MA68) are well-developed in Batu Pahat granite (MA69) due to post-magmatic hydrothermal activities.

sediments that are overlain by Mesozoic carbonates and turbidites (Abdullah, 2009; Ghani *et al.*, 2013). While the Precambrian geology of the Sibumasu terrane is not well understood, Hutchison (2007) suggested that some of the metamorphic outcrops exposed in northern and central Thailand might represent the original Precambrian basement of the Sibumasu terrane. Palaeoproterozoic to Mesoproterozoic basement ages have been given by the inherited zircons extracted by Liew and Page (1985), supported by the detrital zircon core ages presented by Sevastjanova *et al.* (2011), the Nd depleted mantle ages provided in Chapter 3 and the new U-Pb inherited zircon ages presented in Chapter 4. The Main Range Province, sometimes termed as Western Belt granitoids in local literature (Cobbing *et al.*, 1992; Ghani, 2000), has a rather restricted range of lithologies: Most of the granitoids are coarse K-feldspar phyric and biotite bearing, with fewer K-feldspar phyric hornblende–biotite granitoids in the Bintang Batholith near Taiping (Table 2.1). Biotite clots were observed in some of the Main Range granitoids, which may be resulted from retrograde metamorphism of garnet grains (Chenhall *et al.*, 1980). The mineral assemblages of pristine Main Range Province granitoids are K-feldspar, quartz, plagioclase and biotite in decreasing abundance, with accessory minerals such as primary and secondary mucovite, apatite, zircon, secondary epidote, allanite and sphene (Table 2.1 and Plate 2.11) (Ghani, 2000). K-feldspar phenocrysts are observed in all kinds of granites, but can be megacrystic in laths up to a few centimetres in the most fractionated granite. All the Main Range Province granitoids are ilmenite-series granites (Ishihara *et al.*, 1979).

In contrast to the Eastern Province granitoids, the Main Range Province granitoids are more severely altered by hydrothermal activities. The widespread greisenisation of the granitoids and the extensive development of quartz–tourmaline veins and enclaves. The

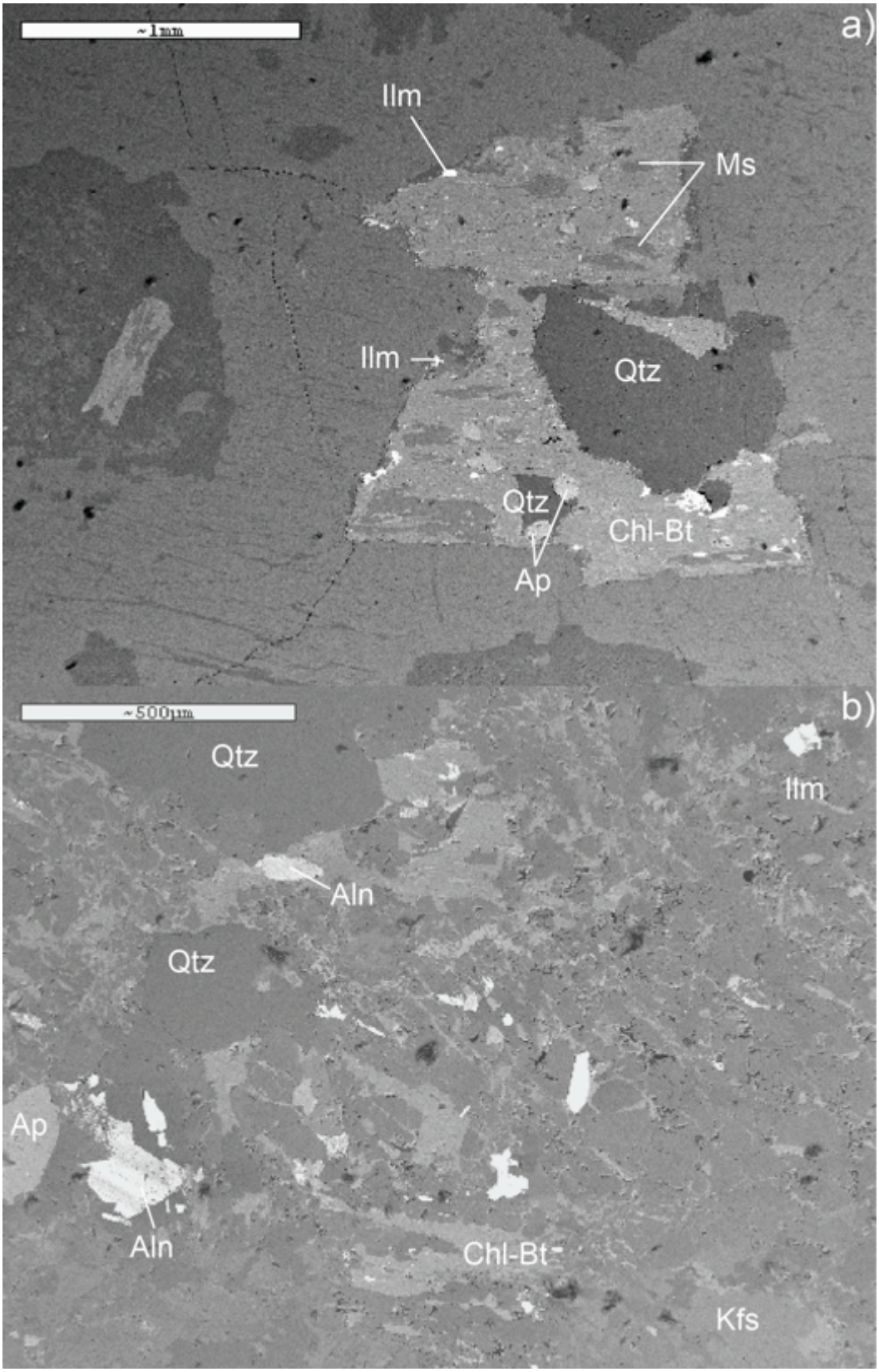

Plate 2.11 Scanning electron microscope images show the common accessory minerals found in the Main Range Province granitoids (MA11: Cameron Highlands).

roof-zones of the plutons were greisenized, and replaced with muscovite + quartz + cordierite assemblage. Quartz–tourmaline veins or miarolitic cavities were often developed. This is particularly important because the tin deposits of the Main Range Province are restricted to these greisen-bordered veins localized in the roof-zones. Famous Main Range primary tin fields are located in the Kinta Valley and near Kuala Lumpur. Secondary muscovite and chlorite are commonly observed, with lesser extent pyrite and fluorite.

Homogeneous fine-grained biotite granitic plutons are found surrounded by homogeneous coarse-grained granite. The boundary between them is often marked by hydrothermally altered granite, which suggests that the finer phase probably represents a second intrusion into the coarser phase.

Hornblende-bearing granitoids with mafic enclaves are found in the Bintang Batholith near Taiping (MA16). Biotite grains in these granites are usually low in Al, and are associated with sphene and sometimes with actinolite (Ghani, 2000). This resembles the lithological characteristics of I-type granitoids. The field relationship between the hornblende-bearing granites and the hornblende-absent granites resembles the relationship observed in the Eastern Province.

Unlike the small batholithic bodies in the Eastern Province, the Main Range Province granitoids were emplaced as large batholithic bodies up to several thousands of square kilometres in area. They are not apparently associated with a regional migmatite terrane, do not appear to have a Barrovian metamorphic sequence (unless it remains unexposed in the lower crust) and are not associated with contemporaneous thrust or normal faults.

These observations contradict the field characteristics of purely-crustal derived S-type Himalayan leucogranites (Searle *et al.*, 2010). Hence, the S-type designation of the Main Range granitoids is controversial. The emplacement of these batholiths into the thick carbonate country rocks caused extensive skarn formation, where tin mineralization could also be associated (Hutchison, 2007). Good exposure of such relationship can be seen on Tuba Island near the Langkawi region (MA27-29, Figure 2.2), in which the skarn body is characterized by the presence of biotite, cordierite, garnet and sphene.

Granitic batholiths in the Western Belt form a large mountain range in western Malay Peninsula, called the Main Range batholith. The Main Range granitoids will be discussed according to their geographical locations.

2.6.1 Northern Main Range (MA06-MA30 in Figure 2.2 and 2.9)

In the northern part of Main Range, natural outcrops are found along the road connecting Ipoh and Cameron Highlands (MA06-MA14); granitoids are also exposed in quarries in Kinta Valley (MA15). The collected roadcut samples (MA06-MA14) are generally homogeneous in grain size. They are dominantly coarse-grained (cordierite)-biotite granite without the presence of hornblende (Plate 2.12a). Similar granitoids could be found in Kulim area on the western coast and the eastern coast of the Penang Island offshore. However, in some localities, meso- to microgranites of similar mineral assemblage are found, such as those in Kinta Valley near the city of Ipoh (Plate 2.12b), central and western Penang Island (Plate 2.12c) and Langkawi Island. These fine-grained phases are usually characterized by the development of greisen and quartz–tourmaline veins (Plate 2.12d), such as the samples collected from the northern coast of

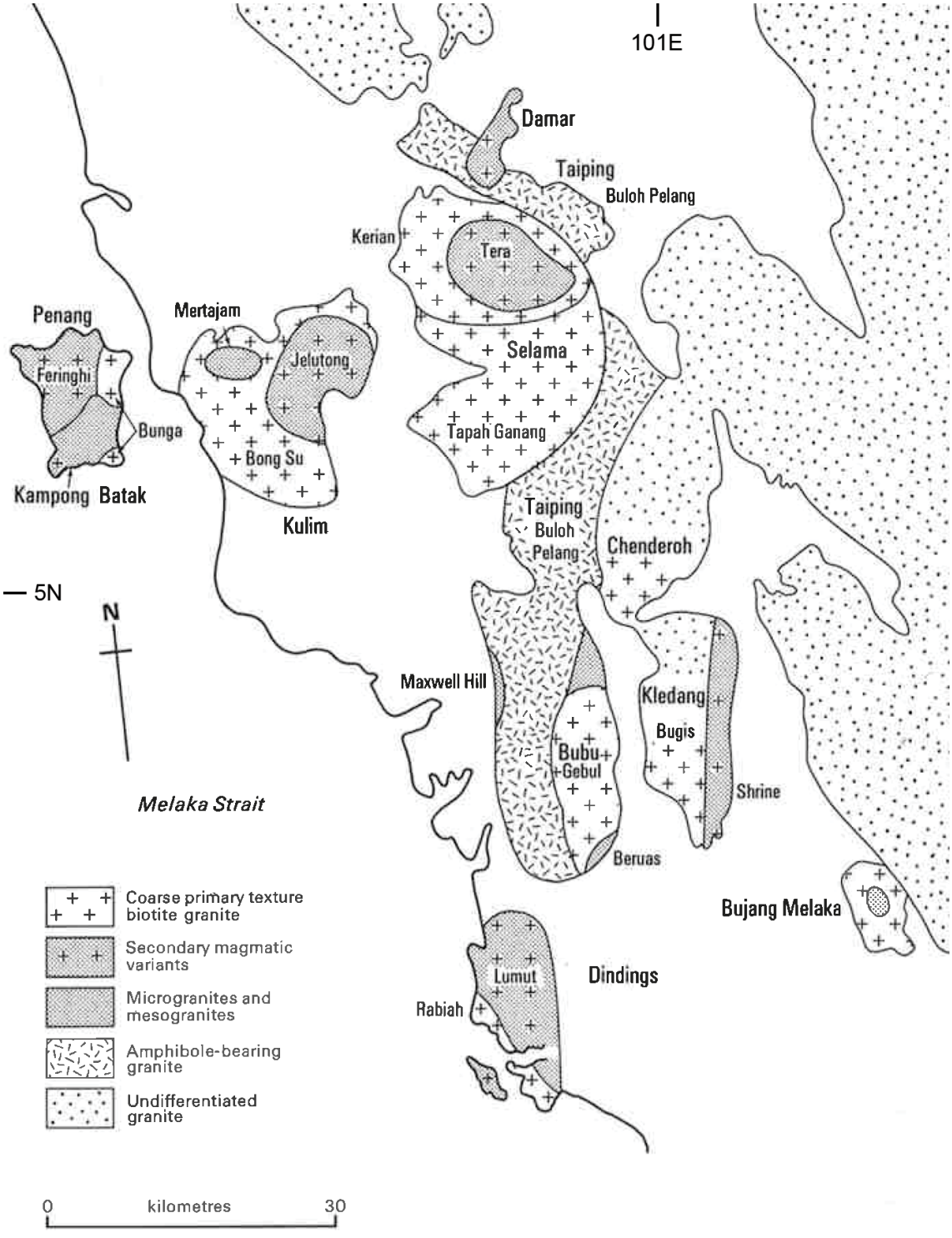

Figure 2.9 Distribution of the northern Main Range Province granitoids (Cobbing *et al.*, 1992).

Plate 2.12 a) Coarse-grained biotite granite is a typical unfractionated Main Range Province granite, fractionated granite usually has much finer grains, may or may not associated with K-feldspar phenocrysts. They can be found b) in the Kinta Valley near Ipoh, in which pyrite is formed as a secondary mineral due to hydrothermal alteration, and c) on Penang Island; Evidences of hydrothermal alteration include d) greisen-bordered quartz-tourmaline vein (Cameron Highlands); e) development of secondary muscovite (MA19: Penang, 40x, cpl); f) Sericitization of K-feldspar and chloritization of biotite (MA13: Cameron Highlands, 40x, cpl).

Penang Island (Feringhi granite) (MA18-MA20). They are also highly fractionated in geochemistry (Cobbing *et al.*, 1992). These granitoids may represent the roof-zones of the plutons and they are usually associated with pegmatite and mineral layering development (Ghani, 2000). Sn content is particularly high, up to 30 ppm, in these fractionated granites (Cobbing *et al.*, 1992), which makes Kinta Valley one of the most tin producing regions in the Malay Peninsula. Other evidences of hydrothermal alteration observed in these fractionated granitoids in the pluton roof-zones include the presence of secondary muscovite (Plate 2.12e) and pyrite (Plate 2.12b), sericitization of K-feldspar and chloritization of biotite (Plate 2.12f). Since the Western Belt has significant amount of carbonate strata in the upper crust, formation of skarn is usually associated with the emplacement of Main Range Province granitoids. On Tuba Island, an endoskarn with garnet, cordierite, biotite and sphene is developed when the granite was emplaced into the Chuping limestone (Plate 2.13). Hornfels is also formed beyond the endoskarn due to hydrothermal alteration.

In contrast to the most of the Main Range granitoids, The Taiping Pluton in the Bintang Batholith has completely different lithology. It is characterized by the presence of hornblende, similar to the Eastern Province granitoids (Plate 2.14a). The biotite also has much lower Al content than those being found in the Main Range granitoids (Ghani, 2000). In the most geochemical fractionated part of the granite, K-feldspar grains exhibit as megacrystic phenocrysts in a hornblende-free microgranitic matrix (Plate 2.14b). Fluorite is found as secondary mineral in the roof-zone of the Taiping granite (Plate 2.14c). Its formation may be related to the hydrothermal breakdown of Li-mica (Manning and Exley, 1984). However, no Li-mica has been reported in the Main Range Province.

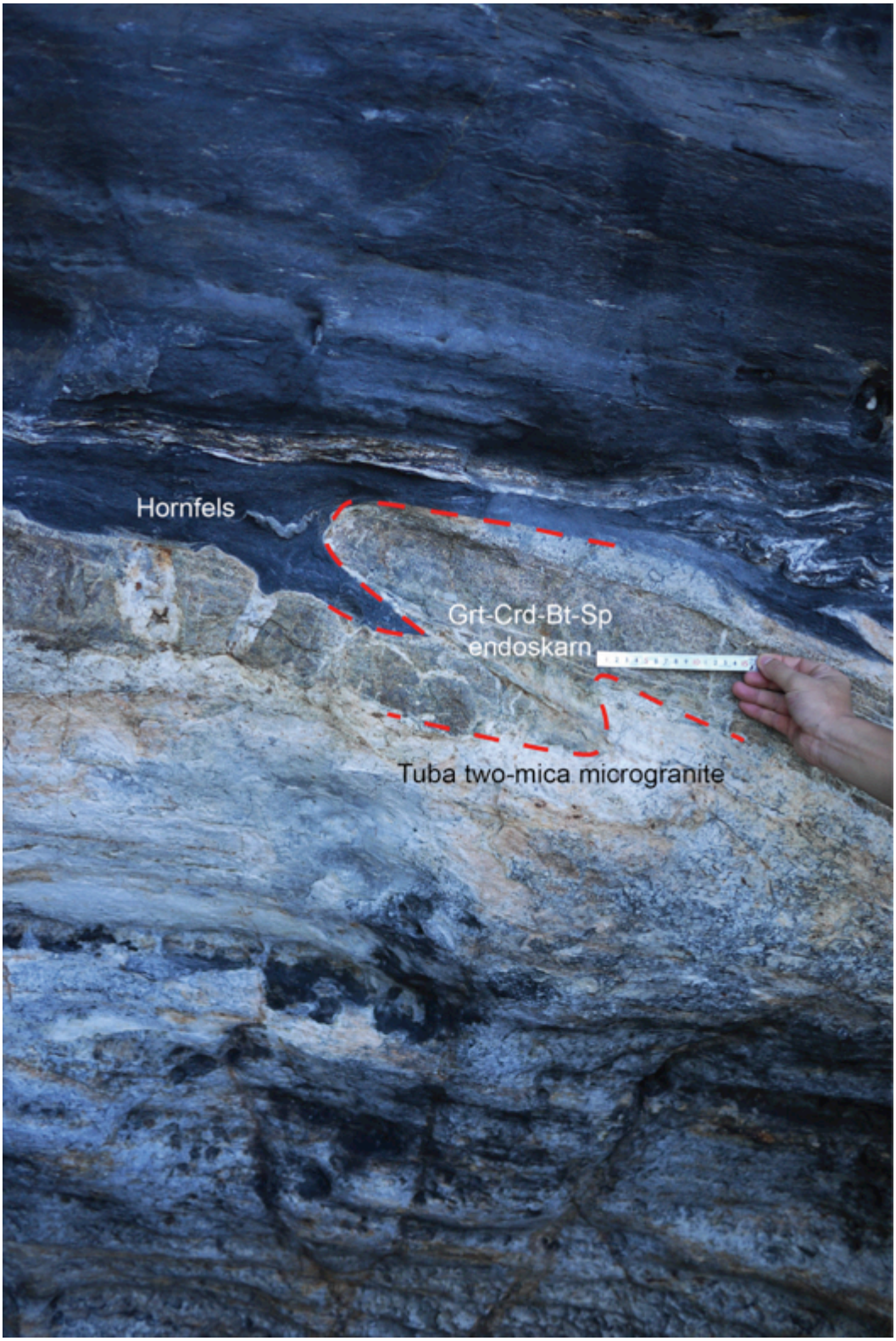

Plate 2.13 Skarn development during the emplacement of the Tuba two-mica microgranite into carbonates. Endoskarn is characterized by the presence of garnet, cordierite, biotite and sphene. Hornfels is developed beyond the skarn.

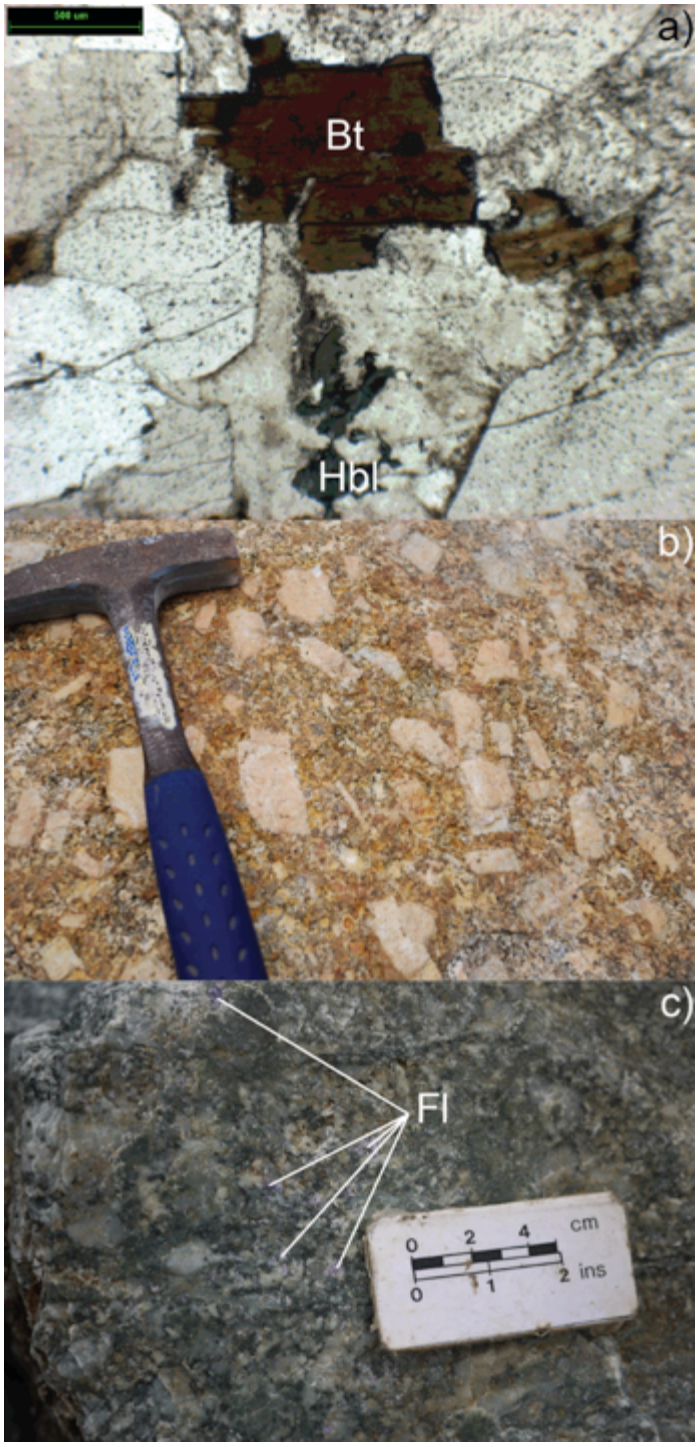

Plate 2.14 a) Hornblende is present in Taiping granite, which makes it more akin to the Eastern Province granitoids (MA16: Taiping, 40x, ppl); b) Megacrystic K-feldspar phenocrysts are developed in fractionated Taiping granite, and can have length up to a few centimetres (MA16); c) Secondary fluorite is associated in Taiping granite as a sign of hydrothermal alteration (MA17).

2.6.2 Southern Western Belt (MA31, MA59-MA63 in Figure 2.2 and 2.8)

Main Range batholiths exposed in the southern part are essentially hornblende-free. Second intrusions with smaller grain size, such as the Jelebu granite, are hosted by the Main Range batholith. These second intrusions crosscut the coarser-grained main granitic body and its roof-zone.

The sample collected from Kuala Lumpur granite (MA31) is more akin to the fractionated granites exposed near Ipoh. It is a medium-grained hornblende-free biotite granite with K-feldspar megacrystic phenocrysts (Plate 2.15). The grain size of the granite can vary along the roof-zone boundary, which separates the hydrothermally altered granite from the pristine granite. Primary and alluvial tin deposits are also abundant in the Kuala Lumpur region, originating from this granite with Sn content up to 60 ppm.

The Bukit Mor granite (MA59-MA63) further south is made up of hornblende-free pure biotite granite, it is cut by later microgranitic sills (Plate 2.16), and the whole section is again cut by the youngest cordierite–muscovite K-feldspar megacrystic pegmatite. The relationship is best seen in the Muar quarry (N01°58'32.8", E102°40'24.5"). It has been suggested that the formation of pegmatite is related to immiscible fluids of different water content and viscosity between pegmatite-forming melt and granitic melt (Thomas and Davidson, 2012). It shows that water played an important role in the latest stage of magmatic evolution of the Main Range Province granitoids, apart from hydrothermal alteration.

Plate 2.15 Textural variation of Kuala Lumpur granite along the pluton roof-zone boundary can be large, ranging from microgranite to coarse-grained biotite granite. This K-feldspar megacrystic mesogranite (MA31) was collected along the Karak Highway (E8) near Kuala Lumpur.

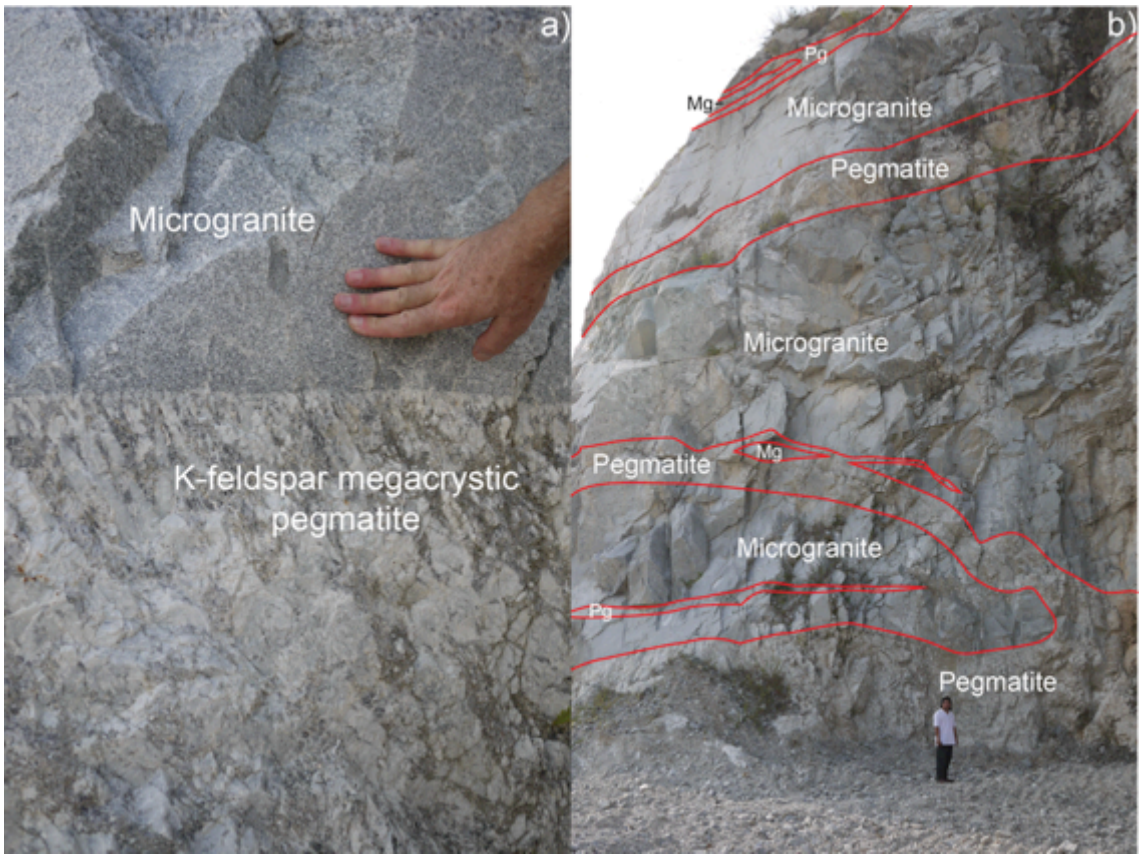

Plate 2.16 a) The Bukit Mor granite exposed at the Muar quarry (N01°58'32.8", E102°40'24.5") exhibits as a series of microgranitic sills intruded into K-feldspar megacrystic pegmatite. This shows a contrast of water content in the fluids (water-rich pegmatitic melt and water-poor granitic melt), which forms the Bukit Mor granite.

2.7 Volcanic rocks in the Malay Peninsula

Highly deformed Ordovician volcanic sequences are found in the Western Belt (Sibumasu). They are mainly foliated rhyolitic flows and tuff, sitting conformably on the Lower Palaeozoic meta-sediments (Ghani, 2009b). However, little has been know about the geochemistry of these volcanic rocks. Petrographically, the tuff exposed in Perak and Gunong Jerai, Kedah in the Western Belt contain fragments of quartz, K-feldspar and plagioclase in a matrix of quartz, mica, tourmaline, chlorite and iron oxide (Jones, 1970; Bradford, 1972; Ghani, 2009b).

The only volcanic succession that has been correlated with the Malaysian Permo-Triassic magmatism in the Western Belt is the Genting Sempah Complex near Kuala Lumpur. This Complex comprises tuff, ignimbritic rhyolite and porphyroclastic rhyodacite (Liew, 1983; Chakraborty, 1995; Singh and Ghani, 2000; Ghani and Singh, 2002; Ghani, 2009b). According to Ghani and Singh (2002), the rhyolite and rhyodacite have similar phenocryst assemblages as the Main Range granitoids, with quartz, biotite, K-feldspar and plagioclase, but the rhyodacite is in addition characterized by the presence of hypersthene (orthopyroxene). These volcanic rocks are peraluminous with high-K calc-alkaline content, showing similar geochemistry as the Main Range Province granitoids. The U-Pb zircon age (226.2 ±1.2 Ma) of the rhyodacite presented in Chapter 4 can also be correlated with the time span of Main Range granite magmatism.

The Eastern Province has been described as a granitic province generated in an Andean-type setting. Related calc-alkaline arc volcanic rocks are exposed in the Kelantan-Pahang region, forming the Pahang volcanic series in south and southeast Johor (Ghani,

2009b). The Pahang volcanic series is dominantly composed of tuff, with subordinate amount of lava and agglomerate. The geochemistry of these volcanic successions is andesitic to rhyolitic, while trachyte is also observed (Ghani, 2009b). The pyroclastics and lava flows in south and southeast Johor are not well understood. Recently, the geochemistry of the Teluk Ramunia Suite in southeast Johor has been studied by Roselee *et al.* (2013) who suggested these volcanics correspond to A-type behaviour, which these authors related to rollback of the Palaeo-Tethyan subduction zone.

Volcanic islands, like Tioman and Sibu, offshore eastern Malaysia in the South China Sea have different geological origins. Sibu is dominantly composed of rhyolite lavas inter-layered with lapilli tuff that gave an Early Permian U-Pb zircon age (287 ±4.5 Ma) (Oliver *et al.*, 2014). In contrast, Tioman Island further north has much younger volcanic and plutonic sequences (Searle *et al.*, 2012). Weakly metamorphosed Carboniferous to Triassic sediments on Tioman Island were intruded by Upper Cretaceous granitoids, overlain by a volcanic suprastructure (Ghani *et al.*, 1999; Ghani and Rashid, 2008; Searle *et al.*, 2012). The lithology of the Tioman granite has been discussed in a previous section. Volcanic rocks include pyroclastic flows (ignimbrite, Plate 2.17) and lava flows, which appear to mingle with granitic lobes (Ghani *et al.*, 1999). Volcanic features like gas pipes are observed on the coast, which brought up gabbroic, dioritic and granitic xenoliths (Plate 2.7b). The geochemistry of the lava flows on Tioman Island ranges from andesitic to rhyolitic compositions. Hornblende is dominant in andesite but insignificant in dacite and rhyolite (Ghani, 2009b).

The Eastern Province granitoids are cut by younger doleritic or basaltic dykes. Radiometric dating (Ar-Ar method) of these dykes suggested that they formed between

Plate 2.17 Ignimbrite (MA92) collected on the eastern coast of Tioman Island.

79 ± 2 Ma and 179 ± 2 Ma (Ghani *et al.*, 2013). They are hence, not related to the Permo-Triassic magmatism, which formed the Malaysian granitoids. Instead, it is suggested that they were related to the mantle upwelling beneath the East Malaya terrane after the slab break-off along the Bentong-Raub subduction zone (Ghani *et al.*, 2013). However, this hypothesis is still highly controversial, as such slab break-off is not supported by any field evidence. Cenozoic post-orogenic alkali basalt is found in Kuantan in eastern Pahang and Segamat in northern Johor (Ghani, 2009b). A K-Ar age of 62 ± 3 Ma has been reported for the Segamat basalt (Bignell and Snelling, 1977). The Kuantan basalt is extremely young, in contrast to the mafic dykes and the Segamat basalt. Early Pleistocene ages of 1.5 to 2.5 Ma have been reported by Haile *et al.* (1983) and Ghani and Taib (2007). The tectonics responsible for the formation of these basalts remained unclear, both Segamat basalt and Kuantan basalt are too young to be correlated with any known tectonic event.

2.8 Structural geology of the Malay Peninsula

The NNW-SSE striking Malay Peninsula is mainly controlled by the emplacement of the Main Range Province granitoids. The terrane has been cut by major faults striking in N-S, NW-SE, NNE-SSW and E-W directions (Shuib, 2009a). The N-S to NNW-SSE structural configuration also defined the three stratigraphic belts in the Malay Peninsula. This follows the strike of the Bentong-Raub suture, where the Sibumasu terrane collided with the East Malaya terrane. It is believed that these NNW-SSE structures were formed almost immediately after the collisional orogeny to accommodate the oblique Palaeo-Tethyan subduction (Hutchison, 2007). The development of the Semanggol marine foredeep basin on the Sibumasu terrane was probably related to the stretching of the continental margin during the Palaeotethyan subduction along the

Bentong-Raub suture (Metcalfe, 2000). The Eastern Belt and Central Belt were separated by the sinistral Lebir Fault, which was active after the intrusion of the granitoids (Tija, 1969; Singh, 1985; Aw, 1990). It is thought that this fault was initially dextral to accommodate the oblique subduction along the Bentong-Raub suture (Shuib, 2009a). Although no field evidence supports the initial dextral motion of the Lebir Fault, the granitic intrusion in the Eastern Belt were terminated by the fault and oriented 20°–30° to the major fault plane, which suggests the granitoids were intruded within the sigmoidal stress field. Its operation also formed the transtensional basins in the Central Belt, so that thick sequences of pebbly alluvium could be deposited in the basins during the Jurassic-Cretaceous time (Tija, 1996; Shuib, 2000, 2009b). The Malay Peninsula is then cut by several terrane-crossing faults, which are oblique to the terranes including the Kuala Lumpur Fault Zone, Bukit Tinggi Fault Zone and Bok Bak Fault Zone. These NW-SE oriented strike-slip faults show mainly sinistral shear. Some major fault systems, such as the Bukit Tinggi Fault Zone apparently show early dextral movement (Shuib, 2009a). The change in fault movement direction may have resulted from the Cenozoic collision of the Indian Plate with the Eurasian Plate (Shuib, 2009a).

2.9 Summary

Southeast Asia is composed of Precambrian micro-continental terranes, which were successively rifted off from Gondwana since Devonian. They reassembled along the Eurasian margin through the closure of the Palaeo-Tethys Ocean, which is characterized by the series of N-S oriented suspected suture lines. In the Malay Peninsula, the closure of the Palaeo-Tethys Ocean is marked by the NNW-SSE oriented Bentong-Raub suture. This suture is a linear belt of serpentinite and deep-sea sediments, separating the two micro-continental terranes, namely the Indochina – East Malaya terrane and the

Sibumasu terrane. To the east of the Bentong-Raub suture (the Eastern Province), the granitoids emplaced into the East Malaya terrane are dominated by hornblende-bearing granites, which eventually fractionated into hornblende-free phases in the roof-zones. These granitoids are relatively older, ranging from early Permian to Middle Triassic, and associated with calc-alkaline arc volcanics. They were interpreted as pre-collision Andean I-type granites (Beckinsale, 1979; Cobbing *et al.*, 1986, 1992). To the west of the Bentong-Raub Line, the granitoids are generally hornblende-free, although hornblende-bearing granitoids outcrop in the Bintang Batholith near Taiping. These granitoids are younger, with ages restricted in Late Triassic. They are batholithic, more fractionated and highly mineralized. Hydrothermal alteration products, such as secondary muscovite, tourmaline and fluorite are commonly observed. These granitoids were interpreted as collision-related S-type granite by Beckinsale (1979) and Cobbing *et al.* (1986, 1992), which were formed during the subsequent East Malaya – Sibumasu collision. However, these field characteristics do not match with those of the purely crustal-derived S-type Himalayan leucogranites. Hence, the nature of the Main Range granitoids requires further geochemical studies, which are presented in Chapter 3. The Palaeo-Tethyan subduction that occurred along the Bentong-Raub suture zone is therefore, interpreted as east-dipping to account for the formation of older I-type Eastern Province granitoids. Deformation occurred during subduction, and the collided terrane is cut by series of NNW-SSE oriented faults, which operated to accommodate the Palaeo-Tethyan oblique subduction. Some of these faults were re-activated during the Caenozoic subduction of the Neo-Tethys Ocean, which was followed by the Indo-Asian collision.

Chapter 3 – Geochemistry of the Malaysian granitoids

3.1 Introduction

Detailed work over several decades resulted in a sub-division of the granitoids of the Malay Peninsula into an I-type Eastern Province to the east of the Bentong-Raub suture zone, and a S-type Main Range Province to the west of the suture (Beckinsale, 1979; Cobbing *et al.*, 1986, 1992). These authors pointed out that the Eastern Province is dominated by hornblende-bearing biotite granitoids, and associated calc-alkaline volcanics, common characteristics of classic I-type granitic terranes (Chappell and White, 1974). They also suggested that, in contrast to the Eastern Province, muscovite is occasionally found in the Main Range granitoids instead of hornblende (Beckinsale, 1979; Cobbing *et al.*, 1986, 1992), and that this feature was a signature of S-type granitoids (Chappell and White, 1974). These authors also used Chappell and White's (1974) I-S classification system to explain the metallogenesis of Cu-Au deposits in the I-type Eastern Province and the Sn-W deposits in the S-type Main Range Province.

However, more recent works (Ghani, 2000; Searle *et al.*, 2012; Ghani *et al.*, 2013) has questioned the traditional I- and S-type classification of the Malaysian granitic belts. The latter authors suggested that the hornblende-free biotite granitoids, which are dominant in the Main Range Province, but exist only in the pluton roof-zones in the Eastern Province, are largely indistinguishable on a broad scale. The muscovite present in the Main Range Province is usually secondary, and resulted from post-magmatic hydrothermal alteration. It is also evident that tin mineralization is present in both provinces, a feature that does not accord with an I-type origin for the Eastern Province. In addition, unlike the collisional S-type leucogranites of the Himalaya, the Main Range

granitoids are batholithic in dimension, and more akin to typical volcanic arc I-type granitoids (such as the Gangdese-Ladakh granitoids of the Himalaya). Hence, the nature of the Main Range granitoids and the tin metallogenesis in the I-type Eastern Province is still controversial and requires further geochemical investigation. The application of the I- and S-type granitic provinces also cannot explain the Sn-W metallogenesis in the Eastern Province. Consequently, the subdivision of Malaysian granitoids into S- and I-type belts is considered problematic and the following section is designed to re-examine the issue from the viewpoint of the samples collected across the peninsula as part of the present study.

3.2 Major and trace element geochemistry

Major and trace element geochemistry are used to examine the differences between the Main Range and Eastern Province granitoids. The sample locations were presented in Figure 2.2. They are also used to compare and contrast the characteristics of Malaysian granitoids with classic Cordilleran I- and S-type examples.

Samples were crushed and powdered by jaw crusher and corundum mill. The samples were then fused into glass beads. Major element composition were determined by **X**-**R**ay **F**luorescence (XRF) using the Rigaku® RIX-2000 spectrometer in the Department of Geosciences, National University of Taiwan (NTU). The analytical procedures are described by Wang *et al.* (2007), with the **L**oss **O**f **I**gnition (LOI) determined separately by routine procedures. For trace element analysis, the glass beads produced for major element analysis were crushed, weighed and digested into sample solutions, which were then analyzed by **I**nductively **C**oupled **P**lasma – **M**ass **S**pectrometry (ICP-MS) using an Agilent 7500cx quadrupole spectrometer also at NTU. Detailed sample handling and

preparation procedures followed those of Lee *et al.* (2012). Reported precision is ±5% (2σ), and the results are presented in Table 3.1. The new geochemical data are interpreted together with the data provided by Cobbing *et al.* (1992), forming a combined data set. The high sample population (n = 197) would allow better geochemical interpretation. The combined data set has been primarily classified into two major groups: the Main Range granitoids (samples collected west of the Bentong-Raub suture zone) and the Eastern Province granitoids (samples collected east of the Bentong-Raub suture zone). Among the Eastern Province samples, it is evident, from the U-Pb zircon dating study (Chapter 4) that certain granitoid samples are Cretaceous in age and they are discussed separately. Alkali granitoids (syenites) are only found in Benom and on the Perhentian Island in the Eastern Province. They will be discussed in separate section.

3.2.1 Geochemical variation of Eastern Province granitoids

The Eastern Province granitoids were emplaced in two distinct sub-units, here termed the Coastal Belt and the Central Belt, as discussed in Chapter 2. Although these two belts were designated according to the country rock stratigraphy, no distinct mineralogical and geochemical differences have been noticed between the granitoids emplaced in these two belts (Figure 3.1) and hence the samples from the two belts are not differentiated in the following discussion. In addition, there are only two samples collected for the alkali granitoids in the Eastern Province. The small sample size does not allow any meaningful petrogenetic and geochemical interpretation for these alkali granitoids. It was suggested that they are related to fractionation of more mafic intrusions (Ghani, 2003, 2006).

TABLE 3.1A. MAJOR AND TRACE ELEMENT DATA OF THE MALAYSIAN EASTERN PROVINCE GRANITOIDS.

Sample	MA03	MA36	MA39	MA47	MA48	MA50	MA52	MA55
Latitude	N04°00'42.1"	N05°08'22.2"	N05°17'49.7"	N05°55'16.5"	N05°55'16.5"	N05°20'47.6"	N04°59'21.6"	N03°50'19.7"
Longitude	E101°57'32.0"	E101°58'49.5"	E101°57'50.2"	E102°43'23.9"	E102°43'23.9"	E103°02'12.5"	E102°28'53.3"	E103°21'07.1"
Rock type	Syenite	Kfs phyric Hbl-Bt tonalite	Migmatitic granite	Bt granite	Syenite	Kfs phyric (Hbl)-Bt granite	Hbl-Bt granite	Hbl-Bt granite
Age (Ma)		231.9 ±0.9	83.9 ±0.8	257.6 ±1.6	284.2 ±1.6	289.4 ±3.4*	248.4 ±1.8	270.0 ±1.4
Major element (wt%)								
SiO_2	53.96	65.09	60.97	74.91	57.24	65.38	64.36	74.17
TiO_2	0.66	0.70	1.17	0.12	0.73	0.13	0.66	0.12
Al_2O_3	17.72	15.17	16.07	12.81	16.57	17.92	16.62	13.69
Fe_2O_3(t)	5.17	4.69	4.63	0.80	6.47	1.19	5.24	1.46
MnO	0.05	0.07	0.08	0.01	0.08	0.02	0.09	0.02
MgO	1.90	2.38	3.05	0.21	3.02	0.27	1.84	0.01
CaO	8.48	3.16	4.89	0.73	5.74	0.62	2.89	0.92
Na_2O	3.47	2.63	3.56	2.53	4.05	3.37	3.95	3.30
K_2O	5.18	4.95	3.60	6.19	4.40	8.11	2.76	5.74
P_2O_5	0.45	0.34	0.54	0.05	0.57	0.22	0.16	0.03
LOI	2.97	1.79	2.00	1.37	1.66	1.62	2.34	1.46
Sum	100.01	100.96	100.55	99.73	100.53	98.84	100.90	100.91
Trace element (ppm)								
P	1950	1600	2540	202	2750	1030	712	102
Sc	10.7	21.8	21.1	5.40	25.2	8.00	10.0	23.2
Ti	3970	4140	6900	583	4380	691	3850	608
V	121	81.3	79.8	9.64	137	10.1	54.3	1.14
Cr	126	133	102	129	97.0	55.0	81.0	57.0
Mn	453	565	626	79.0	640	165	671	196

Sample	MA03	MA36	MA39	MA47	MA48	MA50	MA52	MA55
Latitude	N04°00'42.1"	N05°08'22.2"	N05°17'49.7"	N05°55'16.5"	N05°55'16.5"	N05°20'47.6"	N04°59'21.6"	N03°50'19.7"
Longitude	E101°57'32.0"	E101°58'49.5"	E101°57'50.2"	E102°43'23.9"	E102°43'23.9"	E103°02'12.5"	E102°28'53.3"	E103°21'07.1"
Rock type	Syenite	Kfs phyric Hbl-Bt tonalite	Migmatitic granite	Bt granite	Syenite	Kfs phyric (Hbl)-Bt granite	Hbl-Bt granite	Hbl-Bt granite
Age (Ma)		231.9 ±0.9	83.9 ±0.8	257.6 ±1.6	284.2 ±1.6	289.4 ±3.4*	248.4 ±1.8	270.0 ±1.4
Co	8.30	13.3	11.4	3.80	15.8	2.20	9.60	1.00
Ni	43.7	65.1	53.2	57.6	51.9	25.7	34.4	26.7
Cu	74.2	22.1	10.1	20.4	37.3	6.31	5.58	2.18
Zn	22.0	53.6	70.2	14.5	48.5	24.7	66.7	50.8
Ga	19.6	18.9	20.3	16.8	21.1	22.2	19.1	19.4
Rb	269	317	192	270	187	531	166	190
Sr	1290	416	1790	375	1350	136	394	82.0
Y	25.0	30.4	17.5	32.5	38.6	15.5	22.4	34.7
Zr	442	339	321	122	317	71.0	201	172
Nb	11.6	17.0	30.6	13.6	28.3	6.70	7.60	12.9
Cs	1.43	19.9	5.74	4.92	2.93	28.4	5.18	4.47
Ba	2170	2140	2900	422	1050	395	823	830
La	81.7	83.3	98.6	65.0	120	6.20	24.1	71.1
Ce	153	157	176	114	221	11.8	47.3	149
Pr	18.2	18.6	19.4	12.4	25.5	1.33	5.55	18.3
Nd	67.7	65.2	64.0	38.7	88.3	4.56	20.4	65.5
Sm	12.0	11.3	9.18	6.62	14.6	1.14	4.31	12.5
Eu	3.84	2.49	2.56	0.47	3.17	0.34	1.04	1.18
Gd	8.07	7.83	5.56	5.43	10.4	1.20	3.98	9.24
Tb	1.05	1.07	0.74	0.89	1.41	0.22	0.64	1.28
Dy	5.05	5.51	3.42	5.31	6.99	1.29	3.74	6.75
Ho	0.91	1.05	0.60	1.11	1.31	0.24	0.78	1.29

Sample	MA03	MA36	MA39	MA47	MA48	MA50	MA52	MA55
Latitude	N04°00'42.1"	N05°08'22.2"	N05°17'49.7"	N05°55'16.5"	N05°55'16.5"	N05°20'47.6"	N04°59'21.6"	N03°50'19.7"
Longitude	E101°57'32.0"	E101°58'49.5"	E101°57'50.2"	E102°43'23.9"	E102°43'23.9"	E103°02'12.5"	E102°28'53.3"	E103°21'07.1"
Rock type	Syenite	Kfs phyric Hbl-Bt tonalite	Migmatitic granite	Bt granite	Syenite	Kfs phyric (Hbl)-Bt granite	Hbl-Bt granite	Hbl-Bt granite
Age (Ma)		231.9 ±0.9	83.9 ±0.8	257.6 ±1.6	284.2 ±1.6	289.4 ±3.4*	248.4 ±1.8	270.0 ±1.4
Er	2.21	2.79	1.54	3.22	3.41	0.61	2.16	3.27
Tm	0.29	0.40	0.21	0.52	0.50	0.09	0.33	0.48
Yb	1.71	2.59	1.32	3.51	3.23	0.60	2.12	2.90
Lu	0.26	0.39	0.19	0.51	0.49	0.08	0.32	0.42
Hf	10.1	8.26	6.94	3.43	6.87	0.82	4.86	5.41
Ta	0.78	1.57	1.93	1.28	2.02	1.07	0.65	0.84
W	1.07	0.83	0.26	0.87	0.87	7.06	0.83	0.23
Tl	5.63	9.61	5.75	5.14	3.88	5.39	4.60	4.67
Pb	7.67	102	26.8	14.6	8.91	26.1	32.7	27.7
Th	55.8	49.9	45.7	34.7	32.4	3.35	12.0	25.7
U	5.59	10.3	3.70	8.48	7.53	4.42	3.51	3.31
A/CNK	0.68	1.01	0.89	1.06	0.78	1.18	1.14	1.03
Eu/Eu*	1.19	0.81	1.10	0.24	0.79	0.89	0.77	0.33
M	(2.94)	1.65	(2.02)	1.33	(2.47)	1.40	1.46	1.39
T_{Zr} (°C)	(761)	835	(801)	768	767	720	802	793

Note:

M is defined as the cation ratio (Na + K + 2Ca)/(Al × Si) (Watson and Harrison, 1983).

Data put in brackets were calculated beyond the assumption made by Watson and Harrison (1983) for *M* is less than 2.00.

All the ages are U-Pb zircon ages presented in Chapter 4. Ages in (*) are reference magmatic ages (Chapter 4).

Sample	MA57	MA58	MA64	MA66	MA69	MA73	MA77
Latitude	N02°20'26.1"	N02°20'26.1"	N01°51'29.2"	N01°49'08.8"	N01°49'01.0"	N01°24'29.0"	N01°23'09.6"
Longitude	E102°37'03.9"	E102°37'03.9"	E102°57'19.2"	E102°54'37.3"	E102°54'50.9"	E103°59'21.8"	E104°12'20.5"
Rock type	Kfs phyric (Hbl)-Bt granite	Leuco- Kfs-phyric (Hbl)-Bt granite	(Hbl)-Bt granite	Hbl-Bt granite	Bt granite	Migmatitic granite	Hbl-Btl granite
Age (Ma)				222.2 ±1.8	225.5 ±2.5*	231.0 ±2.6*	
Major element (wt%)							
SiO_2	74.93	75.32	68.43	71.40	77.61	75.69	78.10
TiO_2	0.19	0.17	0.49	0.32	0.16	0.16	0.11
Al_2O_3	13.92	13.71	16.06	15.69	12.76	14.07	12.69
Fe_2O_3(t)	0.63	0.66	2.92	1.90	1.11	1.19	0.98
MnO	0.03	0.05	0.05	0.04	0.03	0.04	0.02
MgO	0.18	0.09	1.08	0.56	0.18	0.19	0.14
CaO	0.92	0.79	2.48	1.98	0.52	0.79	0.13
Na_2O	3.33	3.51	2.99	3.52	2.97	3.36	3.07
K_2O	5.22	5.10	5.30	5.21	4.77	5.22	5.39
P_2O_5	0.06	0.04	0.17	0.10	0.07	0.08	0.03
LOI	0.97	0.95	0.73	1.13	0.83	0.93	1.20
Sum	100.36	100.38	99.97	100.72	100.18	100.78	100.66
Trace element (ppm)							
P	219	92.0	357	271	378	137	412
Sc	3.90	3.50	2.70	3.60	13.5	2.20	11.0
Ti	945	792	1550	733	1050	687	1640
V	7.34	1.24	24.1	4.43	8.85	1.73	17.4
Cr	4.00	3.00	8.00	6.00	10.0	5.00	8.00
Mn	233	361	266	239	382	104	480

Sample	MA57	MA58	MA64	MA66	MA69	MA73	MA77
Latitude	N02°20'26.1"	N02°20'26.1"	N01°51'29.2"	N01°49'08.8"	N01°49'01.0"	N01°24'29.0"	N01°23'09.6"
Longitude	E102°37'03.9"	E102°37'03.9"	E102°57'19.2"	E102°54'37.3"	E102°54'50.9"	E103°59'21.8"	E104°12'20.5"
Rock type	Kfs phyric (Hbl)-Bt granite	Leuco- Kfs-phyric (Hbl)-Bt granite	(Hbl)-Bt granite	Hbl-Bt granite	Bt granite	Migmatitic granite	Hbl-Btl granite
Age (Ma)				222.2 ±1.8	225.5 ±2.5*	231.0 ±2.6*	
Co	0.80	0.40	3.20	1.30	1.80	0.20	3.30
Ni	2.33	2.22	4.63	2.59	3.93	1.93	2.90
Cu	3.09	12.9	4.43	3.19	4.81	6.76	25.1
Zn	26.1	31.6	26.5	27.3	53.2	15.1	52.3
Ga	17.7	17.7	16.8	19.6	28.8	18.1	18.9
Rb	373	312	375	562	872	204	322
Sr	220	121	205	51.0	43.0	238	208
Y	60.4	15.8	25.3	52.0	79.4	23.8	29.7
Zr	133	130	150	116	159	154	182
Nb	16.5	18.0	15.3	18.9	25.7	6.10	12.3
Cs	13.4	11.8	37.6	30.8	114	4.42	35.7
Ba	880	615	686	148	204	1160	898
La	57.6	51.0	28.5	33.5	51.5	24.4	51.1
Ce	93.4	97.3	57.5	72.6	112	39.5	93.3
Pr	12.1	10.2	6.70	8.37	12.9	4.14	9.86
Nd	41.8	31.3	23.6	28.6	44.1	14.7	32.5
Sm	7.26	4.67	5.04	7.05	10.7	2.93	6.15
Eu	2.17	0.88	1.14	0.24	0.36	1.09	0.85
Gd	6.97	3.12	4.22	6.79	10.2	3.15	5.00
Tb	1.12	0.46	0.65	1.23	1.80	0.51	0.78
Dy	7.29	2.51	3.96	7.92	11.7	3.42	4.64
Ho	1.67	0.50	0.82	1.67	2.47	0.78	0.96

Sample	MA57	MA58	MA64	MA66	MA69	MA73	MA77
Latitude	N02°20'26.1"	N02°20'26.1"	N01°51'29.2"	N01°49'08.8"	N01°49'01.0"	N01°24'29.0"	N01°23'09.6"
Longitude	E102°37'03.9"	E102°37'03.9"	E102°57'19.2"	E102°54'37.3"	E102°54'50.9"	E103°59'21.8"	E104°12'20.5"
Rock type	Kfs phyric (Hbl)-Bt granite	Leuco- Kfs-phyric (Hbl)-Bt granite	(Hbl)-Bt granite	Hbl-Bt granite	Bt granite	Migmatitic granite	Hbl-Btl granite
Age (Ma)				222.2 ±1.8	225.5 ±2.5*	231.0 ±2.6*	
Er	5.09	1.40	2.31	4.81	7.11	2.31	2.75
Tm	0.82	0.23	0.37	0.78	1.15	0.36	0.44
Yb	5.48	1.54	2.50	5.14	7.38	2.42	2.96
Lu	0.87	0.24	0.37	0.74	1.06	0.38	0.45
Hf	4.04	4.22	4.34	4.18	5.59	4.61	4.97
Ta	1.35	1.49	2.12	3.93	4.99	0.51	1.51
W	0.86	0.73	2.93	4.10	14.9	0.50	1.93
Tl	8.89	7.75	10.6	15.7	24.9	5.00	11.2
Pb	41.1	41.1	82.3	57.9	92.9	22.4	26.4
Th	25.8	24.6	39.4	26.3	49.5	10.4	39.9
U	7.87	8.26	9.65	27.1	37.4	1.49	12.6
A/CNK	1.09	1.08	1.07	1.05	1.17	1.13	1.14
Eu/Eu*	0.93	0.70	0.76	0.11	0.11	1.10	0.47
M	1.31	1.31	1.48	1.45	1.18	1.27	1.20
T_{Zr} (°C)	777	775	775	755	802	793	813

Note:

M is defined as the cation ratio (Na + K + 2Ca)/(Al × Si) (Watson and Harrison, 1983).

Data put in brackets were calculated beyond the assumption made by Watson and Harrison (1983) for *M* is less than 2.00.

All the ages are U-Pb zircon ages presented in Chapter 4. Ages in (*) are reference magmatic ages (Chapter 4).

Sample	MA78	MA81	MA83	MA87	MA90	MA104	MA109
Latitude	N02°48'26.1"	N02°47'20.7"	N02°52'54.3"	N02°48'36.0"	N02°43'06.9"	N02°18'10.4"	N05°49'11.1"
Longitude	E104°09'20.0"	E104°12'13.8"	E104°10'52.0"	E104°09'12.0"	E104°10'27.0"	E103°39'25.2"	E101°56'07.2"
Rock type	Cpx-Hbl-Bt granite	Bt granite	(Hbl)-Bt granite	(Hbl)-Bt granite	Microgranitic dyke	Hbl-Bt granite	Bt granite
Age (Ma)	80.1 ±0.6				80.2 ±0.7	244.3 ±1.8*	226.7 ±2.2
Major element (wt%)							
SiO_2	71.33	68.32	70.01	69.68	76.72	75.54	69.86
TiO_2	0.39	0.26	0.23	0.22	0.10	0.16	0.66
Al_2O_3	15.28	18.01	16.03	17.48	13.76	13.96	15.14
Fe_2O_3(t)	1.95	1.44	0.90	1.02	0.59	1.58	3.45
MnO	0.04	0.02	0.02	0.01	0.05	0.05	0.04
MgO	0.64	0.26	0.16	0.24	0.14	0.20	1.55
CaO	1.80	0.75	0.82	0.88	0.88	1.02	2.72
Na_2O	3.88	2.82	3.71	4.96	3.75	3.56	2.39
K_2O	5.05	8.95	7.23	6.20	4.53	4.96	4.54
P_2O_5	0.13	0.05	0.04	0.04	0.03	0.06	0.21
LOI	0.83	1.10	0.85	0.50	0.60	0.93	1.03
Sum	100.49	100.88	99.16	100.73	100.56	101.09	100.57
Trace element (ppm)							
P	465	184	144	139	154	235	975
Sc	7.60	2.80	1.20	1.50	10.2	1.00	27.3
Ti	1620	1260	1170	1010	585	726	3260
V	19.3	15.4	7.42	6.20	1.26	4.44	66.9
Cr	8.00	4.00	10.0	3.00	5.00	3.00	40.0

Sample	MA78	MA81	MA83	MA87	MA90	MA104	MA109
Latitude	N02°48'26.1"	N02°47'20.7"	N02°52'54.3"	N02°48'36.0"	N02°43'06.9"	N02°18'10.4"	N05°49'11.1"
Longitude	E104°09'20.0"	E104°12'13.8"	E104°10'52.0"	E104°09'12.0"	E104°10'27.0"	E103°39'25.2"	E101°56'07.2"
Rock type	Cpx-Hbl-Bt granite	Bt granite	(Hbl)-Bt granite	(Hbl)-Bt granite	Microgranitic dyke	Hbl-Bt granite	Bt granite
Age (Ma)	80.1 ±0.6				80.2 ±0.7	244.3 ±1.8*	226.7 ±2.2
Mn	294	149	170	114	469	417	339
Co	2.80	1.20	1.00	0.40	0.50	1.30	7.70
Ni	5.17	3.41	3.90	2.22	2.88	2.36	15.8
Cu	2.33	3.77	3.84	4.38	5.23	2.44	12.4
Zn	38.4	12.2	14.5	35.1	28.3	38.2	44.3
Ga	15.4	17.9	17.7	18.7	19.7	16.2	18.8
Rb	215	359	223	118	413	343	269
Sr	378	164	133	200	147	92.0	230
Y	17.5	15.1	19.8	14.2	26.1	31.2	28.3
Zr	213	369	266	219	120	125	288
Nb	14.9	10.4	18.8	11.4	23.2	11.8	18.8
Cs	8.64	8.80	4.78	2.59	38.5	12.7	10.3
Ba	743	522	461	570	313	495	993
La	53.8	51.2	63.9	70.7	26.9	35.5	65.2
Ce	89.7	84.1	132	143	48.2	61.8	130
Pr	9.03	9.01	15.0	16.3	5.33	6.41	14.8
Nd	28.3	27.4	48.3	53.5	17.7	20.7	51.7
Sm	4.24	3.87	7.44	8.76	3.66	4.25	9.44
Eu	0.95	1.54	1.16	1.51	0.59	0.44	1.61
Gd	2.95	2.64	4.65	5.20	3.39	3.85	6.80
Tb	0.44	0.40	0.66	0.70	0.58	0.64	0.95
Dy	2.48	2.38	3.50	3.18	3.83	4.13	5.00

Sample	MA78	MA81	MA83	MA87	MA90	MA104	MA109
Latitude	N02°48'26.1"	N02°47'20.7"	N02°52'54.3"	N02°48'36.0"	N02°43'06.9"	N02°18'10.4"	N05°49'11.1"
Longitude	E104°09'20.0"	E104°12'13.8"	E104°10'52.0"	E104°09'12.0"	E104°10'27.0"	E103°39'25.2"	E101°56'07.2"
Rock type	Cpx-Hbl-Bt granite	Bt granite	(Hbl)-Bt granite	(Hbl)-Bt granite	Microgranitic dyke	Hbl-Bt granite	Bt granite
Age (Ma)	80.1 ±0.6				80.2 ±0.7	244.3 ±1.8*	226.7 ±2.2
Ho	0.53	0.50	0.67	0.52	0.83	0.93	0.97
Er	1.54	1.53	1.84	1.30	2.47	2.88	2.48
Tm	0.25	0.25	0.28	0.19	0.43	0.51	0.35
Yb	1.73	1.80	1.94	1.18	3.15	3.66	2.12
Lu	0.27	0.29	0.29	0.18	0.50	0.58	0.31
Hf	4.97	8.60	6.66	5.14	4.17	3.98	7.26
Ta	1.35	0.77	1.35	0.60	3.22	1.87	1.22
W	0.91	1.23	0.94	0.39	4.71	0.64	1.01
Tl	5.98	9.28	4.97	2.66	8.57	7.88	7.29
Pb	14.9	42.9	36.1	18.9	40.8	39.1	50.6
Th	19.2	9.10	20.0	12.5	38.9	52.2	47.7
U	7.47	0.99	4.12	1.54	17.2	20.1	3.79
A/CNK	1.02	1.15	1.04	1.06	1.09	1.07	1.12
Eu/Eu*	0.82	1.47	0.60	0.68	0.51	0.34	0.61
M	1.50	1.39	1.48	1.49	1.29	1.34	1.39
T_{Zr} (°C)	804	865	826	807	770	769	841

Note:

M is defined as the cation ratio (Na + K + 2Ca)/(Al × Si) (Watson and Harrison, 1983).

Data put in brackets were calculated beyond the assumption made by Watson and Harrison (1983) for *M* is less than 2.00.

All the ages are U-Pb zircon ages presented in Chapter 4. Ages in (*) are reference magmatic ages (Chapter 4).

TABLE 3.1B. MAJOR AND TRACE ELEMENT DATA OF THE MALAYSIAN MAIN RANGE PROVINCE GRANITOIDS.

Sample	MA06	MA09	MA11	MA13	MA14	MA15	MA16	MA19
Latitude	N04°33'50.4"	N04°34'30.0"	N04°33'19.5"	N04°35'00.3"	N04°34'49.5"	N04°32'56.1"	N04°46'54.9"	N05°27'48.0"
Longitude	E101°11'55.4"	E101°15'45.6"	E101°19'26.6"	E101°24'24.5"	E101°20'22.8"	E101°01'46.8"	E100°44'11.0"	E100°13'58.9"
Rock type	Kfs phyric Crd-Bt granite	Kfs phyric Crd-Bt granite	Tur-Bt granite	Kfs phyric Ms-Bt granite	Kfs phyric Ms-Bt microgranite	Kfs phyric Ms-Bt granite	Kfs phyric Hbl-Bt granite	Kfs phyric Bt granite
Age (Ma)	220.1 ±2.8*			225.4 ±1.3	218.3 ±2.4	220.1 ±1.0	215.7 ±1.6	213.9 ±2.9*
Major element (wt%)								
SiO_2	75.70	71.71	71.80	71.26	77.16	74.62	68.15	74.18
TiO_2	0.06	0.37	0.35	0.57	0.20	0.10	0.55	0.28
Al_2O_3	13.14	14.03	13.84	12.97	11.95	13.76	14.19	12.34
Fe_2O_3(t)	0.52	1.83	2.25	3.19	1.41	0.65	2.95	2.02
MnO	0.03	0.04	0.03	0.05	0.03	0.02	0.05	0.05
MgO	0.06	0.56	0.71	1.33	0.26	0.13	1.56	0.36
CaO	0.71	1.12	0.81	1.53	0.44	0.66	2.74	1.11
Na_2O	3.18	2.57	2.51	2.66	1.73	3.02	2.75	2.49
K_2O	5.20	6.14	5.09	4.14	4.57	5.53	4.71	4.29
P_2O_5	0.04	0.13	0.15	0.18	0.05	0.07	0.18	0.13
LOI	2.14	1.68	2.14	2.48	1.72	0.91	1.98	2.06
Sum	100.78	100.16	99.67	100.35	99.52	99.47	99.82	99.30
Trace element (ppm)								
P	159	511	600	790	306	307	788	558
Sc	35.9	15.4	11.6	10.6	20.5	10.3	10.1	7.10
Ti	381	1950	1730	3330	1020	476	3200	1400
V	1.17	19.0	21.1	33.3	5.57	1.50	43.4	13.6
Cr	42.0	80.0	56.0	68.0	72.0	57.0	96.0	59.0
Mn	210	304	238	388	275	151	411	367

Sample	MA06	MA09	MA11	MA13	MA14	MA15	MA16	MA19
Latitude	N04°33'50.4"	N04°34'30.0"	N04°33'19.5"	N04°35'00.3"	N04°34'49.5"	N04°32'56.1"	N04°46'54.9"	N05°27'48.0"
Longitude	E101°11'55.4"	E101°15'45.6"	E101°19'26.6"	E101°24'24.5"	E101°20'22.8"	E101°01'46.8"	E100°44'11.0"	E100°13'58.9"
Rock type	Kfs phyric Crd-Bt granite	Kfs phyric Crd-Bt granite	Tur-Bt granite	Kfs phyric Ms-Bt granite	Kfs phyric Ms-Bt microgranite	Kfs phyric Ms-Bt granite	Kfs phyric Hbl-Bt granite	Kfs phyric Bt granite
Age (Ma)	220.1 ±2.8*			225.4 ±1.3	218.3 ±2.4	220.1 ±1.0	215.7 ±1.6	213.9 ±2.9*
Co	1.20	3.10	4.50	6.90	1.70	0.70	6.60	3.00
Ni	19.7	36.8	22.2	26.6	34.0	25.1	35.1	28.3
Cu	2.07	2.25	30.1	7.78	4.04	8.16	11.6	5.10
Zn	15.9	32.1	36.6	99.0	22.4	5.50	46.6	43.1
Ga	24.2	19.3	17.2	17.7	19.7	21.1	19.4	18.5
Rb	1100	544	354	400	579	832	428	381
Sr	23.0	131	77.0	85.0	32.0	25.0	201	51.0
Y	108	46.2	23.4	39.2	67.0	47.2	34.2	48.9
Zr	74.0	199	131	247	145	64.0	264	173
Nb	29.1	22.8	13.5	19.1	24.9	25.2	23.0	13.5
Cs	74.9	16.5	12.4	14.0	11.9	50.4	50.2	22.3
Ba	123	545	426	284	81.0	115	575	191
La	28.9	49.0	25.0	45.0	42.6	14.3	58.0	38.1
Ce	62.5	102	52.2	94.4	93.6	31.8	116	82.1
Pr	7.91	12.1	6.12	11.1	11.2	3.71	13.9	9.56
Nd	28.3	41.5	21.8	39.4	37.7	12.0	49.5	33.9
Sm	8.71	8.61	4.63	8.45	8.80	3.25	9.42	7.57
Eu	0.25	0.75	0.65	0.78	0.25	0.15	1.16	0.61
Gd	10.1	7.33	3.78	7.34	8.16	3.62	6.83	7.14
Tb	2.01	1.26	0.61	1.17	1.54	0.76	1.03	1.22
Dy	14.3	7.59	3.44	6.79	10.2	5.69	5.56	7.67
Ho	3.18	1.58	0.68	1.35	2.15	1.28	1.10	1.61

Sample	MA06	MA09	MA11	MA13	MA14	MA15	MA16	MA19
Latitude	N04°33'50.4"	N04°34'30.0"	N04°33'19.5"	N04°35'00.3"	N04°34'49.5"	N04°32'56.1"	N04°46'54.9"	N05°27'48.0"
Longitude	E101°11'55.4"	E101°15'45.6"	E101°19'26.6"	E101°24'24.5"	E101°20'22.8"	E101°01'46.8"	E100°44'11.0"	E100°13'58.9"
Rock type	Kfs phyric Crd-Bt granite	Kfs phyric Crd-Bt granite	Tur-Bt granite	Kfs phyric Ms-Bt granite	Kfs phyric Ms-Bt microgranite	Kfs phyric Ms-Bt granite	Kfs phyric Hbl-Bt granite	Kfs phyric Bt granite
Age (Ma)	220.1 ±2.8*			225.4 ±1.3	218.3 ±2.4	220.1 ±1.0	215.7 ±1.6	213.9 ±2.9*
Er	9.93	4.37	1.85	3.61	6.18	3.99	3.08	4.57
Tm	1.84	0.69	0.28	0.56	1.02	0.72	0.48	0.75
Yb	13.1	4.25	1.79	3.42	6.47	5.02	3.08	4.83
Lu	1.94	0.60	0.26	0.49	0.89	0.72	0.45	0.69
Hf	3.63	5.68	3.14	6.35	4.65	2.47	6.82	4.79
Ta	9.52	2.77	1.47	2.45	3.99	6.34	3.18	2.35
W	8.00	1.28	2.73	1.57	2.72	18.2	7.87	1.10
Tl	26.2	13.4	6.94	8.90	13.3	18.0	10.0	7.89
Pb	53.1	45.2	37.5	32.9	40.8	30.2	65.4	33.2
Th	33.4	52.0	20.4	35.4	51.0	25.2	48.3	29.6
U	17.6	11.5	10.1	10.6	23.4	24.9	18.8	8.34
A/CNK	1.09	1.10	1.26	1.14	1.40	1.14	0.99	1.16
Eu/Eu*	0.08	0.29	0.48	0.30	0.09	0.14	0.44	0.25
M	1.29	1.34	1.16	1.31	0.96	1.25	1.58	1.21
T_{Zr} (°C)	730	810	787	833	811	722	817	807

Note:

M is defined as the cation ratio (Na + K + 2Ca)/(Al × Si) (Watson and Harrison, 1983).

Data put in brackets were calculated beyond the assumption made by Watson and Harrison (1983) for *M* is less than 2.00.

All the ages are U-Pb zircon ages presented in Chapter 4. Ages in (*) are reference magmatic ages (Chapter 4).

Sample	MA20	MA23	MA26	MA30	MA31	MA60	MA62
Latitude	N05°28'13.5"	N05°16'11.3"	N06°24'11.4"	N06°17'56.9"	N03°19'39.6"	N01°58'32.8"	N01°58'32.8"
Longitude	E100°11'31.1"	E100°16'57.3"	E99°48'12.3"	E99°51'10.1"	E101°44'52.0"	E102°40'24.5"	E102°40'24.5"
Rock type	Kfs phyric microgranite	Kfs phyric Bt granite	Kfs phyric Bt granite	Ms-Bt microgranite	Kfs phyric Bt granite	Kfs phyric Ms-Bt granite	Kfs phyric Bt granite
Age (Ma)	215.5 ±1.5*	212.1 ±2.4	215.3 ±2.6	215.9 ±1.7	222.4 ±1.8		217.4 ±1.2
Major element (wt%)							
SiO_2	66.00	68.60	69.72	76.93	69.94	73.95	72.07
TiO_2	0.43	0.41	0.39	0.16	0.51	0.19	0.32
Al_2O_3	16.48	14.71	14.61	12.55	13.98	14.24	14.23
Fe_2O_3(t)	3.69	2.79	2.31	1.16	2.52	1.68	2.71
MnO	0.07	0.04	0.05	0.05	0.05	0.06	0.06
MgO	0.96	0.55	0.19	0.28	1.01	0.21	0.47
CaO	3.34	1.45	1.31	0.35	1.92	0.91	1.95
Na_2O	2.21	2.75	1.43	3.09	2.17	3.58	3.10
K_2O	3.76	6.29	6.28	4.82	5.17	4.83	4.48
P_2O_5	0.10	0.16	0.12	0.13	0.15	0.09	0.10
LOI	3.29	2.05	2.10	1.42	1.96	1.19	1.06
Sum	100.32	99.81	98.51	100.93	99.39	100.92	100.53
Trace element (ppm)							
P	576	687	685	585	726	323	684
Sc	5.60	17.7	19.3	21.3	17.6	5.30	5.90
Ti	2170	2130	2040	793	3030	642	2400
V	52.0	24.9	28.6	8.64	30.5	2.86	41.2
Cr	49.0	78.0	66.0	50.0	62.0	4.00	19.0
Mn	537	358	397	377	366	366	391
Co	7.20	4.40	4.90	2.40	5.70	0.70	5.40

Sample	MA20	MA23	MA26	MA30	MA31	MA60	MA62
Latitude	N05°28'13.5"	N05°16'11.3"	N06°24'11.4"	N06°17'56.9"	N03°19'39.6"	N01°58'32.8"	N01°58'32.8"
Longitude	E100°11'31.1"	E100°16'57.3"	E99°48'12.3"	E99°51'10.1"	E101°44'52.0"	E102°40'24.5"	E102°40'24.5"
Rock type	Kfs phyric microgranite	Kfs phyric Bt granite	Kfs phyric Bt granite	Ms-Bt microgranite	Kfs phyric Bt granite	Kfs phyric Ms-Bt granite	Kfs phyric Bt granite
Age (Ma)	215.5 ±1.5*	212.1 ±2.4	215.3 ±2.6	215.9 ±1.7	222.4 ±1.8		217.4 ±1.2
Ni	21.0	36.8	32.0	24.9	21.1	2.01	7.85
Cu	4.10	8.15	4.62	4.09	8.17	2.16	4.27
Zn	36.4	49.5	43.3	35.3	38.7	26.6	50.1
Ga	17.9	20.4	17.7	16.2	18.4	17.0	18.9
Rb	158	444	470	606	435	420	370
Sr	373	86.0	105	20.0	101	69.0	188
Y	25.8	46.0	34.8	35.0	31.6	48.4	26.1
Zr	186	238	171	82.0	230	104	233
Nb	26.2	16.1	13.5	14.6	17.4	24.4	17.5
Cs	6.55	26.4	46.4	56.1	39.8	13.4	34.4
Ba	1010	604	742	68.0	670	241	937
La	57.9	47.9	31.2	13.7	46.1	27.4	46.5
Ce	97.1	97.5	65.8	30.9	94.9	56.3	92.9
Pr	10.2	11.6	7.81	3.79	11.0	6.52	10.5
Nd	33.0	41.4	27.9	13.4	38.6	22.5	36.4
Sm	5.69	8.67	5.99	3.55	7.53	5.62	6.90
Eu	1.12	1.15	1.20	0.20	0.95	0.34	1.16
Gd	4.59	7.79	5.49	3.71	6.09	5.82	5.38
Tb	0.72	1.27	0.92	0.72	0.94	1.07	0.81
Dy	4.09	7.51	5.55	4.96	5.32	6.37	4.48
Ho	0.88	1.53	1.17	1.10	1.06	1.11	0.88
Er	2.52	4.22	3.35	3.36	2.89	2.80	2.40

Sample	MA20	MA23	MA26	MA30	MA31	MA60	MA62
Latitude	N05°28'13.5"	N05°16'11.3"	N06°24'11.4"	N06°17'56.9"	N03°19'39.6"	N01°58'32.8"	N01°58'32.8"
Longitude	E100°11'31.1"	E100°16'57.3"	E99°48'12.3"	E99°51'10.1"	E101°44'52.0"	E102°40'24.5"	E102°40'24.5"
Rock type	Kfs phyric microgranite	Kfs phyric Bt granite	Kfs phyric Bt granite	Ms-Bt microgranite	Kfs phyric Bt granite	Kfs phyric Ms-Bt granite	Kfs phyric Bt granite
Age (Ma)	215.5 ±1.5*	212.1 ±2.4	215.3 ±2.6	215.9 ±1.7	222.4 ±1.8		217.4 ±1.2
Tm	0.39	0.64	0.53	0.61	0.44	0.43	0.36
Yb	2.58	3.99	3.45	4.24	2.76	2.73	2.25
Lu	0.39	0.58	0.49	0.60	0.40	0.37	0.33
Hf	4.49	5.78	4.49	2.85	6.00	2.92	6.22
Ta	1.43	1.82	2.04	4.89	2.76	8.15	1.68
W	0.34	2.26	8.84	12.5	1.89	0.98	6.55
Tl	3.51	8.70	10.9	12.5	10.6	10.8	10.4
Pb	16.6	43.3	51.9	33.5	52.6	34.5	58.0
Th	17.6	32.3	21.0	15.2	36.1	29.4	47.0
U	2.47	6.67	6.60	17.8	13.9	19.1	11.6
A/CNK	1.21	1.07	1.28	1.16	1.12	1.12	1.06
Eu/Eu*	0.67	0.43	0.64	0.17	0.43	0.18	0.58
M	1.30	1.45	1.15	1.20	1.34	1.29	1.39
T_{Zr} (°C)	807	818	811	745	823	758	821

Note:

M is defined as the cation ratio (Na + K + 2Ca)/(Al × Si) (Watson and Harrison, 1983).

Data put in brackets were calculated beyond the assumption made by Watson and Harrison (1983) for *M* is less than 2.00.

All the ages are U-Pb zircon ages presented in Chapter 4. Ages in (*) are reference magmatic ages (Chapter 4).

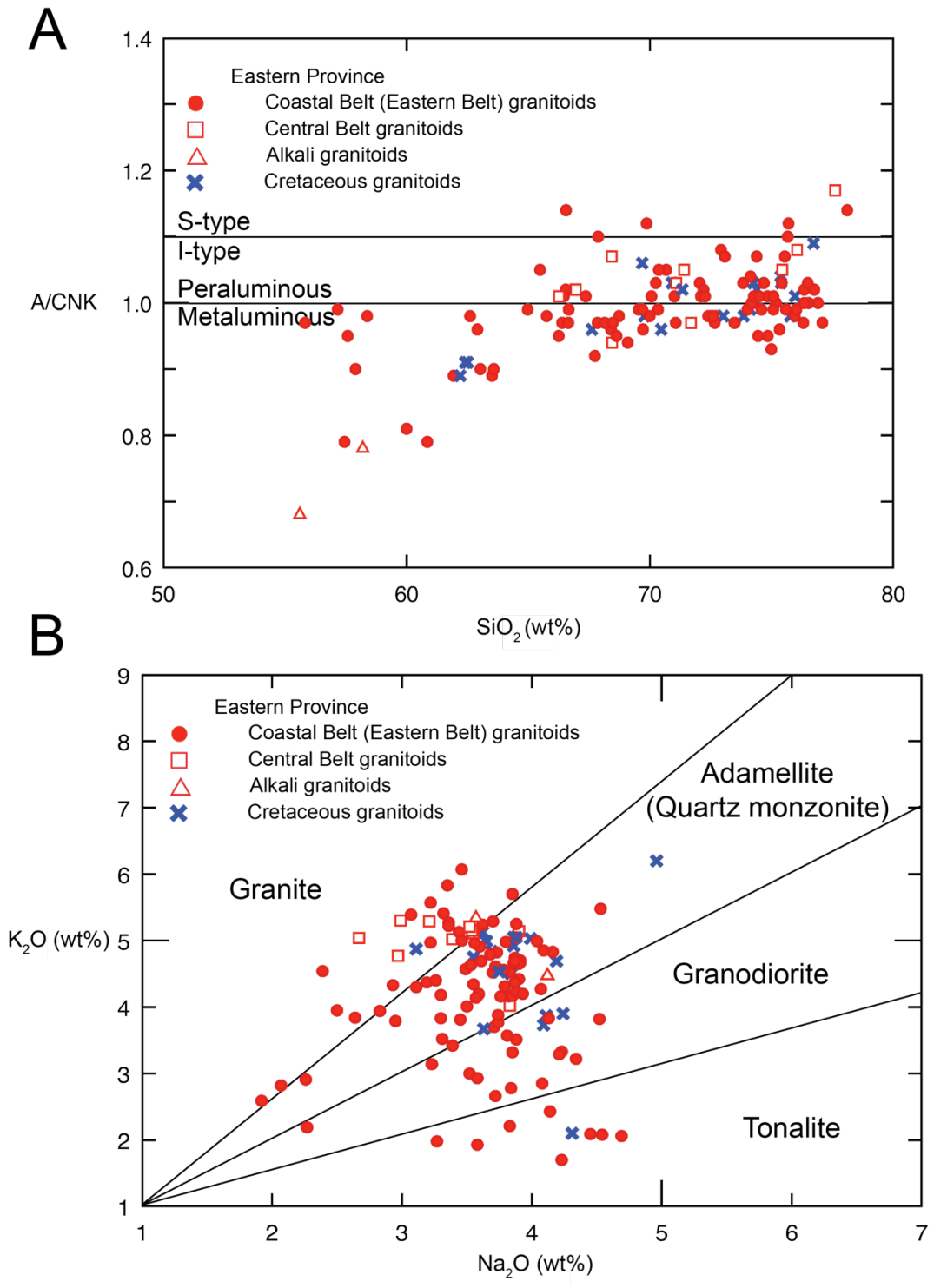

Figure 3.1 Comparison of the Coastal Belt granitoids and Central Belt granitoids in the Eastern Province in terms of aluminium saturation index (ASI or A/CNK) (A) and alkali oxides (B) showing the overlap between the Coastal Belt and Central Belt granitoids. The I-S division was suggested by Chappell and White (1974, 1992), while the granitoid sub-division was suggested by Harpum (1963). Data were provided by this work and Cobbing *et al.* (1992).

3.2.2 Comparison between Eastern Province and Main Range Province granitoids

Aluminium saturation index (ASI or A/CNK): Granitoids of the Eastern Province and the Main Range were originally distinguished according to their "contrasting" mineralogy and geochemistry in Chappell and White's (1974) I-S type granite system. In this system, I- and S-type granitoids are geochemically discriminated primarily by their aluminium saturation index (ASI or A/CNK). The division is drawn when A/CNK = 1.1 (Figure 3.2A), whereby the I-type granitoids are essentially metaluminous and gradually become weakly peraluminous with increasing silica contents, while S-type granitoids are typically peraluminous (Chappell and White, 1974, 1992; Ghani *et al.*, 2013). The Eastern Province granitoids and the Main Range granitoids generally follow the trend of I-type and S-type granitoids respectively. The "S-type" Eastern Province geochemical outliers suggested that some of the Eastern Province granitoids are highly fractionated, while the metaluminous Main Range outliers can be explained by the presence of hornblende-bearing Bintang Batholith in the Main Range Province. There is an overlapping area of A/CNK in between 1.0 and 1.1, where a large number of both Eastern Province and Main Range granitoids can be found. Hence, the A/CNK does not give satisfactory discrimination for these Malaysian granitic provinces.

Alkali oxides: Another geochemical scheme used for I-S type discrimination is the proportion of alkali oxides, namely K_2O and Na_2O, in the granitoids, which is an analogue of the K-feldspar to plagioclase ratio. It is suggested that I-type granites tend to be more sodic, while S-type granites are more potassic (Table 2.1) (Chappell and White, 1974, 1992; Clarke, 1992; Cobbing *et al.*, 1992; Pitcher, 1997; Ghani *et al.*, 2013). This geochemical behaviour is conceptually drawn as an I-S division line in Figure 3.2B. The Eastern and the Main Range Provinces largely follow the I- and S-

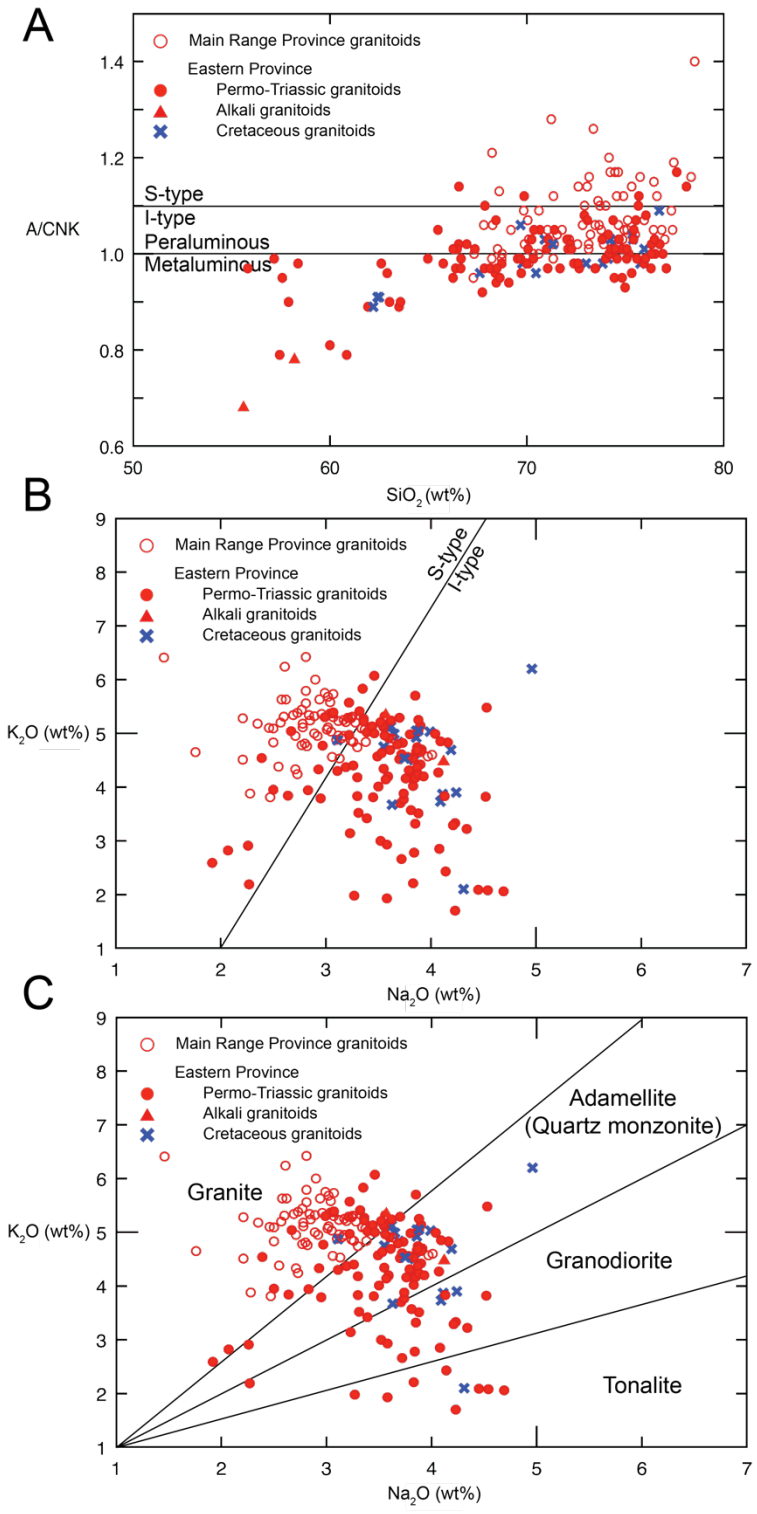

Figure 3.2 Comparison of the Eastern Province and Main Range granitoids in aluminium saturation index (ASI or A/CNK) (A) and alkali oxides (B) showing the overlap between the Eastern Province and the Main Range granitoids in Chappell and White's (1974) I-S granite system. The I-S type division is after Chappell and White (1974, 1992), while the granitoid sub-division was suggested by Harpum (1963) (C).

type geochemical fields respectively. The Na_2O and K_2O pair allows further classification of granitoids as shown by Harpum's (1963) diagram (Figure 3.2C). It is observed that the geochemistry of the Eastern Province granitoids covers a variety of granitoids, including granite, adamellite (or quartz monzonite), granodiorite and tonalite. However, the Main Range granitoids are generally restricted to the granite field.

Trace elements: The trace element compositions of granites are useful in pointing to the tectonic setting, in which granitoids are formed (Pearce *et al.*, 1984; Harris *et al.*, 1986), as discussed in Chapter 2. In the traditional tectonic model proposed by Beckinsale (1979) and Cobbing *et al.* (1986, 1992), the Eastern Province granitoids were interpreted as pre-collision arc-related granites, while the Main Range Province granitoids were interpreted as collisional granites. Pearce *et al.* (1984) and Harris *et al.* (1986) suggested that collisional granites are characterized by high Rb contents, which are related to the incorporation of more evolved source (e.g. felsic precursor) into the parental magma, or to Rayleigh fractional crystallization of the magma (Halliday *et al.*, 1991). In Pearce *et al.*'s (1984) diagram (Figure 3.3A), The present data showed that the majority of the Main Range Province granitoids are restricted to the syn-**COL**lisional **G**ranite field (syn-COLG), with some outliers falling into the **W**ithin-**P**late **G**ranite (WPG), whereas most of the Eastern Province granitoids straddle the syn-collision, within-plate granite and **V**olcanic **A**rc **G**ranite (VAG) fields. This is caused by enrichment of **H**igh **F**ield **S**trength **E**lements (HFSE), such as Y and Nb. In this Harris *et al.*'s (1986) diagram (Figure 3.3B), both Eastern and Main Range Province granitoids generally follow the pattern shown in the Pearce *et al.*'s (1984) diagram (Figure 3.3A). Here, no outliers are found in the within-plate granite field, as no Rb depletion is observed in the Malaysian granitoids. This suggested that the Malaysian granitoids are

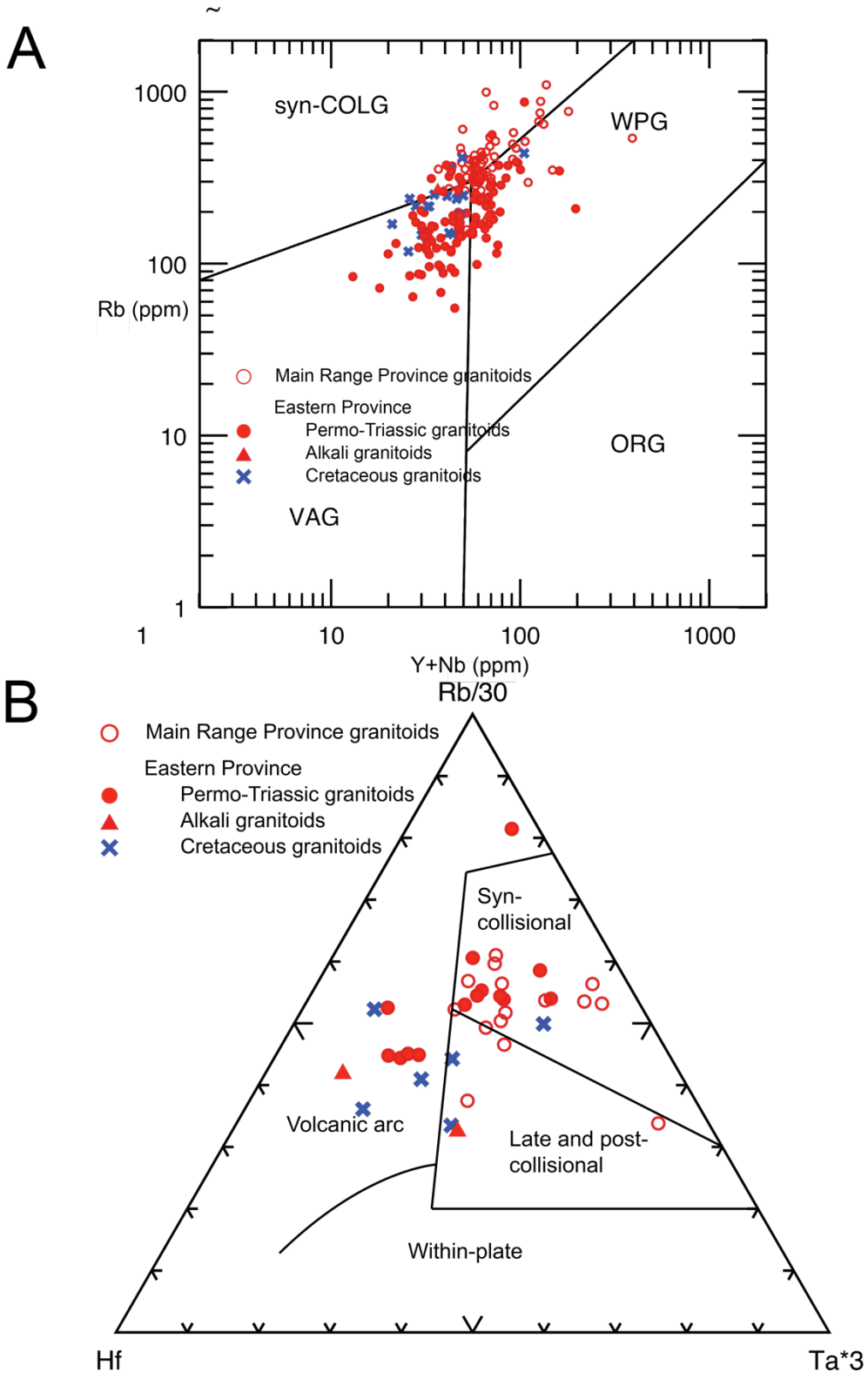

Figure 3.3 Rb vs (Y + Nb) diagram (A) and Hf–Rb/30–Ta×3 diagram (B) illustrating the relatively fractionated nature of some of the Eastern Province granitoids, diagrams after Pearce *et al.* (1984) and Harris *et al.* (1986). Since no Hf and Ta data are available in Cobbing *et al.* (1992), only data from this work are presented in (B).

not real within-plate granites (WPG), as Rb depletion is expected in such granites. These trace element diagrams only showed that the Malaysian granitoids are enriched in HFSE. The cause of such enrichment will be discussed in Section 3.2.3.

Fractionation of the Malaysian granitoids: Harker diagrams (Figure 3.4) show that the Malaysian granitoids in both granitic provinces experience significant fractionation, for which the fractionation trend of the Eastern Province and that of the Main Range Province are largely overlapped. It is also observed that most of the Main Range Province granitoids are more fractionated. In general, as the silica contents increase in the Malaysian granitoids, TiO_2, Al_2O_3, FeO, MgO, CaO and P_2O_5 decrease, while K_2O is the only oxide showing positive correlation with silica contents. No correlation can be found in Na_2O. This suggests that the fractionation here is more complicated in both granitic provinces, and could relate to perthite development in less fractionated granitoids. Trace elements such as Ba, Sr and Fe are selected to compare with Rb (incompatible element) in various bivariate diagrams (Figure 3.5). The Ba, Sr and Fe contents decrease by up to 2 orders of magnitude with increasing silica contents, suggesting that fractionation of feldspars (decrease in Sr and Ba), biotite and hornblende (decrease in Fe) were likely to have played a role in the evolving magmatic systems. A bulk **L**iquid-**L**ines-**O**f-**D**escent (LLOD) was plotted in each diagram to demonstrate the composite effect of K-feldspar, plagioclase, biotite and hornblende fractionation (Figure 3.5). They showed the LLODs of the Eastern Province and Main Range Province have similar slopes, and they may even largely overlap with each other (Figure 3.5A and B). However, it is also clear that the LLODs of the Eastern Province granitoids and the Main Range granitoids have different hypothetical starting points. Moreover, The high

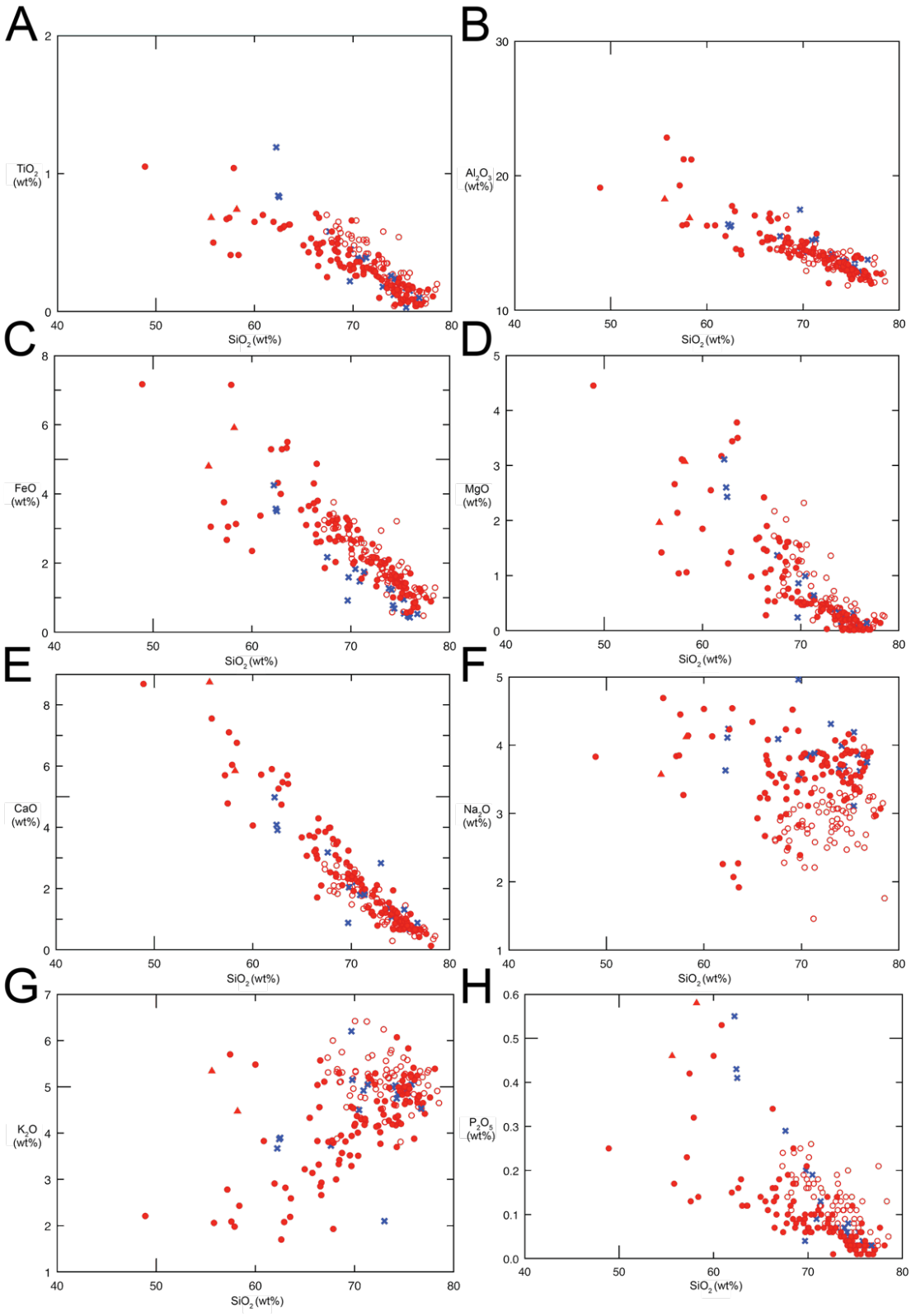

Figure 3.4 Harker diagrams of the Malaysian granitoids on various major oxides, showing the Malaysian granitoids experienced fractionation in their magmatic evolution, with the removal of mafic minerals. Symbols follow Figure 3.2.

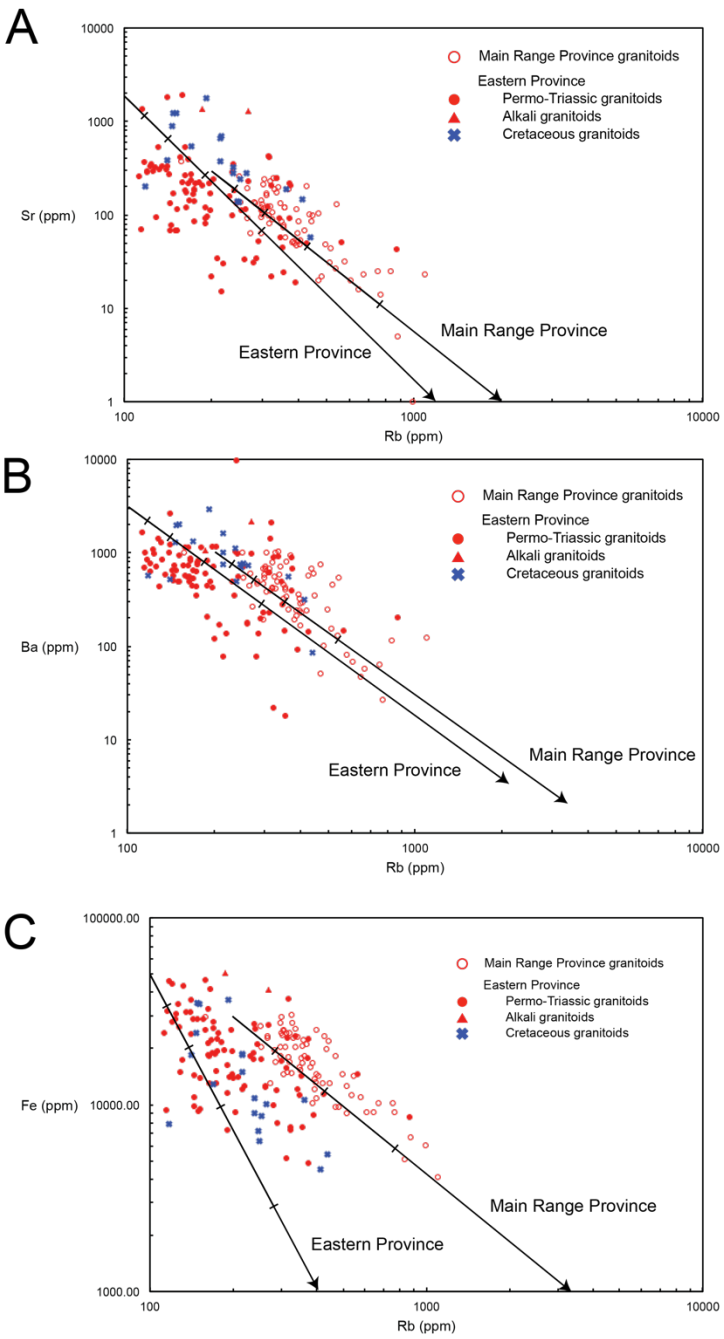

Figure 3.5 Trace element bivariate diagrams in Sr, Ba and Fe with bulk liquid-lines-of descent (LLODs) showing the crystal fractionation trend in the removal of plagioclase (Sr), K-feldspar (Ba), hornblende and biotite (Fe). Each increment represents 20% of bulk fractionation. The bulk LLOD of the Eastern Province granitoids is constructed with the fractionation of 10% hornblende, 1% biotite, 50% plagioclase and 39% K-feldspar. The bulk LLOD of the Main Range Province granitoids is constructed with the fractionation of 5% hornblende, 1% biotite, 50% plagioclase and 44% K-feldspar. Partition coefficients suggested by Mahood and Hildreth (1983) and Ewart and Griffin (1994) are adopted in the calculation of LLODs. These values are shown in Appendix A. Each increment represents 20% of bulk fractionation.

Rb/Sr ratios observed in the Main Range Province granitoids (Figure 3.5A) suggested that they are generally more fractionated than the Eastern Province granitoids.

Granite fractionation and tin metallogenesis: Since Sn data are not available in this work as standard is not available, the study of the relation between granitoid fractionation and their whole-rock Sn contents relied on the data provided by Cobbing *et al.* (1992). In Figure 3.6, trace element ratio Rb/Sr is used as an index of fractionation. It is observed that the whole-rock Sn contents of the granitoids have a positive correlation with the fractionation index Rb/Sr. This explained why the more fractionated Main Range granitoids are usually Sn-bearing.

3.2.3 Comparison between the Malaysian granitoids and the Cordilleran I-S granites

In Figure 3.3A, it is observed that both granitic provinces have data which falls into the WPG field, suggesting the Malaysian granitoids of both granitic provinces show enrichment in some of the HFSE, such as Nb and Y. Although such observation is not shown in the Harris *et al.*'s diagram (Figure 3.3B), enrichment of other HFSE, such as Ga, Zr and Ce, are also supported by Whalen *et al.*'s (1987) diagrams, in which some of Malaysian granitoids fell into the A-type geochemical field (Figure 3.7). Such HFSE anomaly is unusual for typical I- and S-type granites. Spider diagrams (normalized to primitive mantle) of the Malaysian granitoids (Figure 3.8) were plotted to compare the trace element geochemistry of the Malaysian granitoids with the more typical Cordilleran I-S granites (Famatinian magmatic arc in NW Argentina) (Grosse *et al.*, 2011) and the Northeastern China A-type granites (Wu *et al.*, 2002). These spider diagrams show that the Malaysian granitoids are more enriched than the Cordilleran I-S granites in HFSE (e.g. Zr and Nb), and REE). These elements, for example La, Ce, Zr

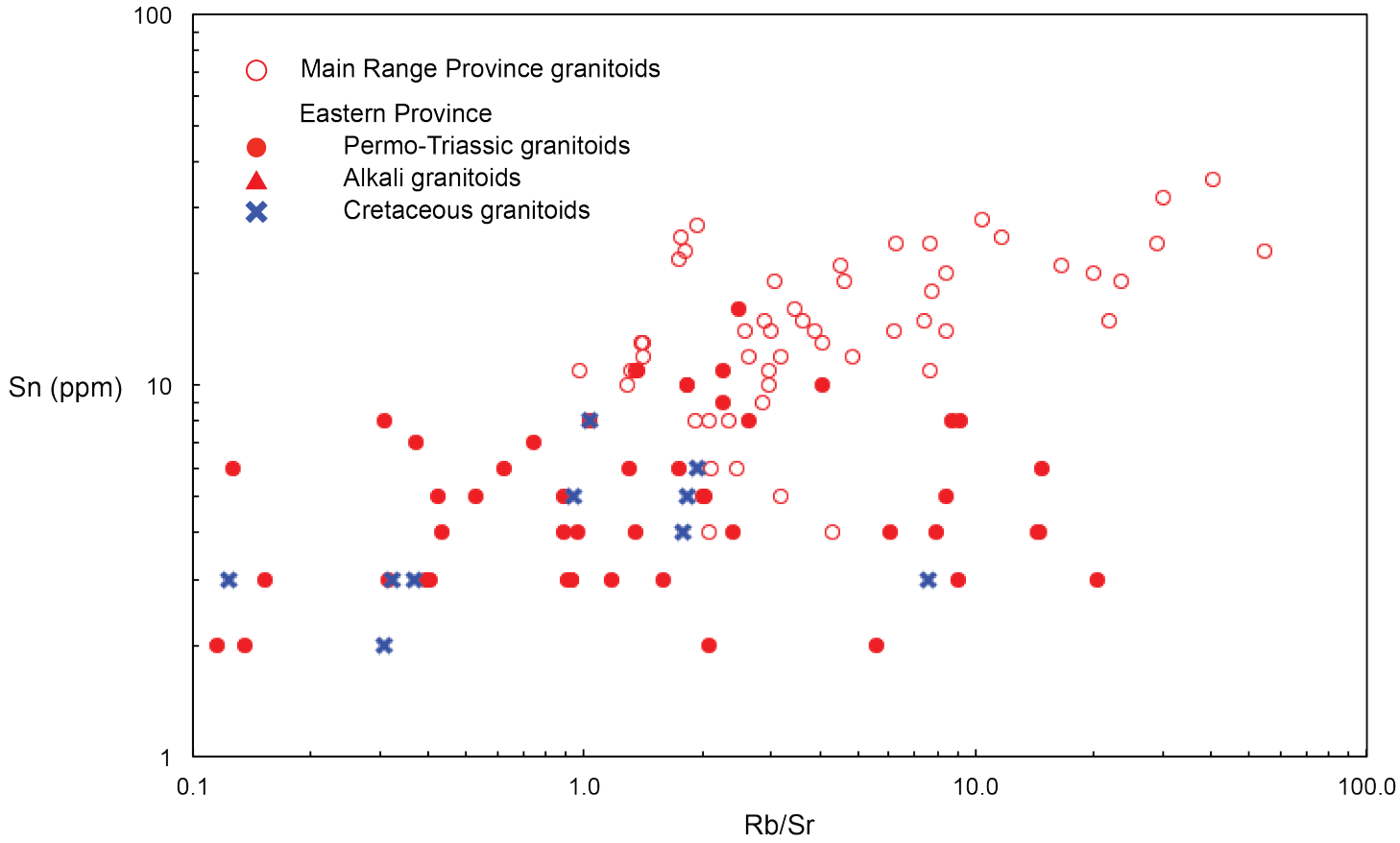

Figure 3.6 Sn vs Rb/Sr diagram showing positive correlation between the whole-rock Sn content and granite fractionation. Hence, the more fractionated Main Range granitoids are more enriched in Sn.

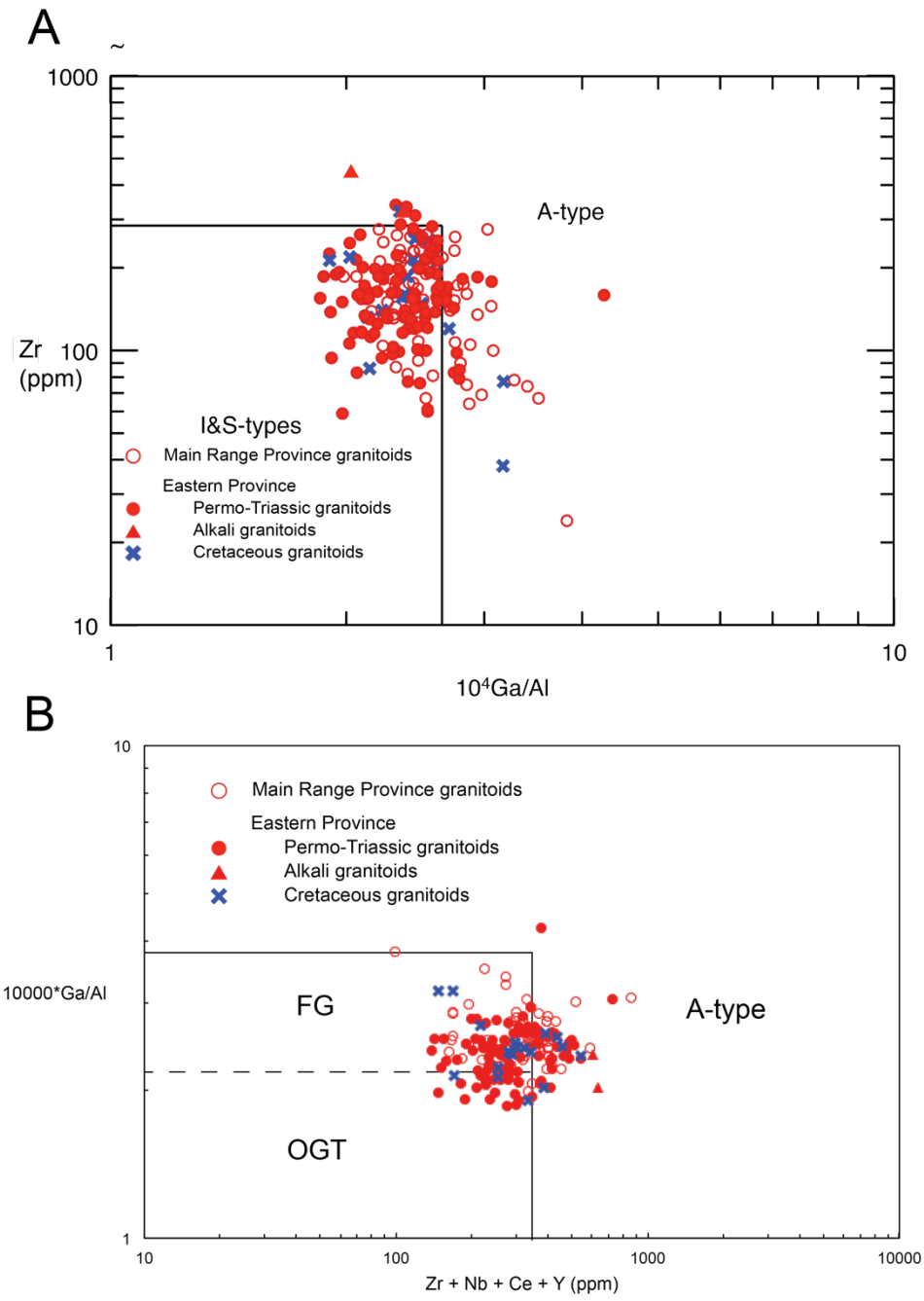

Figure 3.7 Whalen *et al.*'s (1987) diagrams showing the enrichment of HFSE, such as Zr, Nb, Ce, Y and Ga in Malaysian granitoids, compared to ordinary (OGT) and fractionated I-S granitoids (FG).

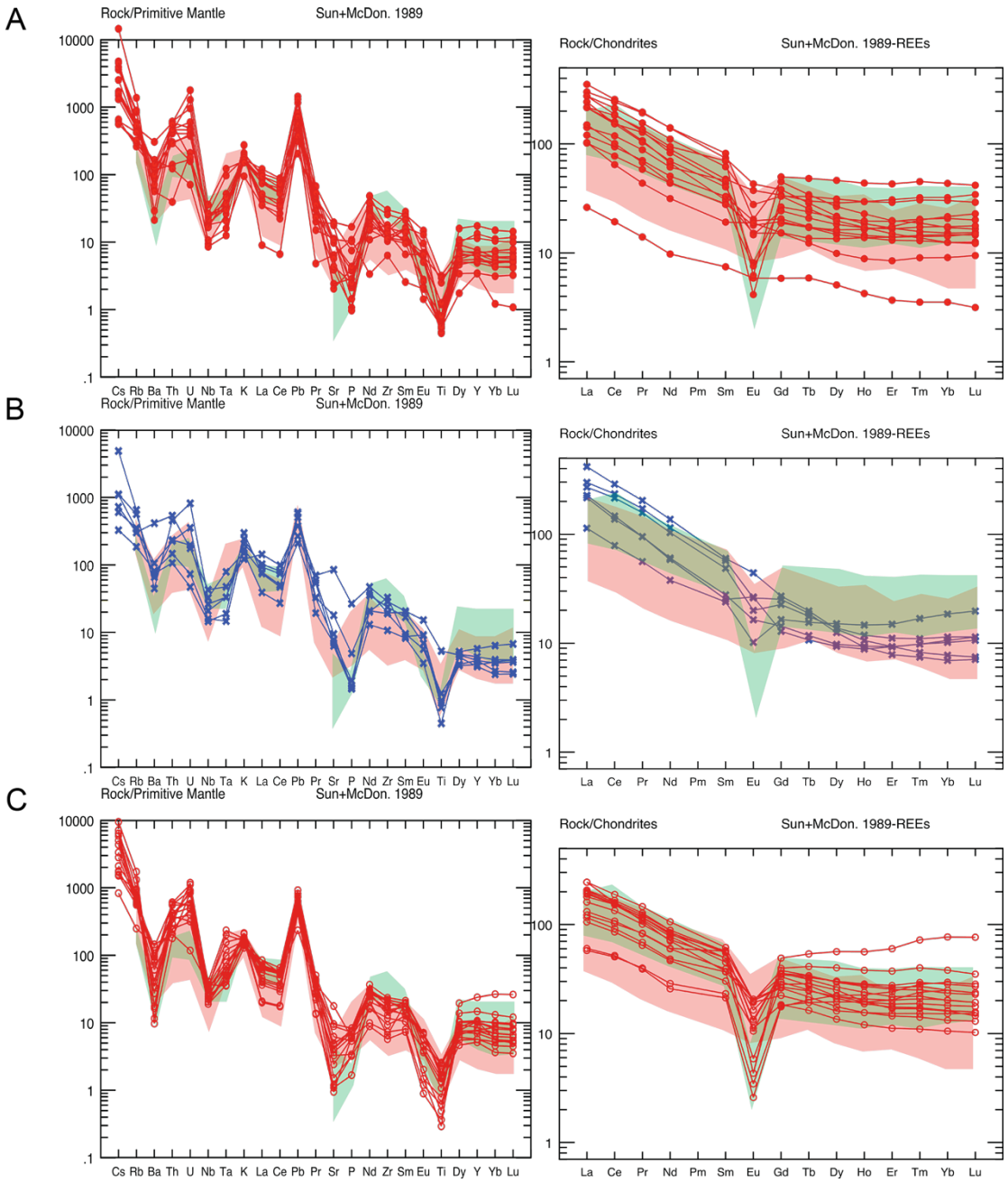

Figure 3.8 Spider diagrams of the Malaysian granitoids (A: Eastern Province Permo-Triassic granitoids, B: Eastern Province Cretaceous granitoids, C: Main Range granitoids) showing the enrichment of HFSE and REE relative to typical Cordilleran I-S granitoids (red shading) (Grosse *et al.*, 2011). These spider diagrams are normalized to primitive mantle (Sun and McDonough, 1989), and the data are plotted with reference to the trace element for Northeastern China A-type granitoids (green shading) as well (Wu *et al.*, 2002).

and Nb, were compared with the Rb/Sr ratios, which have a positive correlation with granite fractionation, in various bivariate diagrams (Figure 3.9). It is seen that the content of the HFSE remains constant with increasing Rb/Sr, suggesting that their enrichment in Malaysian granitoids is not a product of fractionation but possibly a primary concentration inherited from the source. The HFSE enrichment in the Malaysian granitoids is worth noticing because both Sn and W have similar chemical behaviour as these elements. These elements formed larged, highly charged cations, which are not compatible to polymerized framework of granitic magma (Eugster, 1985). They tend to be concentrated in the roof-zones of plutons, where cations are mobile and depolymerization occurs. This implies that high primary Sn and W concentrations could be inherited from the source as well.

3.2.4 Comparison between the Permo-Triassic granitoids and the Cretaceous granitoids

Cretaceous granitoids are found in the Eastern Province, namely in the Stong region and on the Tioman Island. The Cretaceous granitoids does not have distinctive lithological or geochemical differences from the Permo-Triassic granitoids as seen in previous sections. The notable exceptions are the relative depletion of **H**eavy **R**are **E**arth **E**lements (HREE) (i.e. Tb, Dy, Ho, Er, Tm, Yb and Lu) than the Permo-Triassic granitoids (Figure 3.8B). The Cretaceous granitoids are also characterized by low Y/Nb ratios in Eby's (1992) diagram (Figure 3.10). These diagrams were designed for discriminating the plume-related A-type granites (A_1-type) from the post-collisional A-type granites (A_2-type). However, since the Cretaceous granitoids are not depleted in Rb (Figure 3.3B), and many of them do not fall in the A-type geochemical field in Figure 3.7, these diagrams serve for geochemical discrimination of the Cretaceous granitoids

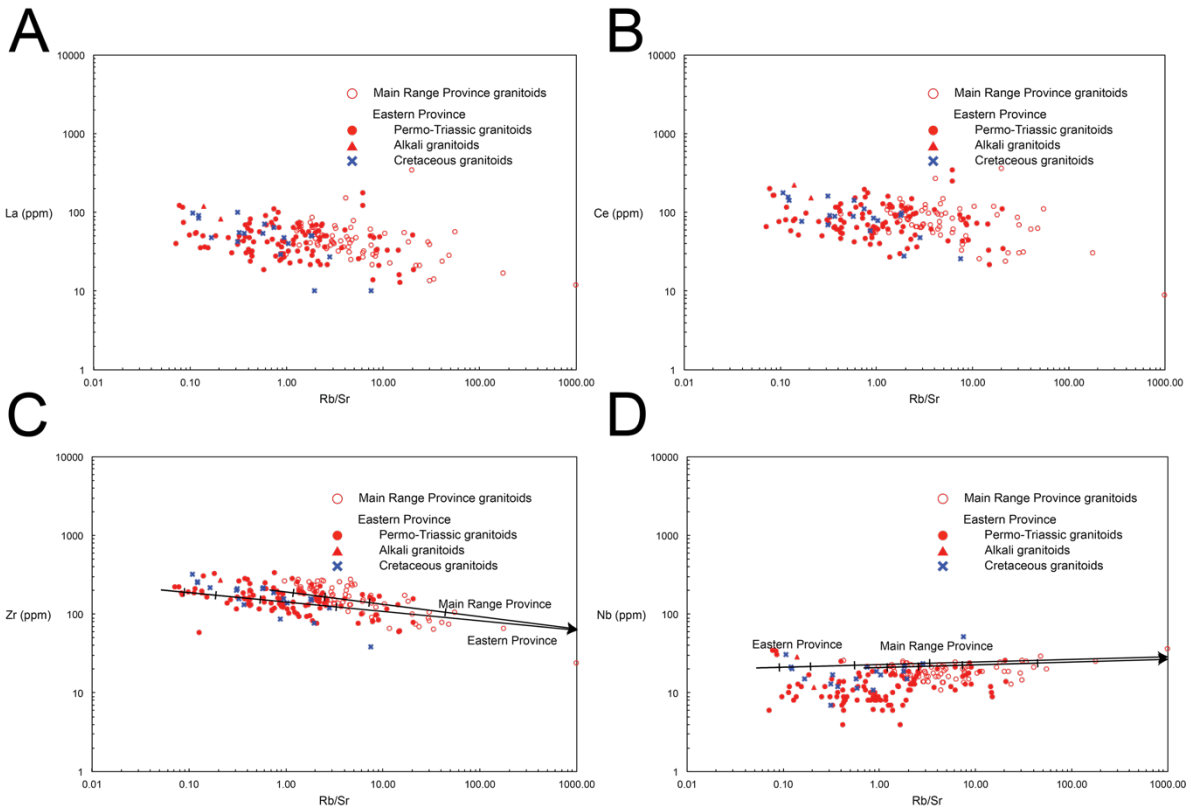

Figure 3.9 Trace element bivariate diagrams of REE (La and Ce) and HFSE (Zr and Nb) against Rb, which has a positive correlation with granite fractionation, showing the enrichment of elements was not significantly affected by granite fractionation. The LLODs were constructed with the removal of plagioclase, K-feldspar, hornblende and biotite with the proportions suggested in Figure 3.5. Partition coefficients suggested by Mahood and Hildreth (1983) and Ewart and Griffin (1994) are adopted in the calculation of LLODs. These values are shown in Appendix A. Each increment represents 20% of bulk fractionation.

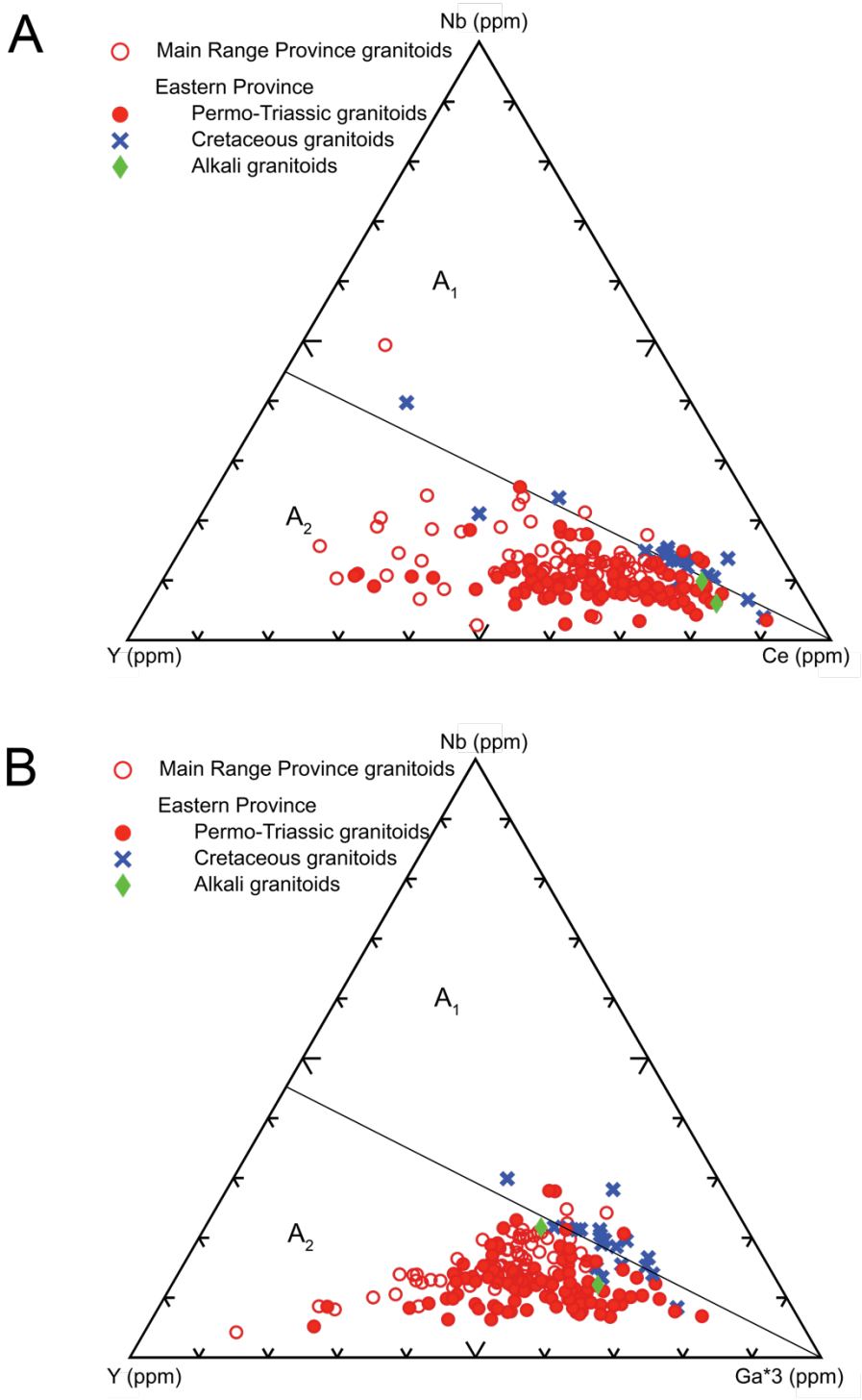

Figure 3.10 Eby's (1992) A-type granite discrimination diagrams showing that the Cretaceous granitoids in the Eastern Province have slightly lower Y/Nb ratios than the dominant Permo-Triassic granitoids.

from the Permo-Triassic Malaysian granites. Hutchison (2007) suggested that the occurrence of Cretaceous rift-related granitoids in the Malay Peninsula could be related to the opening of the Staits of Malacca and the Gulf of Thailand.

3.3 Sr-Nd isotopic analysis

Initial $^{87}Sr/^{86}Sr$ ratios and εNd(*t*) values are often useful as indicators of the nature of the magmatic source for granitoids and have been used to discriminate between I- and S-type granites (Table 3.2) (Cobbing *et al.*, 1986; Chappell and White, 1992; Ghani *et al.*, 2013). In this study, Sr and Nd isotopic data were collected in the Department of Geosciences, National Taiwan University using a **M**ulti-**C**ollector **I**nductively **C**oupled **P**lasma **M**ass **S**pectrometer (MC-ICP-MS), Thermo Electron Finnigan™ Neptune. Detailed sample handling and preparation procedures are described in Lee *et al.* (2012).

3.3.1 Sr-Nd isotopic composition of the Malaysian granitoids

New Sr-Nd isotopic data of the Malaysian granitoids are presented in Table 3.2. It should be noted that the Sr isotopic data for the Main Range granitoids have limited applicability because many of these samples have high (> 10) Rb/Sr ratios resulting in imprecise initial $^{87}Sr/^{86}Sr$ ratio calculations. This is because the calculation involves subtraction of the radiogenic components from the measured $^{87}Sr/^{86}Sr$ ratio. Accordingly, these data are omitted from the discussion. In general, however, the new data of the Eastern Province granitoids show an initial $^{87}Sr/^{86}Sr$ ratio ranging from 0.7004 to 0.7074, while those from the Main Range Province granitoids range from 0.7062 to 0.7159. In contrast, the Nd isotopic data are more reliable, as both Sm and Nd in the isotope system are less mobile than the Rb-Sr pair. The initial Nd isotope ratios for the majority of the Eastern Province granitic samples in the new data range from

TABLE 3.2A. Sr ISOTOPIC DATA OF THE MALAYSIAN GRANITOIDS.

Sample	Rock type	Age (Ma)	Rb (ppm)	Sr (ppm)	$^{87}Rb/^{86}Sr$	$(^{87}Sr/^{86}Sr)_m$	± 2σ	$(^{87}Sr/^{86}Sr)_i$
MA06	Kfs phyric Crd-Bt granite	220.1 ±2.8*	1100	23.0	138	1.030768	1.5E-05	0.5904
MA13	Kfs phyric Ms-Bt granite	225.4 ±1.3	400	85.0	13.6	0.759570	6E-06	0.7159
MA14	Kfs phyric Ms-Bt microgranite	218.3 ±2.4	579	32.0	52.4	0.833845	1.3E-05	0.6713
MA19	Kfs phyric Bt granite	213.9 ±2.9*	381	51.0	21.6	0.771932	1.1E-05	0.7062
MA23	Kfs phyric Bt granite	212.1 ±2.4	444	86.0	15.0	0.756029	5E-06	0.7109
MA26	Kfs phyric Bt granite	215.3 ±2.6	470	105	13.0	0.751779	8E-06	0.7121
MA30	Ms-Bt microgranite	215.9 ±1.7	606	20.0	87.7	0.926408	1.5E-05	0.6572
MA31	Kfs phyric Bt granite	222.4 ±1.8	435	101	12.5	0.754962	9E-06	0.7155
MA36	Kfs phyric Hbl-Bt tonalite	231.9 ±0.9	317	416	2.20	0.728782	9E-06	0.7215
MA39	Migmatitic granite	83.9 ±0.8	192	1790	0.31	0.707854	7E-06	0.7075
MA47	Bt granite	257.6 ±1.6	270	375	2.08	0.712046	9E-06	0.7044
MA48	Syenite	284.2 ±1.6	187	1350	0.40	0.707232	5E-06	0.7056
MA50	Kfs phyric (Hbl)-Bt granite	289.4 ±3.4*	531	136	11.3	0.744183	6E-06	0.6976
MA52	Hbl-Bt granite	248.4 ±1.8	166	394	1.21	0.711707	8E-06	0.7074
MA55	Hbl-Bt granite	270.0 ±1.4	190	82.0	6.71	0.726117	8E-06	0.7004

Note:

All Sr isotope ratios are presented at the 2σ confidence level.

$(^{87}Sr/^{86}Sr)_i = {}^{87}Sr/^{86}Sr - (^{87}Rb/^{86}Sr) \times (e^{\lambda T} - 1)$, $\lambda_{Rb-Sr} = 0.0142\ Ga^{-1}$, $^{87}Rb/^{86}Sr = (Rb/Sr) \times 2.8956$.

All the modern Rb/Sr values in CHUR and DM are suggested by DePaolo (1988) and O'Nions *et al*. (1977).

All the ages are U-Pb zircon ages presented in Chapter 4. Ages in (*) are reference magmatic ages (Chapter 4).

TABLE 3.2B. Nd ISOTOPIC DATA OF THE MALAYSIAN GRANITOIDS.

Sample	Rock type	Age (Ma)	Sm (ppm)	Nd (ppm)	$^{147}Sm/^{144}Nd$	$(^{143}Nd/^{144}Nd)_m$	± 2σ	$f_{Sm/Nd}$	εNd(*t*)	T_{DM} (Ga)	T_{DM2} (Ga)	Nd model age (Ga)
MA06	Kfs phyric Crd-Bt granite	220.1 ±2.8*	8.71	28.3	0.186	0.512213	3.3E-06	-0.05	-8.00	5.16	1.63	1.63
MA13	Kfs phyric Ms-Bt granite	225.4 ±1.3	8.45	39.4	0.130	0.512049	5.5E-06	-0.34	-9.56	1.99		1.99
MA14	Kfs phyric Ms-Bt microgranite	218.3 ±2.4	8.80	37.7	0.141	0.512101	3.2E-06	-0.28	-8.93	2.19	1.72	1.72
MA19	Kfs phyric Bt granite	213.9 ±2.9*	7.57	33.9	0.135	0.512143	2.9E-06	-0.31	-7.98	1.95		1.95
MA23	Kfs phyric Bt granite	212.1 ±2.4	8.67	41.4	0.127	0.512140	3.6E-06	-0.36	-7.82	1.77		1.77
MA26	Kfs phyric Bt granite	215.3 ±2.6	5.99	27.9	0.130	0.512103	2.6E-06	-0.34	-8.60	1.89		1.89
MA30	Ms-Bt microgranite	215.9 ±1.7	3.55	13.4	0.160	0.512132	2.3E-06	-0.19	-8.86	2.86	1.70	1.70
MA31	Kfs phyric Bt granite	222.4 ±1.8	7.53	38.6	0.118	0.512038	2.7E-06	-0.40	-9.48	1.77		1.77
MA36	Kfs phyric Hbl-Bt tonalite	231.9 ±0.9	11.3	65.2	0.105	0.511986	3.0E-06	-0.47	-10.0	1.69		1.69
MA39	Migmatitic granite	83.9 ±0.8	9.18	64.0	0.087	0.512393	3.8E-06	-0.56	-3.60	0.93		0.93
MA47	Bt granite	257.6 ±1.6	6.62	38.7	0.103	0.512358	3.8E-06	-0.47	-2.39	1.09		1.09
MA48	Syenite	284.2 ±1.6	14.6	88.3	0.100	0.512490	4.0E-06	-0.49	+0.62	0.89		0.89
MA50	Kfs phyric (Hbl)-Bt granite	289.4 ±3.4*	1.14	4.56	0.151	0.512358	2.7E-06	-0.23	-3.79	1.92	1.36	1.36
MA52	Hbl-Bt granite	248.4 ±1.8	4.31	20.4	0.128	0.512257	3.3E-06	-0.35	-5.25	1.58		1.58
MA55	Hbl-Bt granite	270.0 ±1.4	12.5	65.5	0.116	0.512364	3.5E-06	-0.41	-2.55	1.22		1.22

Note:

All Nd isotope ratios are presented at the 2σ confidence level.

$(^{143}Nd/^{144}Nd)_i = {}^{143}Nd/^{144}Nd - (^{147}Sm/^{144}Nd) \times (e^{\lambda T} - 1)$, $\lambda_{Sm-Nd} = 0.00654\ Ga^{-1}$, $^{147}Sm/^{144}Nd = (Sm/Nd) \times 0.60456$.

$\varepsilon Nd(t) = [(^{143}Nd/^{144}Nd)_{Sample}(T)/(^{143}Nd/^{144}Nd)_{CHUR}(T) - 1] \times 104$; $(^{143}Nd/^{144}Nd)_{CHUR}(T) = 0.512638 - 0.1967 \times (e^{\lambda T} - 1)$.

$T_{DM} = 1/\lambda_{Sm-Nd} \times ln\{1 + [((^{143}Nd/^{144}Nd)_{Sample} - 0.51315)/((^{147}Sm/^{144}Nd)_{Sample} - 0.2137)]\}$, $f_{Sm/Nd} = [(^{147}Sm/^{144}Nd)/0.1967] - 1$.

$T_{DM2} = T_{DM} - (T_{DM} - t)((-0.4 - f_{Sm/Nd})/(-0.4 - 0.08592))$

All the modern Sm/Nd values in CHUR and DM are suggested by Goldstein *et al.* (1984) and Peucat *et al.* (1988).

All the ages are U-Pb zircon ages presented in Chapter 4. Ages in (*) are reference magmatic ages (Chapter 4).

0.5120 to 0.5123, giving a variety of εNd(t) values ranging from -2.4 to -5.3: (except for MA36 with a rather low εNd(t) value at -10.01 and the Perhentian syenite sample, MA48, with a slight positive value of +0.62). The εNd(t) values calculated for the Main Range Province granitoids are more restricted, varying from -7.8 to -9.6. These data are combined with Cobbing *et al.*'s (1992) and Liew and McCulloch's (1985) isotopic data to form a more representative data set, and presented in Figure 3.11A and B. In the combined data set, the Eastern Province Permo-Triassic granitoids have initial $^{87}Sr/^{86}Sr$ ratios ranging from 0.7004 to 0.7143 and εNd(t) values ranging from -0.7 to -5.8. The Main Range granitoids have initial $^{87}Sr/^{86}Sr$ ratios ranging from 0.7062 to 0.7243 and εNd(t) values ranging from -5.4 to -9.6.

The combined data showed that the Nd isotope ratio is a reliable discriminator of Malaysian granitoids (Figure 3.11). However, the T_{DM} values calculated from the Sm-Nd isotopic values may be unreasonably high if marked fractionation has occurred between Sm and Nd, giving a high $f_{Sm/Nd}$ values compared to the average continental crust where $f_{Sm/Nd}$ = -0.4 (Wu *et al.*, 2002). In such a case, a two-stage neodymium depleted mantle model age (T_{DM2}) may be required to correct for the unrealistically high values obtained, by assuming that the protolith shares the same Sm/Nd ratio as the average continental crust (Keto and Jacobsen, 1987). The Eastern Province granitoids have $f_{Sm/Nd}$ values ranging from -0.23 to -0.56, yielding T_{DM} ranging from 0.89 to 1.92 Ga (Table 3.2). Significant fractionation occurred between Sm and Nd in MA50 ($f_{Sm/Nd}$ = -0.23), T_{DM2} (1.36 Ga) is therefore, adopted as the Nd model age instead of T_{DM} (1.92 Ga). Hence, the Nd model ages of the Eastern Province granitoids range from 0.89 to 1.36 Ga in the new data (Table 3.2). The Main Range Province granitoids have $f_{Sm/Nd}$

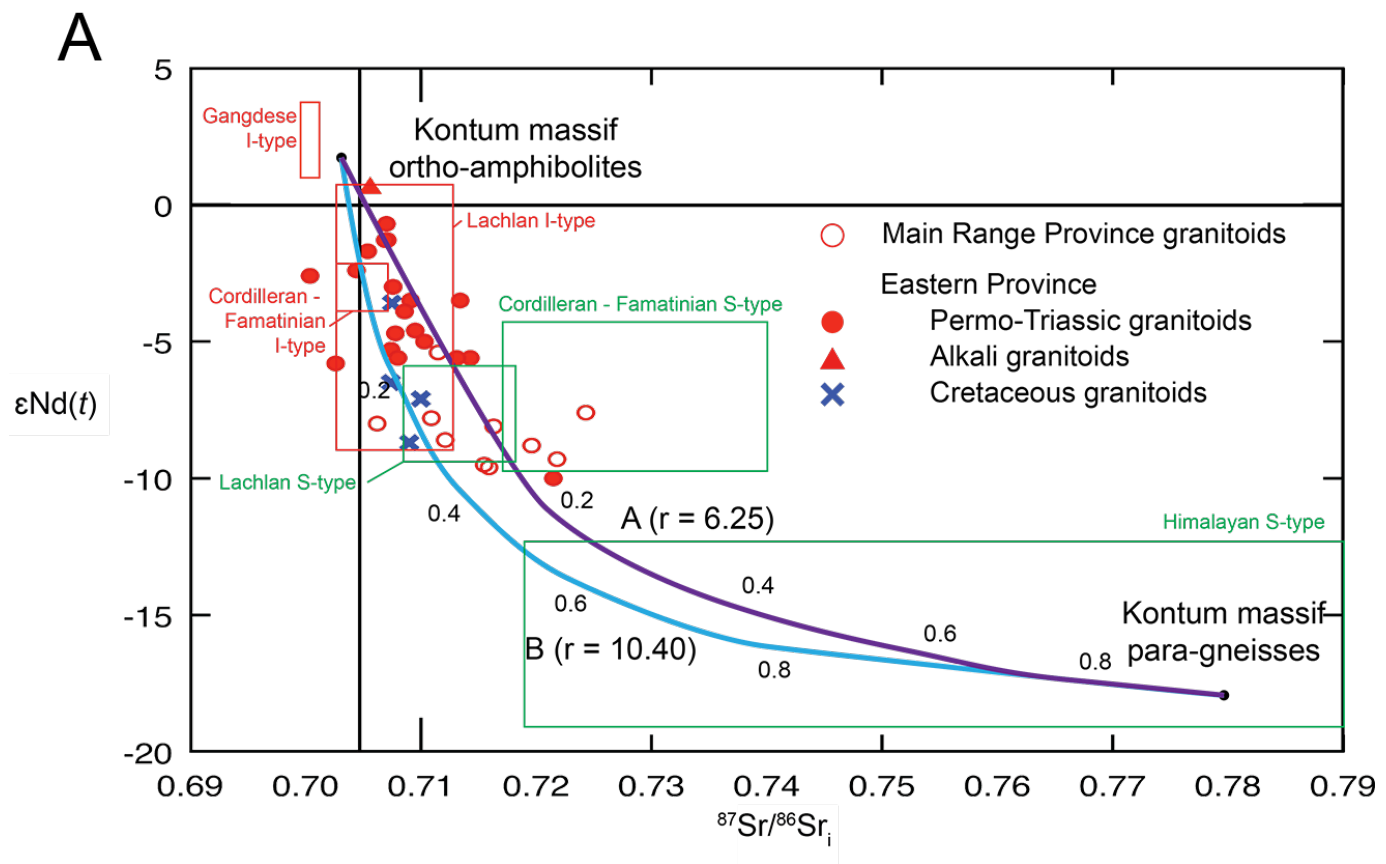

Figure 3.11A Sr-Nd isotope characteristics of the Malaysian granitoids in comparison with other granitic terranes in the world. The Sr-Nd isotope data of the Gangdese I-type granitoids and Himalayan S-type leucogranites were provided by Wen *et al.* (2008) and Guo and Wilson (2012), while those of the Cordilleran – Famatinian I-S granitoids were provided by Grosse *et al.* (2009). The Lachlan Fold Belt Sr-Nd data were provided by Chappell and White (1992). The Kontum massif Sr-Nd data were provided by Lan *et al.* (2003).

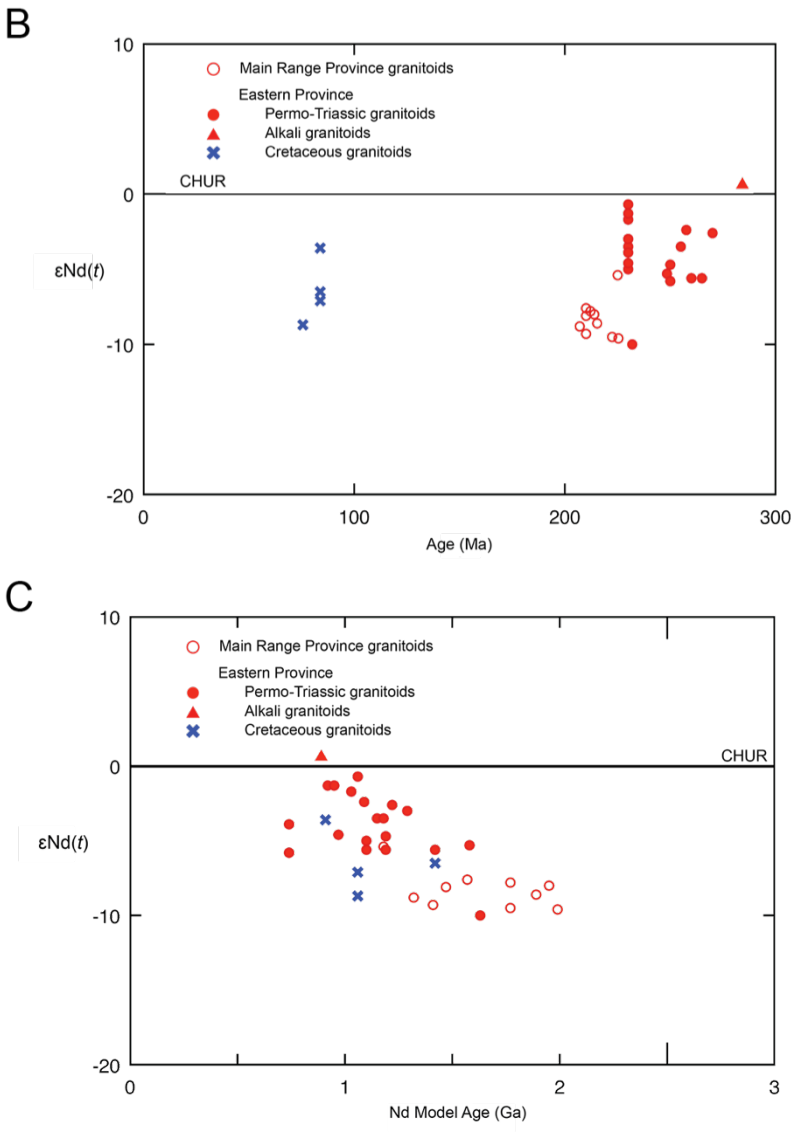

Figure 3.11B and C Nd isotope characteristics of the Malaysian granitoids showing good discrimination between the Eastern Province and Main Range granitoids.

.

values ranging from -0.05 to -0.40. Significant fractionation occurred between Sm and Nd in MA06, MA14 and MA30. T_{DM2} is hence, adopted as Nd model age for these samples. In general, the Main Range Province granitoids have slightly older Nd model ages ranging from 1.63 to 1.99 Ga in the new data (Table 3.2). All these isotopic data are again combined with Cobbing *et al.*'s (1992) and Liew and McCulloch's (1985) isotopic data to form a more representative data set, and presented in Figure 3.11C. In the combined data set, the Eastern Province granitoids have Nd model ages ranging from 0.74 to 1.63 Ga, while those of the Main Range granitoids are ranging from 1.18 to 1.99 Ga.

3.3.2 Comparison of the Malaysian granitoids with other granitic belts in the world

Figure 3.11A also compares the isotopic data of the Malaysian granitoids with other granitic belts in the world. Since the most depleted (igneous-sourced) reservoirs are always plotted in the upper left quadrant, while the most enriched (sedimentary-sourced) reservoirs are always located in the lower right quadrant (Rollinson, 1993). In other words, granites plotting into the upper left quadrant would be purely I-type, while those fell into the lower right quadrant would be close to purely S-type. It is observed that the Gangdese-Ladakh I-type granites and the Himalayan S-type leucogranites could therefore; serve as two end-members of the granitic compositional spectrum. It is worth noting that both of these end-members are not tin-producing. However, the Malaysian Main Range granitoids (and some of the Eastern Province granitoids), Cordilleran – Famatinian S-type granites and the Lachlan Fold Belt S-type granites, which lie between the two end-members, are all tin-producing. Although it is commonly understood that tin deposits are usually associated with S-type granites (Floyd, 1993; Blevin and Chappell, 1995; Grosse *et al.*, 2011), the end-member S-type Himalayan

leucogranites are essentially Sn-barren. Clearly, the two end-members here can be Sn-deficient. However, this may also suggest tin metallogenesis in granites requires the participation of the melts derived from both igneous and sedimentary precursors. Walshe *et al.* (2011) proposed that the input of igneous-sourced melts might sustain a thermal flux in the magmatic system, could induce the segregation of brine and vapour in the magma chamber and the increase of internal fluid pressure. This allows extreme fractionation of the granitoids. However, this proposed mechanism requires further laboratory investigation.

The only comparable example for the Malay Main Range Province granitoids is the Cornubian granites in SW England. Although the Cornubian granites are not as voluminous as the Main Range granitoids, the Sn-W mineralization in both granitic terranes are usually associated with greisen-bordered hydrothermal veins and tourmalinization (Taylor, 1979; Manning, 1986). However, the Cornubian granites are charcherized with late-stage topaz granites, which are enriched in F, Li and P. Such phase is absent in the Main Range, although fluorite is reported in some of the greisenized granites (Plate 2.14c).

3.3.3 Possible source regions of the Malaysian granitoids

Chapter 1 discussed the genesis of granitic magma and suggested that they may form by hybridization of melts derived from igneous and sedimentary precursors (DePaolo, 1988; Keay *et al.*, 1997; Gray and Kemp, 2009; Kemp *et al.*, 2009). Since the Malaysian granitoids lie in between the purely igneous-sourced (I-type) Gangdese-Ladakh granites and the purely sedimentary-sourced (S-type) Himalayan leucogranites, it is likely that the parental magmas of the Eastern and the Main Range Province

granitoids are hybridized melts derived from variable proportions of igneous and sedimentary precursors.

The Kontum massif: Possible source regions for the Malaysian granitoids can be considered by comparing their Sr-Nd isotopic compositions with those of the surrounding basement rocks. Hence, the Sr-Nd isotopic compositions of the Eastern Province granitoids are compared with isotope data obtained from the Kontum massif, an ultrahigh-grade metamorphic complex interpreted as an analogue of the lower continental crust of Indochina. The ortho-amphibolites of the Kontum massif have been interpreted as metamorphosed intraplate basalt, which was dated as Cambro-Ordovician, by Lan *et al.* (2003). These ortho-amphibolites and para-gneisses are essentially enriched in HFSE (Figure 3.12A) (Lan *et al.*, 2003). In Section 3.2.3, it was suggested that the high HFSE concentrations in the sources might contributed to the primary Sn-W enrichment in the Malaysian granitoids. However, no Sn and W data are available in the Kontum massif for such comparison with the average continental crust. The occurrence of the ortho-amphibolites has been linked either with the slab break-off of Proto-Tethyan oceanic lithosphere (Zhu *et al.*, 2012) or to the Pan-African orogeny (Castro *et al.*, 2012; Kawakami *et al.*, 2014) in the Cambro-Ordovician time. The para-gneisses of the Kontum massif have been interpreted as Mesoproterozoic basement of the Indochina continental terrane (Figure 3.12B) (Lan *et al.*, 2003). It is suggested that partial melting of these ortho-amphibolites (initial $^{87}Sr/^{86}Sr$ = 0.7035, $\varepsilon Nd(t)$ = +1.5) and para-gneisses (initial $^{87}Sr/^{86}Sr$ = 0.7800, $\varepsilon Nd(t)$ = -18.0) could provide igneous-sourced and sedimentary-sourced melts respectively for the Eastern Province parental magma. This hypothesis is also supported by the Cambro-Ordovician and

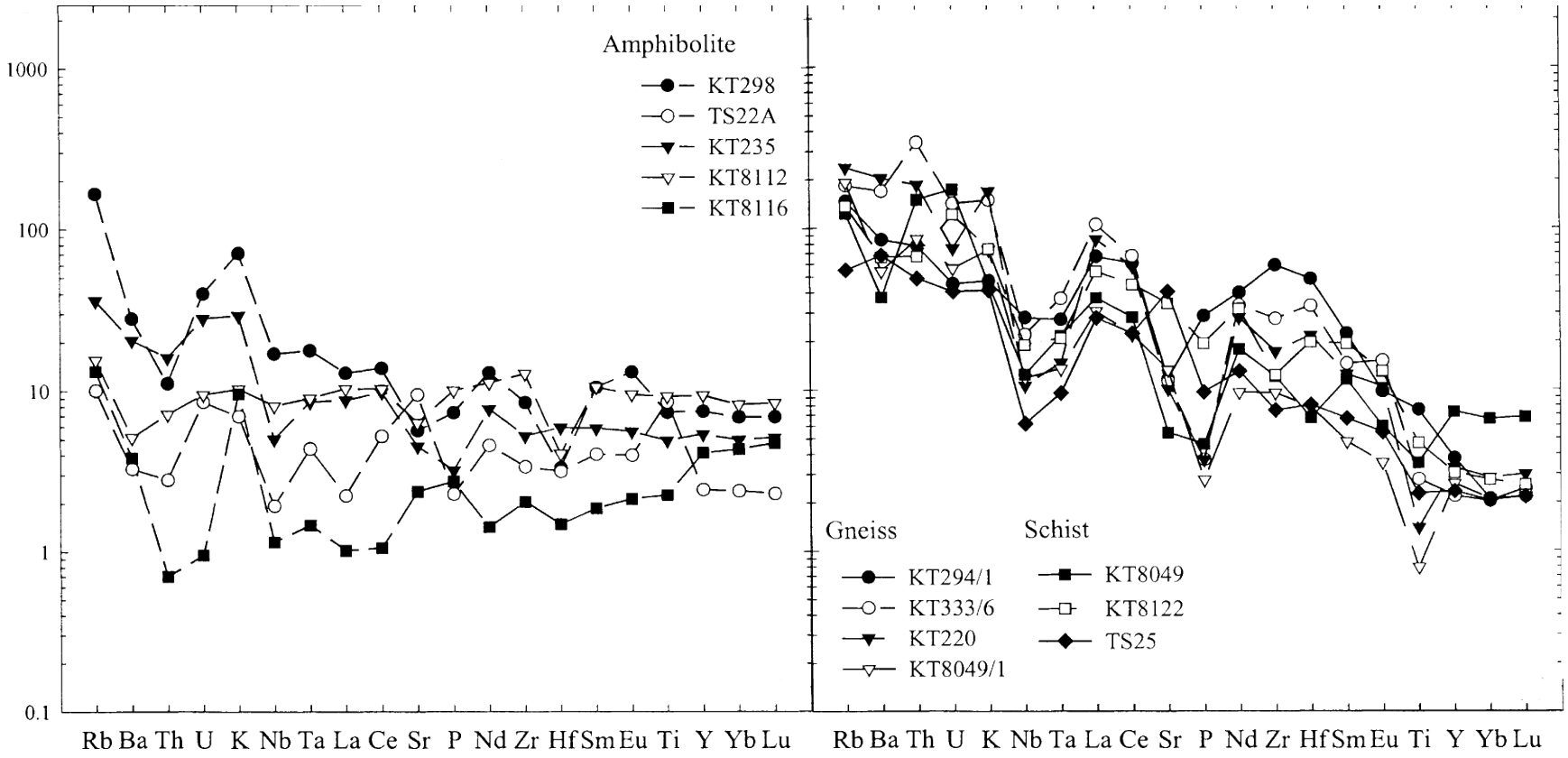

Figure 3.12 Spider diagrams of the Kontum ortho-amphibolites and Kontum para-gneisses provided by Lan *et al.* (2003). TS22A and KT333/6 were selected as end-members in Figure 3.11.

Mesoproterozoic inheritance signature given by the extracted zircons in the Eastern Province granitoids (Chapter 4).

Formation of the Eastern Province parental magma by hybridization of melts derived from Kontum end-members: Two hypothetical mixing curves were constructed between the selected end-members. Curve A uses the Sr and Nd compositions of the Kontum end-member lithologies ($Sr_{igneous}$ = 200 ppm, $Nd_{igneous}$ = 6 ppm, $Sr_{sedimentary}$ = 240 ppm, $Nd_{sedimentary}$ = 45 ppm) (Lan *et al.*, 2003). Curve B uses those of average ocean island and average continental crust as end-members ($Sr_{igneous}$ = 650 ppm, $Nd_{igneous}$ = 25 ppm, $Sr_{sedimentary}$ = 150 ppm, $Nd_{sedimentary}$ = 60 ppm) (Prame andPohl, 1994; Villaseca *et al.*, 1998; Wilson, 2007). It is found that, except for the Berengkat tonalite, which gives extraordinarily low εNd(*t*) values, most of the Eastern Province granitoids were formed from 80-90% of igneous-sourced melt. Since the incorporation of sedimentary-sourced melt is insignificant here, the I-type mineralogy and geochemistry are largely retained in the Eastern Province. It is suggested that the sedimentary involvement in the Eastern Province could give rise to the tin metallogenesis in the highly fractionated granitoids in the province. One possible mechanism is that sedimentary-sourced melt lowered the oxidation state of the Eastern Province parental magma, which promoted the fractionation of Sn into the magma (Lehmann, 1990) and led to the formation of tin deposits after crystal fractionation. This model is supported by the presence of both ilmenite-series granites in the Eastern Province, as discussed in Chapter 2 and in Ishihara *et al.* (1979) and Yeap (1993).

Formation of the Main Range Province parental magma: The Main Range Province hosted by the Sibumasu terrane comprises predominantly biotite granite, with

subordinate amount of Bintang hornblende–biotite granodiorite and adamellite. This implies that the source of the Main Range granitoids would be largely pelitic and psammitic, but small amount of igneous materials were also contributed to form the parental magmas. No Precambrian Sibumasu basement rocks are exposed in the Malay Peninsula. Although high-grade metamorphic rocks were reported in northern and eastern Thailand, no Precambrian ages were reported (MacDonald *et al.*, 2010; Kawakami *et al.*, 2014). Hence, with regards modeling the Main Range granitoids, which were all emplaced into the Sibumasu terrane, there is no basement analogue for source mixing. The Sr-Nd isotopic ratios of samples from the Main Range are nevertheless plotted in Figure 3.11A since they are likely to have been derived from similar precursors as the parental magma of the Eastern Province. This is because the Main Range granitoids also have enriched HFSE signature, with Cambro-Ordovican and Mesoproterozoic inheritance (Chapter 4). These mixing curves show the mixing trend between meta-igneous source and meta-sedimentary source like those found in the Kontum massif. However, the incorporation of sedimentary-sourced melt in the Main Range parental magma is much more significant (up to 40%). This increases the peraluminosity of the Main Range granitoids and does not favour the presence of hornblende (Zen, 1986). Hence, the Main Range Province is dominated by hornblende-free biotite granitoids. The high-degree of involvement of sedimentary-sourced melt also lowered the oxygen fugacity of the Main Range parental magma, producing solely ilmenite-series Main Range granitoids, which favours the formation of tin deposits (Lehmann, 1990).

3.4 Summary

The mineralogical difference between the Eastern Province granitoids and the Main Range Province granitoids is reflected in geochemistry. The Eastern Province granitoids are dominantly hornblende-bearing. They are essentially more sodic, Sr rich, with A/CNK ranging from metaluminous to weakly peraluminous. These agree with the "I-type" definition given by Chappell and White (1974, 1992). The Main Range Province granitoids are generally more potassic, Rb rich and are exclusively peraluminous, except for the hornblende-bearing Bintang Batholith. Nevertheless, discrimination between the Eastern Province granitoids and Main Range Province granitoids using these parameters is not easy, and there is large degree of overlap between the two granitic provinces in terms of granite type and texture, mineralogy, metallogenic affinity and compositional attributes (Figures 3.2 and 3.3). The Harker diagrams (Figure 3.4) and the trace element bivariate plots (Figure 3.5) show that all the Malaysian granitoids can be defined in terms of a largely-overlapping continuous liquid-line-of-descent, in which the Main Range granitoids, or the hornblende-free biotite granites are generally more fractionated than the hornblende-bearing Eastern Province. This supports the field observations that the biotite granites found in the pluton roof-zones are fractionated product of the hornblende-bearing granitic bodies as discussed in Chapter 2. These fractionated granitoids, which are dominant in the Main Range Province but also observed in the Eastern Province, favour tin metallogenesis (Figure 3.6).

Beckinsale (1979) and Cobbing *et al.* (1986, 1992) explained the two "contrasting" granitic provinces in the Malay Peninsula by Chappell and White's (1974) I-S granites model. However, the Malaysian granitoids also differ from the typical Cordilleran I-S granites (e.g. Famatinian arc in NW Argentina), by showing in terms of enrichment in

HFSE and REE (Figures 3.7 and 3.8). The HFSE and REE contents of the Malaysian granitoids remain constant in both unfractionated and fractionated granitoids (Figure 3.9). This suggests that the HFSE anomaly was inherited from the partial melting of enriched sources.

The Sr-Nd isotopic compositions of the Malaysian granitoids assist in distinguishing the granitic provinces from one another and in sources identification. The Eastern Province granitoids generally have low initial Sr ratios (0.7004 – 0.7143), but higher εNd(*t*) values (-0.7 – -5.8) than the Main Range (initial Sr ratios: 0.7062 – 0.7243, εNd(*t*) values: -5.4 – -9.6). Two hypothetical mixing curves were constructed with reference to the Kontum massif (an analogue of Indochinese lower continental crust) (Figure 3.11A). The Kontum massif comprises intraplate ortho-amphibolites and para-gneisses, which could serve as two hypothetical source end-members for the Malaysian granitoids. The model suggests that the geneses of the parental magmas of the Eastern Province and the Main Range Province were related to hybridization of melts derived from both intraplate ortho-amphibolites and para-gneisses, but in differing proportions. The fact that the granites from the two granitic provinces are so similar compositionally and metallogenically, suggests that similar protoliths were involved in their source. These sources are enriched in HFSE and could provide primary Sn-W concentrations to the Malaysian tin granites. In addition, the hybridization of igneous- and sedimentary-sourced melts also promotes fractionation of granitic magma, and hence the Sn metallogenesis in both granitic provinces.

The Eastern Province granitoids are dominantly Permo-Triassic (290-220 Ma) (Chapter 4). Cretaceous granitoids were also found in the Stong region and on Tioman Island in

the Eastern Province. These granitoids do not show significant compositional or geochemical differences from the dominated Permo-Triassic granitoids. However, these Cretaceous granitoids can be discriminated from the Permo-Triassic granitoids by Eby's (1992) diagrams. The Cretaceous granitoids tend to have lower Y/Nb ratios, which put them into the A_1-type geochemical field, while the Permo-Triassic granitoids are in A_2-type geochemical field (Figure 3.10).

Chapter 4 – U-Pb Zircon Geochronology of the Malaysian Granitoids

4.1 Introduction

Existing models for the nature and origin of the tin granite belts in Malaysia have been constructed by Beckinsale (1979) and Cobbing *et al.* (1986, 1992) based largely on the contrasting I- and S-type characteristics of the Eastern Province and Main Range granitoids, respectively. In Chapter 3, the geochemistry of the Malaysian granitoids has been reviewed and it has been shown that the two granitic provinces differ only slightly in terms of their compositional and isotopic characteristics. Existing models also suffer from a paucity of precise time constraints. Previous geochronology has relied on only a few U-Pb zircon ages in addition to numerous K-Ar mica cooling ages and whole-rock Rb-Sr isochron ages (Table 4.1). These studies suggested that the Eastern Province granitoids were formed mainly in the Permo-Triassic periods with a few plutons formed in the Cretaceous, while the Main Range granitoids were emplaced mainly in the Triassic. The K-Ar mica cooling ages and the whole-rock Rb-Sr isochron ages are generally imprecise as the parent and daughter isotopes in the Rb-Sr system are extremely mobile in magmatic-hydrothermal systems and readily reset, while K-Ar ages only represent the cooling age of the rock through the closure temperatures of muscovite and biotite (350-300 °C) (Searle *et al.*, 2012). It is now widely accepted that these methods do not produce reliable crystallization ages for rocks such as the highly mineralized granitoids of the Malay Peninsula. The robustness of the U-Pb isotope system in zircon makes it the preferred method for granitoid dating and, since the development of high spatial resolution U-Pb isotopic analysis using microbeam methods (e.g. SIMS), this has become routine, allowing for the rapid and precise determination of both crystallization ages and possible inherited ages in zircon cores.

TABLE 4.1 SUMMARY OF THE RADIOMETRIC DATING OF THE MALAYSIAN GRANITOIDS PRIOR TO THIS STUDY, DATA COMPILATION AFTER GHANI (2009)

Province	Location	Rb-Sr isochron age (Ma)	K-Ar mica age (Ma)	U-Pb zircon age (Ma)
Eastern Province – Eastern Belt	Bekok[1]		218	
	Belumut[1]		231-234	
	Bidang[1, 2]	213 ±4	140-229	
	Bukit Batu[1]		224	
	Dura[2]	240 ±10		
	Kerai[2]	205 ±25		
	Lata Tungil[3]	215 ±10		
	Lunchoo[2]	217 ±6	205-218	
	Nal[2]	230 ±4		
	Panchor[2]	197 ±30	200	
	Saok[1, 4]		234-262	257
	Chukai[5]		240-243	
	Kemaman[1, 5]		253-275, 327, 271	
	Kuantan[1, 4, 5, 6, 7]		252, 207-247	263
	Paka[1, 4]		220	227
	Sungai Lembing[1, 5]		156	
Eastern Province – Central Belt	Batang Melaka[1, 8]		69-72, 81.9 ±1.1	
	Stong – Kenerong[1, 2]	79 ±3	65	
	Stong – Noring[2]	90 ±3		
	Benom[1, 2, 3]	207 ±7, 219 ±10	123-199, 169	
Main Range Province	Jerai (pegmatite)[1]		47, 59-137	
	Langkawi[1, 8]		79.1 ±0.8, 82	
	Bukit Mor[1]		135-164	
	Kledang Range[1, 8]		198-213, 193-216, 203	

Province	Location	Rb-Sr isochron age (Ma)	K-Ar mica age (Ma)	U-Pb zircon age (Ma)
	Ipoh East[8]		176-204, 193-209	
	Cameron Highlands[8]		105-205	
	Bukit Tinggi[1]		237	
	Ampang[1]		202	
	Berenang[1, 2, 4, 9]	215 ±2	124-214, 156-218	211-215
	Bubu (Bintang)[1, 4]	198		
	Bujang Melaka[1, 2, 5]	207 ±14, 194	192-208, 203-210	
	Dingdings[1, 2]	213 ±7	173-186	
	Genting Sempah[1, 4]		198	219
	Jelutong[2]	211 ±9		
	Jor Dam[1]		100-199	
	Kajang[9]		134-188, 170-217	
	Kulim – Bongsu[1,2]	224 ±5	196-201	
	Penang – Batak[1, 4, 10]		180-199, 185-194	215
	Penang – Bunga[1, 4, 10]	220 ±31	68-204	
	Penang – Feringgi[1, 2, 4, 10]	212 ±7		
	Selama[2]	230 ±9		
	Seremban[1, 9]		82-173, 160-201	
	Sik[1]		135-190, 178	
	Sungai Baru[1]		156	
	Tampin[1, 2]	225 ±12	81-179	
	Tranum[1, 4]		160-165	208
	Ulu Kali[1, 4, 9, 12]	206	93-148, 177	198-206
	Wing Sang Cheong[12]		198-202	

Note: Ages are provided by [1]Bignell and Snelling (1977), [2]Darbyshire (1988), [3]Cobbing *et al.* (1992), [4]Liew (1983), [5]Schwartz and Askury (1990), [6]Liew and McCulloch (1985), [7]Yap (1986), [8]Krähenbuhl (1991), [9]Kwan (1990), [10]Kwan and Yap (1986), [11]Liew and Page (1985) and [12]Yap and Kwan (1984).

Before this work, only twenty reliable U-Pb zircon ages for the Malaysian granitoids were available (Table 4.1). They were mainly obtained from granitoids collected along the eastern and western coast of the Malay Peninsula, and in Singapore (Liew, 1983; Liew and McCulloch, 1985; Liew and Page, 1985; Oliver *et al.*, 2014; Searle *et al.*, 2012). More extensive high precision U-Pb geochronology on the Malaysian granitoids is clearly necessary for the reconstruction of the Malaysian tectonic framework. Thirty-nine new U-Pb zircon ages have been obtained in our study and will be presented in the next section. Twenty-four samples from the Eastern Province and fifteen samples from the Main Range Province were analyzed. Most of the rock samples were collected from road-cuts and quarries. Samples from the Stong region were mainly collected from riverside outcrops along the Kenerong and Renyok Rivers. Samples collected from outlying islands like Perhentian, Tioman, Penang, Langkawi and Ubin were from fresh shoreline outcrops.

4.2 U-Pb zircon geochronology

High-spatial resolution, high-precision secondary ionization mass spectrometry (SIMS) was used to analyze the U-Pb isotopic composition of the extracted zircons. The grains were extracted from rock samples by standard disaggregation, heavy liquid (bromoform) separation and magnetic separation procedures. Handpicked zircons were then mounted in epoxy, polished and imaged using a Robinson cathodoluminescence detector, mounted to a Hitachi S4300 Scanning Electron Microscope (SEM). U-Pb isotope ratios were collected using a Cameca IMS1280 ion microprobe at the NordSIM facility, Swedish Museum of Natural History, Stockholm, following the protocols described by Whitehouse *et al.* (1999) and Whitehouse and Kamber (2005). Discussion of the data is presented in groups according to the geographical locality of samples. Data are

summarized in Tables 4.2 and 4.3, and the ages obtained were mapped on Figure 4.1. Selected cathodoluminescence (CL) images of dated zircons and Tera-Wasserburg concordia diagram interpretations of all analyzed samples are presented in Figures 4.2 and 4.3 respectively. Given the ubiquitous presence of post-crystallization, possibly recent, Pb-loss causing a skewed age dispersion towards apparently younger ages, as well as the presence in some zircons of clear inherited cores, we used a consistent filtering approach to extract the probable crystallization age. This involved initially excluding any obvious older cores. This is followed by rejecting the youngest analyses ($^{238}U/^{206}Pb$ age) interpreted on the basis of CL images to belong to the main magmatic crystallization group, which most likely reflect Pb-loss, until the remaining group of ages yielded a concordia age, *sensu* Ludwig (1998), with a statistically significant low **M**ean **S**quare **W**eighted **D**eviation (MSWD). This value indicates the coherence of data, comparing with analytical uncertainties. Value less than the unity indicates the analytical uncertainties have been overestimated, while if it is greater than the unity, either the uncertainties were underestimated or other geological scatters are present. The rule of thumb is MSWD less than 1.50 is considered as acceptable. In general, we consider concordia ages obtained from five or more pooled analyses to be robust indicators of the magmatic crystallization age, while those incorporating fewer analyses are given as reference ages that are accorded somewhat lower significance in our interpretation. All ages are presented at 2σ (or, where appropriate, 95% confidence level) including decay constant errors, with the MSWD value representing that of both concordance and equivalence following the recommendation of Ludwig (1998). Decay constants follow the recommendations of Steiger and Jäger (1977).

TABLE 4.2A. ZIRCON PROPERTIES OF THE EASTERN PROVINCE PERMO-TRIASSIC GRANITOIDS.

Sample No.	Location	Zircon Size in Diameter (nm)	Zircon Shape	Core	Texture	U Content in Age Yielding Group (ppm)	Th/U Ratio in Age Yielding Group	Highest U Grain in the Sample (ppm)
MA33	Penjom Gold Mine	100-200	Mainly fragmented	CL-bright	Faint oscillatory zoning	440-3200	0.46-1.93	32200
MA36	Berengkat – Kampong Jerek	80-200	Well-faceted prisms	Both CL-dark and CL-bright can be found	Core-rim, faint oscillatory zoning	270-1100	0.11-1.52	1500
MA42	Berengkat – Renyok River	100-250	Well-faceted prisms	Both CL-dark and CL-bright can be found	Cloudy, core-rim, clear oscillatory zoning	1300-3900	0.09-0.69	56400
MA47	Perhentian Island	100-220	Well-faceted prisms	CL-dark	Clear oscillatory zoning	1100-4100	0.14-0.39	4700
MA48		100-200	Well-faceted prisms	Both CL-dark and CL-bright can be found	Cloudy, core-rim, clear oscillatory zoning	340-1200	0.19-1.14	3200
MA50	Maras-Jong	100-220	Well-faceted prisms	Most of them are CL-dark, some are CL-bright	Core-rim, faint oscillatory zoning	3700-7000	0.13-0.65	9400
MA51	Kapal Range	50-220	Well-faceted prisms	CL-bright	Core-rim, clear oscillatory zoning	410-2000	0.39-0.53	8000
MA52	Boundary Range	50-180	Well-faceted prisms	Both CL-dark and CL-bright can be found	Clear oscillatory zoning	660-3200	0.27-0.95	30100
MA54	Kerteh	50-220	Fragmented	CL-bright	Homogenous unzoned to faint oscillatory zoning	180-380	0.40-0.76	1300

Sample No.	Location	Zircon Size in Diameter (nm)	Zircon Shape	Core	Texture	U Content in Age Yielding Group (ppm)	Th/U Ratio in Age Yielding Group	Highest U Grain in the Sample (ppm)
MA55	Kuantan	50-150	Well-faceted prisms	CL-dark	Clear oscillatory zoning	420-3200	0.29-0.63	6800
MA66	Minyak Beku	50-180	Fragmented	CL-dark	Faint oscillatory zoning	380-2200	0.09-0.96	12600
MA68	Batu Pahat – Hanson	50-100	Well-faceted prisms	Both CL-dark and	Core-rim, clear	490-3200	0.11-0.66	16400
MA69	Quarry	50-120	and fragments	CL-bright can be found	oscillatory zoning	590-3900	0.31-0.52	22000
MA73	Ubin Island	80-180	Well-faceted prisms	CL-bright	Faint oscillatory zoning	210-660	0.57-0.66	2500
MA76	Musoh River Mouth	80-180	Fragmented	CL-medium to CL-bright	Faint oscillatory zoning	240-1500	0.61-1.06	29000
MA104	Jemaluane – Kluang	80-200	Well-faceted prisms	CL-dark	Faint oscillatory zoning	690-890	0.58-0.98	10200
MA109	Kemahan	80-220	Well-faceted prisms	CL-bright	Core-rim, clear oscillatory zoning	440-920	0.15-0.25	1800

TABLE 4.2B. ZIRCON PROPERTIES OF THE EASTERN PROVINCE CRETACEOUS GRANITOIDS.

Sample No.	Location	Zircon Size in Diameter (nm)	Zircon Shape	Core	Texture	U Content in Age Yielding Group (ppm)	Th/U Ratio in Age Yielding Group	Highest U Grain in the Sample (ppm)
MA43	Kenerong - Renyok River	50-100	Well-faceted prisms	CL-bright	Clear oscillatory zoning	450-1200	1.55-4.05	6600
MA45	Noring	120-220	Well-faceted prisms	CL-bright	Clear oscillatory zoning	620-2300	0.50-1.70	3000
MA78	Tioman Island	80-150	Well-faceted prisms	CL-bright	Homogenous unzoned, cloudy	60-1600	0.45-1.25	5900
MA90		50-100	Well-faceted prisms	Both CL-dark and CL-bright can be found	Homogenous unzoned, cloudy, core-rim	50-730	1.40-1.79	85400
MA91		50-100	Well-faceted prisms	Both CL-dark and CL-bright can be found	Homogenous unzoned, cloudy, core-rim	220-810	0.36-0.58	376600
MA97		80-220	Well-faceted prisms	CL-bright	Cloudy, core-rim, faint oscillatory zoning	120-750	0.55-1.86	1100
MA100		80-220	Well-faceted prisms	CL-medium to CL-bright	Homogenous unzoned, cloudy, core-rim	90-300	0.59-1.07	1700

TABLE 4.2C. ZIRCON PROPERTIES OF THE MAIN RANGE PROVINCE GRANITOIDS.

Sample No.	Location	Zircon Size in Diameter (nm)	Zircon Shape	Core	Texture	U Content in Age Yielding Group (ppm)	Th/U Ratio in Age Yielding Group	Highest U Grain in the Sample (ppm)
MA06	Cameron Highlands	50-150	Well-faceted prisms	Both CL-dark and CL-bright can be found	Clear oscillatory zoning	320-1200	0.08-0.73	47400
MA07		50-150	Well-faceted prisms	CL-dark	Homogenous unzoned, cloudy	1500-8500	0.35-1.17	19300
MA13		100-250	Well-faceted prisms	CL-bright	Core-rim, clear oscillatory zoning	100-320	0.27-0.76	4040
MA14		80-200	Well-faceted prisms and fragments	CL-bright	Core-rim, faint oscillatory zoning	460-1500	0.04-0.69	1510
MA15	Ipoh	40-220	Well-faceted prisms	Both CL-dark and CL-bright can be found	Core-rim, faint oscillatory zoning	280-3000	0.13-1.03	5320
MA16	Taiping	40-200	Well-faceted prisms and fragments	Both CL-dark and CL-bright can be found	Clear oscillatory zoning	480-1820	0.11-1.17	8440
MA19	Penang Island	80-300	Well-faceted prisms and fragments	CL-bright	Core-rim, faint oscillatory zoning	240-1450	0.23-0.61	5540
MA20		80-300	Well-faceted prisms and fragments	CL-dark	Core-rim, faint oscillatory zoning	770-1460	0.40-0.54	6520
MA23		40-300	Well-faceted prisms and fragments	CL-bright	Core-rim, faint oscillatory zoning	70-520	0.33-0.73	950
MA26	Langkawi Island	150-300	Well-faceted prisms	CL-bright	Core-rim, faint	160-720	0.13-1.35	4450

Sample No.	Location	Zircon Size in Diameter (nm)	Zircon Shape	Core	Texture	U Content in Age Yielding Group (ppm)	Th/U Ratio in Age Yielding Group	Highest U Grain in the Sample (ppm)
					oscillatory zoning			
MA30		150-300	Well-faceted prisms	CL-bright	Core-rim, faint oscillatory zoning	160-660	0.25-0.68	2340
MA29	Tuba Island	120-280	Fragmented	CL-bright	Core-rim, faint oscillatory zoning	450-1550	0.12-0.41	3965
MA31	Kuala Lumpur	50-150	Well-faceted prisms	CL-bright	Core-rim, clear oscillatory zoning	540-1160	0.10-0.94	6180
MA62	Bukit Mor	50-120	Well-faceted prisms	CL-dark	Clear oscillatory zoning	360-1020	0.46-0.90	3040
MA110	Genting Sempah	80-220	Fragmented	CL-dark	Core-rim, clear oscillatory zoning	650-1480	0.19-0.68	4710

TABLE 4.3A. U-PB ZIRCON AGES OF THE EASTERN PROVINCE GRANITOIDS

Sample No.	Lithology	Location			Age (Ma)	MSWD of conc. & equiv.	n-total	n-age cluster
MA33	Felsite dyke	Penjom Gold Mine	N04°08'40.0"	E101°59'29.3"	222.4 ±1.8	1.20	32	5
MA36	Kfs phyric Hbl-Bt tonalite	Berengkat – Kampong Jerek	N05°08'22.2"	E101°58'49.5"	231.8 ±1.7	0.95	20	5
MA42	Migmatitic tonalite	Berengkat – Renyok River	N05°34'47.1"	E101°52'25.5"	220.4 ±3.9*	2.40	12	4
MA47	Bt granite	Perhentian Island	N05°55'16.5"	E102°43'23.9"	257.6 ±1.6	0.62	12	9
MA48	Syenite				284.2 ±1.6	1.17	33	10
MA50	Kfs phyric (Hbl)-Bt granite w/ Qtz-Tour miarolitic cavities	Maras-Jong	N05°20'47.6"	E103°02'12.5"	289.3 ±2.4*	1.15	20	4
MA51	Hbl-Bt granite	Kapal Range	N05°09'04.2"	E102°46'59.2"	247.8 ±1.7	0.53	25	7
MA52	Hbl-Bt granite	Boundary Range	N04°59'21.6"	E102°28'53.3"	248.4 ±1.8	1.60	12	7
MA54	Kfs-Pl phyric dacite	Kerteh	N04°37'12.1"	E103°24'20.8"	250.5 ±1.7	0.60	38	7
MA55	Hbl-Bt granite	Kuantan	N03°50'19.7"	E103°21'07.1"	270.0 ±1.4	1.40	25	12
MA66	Cpx-Hbl-Bt granite	Minyak Beku	N01°49'08.8"	E102°54'37.3"	222.2 ±1.8	0.96	15	5
MA68	Kfs phyric Bt microgranite	Batu Pahat – Hanson Quarry	N01°49'01.0"	E102°54'50.9"	227.2 ±1.9	0.67	15	5
MA69	Kfs phyric Bt granite				225.5 ±2.5*	0.24	15	3
MA73	Migmatitic granite	Ubin Island	N01°24'29.0"	E103°59'21.8"	231.0 ±2.6*	2.10	15	3
MA76	Kfs phyric rhyolite	Musoh River Mouth	N01°22'13.0"	E104°16'50.9"	238.5 ±1.7	1.02	15	6
MA104	Kfs phyric Hbl-Bt granite	Jemaluane – Kluang	N02°18'10.4"	E103°39'25.2"	244.5 ±3.1*	1.70	15	3
MA109	Kfs phyric Bt granite	Kemahan	N05°49'11.1"	E101°56'07.2"	226.7 ±2.2	2.00	15	5

Note: Ages with (*) represent reference ages yielded by a group of less than five but more than three pooled analyses in the Tera-Wasserburg diagram.

TABLE 4.3B. U-PB ZIRCON AGES OF THE CRETACEOUS GRANITOIDS IN THE EASTERN PROVINCE

Sample No.	Lithology	Location			Age (Ma)	MSWD of conc. & equiv.	n-total	n-age cluster
MA43	Leucogranitic dyke	Kenerong - Renyok River	N05°34'47.1"	E101°52'25.5"	83.9 ±0.8	0.70	12	7
MA45	Kfs phyric Hbl-Bt granite	Noring	N05°39'42.5"	E101°41'26.7"	75.7 ±0.6	1.17	20	5
MA78	Cpx-Hbl-Bt granite	Tioman Island	N02°48'26.1"	E104°09'20.0"	80.1 ±0.6	1.20	15	7
MA90	Microgranitic dyke		N02°43'06.9"	E104°10'27.0"	80.2 ±0.7	1.50	15	5
MA91	Diorite				81.5 ±0.7	1.40	14	5
MA97	Ms-Tour granite		N02°49'48.8"	E104°11'44.2"	79.7 ±0.7	1.01	15	5
MA100	Migmatitic granite		N02°46'39.4"	E104°12'59.9"	80.7 ±0.5	1.30	14	8

Note: Ages with (*) represent reference ages yielded by a group of less than five but more than three pooled analyses in the Tera-Wasserburg diagram.

TABLE 4.3C. U-PB ZIRCON AGES OF THE MAIN RANGE PROVINCE GRANITOIDS.

Sample No.	Lithology	Location			Age (Ma)	MSWD of conc. & equiv.	n-total	n-age cluster
MA06	Kfs phyric Crd-Bt granite	Cameron Highlands	N04°33'50.4"	E101°11'55.4"	220.1 ±2.8*	1.60	34	4
MA07	Fe-stainning Bt granite				219.4 ±1.5	0.57	20	6
MA13	Kfs phyric Ms-Bt granite		N04°35'00.3"	E101°24'24.5"	225.4 ±1.3	1.09	38	10
MA14	Kfs phyric Ms-Bt microgranite		N04°34'49.5"	E101°20'22.8"	218.3 ±2.4	1.18	11	9
MA15	Kfs phyric Ms-Bt granite	Ipoh	N04°32'56.1"	E101°01'46.8"	220.1 ±1.0	0.79	20	13
MA16	Kfs phyric Hbl-Bt granite	Taiping	N04°46'54.9"	E100°44'11.0"	215.7 ±1.6	1.09	20	7
MA19	Kfs phyric Bt granite	Penang Island	N05°27'48.0"	E100°13'58.9"	213.9 ±2.9*	0.38	11	4
MA20	Kfs phyric microgranite		N05°28'13.5"	E100°11'31.1"	215.5 ±1.5*	1.50	10	4
MA23	Kfs phyric Bt granite		N05°16'11.3"	E100°16'57.3"	212.1 ±2.4	1.60	20	6
MA26	Kfs phyric Bt granite	Langkawi Island	N06°24'11.4"	E99°48'12.3"	215.3 ±2.6	1.90	12	6
MA30	Kfs phyric Ms-Bt microgranite		N06°17'56.9"	E99°51'10.1"	215.9 ±1.7	0.58	12	6
MA29	Ms-Bt microgranite	Tuba Island	N06°15'45.6"	E99°51'02.1"	200.8 ±2.0*	1.90	34	4
MA31	Kfs phyric Bt granite	Kuala Lumpur	N03°19'39.6"	E101°44'52.0"	222.4 ±1.8	0.91	35	5
MA62	Kfs phyric Bt granite	Bukit Mor	N01°58'32.8"	E102°40'24.5"	217.4 ±1.2	1.20	15	6
MA110	Qtz phyric Opx dacite	Genting Sempah	N03°21'10.9"	E101°48'39.9"	226.2 ±1.2	1.30	15	6

Note: Ages with (*) represent reference ages yielded by a group of less than five but more than three pooled analyses in the Tera-Wasserburg diagram.

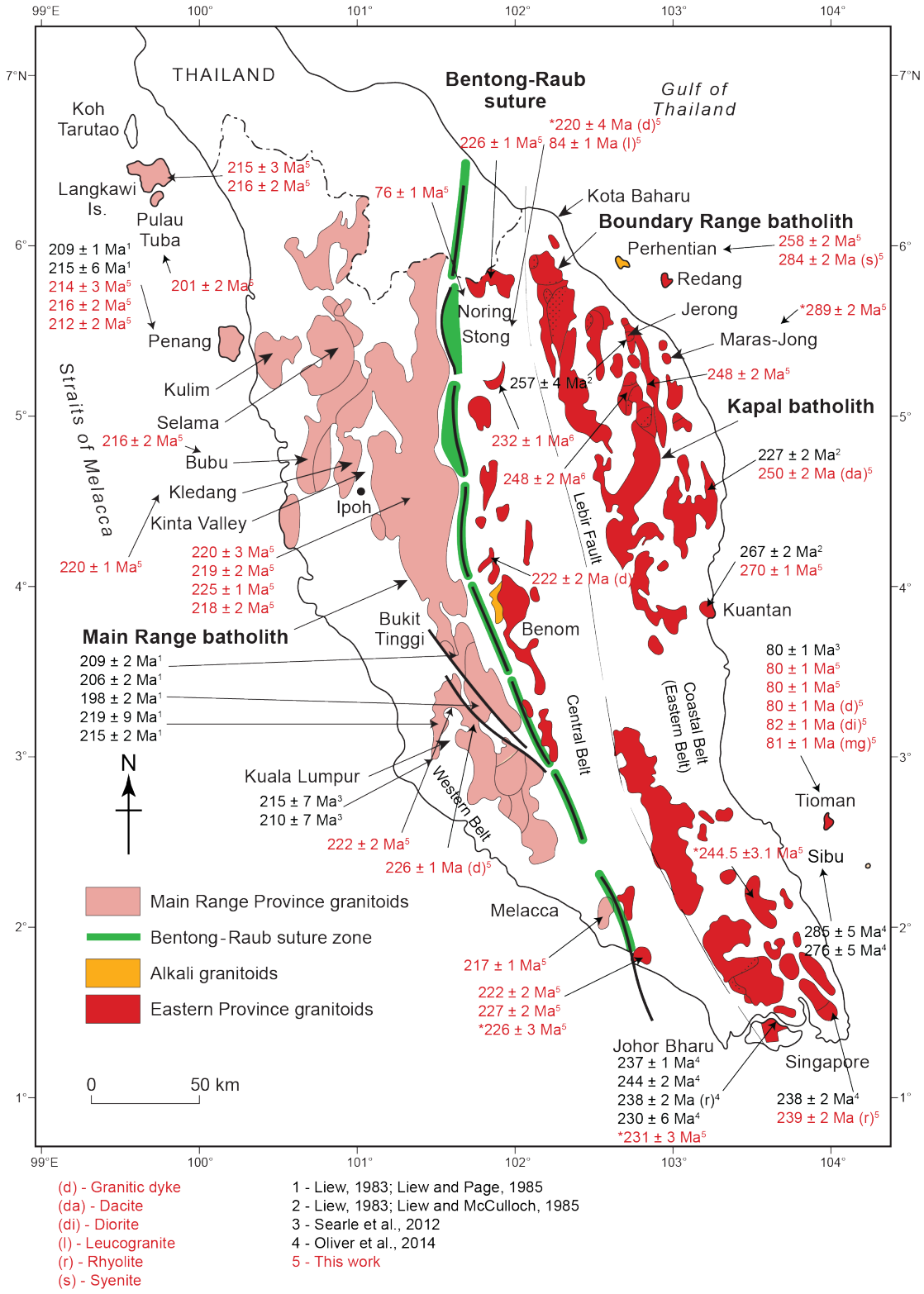

Figure 4.1 U-Pb zircon ages of the Malaysian granitoids presented in this research (in red) and those provided by previous workers (Liew, 1983; Liew and McCulloch, 1985; Liew and Page, 1985; Searle *et al.*, 2012; Oliver *et al.*, 2014) (in black).

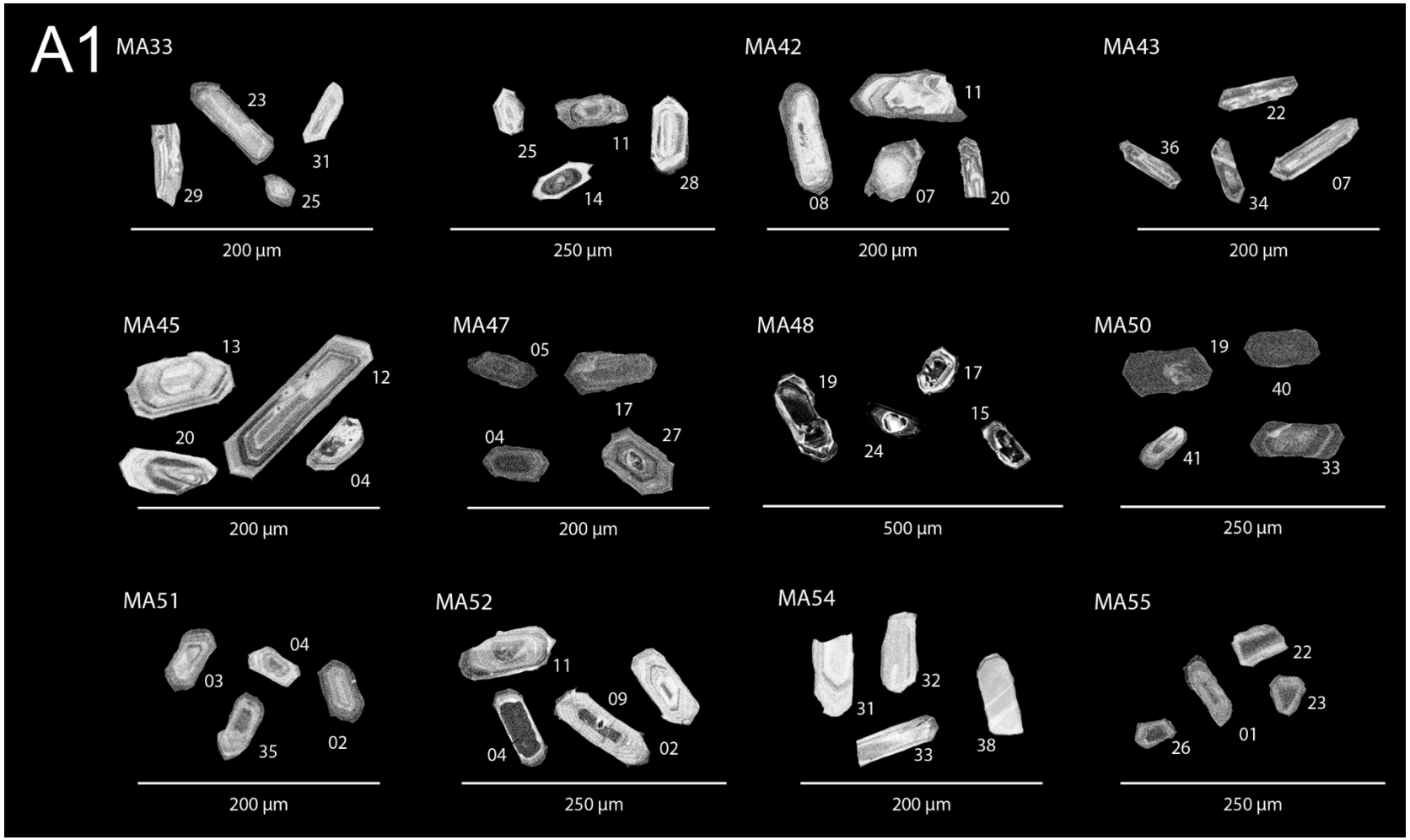

Figure 4.2A Representative cathodoluminescence (CL) images of extracted zircons from the Eastern Province granitoids.

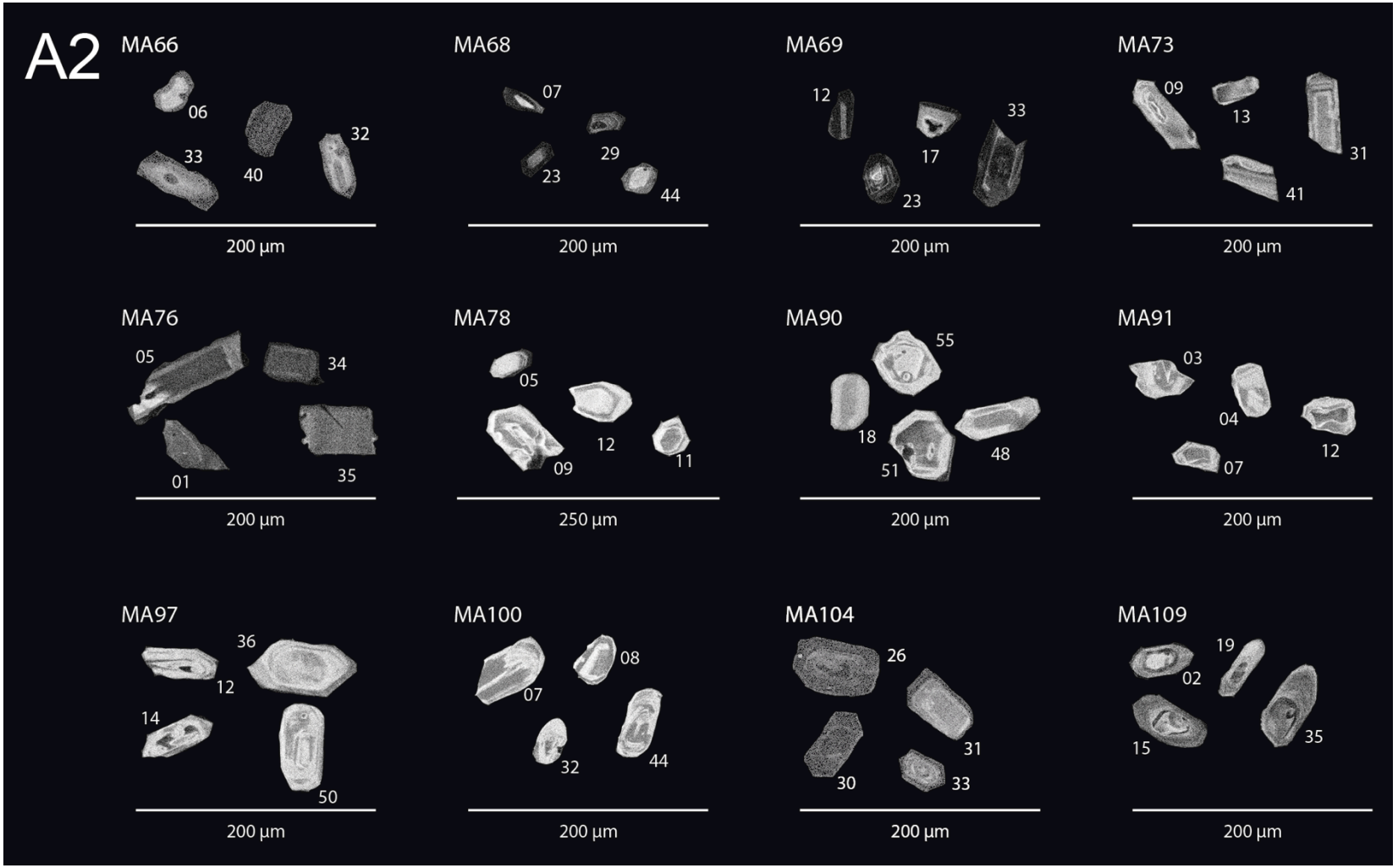

Figure 4.2A (Cont'd) Representative cathodoluminescence (CL) images of extracted zircons from the Eastern Province granitoids.

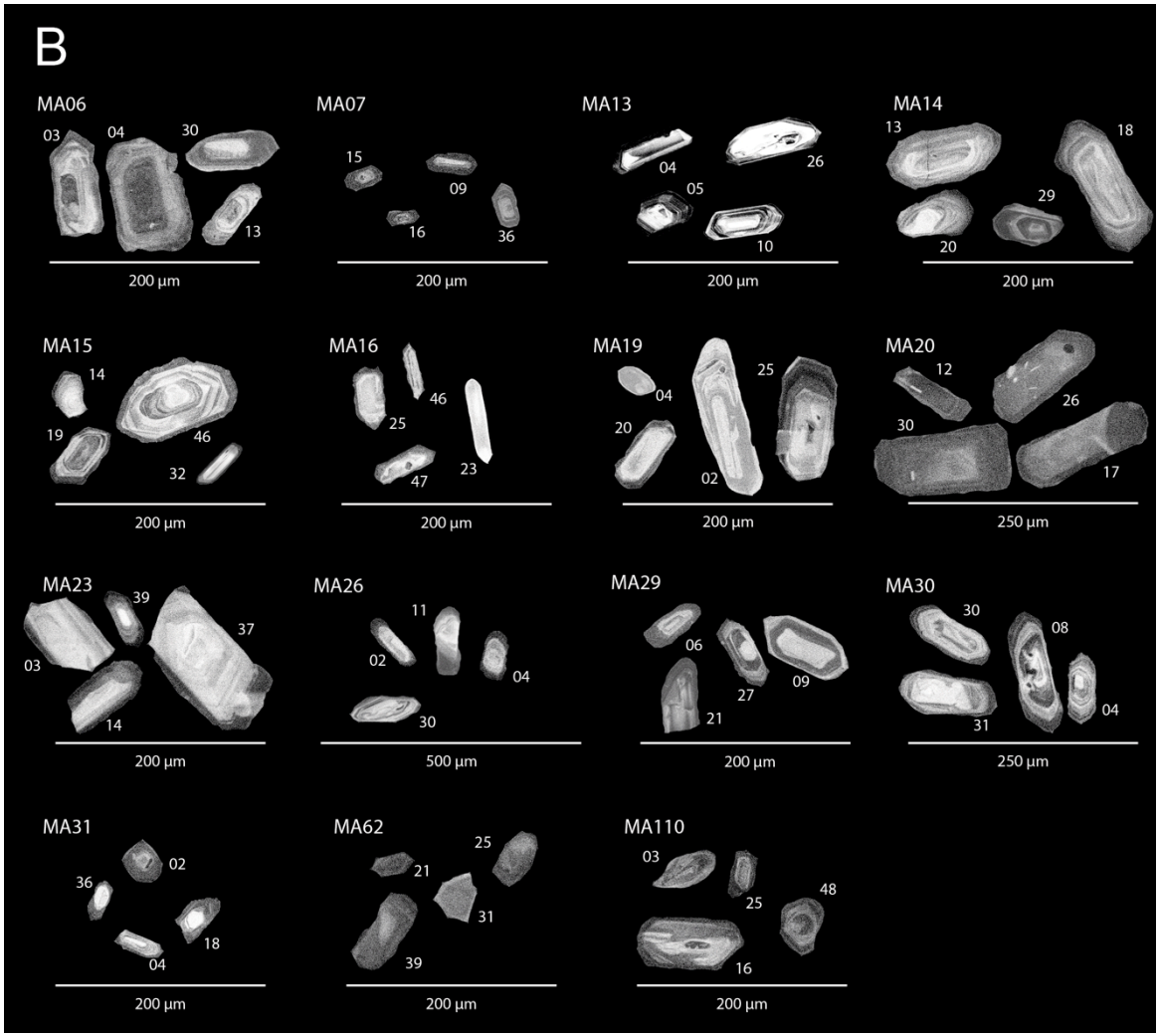

Figure 4.2B Representative cathodoluminescence (CL) images of extracted zircons from the Main Range Province granitoids.

A. Eastern Province Permo-Triassic granitoids

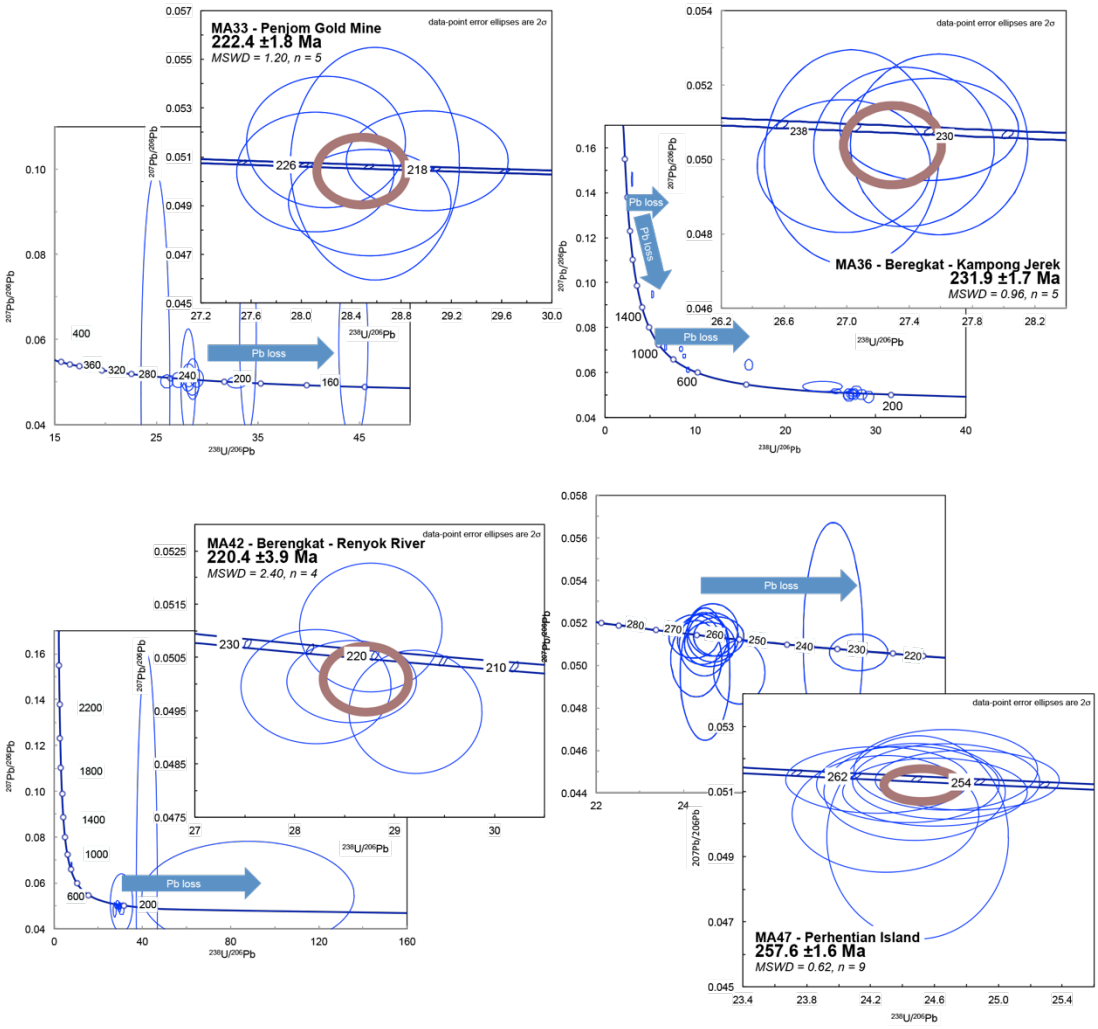

Figure 4.3A Terra-Wasserburg diagrams for all dated Eastern Province granitoids.

B. Eastern Province Permo-Triassic granitoids

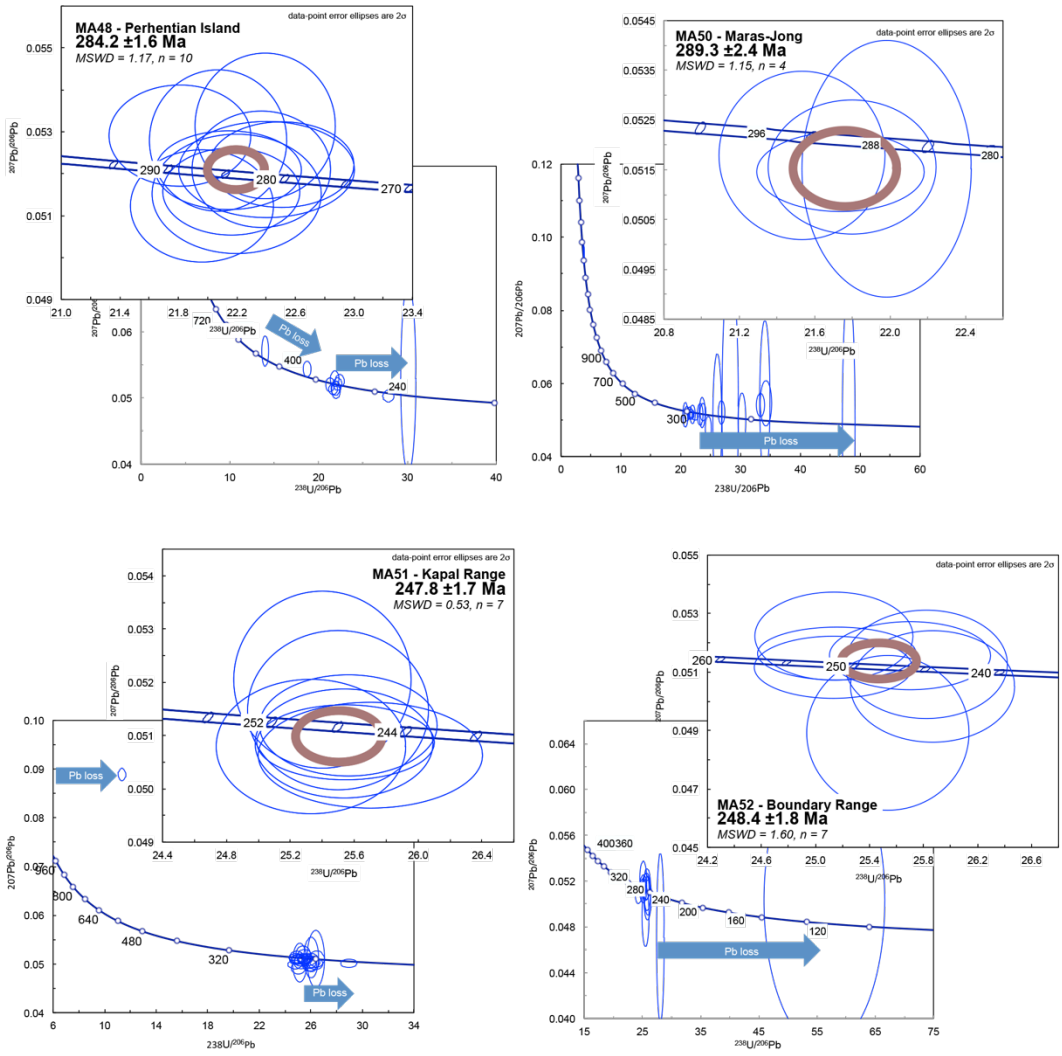

Figure 4.3B (Cont'd) Terra-Wasserburg diagrams for all dated Eastern Province granitoids.

C. Eastern Province Permo-Triassic granitoids

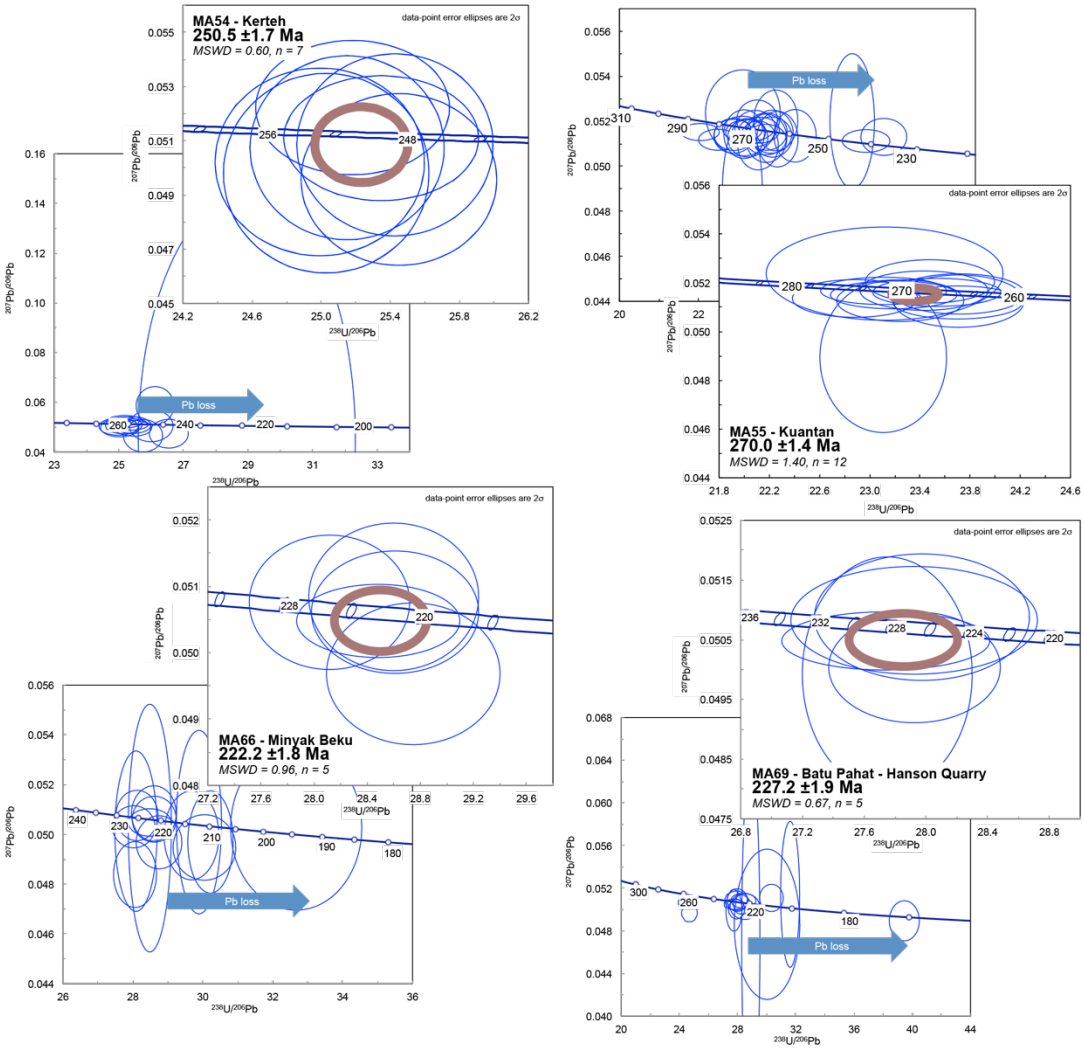

Figure 4.3C (Cont'd) Terra-Wasserburg diagrams for all dated Eastern Province granitoids.

D. Eastern Province Permo-Triassic granitoids

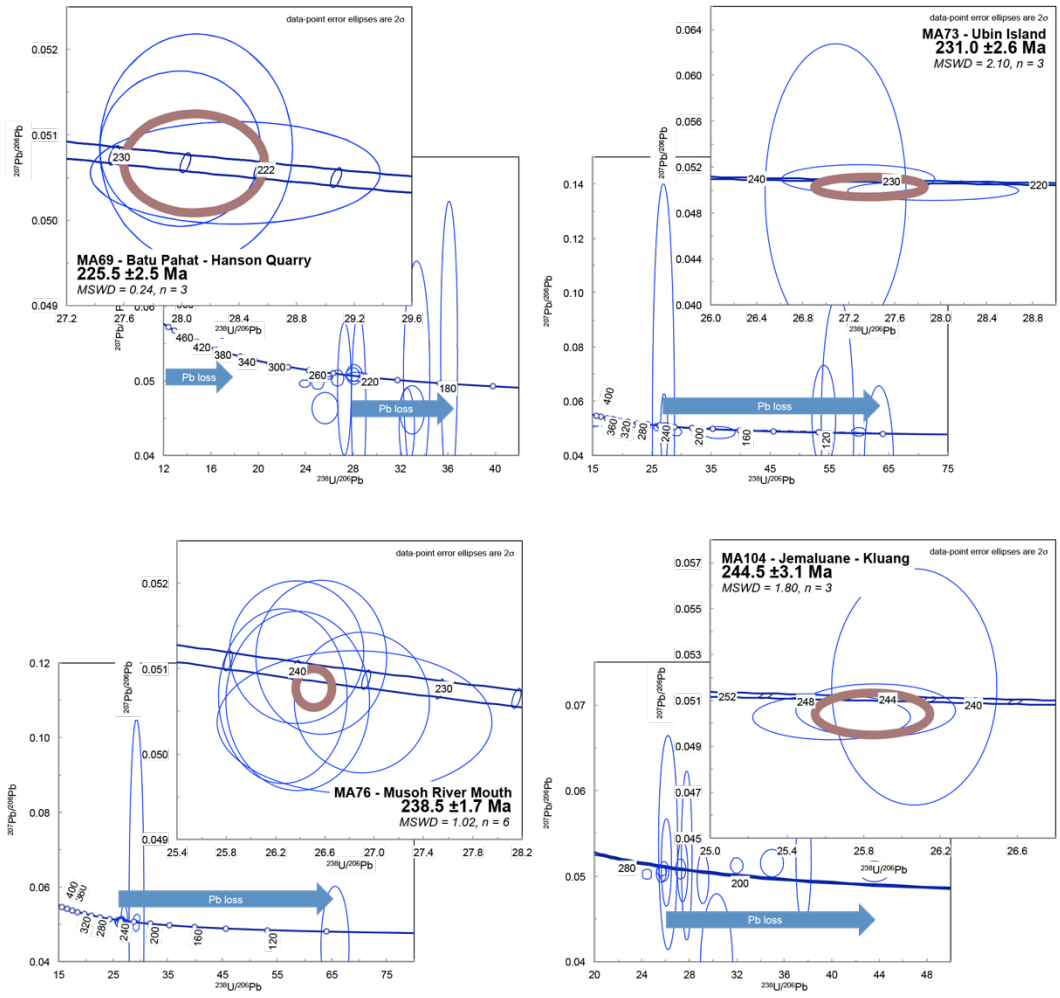

Figure 4.3D (Cont'd) Terra-Wasserburg diagrams for all dated Eastern Province granitoids.

E. Eastern Province Kemahan granite and Cretaceous granitoids

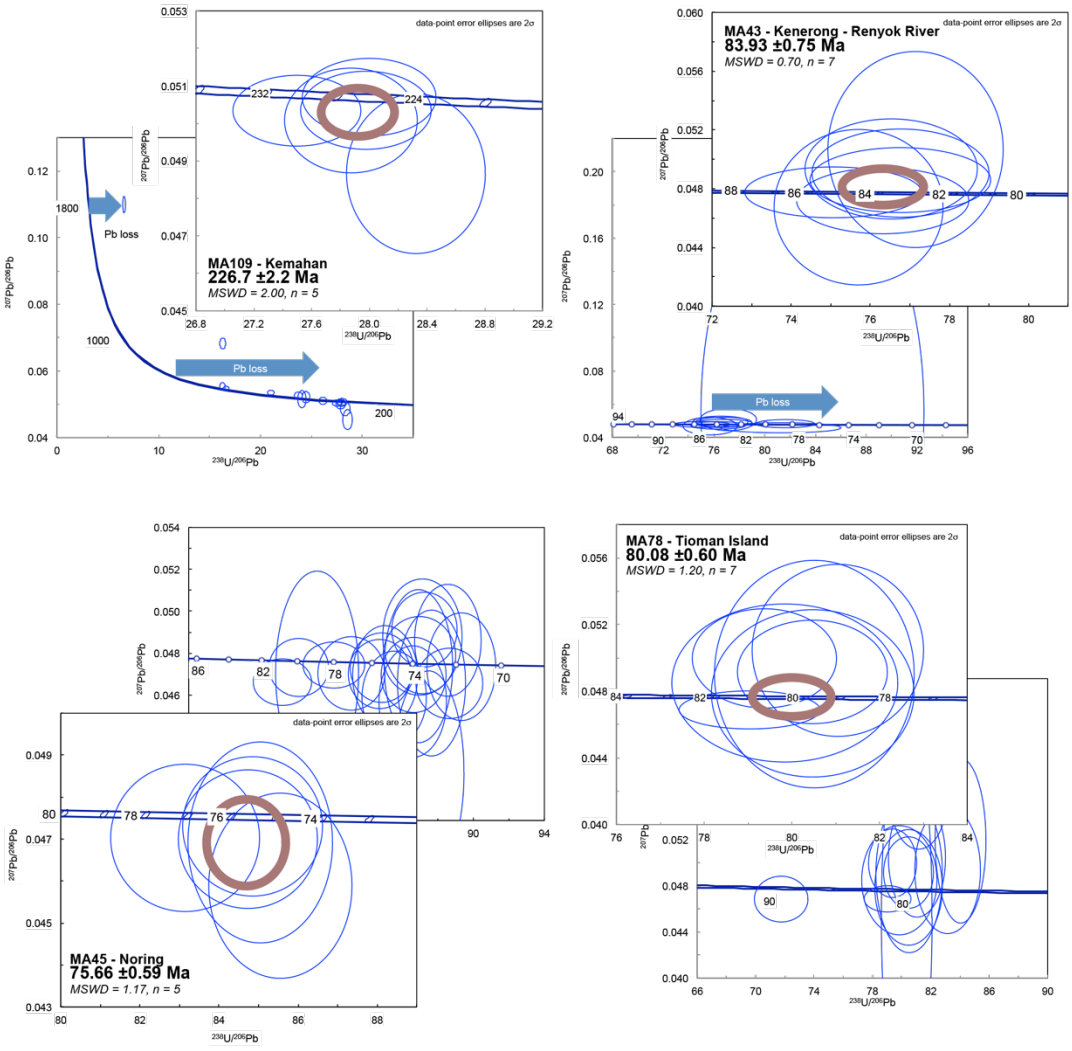

Figure 4.3E Terra-Wasserburg diagrams for the Eastern Province Kemahan granite and Cretaceous granitoids.

F. Eastern Province Cretaceous Tioman granites

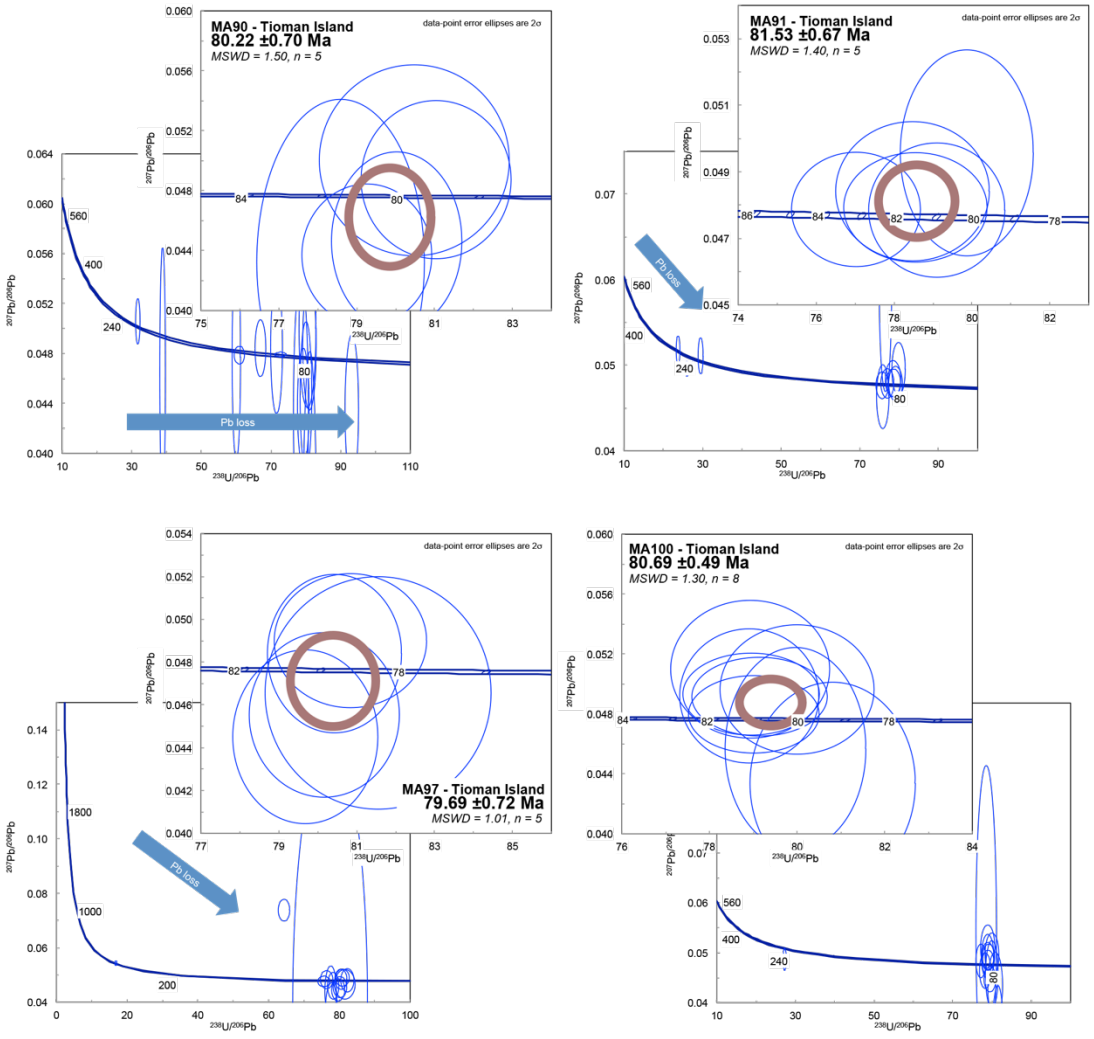

Figure 4.3F Terra-Wasserburg diagrams for all dated Cretaceous Tioman granites.

G. Main Range Province granitoids

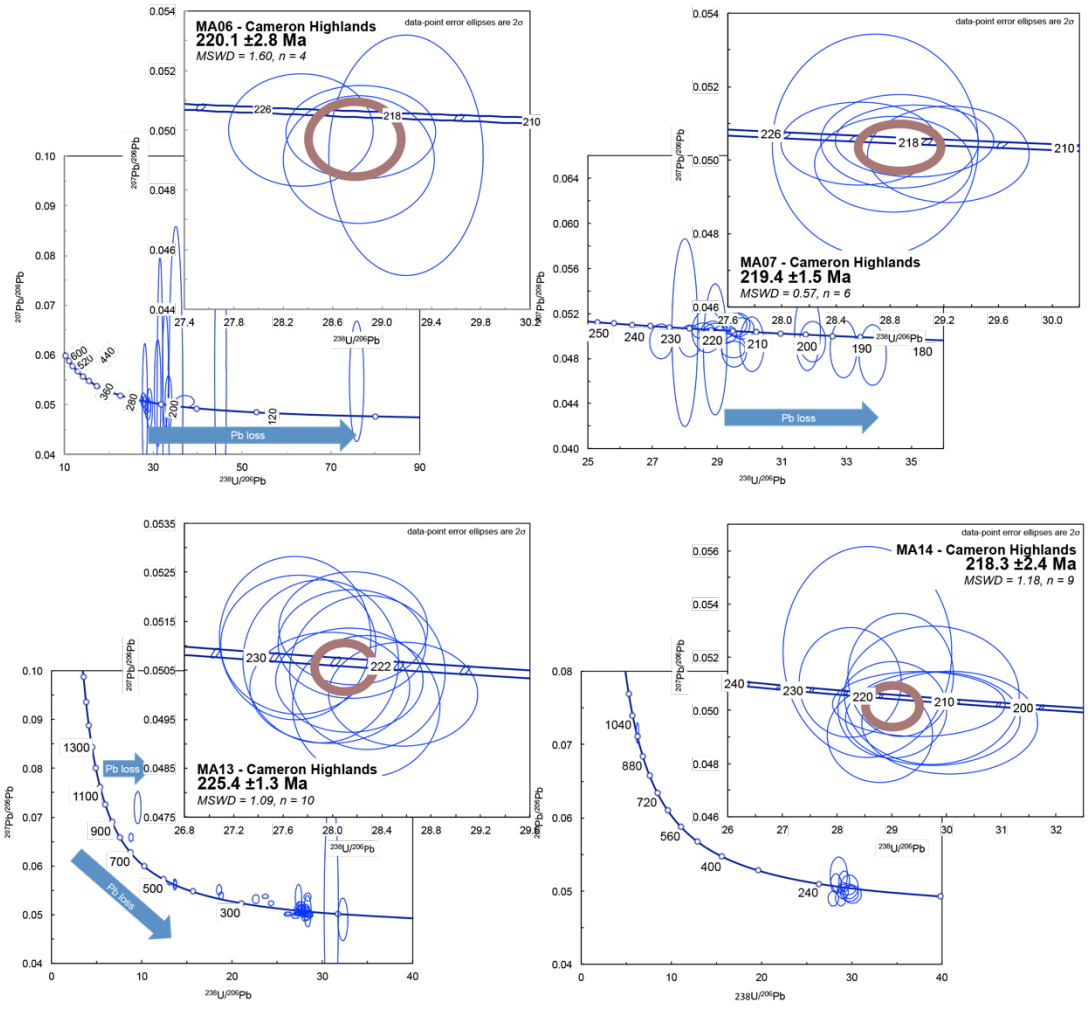

Figure 4.3G Terra-Wasserburg diagrams for all dated Main Range Province granitoids.

H. Main Range Province granitoids

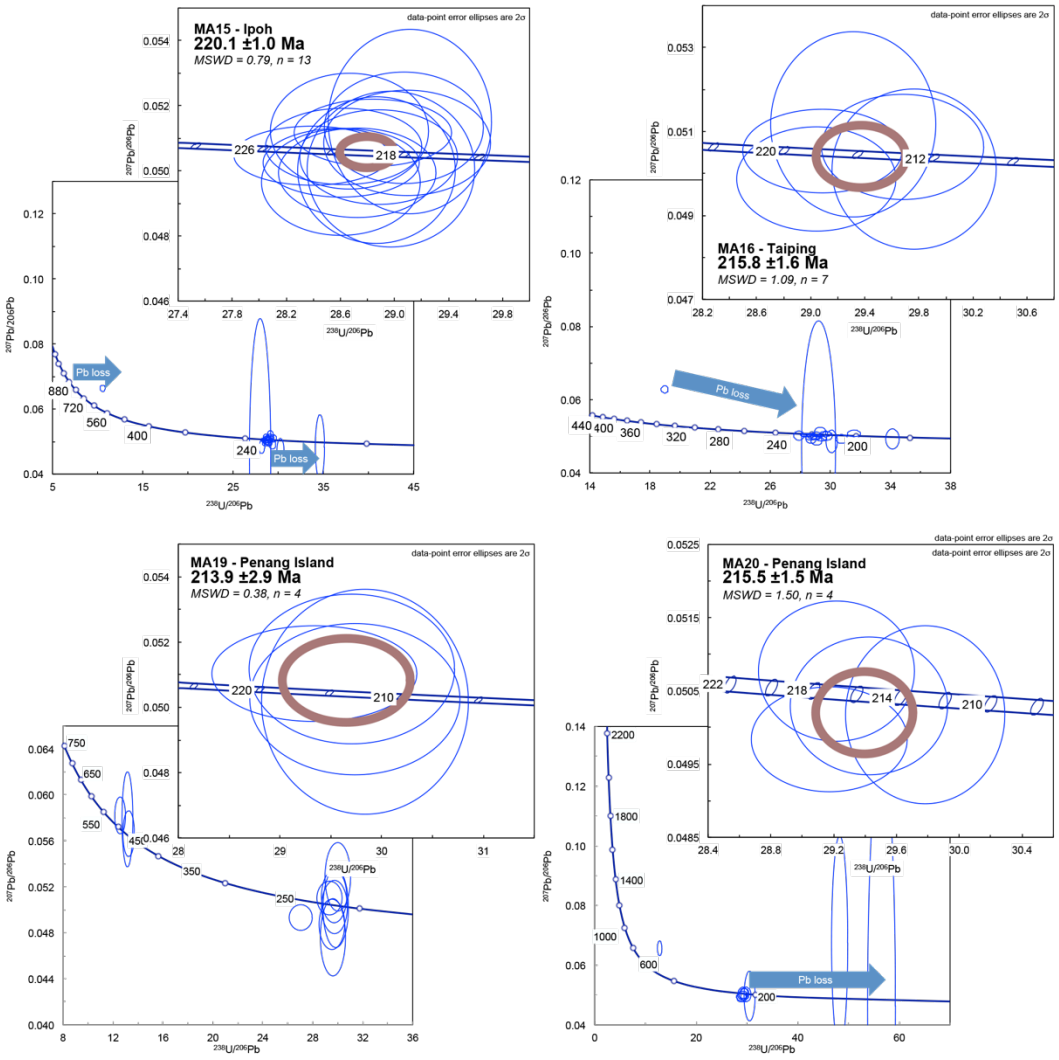

Figure 4.3H (Cont'd) Terra-Wasserburg diagrams for all dated Main Range granitoids.

I. Main Range Province granitoids

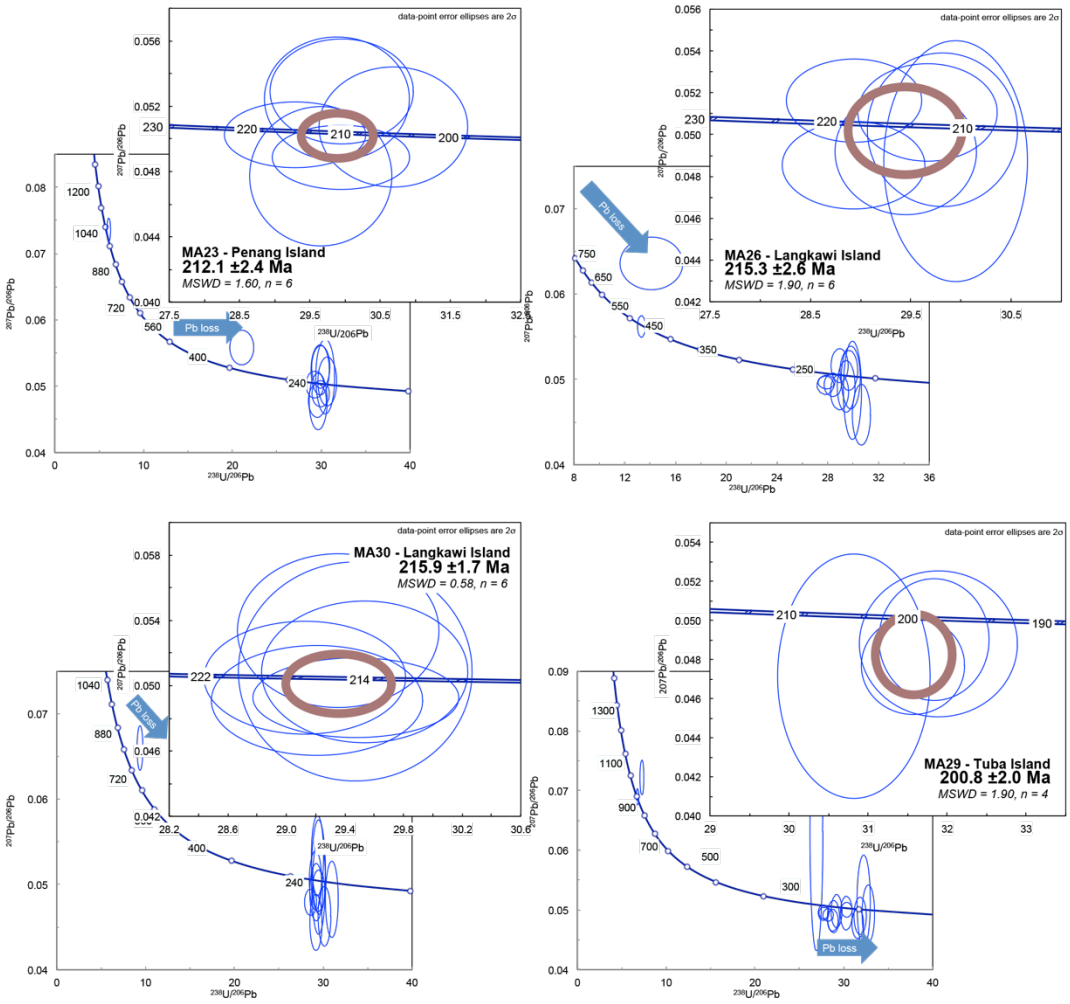

Figure 4.3I (Cont'd) Terra-Wasserburg diagrams for all dated Main Range Province granitoids.

J. Main Range Province granitoids

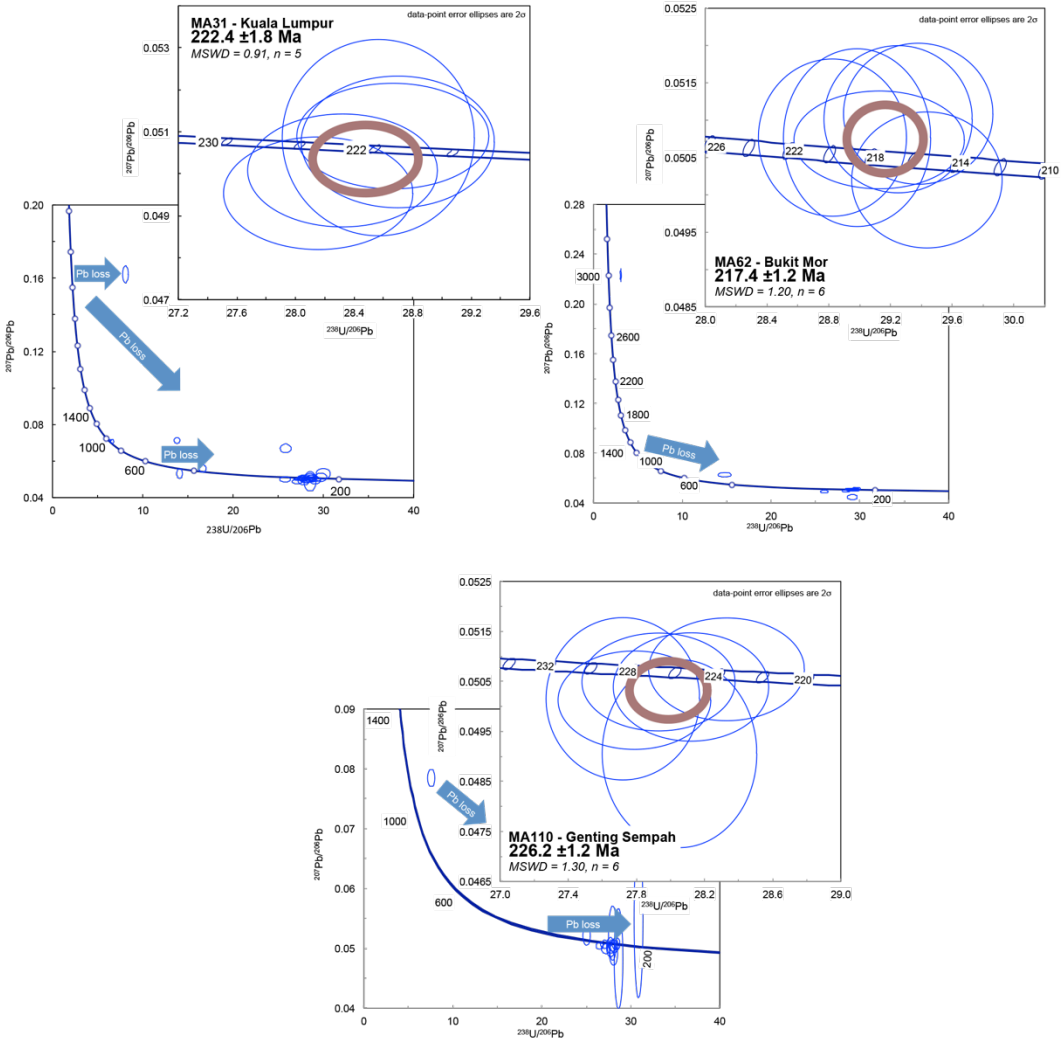

Figure 4.3J (Cont'd) Terra-Wasserburg diagrams for all dated Main Range Province granitoids.

In this section, the U-Pb zircon data and ages of the Eastern Province and Main Range granitoids are presented separately. The Eastern Province granitoids are further divided into Coastal Belt (Eastern Belt) granitoids, Central Belt granitoids and Cretaceous granitoids. This is just for the convenience of data presentation. It should be noted that there is no significant compositional and geochemical difference between the granitoids in the Coastal Belt (Eastern Belt) and the Central Belt as discussed in Chapter 3.

4.2.1 Eastern Province Permo-Triassic granitoids in the Coastal Belt (Eastern Belt)

Zircons extracted from granitic samples collected on the Coastal Belt are mostly well-faceted prisms exhibiting oscillatory zoning with CL-dark cores, while those extracted from the Kerteh dacite (MA54) are fragmented and homogeneous (Figure 4.2A). The CL-dark domains in such images typically reflect high U contents, as confirmed by SIMS analyses (Table 4.2A). The age yielding clusters have U contents ranging from 300 to 4000 ppm and Th/U ratios ranging from 0.11 to 1.14. MA50 from Maras-Jong has much higher U contents in the age-yielding zircons than on average, ranging from 3700 to 7000 ppm, while the zircons extracted from the Kerteh dacite sample (MA54) has much lower U contents, ranging from 180 to 380 ppm. Although both U contents and Th/U ratios vary over a large range between samples, they are consistent within individual samples, adding confidence to our interpretation of magmatic ages from each pooled group of analyses. Exceptions are the Maras-Jong granite (MA50), the Jemaluang– Kluang granite and the Ubin migmatitic granite (MA73), all of which have zircons that exhibit Pb loss and variable Th/U ratios even within individual sample. For the latter granitoids the number of pooled analyses available for age calculation was reduced, and hence, only reference magmatic ages could be calculated. Inherited zircons

are identified as cores to younger zircon overgrowths and record ages of 444.3, 467.7 and 1044.7 Ma (Figures 4.3A and 4.4A).

The oldest granitoids dated in this study were found in the Coastal Belt. Granites formed on the eastern coast have U-Pb ages ranging from 289.3 ± 2.4 to 231.0 ± 2 (Figure 4.1), spanning the Permo-Triassic periods. The age data are summarized Table 4.3A. The oldest sample dated is a K-feldspar phyric, (hornblende)–biotite granite (MA50) from Maras-Jong. However, zircons extracted from this sample exhibit significant post-magmatic Pb loss. Omitting the analyses interpreted as showing Pb-loss, a group of four analyses yield a reference concordia age of 289.3 ±2.4 Ma. The oldest robust U-Pb age obtained is obtained from the Perhentian Island syenite (MA48). A group of thirteen analyses yields a magmatic age of 284.2 ± 1.6 Ma. This syenite is intruded by a biotite granite (MA47) that yields an age of 257.6 ± 1.6 Ma. Other robust east coast ages obtained from Terengganu and Pahang include 250.5 ± 1.7 Ma for the K-feldspar phyric Kerteh dacite (MA54) and 270.0 ± 1.4 Ma for the hornblende–biotite Kuantan granite. The inland hornblende–biotite granites of the Kapal Batholith (MA51) and Boundary Range (MA52) yielded robust concordia ages of 247.8 ± 1.7 Ma and 248.4 ± 1.8 Ma respectively. They are younger than the coastal samples. Only one robust age was obtained in the southern part of the Malay Peninsula, namely 238.5 ± 1.7 Ma from a K-feldspar phyric rhyolite collected at the Musoh River Mouth. The other two ages obtained are reference ages of 244.5 ± 3.1 Ma for the Jemaluang – Kluang K-feldspar phyric hornblende–biotite granite and 231.0 ± 2.6 Ma for the Ubin Island migmatitic granite in Singapore. Zircons extracted from these two samples have suffered severe Pb loss, which hindered the age interpretation. Most of the U-Pb zircon

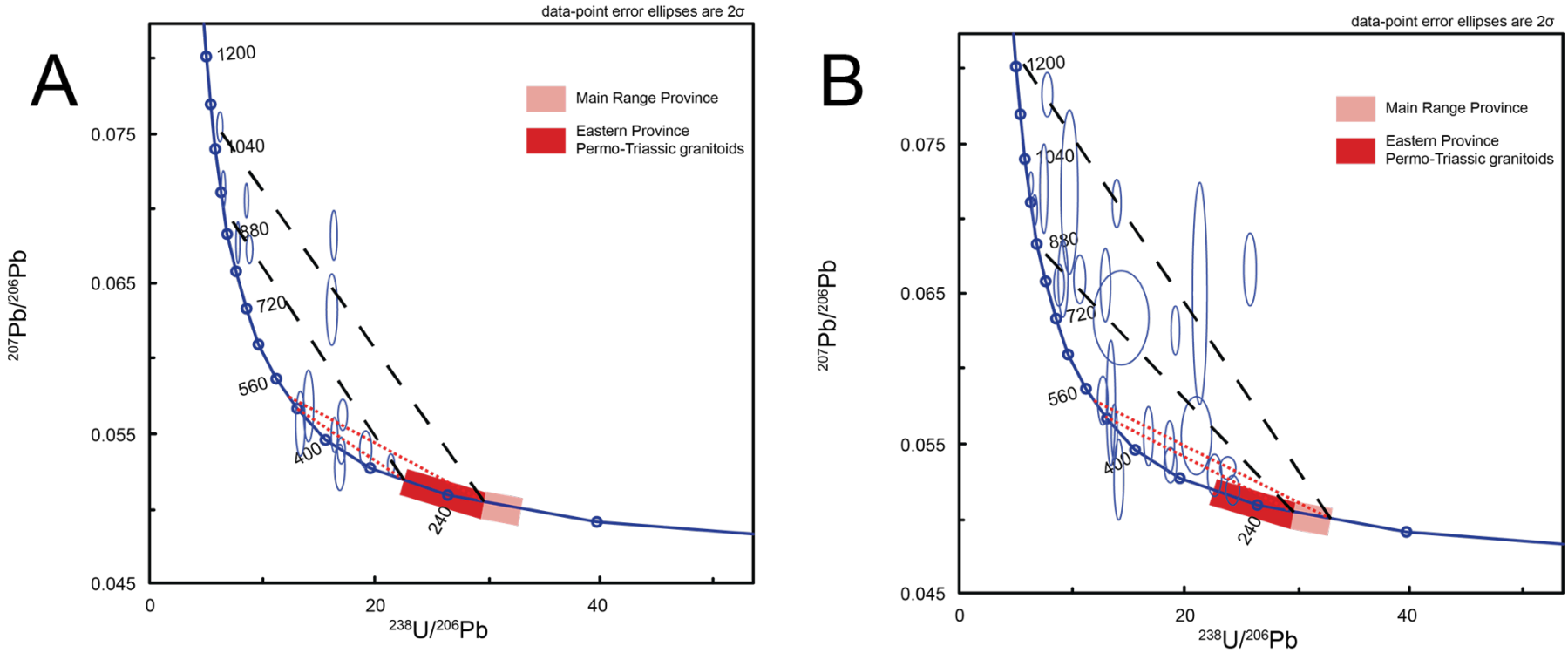

Figure 4.4 Inherited zircon ages and likely inheritance chords yielded from the Eastern Province (A) and the Main Range Province granitoids (B).

ages presented here agree with those obtained by Liew (1983) and Liew and McCulloch (1985).

4.2.2 Eastern Province Permo-Triassic granitoids in the Central Belt

Similar to the zircons extracted from the Coastal Belt samples of the Eastern Province, zircons extracted from the Central Belt granitoids are mostly well-faceted oscillatory-zoned prisms, with either CL-bright or CL-dark core (Figure 4.2A). Zircons extracted from Minyak Beku (MA66) and Batu Pahat (MA68 and MA69) usually have CL-dark cores, which indicates high U contents as shown in Table 2A. Zircons extracted from the Berengkat tonalitic migmatite on Renyok River (MA42) have metamorphic overgrowths, which display growth zoning. The age-yielding clusters have U contents ranging from 270 to 4000 ppm, while Th/U ratios range from 0.09 to 1.52. Generally, both U contents and Th/U ratios are consistent within samples. Exceptions are the Berengkat migmatitic tonalite collected from the Renyok River (MA42) and the K-feldspar phyric biotite granite of Batu Pahat (MA69). Both of these samples have zircons exhibiting Pb loss and in MA69 extremely high U metamict zircons were encountered which adversely affects the accuracy of the ages. Metamorphic rims were found in the zircons extracted from the Berengkat migmatitic tonalite (MA42). No good rim ages have been calculated because of Pb loss, which is also a problem in inherited zircons found in MA36 and MA109. Most of the core data obtained from these grains are discordant. Although they are not useful in determining individual sample ages, they are useful in identifying possible inherited or source components of the granitic magmas – zircon core ages indicate upper intercept ages at Cambro-Ordovician and Proterozoic times (Figure 4.4A).

The granitoids sampled in this area have ages ranging from 231.8 ± 1.7 to 222.2 ± 1.8 Ma (Figure 4.1). The age data are summarized in Table 4.3A. Robust U-Pb zircon ages were obtained from the K-feldspar phyric hornblende–biotite granite of the Jeli Blunero Quarry (MA109: 226.7 ± 2.2 Ma), felsite from the Penjom Gold Mine (MA33: 222.4 ± 1.8 Ma), K-feldspar phyric hornblende–biotite tonalite from Berengkat in the Stong region (MA36: 231.8 ± 1.7 Ma), clinopyroxene–hornblende–biotite granite from Minyak Beku (MA66: 222.2 ± 1.8 Ma), and K-feldspar phyric biotite microgranite from Batu Pahat (MA68: 227.2 ± 1.9 Ma). Compared to the U-Pb zircon ages obtained in the Coastal Belt, the ages obtained here is much younger. Reference ages only were obtained from MA42 and MA69 due to the presence of zircons with Pb loss. For MA42, clusters of four analytical spots yield reference age at 220.4 ± 3.9 Ma. This reference age is broadly consistent with the other Berengkat sample collected at Kampong Jerek (MA36), and other robust ages obtained in the Central Belt. It also confirms the temporal relationship between the hosting tonalite and the Cretaceous Kenerong–Renyok leucogranitic dyke (MA43). For the Batu Pahat K-feldspar phyric biotite granite (MA69), a cluster of four pooled analyses yield a reference age at 225.5 ± 2.5 Ma. This age is consistent with MA68 collected at the same locality, which has robust age at 227.2 ± 1.9 Ma. Although field relationships suggested that the Batu Pahat Bt microgranite (MA68) cuts the coarser-grained granite (MA69), the age difference is within error of both ages and the two granitic bodies are considered to have formed contemporaneously.

4.2.3 Eastern Province Cretaceous granitoids

Granitoids outcropping in the Stong region (Kenerong and Noring) and on Tioman Island are Late Cretaceous in age. Zircons extracted from a leucogranitic dyke (MA43)

at Renyok are mainly multi-faceted prismatic grains considered to be of metamorphic origin. They are homogeneous and unzoned. In contrast, grains from the Noring Kfs-phyric Hbl-Bt granite (MA45) are well-faceted, oscillatory-zoned, magmatic zircons. U contents of zircons from both Stong samples are high, ranging from 450 to 6600 ppm. The Tioman zircons are well-faceted prisms (Figure 4.2A). They are mainly homogeneous, unzoned to faint-oscillatory-zoned, magmatic zircons. These zircons generally have lower U contents than those extracted from the Peninsula samples. They usually have U contents less than 1000 ppm (Table 4.2B). However, the Th/U ratios of all of the Cretaceous zircons are variable, in the range of 0.36 to 4.05, and generally higher than the Permo-Triassic granitoids. Older inherited zircons were also extracted from these samples and most of these yielded discordant data similar to the inherited zircons extracted from the Permo-Triassic granitoids in the Eastern Province. Although two of them give Carboniferous to Triassic concordant ages, no relevant petrologic or tectonic interpretation can be made.

Robust U-Pb zircon ages are provided for the Renyok leucogranitic dyke (MA43) at 83.9 ± 0.8 Ma and the Noring K-feldspar phyric hornblende–biotite granite (MA45) at 75.7 ± 0.6 Ma. The granitic samples collected from different parts of Tioman Island (MA78, MA90, MA91, MA97 and MA100) all yielded robust ages at 80.0 ± 1.0 Ma (Table 4.3B and Figure 4.3F).

4.2.4 Main Range Province

Zircons extracted from the Main Range Province granitoids are mostly well-faceted prismatic grains that are typically coarser grained than those extracted from the Eastern Province granitoids (Figure 4.2B). Both CL-dark and CL-bright cores can be found in

the grains with oscillatory zoning. Fragmented zircons are found in the volcanic sample collected from Genting Sempah (MA110). Zircon in the age yielding group usually have U contents ranging from 100 to 3000 ppm (Table 4.2C). MA07 from the Cameron Highlands has higher U contents in its age yielding group lying between 1500 and 8500 ppm, with the Th/U ratios in this group ranging from 0.04 to 1.35, similar to the Eastern Province. In contrast to the Eastern Province samples, the Main Range zircons have a relatively limited range of Th and U contents. Core-rim relationships were found in some of the extracted zircons from most samples. The core ages, if concordant, usually suggest a Cambro-Ordovician or Neoproterozoic upper intercept ages (Figure 4.4B).

Fifteen samples were dated in the Main Range Province. The U-Pb zircon ages range from 226.2 ± 1.2 to 200.8 ± 2.0 Ma (Figure 4.1). The oldest samples with robust ages were found in the inland, i.e. from the Cameron Highlands (MA07: 219.4 ± 1.5 Ma, MA13: 225.4 ± 1.3Ma, MA14: 218.3 ± 2.4 Ma), Ipoh (MA15: 220.1 ± 1.0 Ma), Kuala Lumpur (MA31: 222.4 ± 1.8 Ma) and Bukit Mor (MA62: 217.4 ± 1.2 Ma). All these ages were obtained from K-feldspar phyric (muscovite)–biotite granites. Younger samples were found on the western coast and outlying islands like Penang (MA23: 212.1 ± 2.4 Ma) and Langkawi (MA26: 215.3 ± 2.6 Ma and MA30: 215.9 ± 1.7 Ma). The only hornblende-bearing granite in the Main Range Province, the Taiping granite (MA16) of the Bintang Batholith, also gives a robust age of 215.7 ± 1.6 Ma. Hence, it is formed at the same time as the other hornblende-free Main Range granitoids. Reference ages are provided when the zircons suffered from severe Pb loss and these include samples from a K-feldspar phyric cordierite–biotite granite of the Cameron Highlands (MA06: 220.1 ±2.8 Ma), the K-feldspar phyric biotite granites from Penang (MA19: 213.9 ±2.9 Ma and MA20: 215.5 ± 1.5 Ma), and the Ms-Bt microgranite at Tuba

(MA30: 200.8 ± 2.0 Ma). The reference ages provided are comparable to the robust ages obtained in nearby samples. All these ages are reported in Table 4.3D.

4.2.5 Westward younging of the Malaysian granitoids

The age younging trend observed in the Eastern Province also follows in the Main Range Province. In other words, the granitoids on the eastern coast are the oldest, while the youngest granitoids are found on the western coast (Figures 4.1 and 4.5). The Eastern Province granitoids have U-Pb ages ranging from 289 Ma to 222 Ma (Coastal Belt: 289 – 231 Ma, Central Belt: 226 – 220 Ma). The Main Range Province granitoids have U-Pb ages ranging from 227 Ma to 201 Ma. However, it is also observed that the chronological isolines 220 Ma and 210 Ma in the Main Range Province are close to each other, and they are not as well defined as other isolines in the Eastern Province (Figure 4.5). The Genting Sempah volcanics have been correlated with the Main Range magmatism due to their similar geochemistries (Ghani and Singh, 2002, 2005). The orthopyroxene-bearing dacite (MA110) there was dated at 226.2 ± 1.2 Ma (2σ, MSWD of concordance and equivalence = 1.30), which provides temporal evidence for such a conclusion.

4.2 U and Th contents and Th/U ratios of zircons in the Malaysian granitoids

Compared to the common U and Th contents of zircon in granitic rocks (median values 350 ppm of U and 140 ppm of Th, n = 1684) (Wang *et al.*, 2011), the zircons in the Malaysian granitoids are generally more enriched in U and Th than typical granitoids. The U contents can be 10-fold of those values in normal zircons extracted from granitoids. Zircons with thousands ppm of U contents are common (Tables 4.2). Radiation damage to the crystal lattice will enhance Pb mobility rates, which can

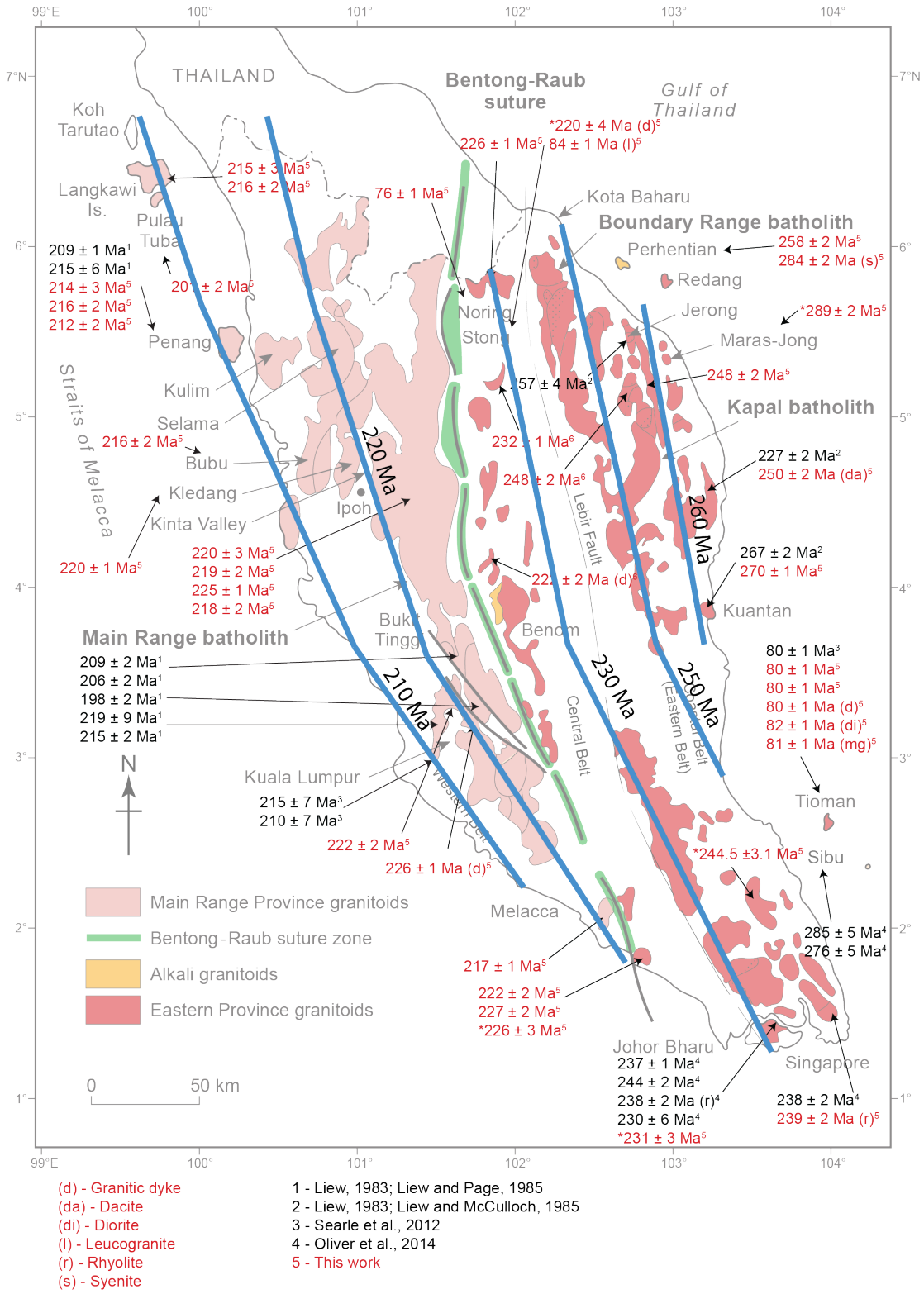

Figure 4.5 Chronological isolines drawn according to the U-Pb zircon ages presented in this chapter.

explain the ubquitious Pb loss problem in these samples. The U and Th geochemistry does however suggest a subtle difference in the source region and/or petrogenesis of the different sample groups. Compared to the Permo-Triassic Malaysian granitoids (Th/U ratios ranges from 0.2 to 1.2, with average Th/U = 0.5), the Cretaceous plutons generally have higher Th/U ratios, ranging from 0.5 to 2.5 and average Th/U = 1.3 (Figure 4.6). Since the U and Th contents of the zircons are primarily controlled by the U and Th contents of the melt, the difference observed here may be attributed to the compositional difference of the sources.

4.3 Summary

Thirty-seven granitic samples and two volcanic samples were collected throughout the Malay Peninsula for U-Pb zircon geochronology, of which twenty-four samples were from the Eastern Province and fifteen from the Main Range Province. The Eastern Province magmatism is bracketed by the Perhentian syenite at 289.3 ± 2.4 Ma and the Berangkat migmatitic tonalite at 220.4 ± 3.9 Ma. An obvious trend is evident in these data whereby granite ages young progressively from the eastern coast to the Bentong-Raub suture (Figure 4.5). The Main Range Province magmatism is bracketed by the Genting Sempah dacite at 226.2 ± 1.2 Ma and the Tuba microgranite at 200.8 ± 2.0 Ma. The ages of granite magmatism in the Main Range also appear to young progressively westwards, from the Bentong-Raub suture to the west coast of the peninsula, although the pattern is not as well defined as that in the Eastern Province. The duration of Main Range magmatism (25 million years) appears to be shorter than that applicable to the Eastern Province magmatism (69 million years). Cretaceous granitoids are reported in the Stong region (Kenerong leucogranite: 83.9 ± 0.8 Ma, Noring granite: 75.7 ± 0.6 Ma) and on the Tioman Island (*ca.* 80 ± 1 Ma).

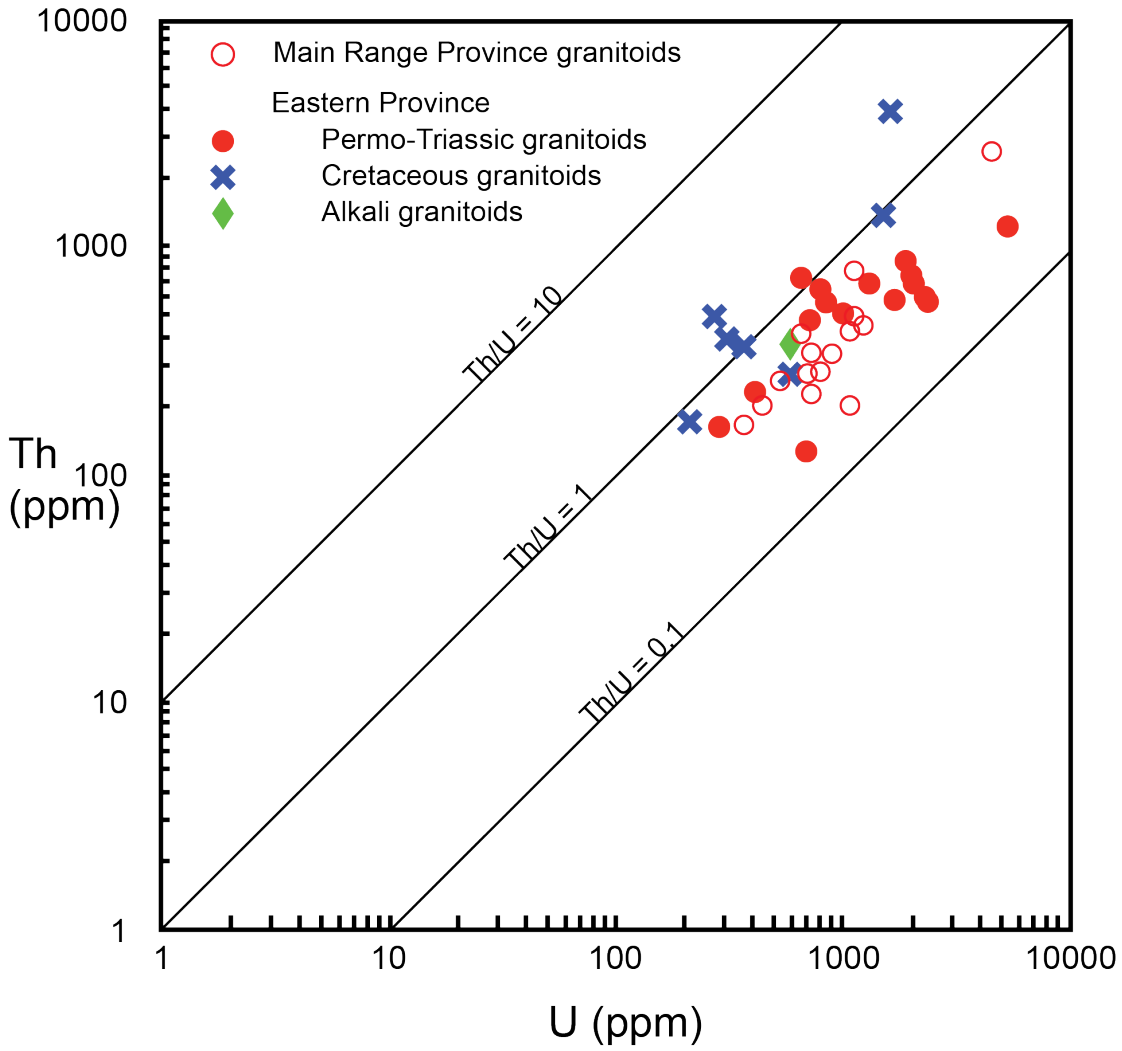

Figure 4.6 The average Th concentration of the age-yielding group of each sample is plotted against the average U concentration.

Both the Eastern Province and Main Range granites carry Cambro-Ordovician and Mesoproterozoic inheritance signatures provided by zircon core ages and defined by upper intercepts on the Tera-Wasserburg plot (Figure 4.4). This suggests that unexposed basement in both continental terrane, namely the East Malaya terrane (Eastern Province) and the Sibumasu terrane (Main Range) comprise early Phanerozoic and Mesoproterozoic rocks, which were the hosts for emplacement, and possibly also the source rocks, of the Malaysian granitoids.

The zircons extracted from the Permo-Triassic and Cretaceous Malaysian granitoids have different Th and U contents. Zircons extracted from the Permo-Triassic granitoids typically have Th/U ranging from 0.2 to 1.2, with average Th/U = 0.5, while the those extracted from Cretaceous granitoids can have Th/U ratios ranging from 0.5 to 2.5, with average Th/U = 1.3. The difference could be attributed by the compositional difference of the melting sources.

Chapter 5 – Discussion and Conclusion

5.1 Synopsis

In Chapter 1, concepts of granite petrogenesis were reviewed. It is widely accepted that the composition of granites is mainly determined by the source regions in the middle and lower crust (Chappell and White, 1974; Clemens and Stevens, 2012). The parental granitic magma usually involves hybridization of melts derived from different source regions (protoliths), which can be either of igneous or sedimentary origin in upper amphibolite to granulite metamorphic facies (Gray, 1984; Keay *et al.*, 1997; Kemp *et al.*, 2007). Partial melting of these protoliths is facilitated by the heat and fluids introduced by the subduction system and the breakdown of hydrous minerals. Heat can be generated by crustal thickening, internal radiogenic heat production or by basaltic underplating.

In Chapter 2, the geological framework of the Malay Peninsula has been presented. The Malaysian granitoids were formed and emplaced during the re-assembly of Gondwana-originated Precambrian micro-continental terranes, namely Indochina – East Malaya terrane and Sibumasu terrane in the Malay Peninsula. The Eastern Province is bounded to the west by the Bentong-Raub suture zone, and is dominated by hornblende-bearing, pre-collision I-type granites. The younger Main Range Province biotite granites west of the suture zone have been interpreted as "syn-collision S-type granites" by previous authors (Beckinsale, 1979; Cobbing *et al.*, 1986, 1992). Field observations suggest that the hornblende-bearing granitoids in the Eastern Province usually have a more fractionated roof-zone which is hornblende-free and characterized by hydrothermal alteration. The hornblende-free roof-zones in the Eastern Province are mineralogically

similar to the biotite granitoids that dominate in the Main Range Province. On the other hand, the Bintang Batholith in the Main Range Province also exhibits hornblende-bearing granitoids that are mineralogically similar to those in the Eastern Province. In addition, both granitic provinces share commonality in accessory mineral assemblages in containing sphene, allanite, apatite and ilmenite. This shows that the two granitic provinces being defined are not as mineralogically contrasting as previous authors (Beckinsale, 1979; Cobbing *et al.*, 1986, 1992) suggested.

In Chapter 3, the geochemistry of the Malaysian granitoids was reviewed. The Eastern Province granitoids are akin to typical I-type granites in major element geochemistry, but this study also shows that some of the Main Range Province granitoids cannot be distinguished geochemically from the Eastern Province granitoids. It further shows that all the Malaysian granitoids follow a common LLOD, while the hornblende-free granitoids in both granitic provinces are geochemically more fractionated. In other words, the Main Range Province granitoids are generally more fractionated than the Eastern Province granitoids. Positive correlation has been found between Sn metallogenesis and fractionated granitoids. The trace element geochemistry of the Malaysian granitoids suggests that they are all enriched in HFSE and REE. The enrichment signature is likely inherited from the protoliths, which are also enriched in these elements. The Sr-Nd isotopic data shows that the Eastern Province were formed from hybridized magmas made of both igneous protolith and sedimentary protolith similar to the Kontum ortho-amphibolites and para-gneisses, analogues to the two end-member sources of the Indochina basement. The Main Range granitoids of the Western Province have a similar source but the incorporation of sedimentary-sourced melt is much more significant in the parental magma, in contrast to that of the Eastern Province,

which comprised predominantly igneous-sourced melt. It is suggested that the incorporation of both igneous- and sedimentary-sourced melts can promote the formation of Sn deposits.

In Chapter 4, thirty-nine new U-Pb zircon ages from the Malaysian granitoids were presented. These new data show that the Eastern Province magmatism occurred between 289.3 ± 2.4 Ma and 220.4 ± 3.9 Ma, while the Main Range Province magmatism occurred between 226.2 ±1.2 Ma and 200.8 ± 2.0 Ma. Late Cretaceous magmatism is restricted in the Eastern Province, with granitoids outcropped in the Stong region and on Tioman Island. A westward younging trend is prominent in the Eastern Province, but becomes poorly defined in the Main Range Province. All the Malaysian granitoids in both granitic provinces have Cambro-Ordovician and Mesoproterozoic inheritance signature, which are interpreted as the ages of the source regions. In addition, zircons extracted from the Cretaceous granitoids are characterized by high Th/U ratios.

5.2 The Malaysian granitoids in Chappell and White's (1974) I-S granite classification system

Beckinsale (1979) and Cobbing *et al.* (1986, 1992) separated the Malaysian granitoids into an I-type Eastern Province and a S-type Main Range Province according to their lithological and geochemical differences. The field observations and geochemistry presented in Chapters 2 and 3 confirm that the hornblende-bearing granitoids in the Eastern Province have typical I-type mineralogy and geochemical signatures. Mineralogically, they contain I-type indicative minerals like hornblende and sphene. Geochemically, they are metaluminous to weakly peraluminous, and tend to be more

sodic. These I-type granites are however not wholly restricted to the Eastern Province; the hornblende-bearing Bintang Batholith in the Main Range Province is also I-type. Although Sr-Nd isotopic data suggests that up to 10 – 20% of sedimentary-sourced melt was incorporated into the parental magma of the Eastern Province granitoids, the I-type mineralogy and geochemistry are still largely retained. Some of them could be highly fractionated, and may host Sn-W deposits.

In contrast, the Main Range Province is dominated by hornblende-free biotite granites, interpreted as "S-type" because they are generally more potassic and peraluminous (Beckinsale, 1979; Cobbing *et al.*, 1986, 1992). However, these characteristics are also found in fractionated I-type roof-zone granites in the Eastern Province, and make the Main Range granitoids mineralogically and geochemically indistinguishable from the fractionated hornblende-free pluton roof-zone in the Eastern Province. The only way to discriminate Main Range granitoids from the Eastern Province is using Sr-Nd isotope compositions. The Main Range granites have higher initial Sr isotope ratios, but lower $\varepsilon Nd(t)$ values. These values are in the middle of the range of values of igneous and sedimentary end-member sources (Figure 3.11A), suggesting these granitoids are formed from hybridized parental magma with significant input from both an igneous precursor and a sedimentary precursor. Hence, it is suggested that the Main Range Province granitoids are transitional I/S-type here, instead of S-type.

5.3 Comparison of the Malaysian granitoids and the Himalaya-Tibet granitoids

The tectonic relationship between pre-collision I-type granites and syn-collision S-type granites is best demonstrated by the granitoids intruded along the Himalaya-Tibet collision zone (Figure 1.6). The Malay Eastern Province granitoids are comparable to

the pre-collision arc-related I-type Gangdese-Ladakh granites in lithology and geochemistry (Searle *et al.*, 2010). Both of them are of batholithic size and are associated with contemporaneous calc-alkaline volcanic rocks (Linzizong volcanics in Tibet and Pahang volcanics in the Eastern Province). Although the Eastern Province granitoids have lower εNd(*t*) values than the Gangdese-Ladakh granites (Figure 3.11A) (Wen *et al.*, 2008), this probably reflects the incorporation of meta-sedimentary material into the parental magma of the Malay Eastern Province granites. The formation of large granitic batholiths involves large amounts of heat and water, and could only be supplied by fluids driven off a subduction zone as discussed in Chapter 1. In Beckinsale's (1979) and Cobbing *et al.*'s (1986, 1992) traditional model, the Greater Himalayan leucogranites would be an analogue to the "collision-related" Main Range Province granitoids.

The Greater Himalayan two-mica tourmaline leucogranites are entirely of sedimentary origin, occur as in situ melts within sillimanite-grade gneisses and are associated with widespread regional Barrovian metamorphism and partial melting at pressures varying from ~10 – 4 kbar (Searle *et al.*, 2010). These leucogranites and their migmatitic host occur along a mid-crustal channel, bounded by a crustal-scale thrust fault along the base (Main Central Thrust) and by a crustal-scale low-angle normal fault (the South Tibetan Detachment) along the top. None of these features compare with the morphology and lithology of the Main Range Province granitoids. The Main Range Province granitoids are also batholithic, and they are even more voluminous than the Eastern Province granitoids. The Malay Main Range granitoids are not apparently associated with a regional migmatite terrane (at least not an exposed one), do not appear to have a Barrovian metamorphic sequence (unless it remains unexposed in the lower crust) and

are not associated with contemporaneous thrust or normal faults. Clearly the Main Range granitoids require a far greater heat source that the Himalayan leucogranites. Internally derived heat from crustal thickening is only sufficient to derive relative small volumes of Himalayan leucogranite melts, not large batholiths. Besides, the surface geological evidence for major crustal thickening (e.g. the uplifting of 1500 m Cameron Highlands) and regional metamorphism (typically in greenschist facies) in western Malaysia cannot explain the enormous heat required for the Main Range magmatism. The only other source of heat is from the mantle, therefore some sort of magmatic underplating above a Triassic subduction zone is proposed to account for this extra heat.

5.4 Petrogenetic model of the Malaysian granitoids

We have seen that the generation of both the Eastern Province granitoids and the Main Range Province granitoids require huge amounts of heat and water provided by subduction zone(s). During subduction, fluids are driven off the subducting slab and these fluids can induce melting at the base of the crust. Magmatic underplating seems to be the best process to generate both extra heat and the fluid-induced melting to make the Main Range batholith. Partial melting of the upper amphibolite to granulite facies middle and lower crust could be achieved with or without the presence of water by the fluid-present or fluid-absent melt reactions addressed in Chapter 1. To produce voluminous Malaysian granitoids, water-present melting is preferred.

The mineralogical and geochemical differences between the Eastern Province granitoids and the Main Range Province granitoids is mainly controlled by the compositional difference between their source regions (Chappell and White, 1974; Clemens and Stevens, 2012). In the previous section, we have seen that the parental magma of the

Eastern Province was mainly derived from an igneous precursor (I-type), hybridized with a minor amount of sedimentary-sourced melt, as suggested by the Sr-Nd isotope data. This implies that the lower crust basement of the Indochina – East Malaya terrane is dominated by granulite facies meta-igneous material. On the contrary, the parental magma forming the Main Range Province granitoids was probably a hybridized magma with significant input from both igneous and sedimentary precursors (transitional I/S-type). Hence, the lower crustal basement of the Sibumasu terrane should also have both igneous and sedimentary precursors. According to the field relationship and geochemistry of the Malaysian granitoids in both provinces (Chapters 2 and 3), hornblende-bearing granitoids were fractionated to form hornblende-free roof-zone at the top of plutons, which is essentially a zone characterized by hydrothermal alteration and mineralization. In the Main Range Province, some of the microgranitic plutons are hosted by coarser-grained granites (Figure 2.8), suggesting multiple phases of intrusion of granitic magma may have occurred. Contact metamorphic skarns are developed where the Main Range granites are in contact with the country rock sedimentary rocks, dominantly carbonates (Plate 2.13). All these observations are also summarized into the petrogenetic model of the Malaysian granitoids (Figure 5.1).

5.5 Tin metallogenesis in the Malaysian granitoids

Tin mineralisation is usually hosted within greisen veins associated with fractionated S-type granites (Groves and McCarthy, 1978; Babu, 1993; Esmaeily *et al.*, 2005; Mlynarczyk and Williams-Jones, 2005). In the Malay Peninsula, tin deposits are mainly hosted in the greisen-bordered veins and pegmatite of the transitional I/S-type hornblende-free, biotite granites in the Main Range Province, which is more fractionated than the Eastern Province granitoids. Some of them are hosted in the

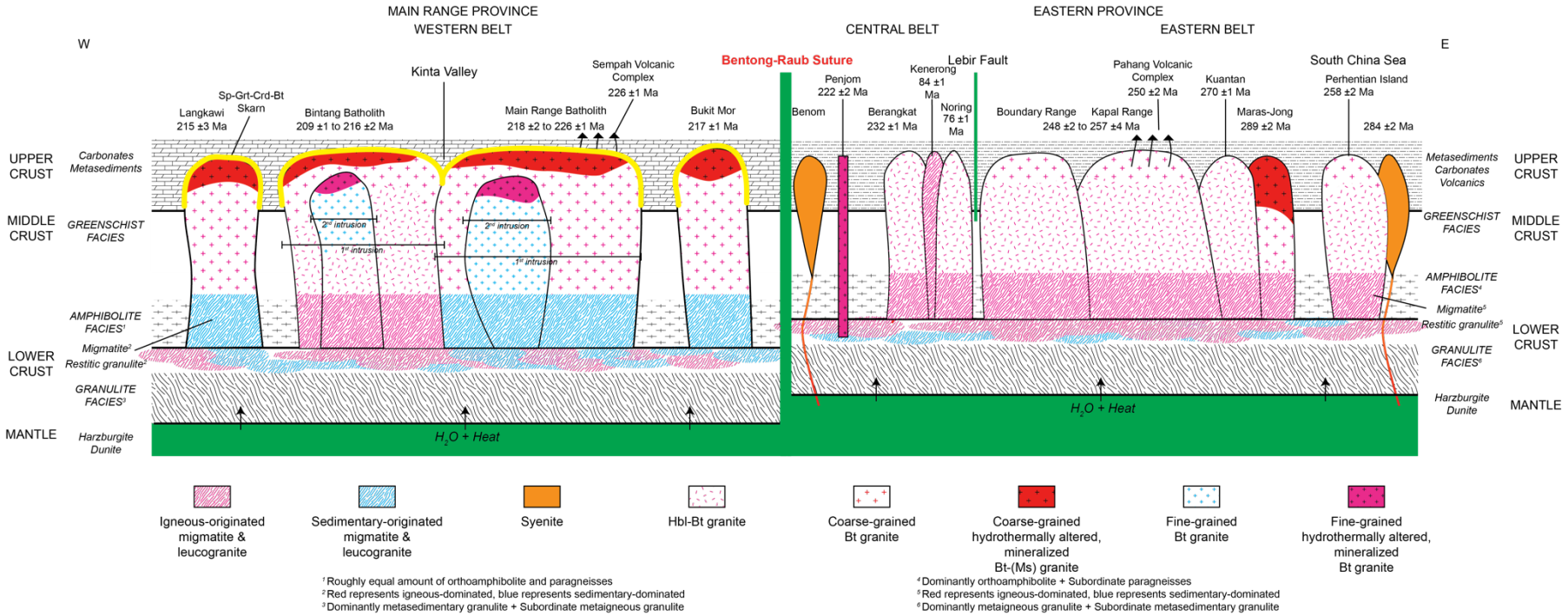

Figure 5.1 Petrogenetic model of the Malaysian granitoids.

hornblende-free pluton roof-zones of the I-type Eastern Province granitoids, where the granitoids are often greisenized, hydrothermally altered and also geochemically fractionated. Hence, there is a correlation between fractionated granites and tin metallogenesis. The association of tin with I-type granitoids is rarely seen worldwide. This is because tin tends to be fractionated into aqueous fluid in a more reduced environment (Taylor, 1979). In Chapter 2, it was suggested that ilmenite-series granites are found in both granitic provinces, including the I-type dominated Eastern Province. Hence, the Eastern Province granitoids are more reduced than typical Cordilleran I-type granites, which usually belong to magnetite-series (Ishihara, 1977; Ishihara *et al.*, 1979; Clarke, 1992; Pitcher, 1997; Frost *et al.*, 2001). The incorporation of sedimentary-sourced melts into the Eastern Province parental magma may have played a role here, as suggested in Chapter 3. Moreover, the Malaysian granitoids are generally enriched in HFSE, such as Nb and Ta, which are primary concentration inherited from the protoliths. These elements have a similar geochemical behaviour to Sn and W, in forming large, highly charged cations, which are readily rejected by polymerized granitic magma. Hence, the Malaysian granitoids may have high primary concentration in Sn and W as well (Chapter 3). These geochemical features might explain the formation of the tin deposits in the greisen-bordered veins and pegmatite associated with the fractionated granitoids in both Malaysian granitic provinces.

5.6 U-Pb ages of the Eastern Province and temporal constraints on the closure of the Palaeo-Tethys Ocean

The new U-Pb age data presented in Chapter 4 support the earlier contention that the Eastern Province granitoids were formed in an Andean-type continental setting along the western margin of Indochina above an east-dipping subduction zone during the

period Early Permian to Mid-Late Triassic (Mitchell, 1977; Cobbing *et al.*, 1986, 1992). The new U-Pb zircon ages obtained in this study are generally compatible with zircon age data from previous authors in the Eastern Province (Liew, 1983; Liew and McCulloch, 1985; Liew and Page, 1985; Searle *et al.*, 2012; Oliver *et al.*, 2014).

The U-Pb zircon ages from the dominantly hornblende-bearing granitoids of the Eastern Province span the period 289 – 220 Ma, which it is interpreted to reflect the timing of active Palaeo-Tethyan subduction and Andean-type magmatism along the Indochina terrane. Although the Bentong-Raub suture zone only contains serpentinites, deep-sea radiolarian cherts and sedimentary rocks spanning Middle Devonian (*ca.* 390 Ma) to Upper Permian age (*ca.* 250 Ma) (Metcalfe, 2000; Sevastjanova *et al.*, 2011), the Palaeo-Tethyan main suture in Thailand (Changning-Menglian suture zone, Inthanon suture zone, and the Klaeng tectonic line) contain marine sediments as young as Mid-Triassic (*ca.* 230 Ma) (Sone and Metcalfe, 2008; Sone *et al.*, 2012). This age correspond closely to the youngest I-type arc-related granite ages from the Eastern Province and thus these data are interpreted to correspond with the timing of closure of Palaeo-Tethys along the Bentong-Raub suture between 230 – 220 Ma (Hutchison, 2009). Continental red-bed clastic sediments overlie older marine sediments both along the suture zone and across the Indochina terrane (Sone *et al.*, 2012). In Singapore, Oliver and Prave (2013) also demonstrated the change to continental sedimentation during the Late Triassic using detrital zircon age data (Sevastjanova *et al.*, 2011).

5.7 Tectonic model of the Malay Peninsula in the Permo-Triassic period

Geological, geochemical and geochronological data can now be used to determine a suitable tectonic model for the evolution of the Malay granite provinces. Two main tectonic models have been proposed which are discussed individually below.

5.7.1 Tectonic Model A – two east-dipping subduction zones

The model generally accepted for the evolution of the Malaysian granitoids (Metcalfe, 2000; Barber and Crow, 2003; Sone and Metcalfe, 2008; Barber *et al.*, 2011; Metcalfe, 2011; Searle *et al.*, 2012) involves eastward subduction of Palaeo-Tethyan lithosphere along the Bentong-Raub suture zone. It resulted in subduction-related, Andean I-type granite magmatism along the over-riding Indochina – East Malaya Block in the Eastern Province (Figure 5.2). The "Central belt granitoids" of Chu *et al.* (1988) and Hutchison and Tan (2009) has been interpreted as products related to the Sukhothai island arc in the Malay Peninsula (Sevastjanova *et al.*, 2011; Metcalfe, 2013). However, in Chapter 3, it was shown that these "Central Belt plutons" have similar geochemistry to those in the Coastal Belt, a proposal also made by Ghani (2009). Hence, the "Central Belt' plutons are grouped with the Eastern Province granitoids in this study. The intervening Lebir fault is a later structure that truncates the granites and has limited offsets; it cannot have been a terrane bounding fault during the Permo-Triassic. The U-Pb age data presented in Chapter 4 show the age range of the Eastern Province granites from Early Permian to Middle-Late Triassic (*ca.* 289 – 220 Ma). The geographical distribution also suggests a progressive westward younging trend for the formation of these granitoids. This may imply a Palaeo-Tethyan subduction rollback along Bentong-Raub suture zone. Following closure of the Palaeo-Tethys Bentong-Raub Ocean, and continental collision of Sibumasu and East Malaya, oceanic subduction beneath Indochina ceased. I-type

magmatism ended soon after and magmatism started in the Main Range Province (Sibumasu) where voluminous crustal-melt granites were intruded forming the Main Range batholith during the Late Triassic. New U-Pb zircon ages presented here suggest a restricted period of intrusion of these granites spanning 227 – 201 Ma (Figure 5.2).

This model has some similarity to the well-known tectonic evolution of the Himalaya-Tibet collision. In the Himalaya-Tibet collision zone, the earlier, pre-collision (*ca.* 180 – 50 Ma) I-type granites (Gangdese-Ladakh granites) and calc-alkaline volcanics (Linzizong Group) occur on the Eurasian plate above a northward-dipping oceanic subduction zone, while the later (*ca.* 26 – 19 Ma) post-collision S-type leucogranites occur along the Indian plate south of the suture zone (Figure 1.6). The major difference with the Himalaya is that the Main Range granites are of much larger extent, batholithic proportions, lithologically and geochemically more akin to transitional I/S-type.

Searle *et al.* (2012) suggested that a second east-dipping subduction zone was required west of the Sibumasu Main Range province in order to explain another belt of subduction-related I-type granites extending from western Phuket Island along western Thailand and southeastern Burma (Figure 5.2). Cobbing *et al.* (1986, 1992) referred to this zone as the Western (Peninsula Thailand – Burma) Province composed of large batholiths of tin-bearing granites and smaller I-type plutons. However, most of the granites along the west coast of Phuket Island are hornblende-bearing granitoids that continue north along the Mergui coast of Southeast Burma. In Burma these granitoids are dominantly either tin-bearing Main Range transitional I/S-type or fractioned I-type granites but appear to be much younger with Cretaceous ages (Barley and Zaw, 2009).

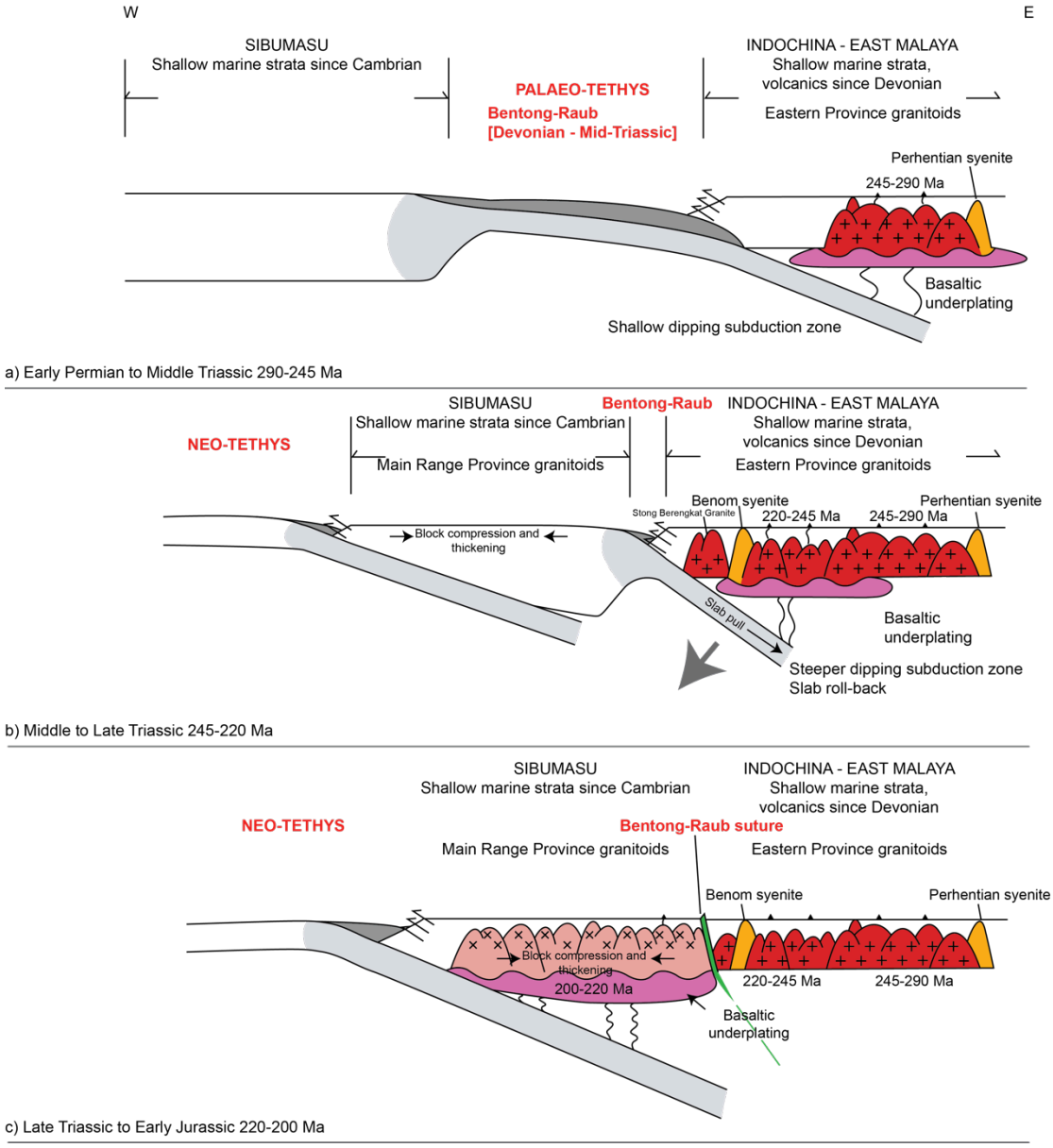

Figure 5.2 Schematic diagram of Tectonic Model A explains the formation and the emplacement of the Malaysian granitoids in the Permo-Triassic period, modified after Searle *et al.* (2012).

A lack of U-Pb zircon age data in this western Thailand – southeast Burma region precludes any detailed tectonic correlations, but in the Mogok belt of Burma (Myanmar) Andean I-type granitoids have U-Pb ages spanning Jurassic to mid-Cretaceous (Barley *et al.*, 2003; Mitchell *et al.*, 2012). However, Searle *et al.* (2012) provided new U-Pb zircon core ages of 212 ± 2 and 214 ± 2 Ma for the Phuket granite, while Late Triassic zircon xenocrysts (209 ± 4 Ma) was reported previously in the Kyanigan gneiss further north in Mandalay of Burma by Barley *et al.* (2003). More precise U-Pb zircon ages are needed along this belt in order to constrain the tectonic evolution of Neo-Tethyan closure along this part of the India-Burma-Sibumasu collision zone. Although the evidence lies mostly north of Malaysia in Thailand and Burma, the presence of Late Triassic Andean I-type granitoids and calc-alkaline volcanics along this province would seem to require a second east-dipping subduction zone to the west of Sibumasu. It is possible that once the Palaeo-Tethyan subduction zone ceased along the Bentong-Raub suture during the Late Triassic, the Neo-Tethyan subduction zone initiated to the west of Sibumasu, but until more age data becomes available, this model remains speculative.

5.7.2 Tectonic model B – westward underthrusting of Sibumasu by Indochina

An alternative tectonic model was proposed by Oliver *et al.* (2014) who demonstrated a progressive decrease of age in subduction-related gabbros, granitoids and rhyolites from east to west, from Sibu Island (with 285 Ma early magmatic zircon) off the SE coast of Malaysia to Singapore (Ketam granite, 230 ± 6 Ma). Based on limited sampling, they suggested that the subduction zone steepened and progressively rolled back, resulting in stretching of the lithosphere and a westward migrating magmatic front (Figure 5.3). The new U-Pb zircon age data obtained in this study supports this model with 15 new zircon ages across the Eastern Province also showing a pronounced westward decrease in ages

(Figure 5.3). Oliver *et al.* (2014) further suggested that following collision, the Main Range Province (Sibumasu) overthrusted the Indochina province along the Bentong-Raub suture zone, resulting in partial melting of thickened crust in Sibumasu and intrusion of transitional I/S-type tin granites along the Main Ranges of Western Malaysia.

This model is also not without problems. First, there is no geological evidence for westward underthrusting (or easting overthrusting) of the Main Range Province over the Eastern Province. Second, the source for the Main Range crustal melt granites is unlikely to be the underthrust Eastern Province hornblende-bearing I-type granitoids. And third, the Main Range tin-granites are also present in the western Sibumasu terrane, along the western part of the Malay Peninsula (Kinta valley and west coast), and are not restricted to the eastern part of the Main Range Province as shown on Oliver *et al.*'s model (2014) (Figure 5.3). Ghani *et al.* (2013) and this study both show that the Main Range granites were fractionated transitional I/S-types with many characteristics typical of S-types (elevated $^{87}Sr/^{86}Sr$ ratios > 0.706, presence of ilmenite and occasional cordierite and andalusite, and presence of meta-sedimentary enclaves), but also some characteristics of I-types (presence of sphene and amphibole, meta-igneous enclaves). These granitoids are more likely to have been sourced by a lower crust with a dominant meta-sedimentary source than a hornblende-biotite granodiorite-granite as required in the Oliver *et al.* (2014) model.

A study of U-Pb detrital zircon ages in modern rivers across Malaysia by Sevastjanova *et al.* (2011) concluded that it was not possible to distinguish between Eastern and Western Province basement rocks, both of which have a common Proterozoic (or

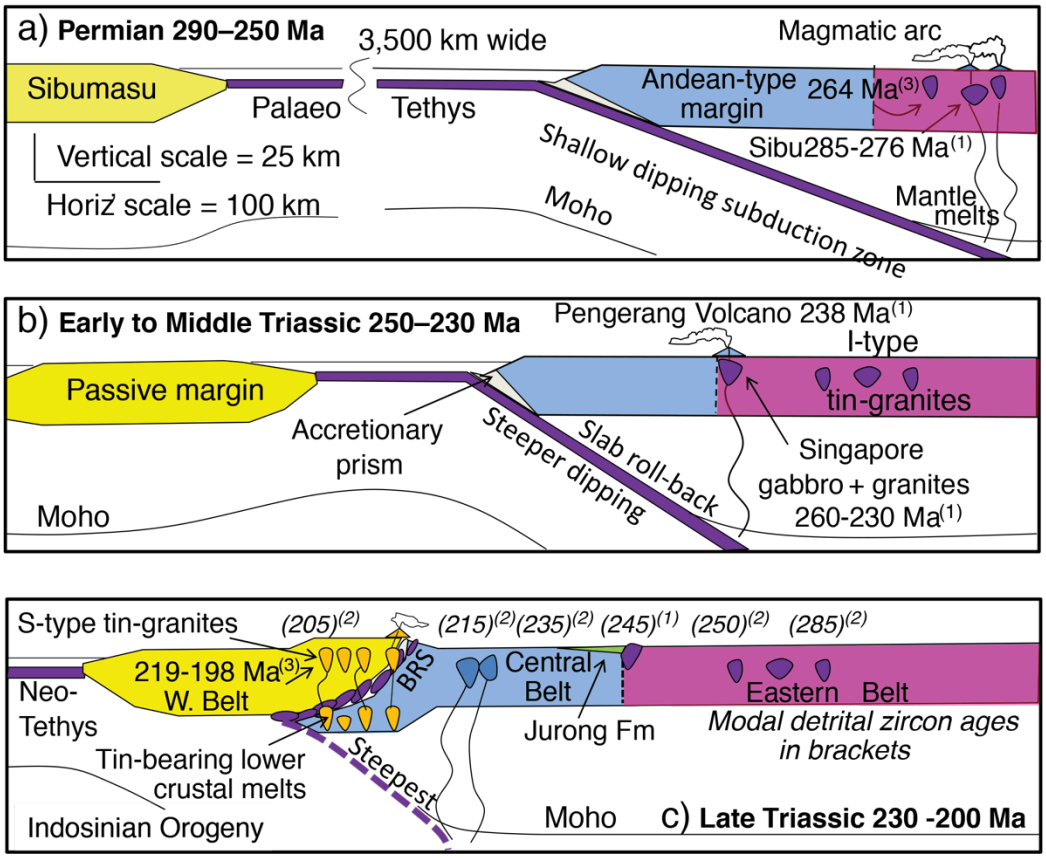

Figure 5.3 Schematic diagram of Tectonic Model B explains the formation and the emplacement of the Malaysian granitoids in the Permo-Triassic period, proposed by Oliver *et al.* (2014).

possibly Neo-Achaean) age. Although detrital zircon ages and particularly zircon Hf isotopes can potentially provide good indicators of provenance, the Hf results from the Main Range Province are essentially inconclusive.

5.8 Conclusion

This study has reviewed the formation and the emplacement of the Malaysian granitoids. The data provides new geochemical and U-Pb zircon geochronological constraints that can be applied to interpreting the tectonics of the Malay Peninsula during the Permo-Triassic period. Table 5.1 summarizes the characteristics of Malaysian granitoids in both the Eastern Province and the Main Range Province that have been presented in Chapters 2-4. In general, the Malaysian granitoids were divided into a pre-collision Andean-type, arc-related I-type Eastern Province (289 – 220 Ma) in Indochina – East Malaya, and a transitional I/S-type Main Range Province (226 – 201 Ma) in Sibumasu. Although both granitic provinces have the same source signatures of HFSE enrichment, and Cambro-Ordovican and Mesoproterozoic zircon inheritance, they were emplaced into different continental terranes. The HFSE enrichment and the Cambro-Ordovician inheritance were interpreted as source signature (Castro *et al.*, 2012; Zhu *et al.*, 2012; Kawakami *et al.*, 2014). Tin metallogenesis is related to the hybridization of igneous- and sedimentary-sourced melts during the granite formation and subsequent fractionation.

The petrogenesis and emplacement of the Malaysian granitoids could be explained by two possible tectonic models. Both tectonic models involve an east-dipping subduction zone along Bentong-Raub suture, along which rollback subsequently to resulted in westward younging I-type Eastern Province granitoids on the over-riding Indochina –

TABLE 5.1 LITHOLOGICAL AND GEOCHEMICAL CHARACTERISTICS OF THE MALAYSIAN GRANITOIDS

Characteristics	Main Range Province	Eastern Province
Morphology	Batholithic	
Age (Ma)	227 – 201	289 – 220
Indicative minerals	Biotite, sphene, ilmenite, (muscovite but usually secondary), (hornblende in Bintang Batholith)	Biotite, hornblende, sphene, ilmenite, (magnetite)
A/CNK	> 1.1, except Bintang Hbl-bearing granite	< 1.1
Major element geochemistry[1]	Transitional I/S-type	I-type
Trace element geochemistry[2]	Syn-collision granite	Volcanic arc granite to syn-collision granite
$(^{87}Sr/^{86}Sr)_i$	0.7062 – 0.7159	0.7044 – 0.7074
$\varepsilon Nd(t)$	-7.82 – -9.56	-2.39 – -5.25 (+0.62 for Perhentian syenite and -10.01 for Berangkat tonalite)
Nd model age (Ga)	1.63 – 1.99	0.89 – 1.36 (1.69 for Berangkat tonalite)
Parental magma	Hybridized magma with significant input of igneous and sedimentary melts	Hybridized magma with dominantly igneous melt
Source signature	Enrichment in HFSE Cambro-Ordovician and Mesoproterozoic zircon inheritance	

East Malaya terrane. However, these two tectonic models have different interpretation on the formation of transitional I/S-type Main Range Province. Tectonic Model A is modified after Searle *et al.* (2012), which suggests the Main Range was formed in response to a new east-dipping subduction of Neo-Tethys Ocean lithosphere started in the mid-Triassic to the west of Sibumasu, after the Sibumasu – East Malaya collision. The Main Range Province granitoids were produced by similar processes as the Eastern Province granitoids, but involved melting of both igneous and sedimentary crustal sources. The Main Range granites are extremely radiogenic with very high U concentrations (8900 – 40,000 ppm) (Searle *et al.*, 2012) so some of the extra hear required to melt the Main Range batholith was probably internal from high heat-producing elements. Extra heat could also have been derived from magmatic underplating during subduction. Fluids driven off the subduction zone could also have contributed to lowering of the granite solidus promoting extensive lower crustal melting. This model also explains the I-type granitoids in Phuket Island and along the Mergui Coast of Burma, although the ages of these I-type granitoids remains poorly constrained.

Tectonic Model B was proposed by Oliver *et al.* (2014). This model involves slab roll-back along the Bentong-Raub Palaeo-Tethyan subduction zone during the Sibumasu – East Malaya collision, followed by underthrusting of East Malaya beneath Sibumasu (or overthrusting of Sibumasu over East Malaya). In this model the Main Range granitoids were produced by partial melting of underthrust I-type Eastern Province granitoids. However, there is no geological evidence for such underthrusting (overthrusting), and partial melting of I-type granitoids to form transitional I/S-type Main Range granitoids is unlikely. Overall, Tectonic geological and geochronological data tend to suuport Model A as the preferred option.

Bibliography

Abdullah, N. T., 2009, Mesozoic Stratigraphy, *in* Hutchison, C. S. and Tan, D. N.-K., eds., Geology of Peninsular Malaysia: Kuala Lumpur, The University of Malaya, The Geological Society of Malaysia, p. 87-132.

Ahmad, J., 1979, The Petrology of the Benom Igneous Complex, Kuala Lumpur, Geological Survey of Malaysia, Geological Survey of Malaysia Special Paper, 141 p.:

Annen, C., Blundy, J. D. and Sparks, R. S. J., 2006, The genesis of intermediate and silicic magmas in deep crustal hot zones: Journal of Petrology, v. 47, no. 3, p. 505-539.

Archbold, N. W., Pigram, C. J., Ratman, N. and Hakim, S., 1982, Indonesian Permian brachiopod fauna and Gondwana–South-East Asia relationships: Nature, v. 296, no. 5857, p. 556-558.

Asama, K., 1984, *Gigantopteris* flora in China and Southeast Asia, *in* Kobayashi, T., Toriyama, R. and Hashimoto, W., eds., Geology and Palaeontology of Southeast Asia, Volume 25: Tokyo, University of Tokyo Press, p. 311-325.

Aw, P. C., 1990, Geology and mineral resources of the Sungai Aring area, Kelantan Darul Naim, Geological Survey West Malaysia District Memoir, 116 p.:

Babu, T. M., 1993, Comparative studies of tin fertile granitic rocks in space and time: Resource Geology, v. 43, no. 5, p. 355-363.

Barber, A. J. and Crow, M. J., 2003, An Evaluation of Plate Tectonic Models for the Development of Sumatra: Gondwana Research, v. 6, no. 1, p. 1-28.

Barber, A. J., Ridd, M. F. and Crow, M. J., 2011, The origin, movement and assembly of the pre-Tertiary tectonic units of Thailand, *in* Ridd, M. F., Barber, A. J. and

Crow, M. J., eds., The Geology of Thailand: London, Geological Society of London, p. 507-537.

Barley, M. E., Pickard, A. L., Zaw, K., Rak, P. and Doyle, M. G., 2003, Jurassic to Miocene magmatism and metamorphism in the Mogok metamorphic belt and the India-Eurasia collision in Myanmar: Tectonics, v. 22, no. 3, p. 1019, doi:1010.1029/2002TC001398.

Barley, M. E. and Zaw, K., 2009, SHRIMP U-Pb in zircon geochronology of granitoids from Myanmar: temporal constraints on the tectonic evolution of Southeast Asia [Geophysical Research Abstract], Vienna: European Geosciences Union General Assembly 2009.

Barth, T. F. W., 1952, Theoretical Petrology, New York, J. Wiley & Sons, 416 p.:

Beckinsale, R. D., 1979, Granite magmatism in the tin belt of Southeast Asia, *in* Atherton, M. P. and Tarney, J., eds., Origin of Granite Batholiths: Geochemical Evidence: Orpington, Kent, Shiva Publishing, p. 34-44.

Bignell, J. D. and Snelling, N. J., 1977, The geochronology of Malayan granites: Overseas Geology and Mineral Resources, v. No. 47, p. 1-72.

Bird, M. I., Taylor, D. and Hunt, C., 2005, Palaeoenvironments of insular Southeast Asia during the Last Glacial Period: a savanna corridor in Sundaland?: Quaternary Science Reviews, v. 24, p. 2228-2242.

Blevin, P. L. and Chappell, B. W., 1995, Chemistry, origin and evolution of mineralized granites in the Lachlan Fold Belt, Australia: The metallogeny of I- and S-type granites: Economic Geology, v. 90, no. 6, p. 1604-1619.

Bons, P. D. and Elburg, M. A., 2001, Fractal size distribution of plutons: An example from the Lachlan Fold Belt, Australia, *in* Chappell, B. W. and Fleming, P. D., eds., S-type Granites and Related Rocks, Australian Geological Survey.

Bowen, N. L., 1948, The granite problem and the method of multiple prejudices: Geological Society of America Memoir, v. 28, p. 79-90.

Bowring, S. A. and Schmitz, M. D., 2003, High-precision U-Pb zircon geochronology and the stratigraphic record, *in* Hancher, J. M. and Hoskin, P. W. O., eds., Zircon, Volume 53: Washington, D.C., The Mineralogical Society of America, p. 305-326.

Bradford, E. F., 1972, The Geology and Mineral Resources of the Gunong Jerai Area, Kedah, Geological Survey West Malaysia District Memoir, 242 p.:

Brown, M., 1994, The generation, segregation, ascent and emplacement of granite magma: The migmatite-to-crustally-derived granite connection in thickened orogens: Earth-Science Reviews, v. 36, no. 1-2, p. 83-130.

Brown, M., 2001a, Crustal melting and granite magmatism: Key issues: Physics and Chemistry of the Earth, v. 26, no. 4-5, p. 201-212.

Brown, M., 2001b, Orogeny, migmatites and leucogranites: A review: Journal of Earth System Science, v. 110, no. 4, p. 313-336.

Brown, M., 2004, Melt extraction from lower continental crust: Transactions of the Royal Society of Edinburgh: Earth Sciences, v. 95, no. 1-2, p. 35-48.

Brown, M., 2007, Crustal melting and melt extraction, ascent and emplacement in orogens: Mechanisms and consequences: Journal of the Geological Society, v. 164, no. 4, p. 709-730.

Brown, M., 2010a, Melting of the continental crust during orogenesis: the thermal, rheological, and compositional consequences of melt transport from lower to upper continental crust: Canadian Journal of Earth Sciences, v. 47, no. 5, p. 655-694.

Brown, M., 2010b, The spatial and temporal patterning of the deep crust and implications for the process of melt extraction: Philosophical Transactions of the Royal Society A: Mathematical, Physical and Engineering Sciences, v. 368, no. 1910, p. 11-51.

Brown, M., 2013, Granite: From genesis to emplacement: Geological Society of America Bulletin, v. 125, no. 7-8, p. 1079-1113.

Brown, M., Averkin, Y. A., McLellan, E. L. and Sawyer, E. W., 1995, Melt segregation in migmatites: Journal of Geophysical Research: Solid Earth, v. 100, no. B8, p. 15655-15679.

Brown, M. and Korhonen, F. J., 2009, Some remarks on melting and extreme metamorphism of crustal rocks, *in* Dasgupta, S., ed., Physics and Chemistry of the Earth: New York, Indian National Science Academy, Springer, p. 67-87.

Brown, M. and Solar, G. S., 1998, Shear zone systems and melts: Feedback relations and self-organization in orogenic belts: Journal of Structural Geology, v. 20, no. 2-3, p. 211-227.

Brown, M. and Solar, G. S., 1999, The mechanism of ascent and emplacement of granite magma during transpression: A syntectonic granite paradigm: Tectonophysics, v. 312, no. 1, p. 1-33.

Castro, N. A., Grande de Araujo, C. E., Basei, M. A. S., Osako, L. S., Nutman, A. A. and Liu, D.-Y., 2012, Ordovician A-type granitoid magmatism on the Ceará Central Domain, Borborema Province, NE Brazil: Journal of South American Earth Sciences, v. 36, p. 18-31.

Chakraborty, K. R., 1995, Genting Sempah Volcanic Complex: Genetic implication for Main Range granite: Warta Geology, v. 21, p. 216-217.

Charkraborty, K. R. and Metcalfe, I., 1985, Analysis of mesoscopic structures at Mersing and Tanjung Kempit, Johore, Peninsular Malaysia: Geological Society of Malaysia Bulletin, v. 17, p. 357-371.

Chappell, B. W., Bryant, C. J. and Wyborn, D., 2012, Peraluminous I-type granites: Lithos, v. 153, p. 142-153.

Chappell, B. W. and White, A. J. R., 1974, Two contrasting granite types: Pacific Geology, v. 8, p. 173-174.

Chappell, B. W. and White, A. J. R., 1992, I- and S-type granites in the Lachlan Fold Belt: Transactions of the Royal Society of Edinburgh: Earth Sciences, v. 83, no. 1-2, p. 1-26.

Chappell, B. W., White, A. J. R. and Wyborn, D., 1987, The importance of residual source material (restite) in granite petrogenesis: Journal of Petrology, v. 28, no. 6, p. 1111-1138.

Chenhall, B. E., Phillips, E. R. and Gradwell, R., 1980, Spotted Structures in Gneiss and Veins from Broken Hill, New South Wales, Australia: Mineralogical Magazine, v. 43, no. 330, p. 779-787.

Chiu, H.-Y., Chung, S.-L., Wu, F.-Y., Liu, D.-Y., Liang, Y.-H., Lin, I.-J., Iizuka, Y., Xie, L.-W., Wang, Y.-B. and Chu, M.-F., 2009, Zircon U–Pb and Hf isotopic constraints from eastern Transhimalayan batholiths on the precollisional magmatic and tectonic evolution in southern Tibet: Tectonophysics, v. 477, no. 1-2, p. 3-19.

Chu, L.-H., Chand, F. and Santokh Singh, D., 1988, Primary tin mineralization in Malaysia: Aspects of geological setting and exploration strategy, *in* Hutchison, C. S., ed., Geology of Tin Deposits in Asia and the Pacific, Volume 3: Berlin, Heidelberg, New York, Springer-Verlag, p. 593-613.

Chu, M.-F., Chung, S.-L., Song, B., Liu, D.-Y., O'Reilly, S. Y., Pearson, N. J., Ji, J.-Q. and Wen, D.-J., 2006, Zircon U-Pb and Hf isotope constraints on the Mesozoic tectonics and crustal evolution of southern Tibet: Geology, v. 34, no. 9, p. 745-748.

Chung, S.-L., Liu, D.-Y., Ji, J.-Q., Chu, M.-F., Lee, H.-Y., Wen, D.-J., Lo, C.-H., Lee, T.-Y., Qian, Q. and Zhang, Q., 2003, Adakites from continental collision zones: Melting of thickened lower crust beneath southern Tibet: Geology, v. 31, no. 11, p. 1021-1024.

Clarke, D. B., 1992, Granitoid Rocks, London, Chapman & Hall, Topics in the Earth Sciences, 283 p.:

Clemens, J. D., 2006, Melting of the continental crust: Fluid regimes, melting reactions, and source-rock fertility, *in* Brown, M., and Rushmer, T., eds., Evolution and Differentiation of the Continental Crust: Cambridge, Cambridge University Press, p. 297-331.

Clemens, J. D. and Stevens, G., 2012, What controls chemical variation in granitic magmas?: Lithos, v. 134-135, p. 317-329.

Clemens, J. D., Stevens, G. and Farina, F., 2011, The enigmatic sources of I-type granites: The peritectic connexion: Lithos, v. 126, no. 3-4, p. 174-181.

Cobbing, E. J. and Mallick, D. I. J., 1987, South East Asia Granite Project: Field Report for Peninsula Malaysia, British Geological Survey, 129 p.:

Cobbing, E. J., Mallick, D. I. J., Pitfield, P. E. J. and Teoh, L.-H., 1986, The granites of the Southeast Asian Tin Belt: Journal of Geological Society, v. 143, p. 537-550.

Cobbing, E. J., Pitfield, P. E. J., Darbyshire, D. P. F. and Mallick, D. I. J., 1992, The Granites of the South-East Asian Tin Belt, London, British Geological Survey, Overseas Memoir of the British Geological Survey, 369 p.:

Cross, C. W., Iddings, J. P., Pirsson, L. V. and Washington, H. S., 1903, Quantitative classification of igneous rocks: based on chemical and mineral characters, with a systematic nomenclature, Chicago, The University of Chicago Press, 286 p.:

Cruden, A. R., 1998, On the emplacement of tabular granites: Journal of the Geological Society, v. 155, no. 5, p. 836-862.

Cruden, A. R. and McCaffrey, K. J. W., 2001, Growth of plutons by floor subsidence: implications for rates of emplacement, intrusion spacing and melt-extraction mechanisms: Physics and Chemistry of the Earth, v. 26, no. 4-5, p. 303-315.

Cruden, A. R. and McCaffrey, K. J. W., 2002, Different scaling laws for sills, laccoliths and plutons: Mechanical thresholds on roof lifting and floor depression, *in* Breitkreuz, C., Mock, A. and Petford, N., eds., First International Workshop: Physical Geology of Subvolcanic Systems - Laccoliths, Sills and Dikes (LASI), Volume 20/2002: Freiberg, Wissenschaftliche Mitteilung des Institute für Geologie, Technische Universität Bergakademie Freiberg, p. 15-17.

Daniel, C., Vidal, P., Fernandez, A., LeFort, P. and Peucat, J. J., 1987, Isotopic study of the Manaslu granite (Himalaya, Nepal) - Inferences on the age and source of Himalayan leucogranite: Contribution to Mineralogy and Petrology, v. 96, no. 1, p. 78-92.

Darbyshire, D. P. F., 1988a, South-east Asia Granite Project - Geochronology of Malaysian Granites, Nat. Environment Research Council Isotope Geol. Centre, London, Rep., v. 88(3), 60 p.:

Darbyshire, D. P. F., 1988b, South-east Asia Granite Project - Geochronology of Thai Granites, Nat. Environment Research Council Isotope Geol. Centre, London, Rep., v. 88(5), 46 p.:

Darbyshire, D. P. F., 1988c, South-east Asia Granite Project - Geochronology of Tin Islands Granites, Indonesia, Nat. Environment Research Council Isotope Geol. Centre, London, Rep., v. 88(4), 32 p.:

Darbyshire, D. P. F. and Swainbank, I. G., 1988, South-east Asia Granite Project - Geochronology of a Selection of Granites from Burma, Nat. Environment Research Council Isotope Geol. Centre, London, Rep., v. 88(6), 44 p.:

Davis, D. W., Williams, I. S. and Krough, T. E., 2003, Historical development of zircon geochronology, *in* Hancher, J. M. and Hoskin, P. W. O., eds., Zircon, Volume 53: Washington, D.C., The Mineralogical Society of America, p. 145-181.

Dell'Angelo, L. N. and Tullis, J., 1988, Experimental deformation of partially melted granitic aggregates: Journal of Metamorphic Geology, v. 6, no. 4, p. 495-515.

DePaolo, D. J., 1981, Trace element and isotopic effects of combined wallrock assimilation and fractional crystallization: Earth and Planetary Science Letters, v. 53, no. 2, p. 189-202.

DePaolo, D. J., 1988, Neodymium Isotope Geochemistry: An Introduction, Berlin, Heidelberg, New York, London, Paris, Tokyo, Springer-Verlag, Minerals and Rocks Series, v. 20, 187 p.:

Eby, G. N., 1992, Chemical subdivision of the A-type granitoids: Petrogenetic and tectonic implications: Geology, v. 20, no. 7, p. 641-644.

Eskola, P. E., 1932, Mineralogie und Petrologie Mitteilungen, v. 42, p. 455-481.

Esmaeily, D., Nédélec, A., Valizadeh, M. V., Moore, F. and Cotten, J., 2005, Petrology of the Jurassic Shah-Kuh granite (eastern Iran), with reference to tin mineralization: Journal of Asian Earth Sciences, v. 25, no. 6, p. 961-980.

Eugster, H. P., 1985, Granites and hydrothermal ore deposits: a geochemical framework: Mineralogical Magazine, v. 49, p. 7-23.

Ewart, A. and Griffin, W. L., 1994, Application of proton-microprobe data to trace-element partitioning in volcanic-rocks: Chemical Geology, v. 117, no. 1-4, p. 251-284.

Floyd, P. A., 1993, Igneous Rocks of South-west England, London, Chapman & Hall, Geological Conservation Review Series, 256 p.:

Foley, S. F., Buhre, S. and Jacob, D. E., 2003, Evolution of the Archaean crust by delamination and shallow subduction: Nature, v. 421, no. 6920, p. 249-252.

Fontaine, H. and Workman, D. R., 1978, Review of the geology and mineral resources of Kampuchea, Laos and Vietnam, *in* Nutalaya, P., ed., Geology and Mineral Resources of Southeast Asia: Bangkok, Asian Institute of Technology, p. 538-603.

Frost, B. R., Barnes, C. G., Collins, W. J., Arculus, R. J., Ellis, D. J. and Frost, C. D., 2001, A geochemical classification for granitic rocks: Journal of Petrology, v. 42, no. 11, p. 2033-2048.

Frost, B. R., Frost, C. D., Hulsebosch, T. P. and Swapp, S. M., 2000, Origin of the charnockites of the Louis Lake Batholith, Wind River Range, Wyoming: Journal of Petrology, v. 41, no. 12, p. 1759-1776.

Ghani, A. A., 2000, The Western Belt granite of Peninsular Malaysia: some emergent problems on granite classification and its implication: Geosciences Journal, v. 4, no. 4, p. 283-293.

Ghani, A. A., 2001, Petrology and geochemistry of granite and syenite from Perhentian Island, Peninsula Malaysia: Geosciences Journal, v. 5, no. 2, p. 123-137.

Ghani, A. A., 2003a, Geochemistry of the main rock forming minerals in the Perhentian Kecil Syenite, Besut, Terengganu: Malaysian Journal of Science, v. 22, p. 77-85.

Ghani, A. A., 2003b, Geochemistry of tourmaline-bearing granite from Maras-Jong Terengganu, Peninsula Malaysia: Geological Society of Malaysia Bulletin, v. 46, p. 19-24.

Ghani, A. A., 2005a, Geochemical characteristics of S- and I-type granites: Example from Peninsular Malaysia granites: Geological Society of Malaysia Bulletin, v. 51, p. 123-134.

Ghani, A. A., 2005b, Highly evolved S type granite: Selim Granite, Main Range Batholith, Peninsular Malaysia: Geological Society of Malaysia Bulletin, v. 51, p. 95-101.

Ghani, A. A., 2006, Field evidence of magma mixing in plutonic rock from the Benom Complex, Central Belt of Peninsular Malaysia: Geological Society of Malaysia Bulletin, v. 52, p. 55-58.

Ghani, A. A., 2009a, Plutonism, *in* Hutchison, C. S. and Tan, D. N.-K., eds., Geology of Peninsular Malaysia: Kuala Lumpur, The University of Malaya, The Geological Society of Malaysia, p. 211-232.

Ghani, A. A., 2009b, Volcanism, *in* Hutchison, C. S. and Tan, D. N.-K., eds., Geology of Peninsular Malaysia: Kuala Lumpur, The University of Malaya, The Geological Society of Malaysia, p. 197-210.

Ghani, A. A., Lo, C.-H. and Chung, S.-L., 2013, Basaltic dykes of the Eastern Belt of Peninsular Malaysia: The effects of the difference in crustal thickness of Sibumasu and Indochina: Journal of Asian Earth Sciences, v. 77, p. 127-139.

Ghani, A. A., Ramesh, V., Yong, B.-T. and Khoo, T.-T., 2006, Geochemistry and petrology of syenite, monzonite and gabbro from the Central Belt of Peninsular Malaysia: Geological Society of Malaysia Bulletin, v. 49, p. 25-30.

Ghani, A. A., Ramesh, V., Yong, B.-T., Khoo, T.-T. and Muda, S., 2002, High Ba igneous rocks from the Central Belt of Peninsula Malaysia and its implication, Geological Society of Malaysia Annual Geological Conference: Kota Bharu, p. 45-49.

Ghani, A. A. and Rashid, A. A., 2008, Petrology and geochemistry of the plutonic igneous rock from Tioman Island, *in* Phang, S.-M., Amri, A. Y., Ooi, J. L.-S. and Jamal, M. A., eds., Natural History of the Pulau Tioman Group of Islands: Kuala Lumpur, Institute of Ocean and Earth Sciences, University of Malaya, p. 5-9.

Ghani, A. A., Searle, M. P., Robb, L. J. and Chung, S.-L., 2013, Transitional I-S type characteristic in the Main Range Granite, Peninsular Malaysia: Journal of Asian Earth Sciences, v. 76, p. 225-240.

Ghani, A. A., Shaarani, N. A. and Anuar, H. A. A., 1999, Field relation of granite-volcanics interaction at Tioman Island, Pahang: more evidence for the occurrence of an older granite: Warta Geology, v. 25, no. 5, p. 229-233.

Ghani, A. A. and Singh, N., 2002, Sempah volcanic complex, Western Belt of Peninsular Malaysia, Preliminiary study of petrology and geochmistry: Malaysian Journal of Science, v. 21, no. 1-2, p. 123-130.

Ghani, A. A. and Singh, N., 2005, Petrology and geochemistry of the Sempah volcanic complex, Peninsular Malaysia: Geological Society of Malaysia Bulletin, v. 51, p. 103-121.

Ghani, A. A. and Taib, N. I., 2007, New trace, major and rare earth element data for early Pleistocene alkali olivine basalt and olivine nephelinites from Kuantan, Pahang: plume related rift volcanics or wrench related crustal extension: Geological Society of Malaysia Bulletin, v. 53, p. 111-117.

Goldstein, S. L., Onions, R. K. and Hamilton, P. J., 1984, A Sm-Nd Isotopic Study of Atmospheric Dusts and Particulates from Major River Systems: Earth and Planetary Science Letters, v. 70, no. 2, p. 221-236.

Gray, C. M., 1984, An isotopic mixing model for the origin of granitic rocks in southeastern Australia: Earth and Planetary Science Letters, v. 70, no. 1, p. 47-60.

Gray, C. M. and Kemp, A. I. S., 2009, The two-component model for the genesis of granitic rocks in southeastern Australia - Nature of the metasedimentary and basaltic end members: Lithos, v. 111, no. 3-4, p. 113-124.

Green, O. R., Searle, M. P., Corfield, R. I. and Corfield, R. M., 2008, Cretaceous-Tertiary carbonate platform evolution and the age of the India-Asia collision along the Ladakh Himalaya (Northwest India): Journal of Geology, v. 116, no. 4, p. 331-353.

Green, T. H. and Ringwood, A. E., 1968, Genesis of the calc-alkaline igneous rock suite: Contribution to Mineralogy and Petrology, v. 18, no. 2, p. 105-162.

Grosse, P., Bellos, L. I., de los Hoyos, C. R., Larrovere, M. A., Rossi, J. N. and Toselli, A. J., 2011, Across-arc variation of the Famatinian magmatic arc (NW Argentina) exemplified by I-, S- and transitional I/S Early Ordovician granitoids of the Sierra de Velasco: Journal of South American Earth Sciences, v. 32, no. 1, p. 110-126.

Groves, D. I. and McCarthy, T. S., 1978, Fractional crystallization and the origin of Sn deposits in granitoids: Mineralium Deposita, v. 13, no. 1, p. 11-26.

Guo, Z.-F. and Wilson, M., 2012, The Himalayan leucogranites: Constraints on the nature of their crustal source region and geodynamic setting: Gondwana Research, v. 22, no. 2, p. 360-376.

Haile, N. S., 1973, The recognition of former subduction zones in Southeast Asia, *in* Tarling, D. H. and Runcorn, S. K., eds., Implications of Continental drift in the Earth Sciences, Volume 2: London, Academic Press, p. 885-892.

Haile, N. S., Beckinsale, R. D., Chakraborty, K. R., Abdul, H. H. and Hardjono, T., 1983, Palaeomagnetism, geochronology and petrology of the dolerite dykes and basaltic lavas from Kuantan: Geological Society of Malaysia Bulletin, v. 16, p. 71-85.

Halliday, A. N., Davidson, J. P., Hidreth, W. and Holden, P., 1991, Modelling the petrogenesis of high Rb/Sr silicic magmas: Chemical Geology, v. 92, no. 1-3, p. 107-114.

Harpum, J. R., 1963, Petrographic classification of granitic rocks in Tanganyika by partial chemical analyses, Tanganyika Geological Survey Report, Volume 10, Geological Survey of Tanganyika, p. 80-86.

Harris, N. B. W., Pearce, P. A. and Tindle, A. G., 1986, Geochemical characteristics of collision-zone magmatism, *in* Coward, M. P. and Ries, A. C., eds., Collision Tectonics, Volume 19: London, Geological Society of London, p. 67-81.

Henderson, P., 1982, Inorganic Geochemistry, Oxford, New York, Seoul, Tokyo, Pergamon Press, 353 p.:

Hervé, F., Pankhurst, R. J., Fanning, C. M., Calderón, M. and Yaxley, G. M., 2007, The South Patagonian batholith: 150 my of granite magmatism on a plate margin: Lithos, v. 97, no. 3-4, p. 373-394.

Hildreth, E. W. and Moorbath, S., 1988, Crustal contributions to arc magmatism in the Andes of Central Chile: Contribution to Mineralogy and Petrology, v. 98, no. 4, p. 455-489.

Huppert, H. E. and Sparks, R. S. J., 1988, The generation of granitic magmas by intrusion of basalt into continental crust: Journal of Petrology, v. 29, no. 3, p. 599-624.

Hutchison, C. S., 1971, The Benta Migmatite Complex: Petrology of two important localities: Geological Society of Malaysia Bulletin, v. 4, p. 49-70.

Hutchison, C. S., 1973a, Plutonic activity, *in* Gobbett, D. J. and Hutchison, C. S., eds., Geology of the Malay Peninsula: West Malaysia and Singapore: New York, Wiley-Interscience, p. 215-252.

Hutchison, C. S., 1973b, Tectonic evolution of Sundaland: a Phanerozoic synthesis: Geological Society of Malaysia Bulletin, v. 6, p. 61-86.

Hutchison, C. S., 1977, Granite emplacement and tectonic subdivision of Peninsular Malaysia: Bulletin of the Geological Society of Malaysia, v. 9, p. 197-207.

Hutchison, C. S., 2007, Geological Evolution of South-East Asia, Kuala Lumpur, Geological Society of Malaysia, 433 p.:

Hutchison, C. S., 2009, Bentong-Raub suture, *in* Hutchison, C. S. and Tan, D. N.-K., eds., Geology of Peninsular Malaysia: Kuala Lumpur, The University of Malaya, The Geological Society of Malaysia, p. 43-53.

Hutchison, C. S. and Tan, D. N. K., 2009, Geology of Peninsular Malaysia: Kuala Lumpur, The University of Malaya, The Geological Society of Malaysia, 479 p.:

Hutchison, C. S. and Taylor, D., 1978, Metallogenesis in SE Asia: Journal of the Geological Society v. 135, no. 4, p. 407-428.

Ishihara, S., 1977, The magnetite-series and ilmenite-series granitic rocks: Mining Geology, v. 27, p. 293-305.

Ishihara, S., Sawata, H., Arpornsuwan, S., Busaracome, P. and Bungrakearti, N., 1979, The magnetite-series and ilmenite-series granitoids and their bearing on tin mineralization, particularly of the Malay peninsula region: Bulletin of the Geological Society of Malaysia, v. 11, p. 103-110.

Jones, C. R., 1970, The Geology and Mineral Resources of the Grik Area, Upper Perak, Geological Survey West Malaysia District Memoir, 144 p.:

Kawakami, T., Nakano, N., Higashino, F., Hokada, T., Osanai, Y., Yuhara, M., Charusiri, P., Kamikubo, H., Yonemura, K. and Hirata, T., 2014, U-Pb zircon and CHIME monazite dating of granitoids and high-grade metamorphic rocks from the Eastern and Peninsular Thailand - A new report of Early Paleozoic granite.pdf: Lithos, v. 200-201, p. 64-79.

Keay, S., Collins, W. J. and McCulloch, M. T., 1997, A three-component Sr-Nd isotopic mixing model for granitoid genesis, Lachlan fold belt, eastern Australia: Geology, v. 25, no. 307-310.

Kemp, A. I. S., Hawkesworth, C. J., Collins, W. J., Gray, C. M. and Blevin, P. L., 2009, Isotopic evidence for rapid continental growth in an extensional accretionary orogen: The Tasmanides, eastern Australia: Earth and Planetary Science Letters, v. 284, no. 3-4, p. 455-466.

Kemp, A. I. S., Hawkesworth, C. J., Foster, G. L., Paterson, B. A., Woodhead, J. D., Hergt, J. M., Gray, C. M. and Whitehouse, M. J., 2007, Magmatic and crustal

differentiation history of granitic rocks from Hf-O isotopes in zircon: Science, v. 315, no. 5814, p. 980-983.

Keto, L. S. and Jacobsen, S. B., 1987, Nd and Sr isotopic variations of Early Paleozoic oceans: Earth and Planetary Science Letters, v. 84, no. 1, p. 27-41.

Kilpatrick, J. A. and Ellis, D. J., 1992, C-type magmas: igneous charnockites and their extrusive equivalents: Transactions of the Royal Society of Edinburgh: Earth Sciences, v. 83, no. 1-2, p. 155-164.

Krähenbuhl, R., 1991, Magmatism, tin mineralization, and tectonics of the Main Range Malaysian Peninsula: consequences for the plate tectonic model of Southeast Asia based on Rb-Sr, K-Ar and fission track data: Bulletin of the Geological Society of Malaysia, v. 29, p. 1-100.

Kwan, T.-S. and Yap, F.-L., 1986, The pattern of K/Ar ages of biotites from the granites of Penang: its interpretation in the light of available Rb/Sr and U/Pb data: Geological Society of Malaysia Bulletin, v. 19, p. 181-189.

Lan, C.-Y., Chung, S.-L., Long, T.-V., Lo, C.-H., Lee, T.-Y., Mertzman, S. A. and Shen, J. J.-S., 2003, Geochemical and Sr-Nd isotopic constraints from the Kontum massif, central Vietnam on the crustal evolution of the Indochina block: Precambrian Research, v. 122, no. 1-4, p. 7-27.

Lee, C.-P., 2009, Palaeozoic Stratigraphy, *in* Hutchison, C. S. and Tan, D. N.-K., eds., Geology of Peninsular Malaysia: Kuala Lumpur, The University of Malaya, The Geological Society of Malaysia, p. 55-86.

Lee, H.-Y., Chung, S.-L., Lo, C.-H., Ji, J.-Q., Lee, T.-Y., Qian, Q. and Zhang, Q., 2009, Eocene Neotethyan slab breakoff in southern Tibet inferred from the Linzizong volcanic record: Tectonophysics, v. 477, no. 1-2, p. 20-35.

Lehmann, B., 1990, Metallogeny of Tin, Springer, Lecture Notes in Earth Sciences, 211 p.:

Liew, T.-C., 1983, Petrogenesis of the Peninsular Malaysian Granitoid Batholiths [Ph. D.: Australian National University, 291 p.

Liew, T.-C. and McCulloch, M. T., 1985, Genesis of granitoid batholiths of Peninsular Malaysia and implications for models of crustal evolution: Evidence from Nd-Sr isotopic and U-Pb zircon study: Geochimica et Cosmochimica Acta, v. 49, p. 589-600.

Liew, T.-C. and Page, R. W., 1985, U-Pb zircon dating of granitoid plutons from the West Coast Province of Peninsular Malaysia: Journal of the Geological Society, v. 142, p. 515-526.

Loiselle, M. C. and Wones, D. R., 1979, Characteristics and origin of anorogenic granites: Geological Society of America Abstract with Program, v. 11, p. 468.

Ludwig, K. R., 1998, On the treatment of concordant uranium-lead ages: Geochimica et Cosmochimica Acta, v. 62, no. 4, p. 665-676.

Ludwig, K. R., 2001, Isoplot/Ex, rev. 2.49. A Geochronological Toolkit for Microsoft Excel: Berkeley Geochronology Center, Special Publication v. 1a.

MacDonald, A. S., Barr, S. M., Miller, B. V., Reynolds, P. H., Rhodes, B. P. and Yokart, B., 2010, P–T–t constraints on the development of the Doi Inthanon metamorphic core complex domain and implications for the evolution of the western gneiss belt, northern Thailand: Journal of Asian Earth Sciences, v. 37, no. 1, p. 82-104.

Mahood, G. A. and Hildreth, E. W., 1983, Large partition coefficients for trace elements in high-silica rhyolites: Geochimica et Cosmochimica Acta, v. 47, no. 1, p. 11-30.

Maniar, P. D. and Piccoli, P. M., 1989, Tectonic discrimination of granitoids: Geological Society of America Bulletin, v. 101, no. 5, p. 636-643.

Manning, D. A. C. and Exley, C. S., 1984, The origins of late-stage rocks in the St Austell granite—a re-interpretation: Journal of the Geological Society, v. 141, no. 3, p. 581-591.

McCaffrey, K. J. W. and Cruden, A. R., 2002, Dimensional data and growth models for intrusions, *in* Breitkreuz, C., Mock, A. and Petford, N., eds., First International Workshop: Physical Geology of Subvolcanic Systems - Laccoliths, Sills and Dikes (LASI), Volume 20/2002: Freiberg, Wissenschaftliche Mitteilung des Institute für Geologie, Technische Universität Bergakademie Freiberg, p. 37-39.

McCaffrey, K. J. W. and Petford, N., 1997, Are granitic intrusions scale invariant?: Journal of the Geological Society, v. 154, no. 1, p. 1-4.

McCulloch, M. T. and Chappell, B. W., 1982, Nd isotopic characteristics of S- and I-type granites: Earth and Planetary Science Letters, v. 58, no. 1, p. 51-64.

Metcalfe, I., 1984, Stratigraphy, palaeontology and palaeogeography of the Carboniferous of Southeast Asia: Memoires de la Societe geologique de France, v. 147, p. 107-118.

Metcalfe, I., 1988, Origin and assembly of south-east Asian continental terranes, *in* Audley-Charles, M. G. and Hallam, A., eds., Gondwana and Tethys, Volume 37: London, Geological Society of London, p. 101-118.

Metcalfe, I., 1994, Gondwanaland origin, dispersion, and accretion of East and Southeast Asian continental terranes: Journal of South American Earth Sciences, v. 7, no. 3/4, p. 333-347.

Metcalfe, I., 1996, Pre-Cretaceous evolution of SE Asian terranes, *in* Hall, R. and Blundell, D. J., eds., Tectonic Evolution of Southeast Asia, Volume 106: London, Geological Society of London, p. 97-122.

Metcalfe, I., 2000, The Bentong-Raub suture zone: Journal of Asian Earth Sciences, v. 18, p. 691-712.

Metcalfe, I., 2002, Permian tectonic framework and palaeogeography of SE Asia: Journal of Asian Earth Sciences, v. 20, no. 6, p. 551-556.

Metcalfe, I., 2005, Asia: South-East *in* Selley, R. C., Cocks, L. R. M., and Plimer, I. R., eds., Encyclopedia of Geology, Volume 1: Oxford, Elsevier, p. 169-198.

Metcalfe, I., 2011, Tectonic framework and Phanerozoic evolution of Sundaland: Gondwana Research, v. 19, p. 3-21.

Metcalfe, I., 2013, Tectonic evolution of the Malay Peninsula: Journal of Asian Earth Sciences, v. 2013, no. 76, p. 195-213.

Mielke, P. and Winkler, H. C. F., 1979, Eine bessere berechnung der mesonorm für granitische gesteine: Neues Jahrbuch für Mineralogie - Monatshefte, v. 10, p. 471-480.

Mitchell, A. H. G., 1977, Tectonic settings for emplacement of Southeast Asian tin granites: Bulletin of the Geological Society of Malaysia, v. 9, p. 123-140.

Mitchell, A. H. G., Chung, S.-L., Oo, T., Lin, T.-H. and Hung, C.-H., 2012, Zircon U-Pb ages in Myanmar: Magmatic-metamorphic events and the closure of a neo-Tethys ocean?: Journal of Asian Earth Sciences, v. 56, p. 1-23.

Mitchell, A. H. G. and Garson, M. S., 1981, Mineral Deposits and Global Tectonic Settings, London, Sydney, Academic Press, 405 p.:

Mlynarczyk, M. S. J. and Williams-Jones, A. E., 2005, The role of collisional tectonics in the metallogeny of the Central Andean tin belt: Earth and Planetary Science Letters, v. 240, no. 3-4, p. 656-667.

Niggli, P., 1936, Über molekularnormen zur gesteinsberechnung: Schweizer Mineralogische and Petrographische Mitteilungen, v. 16, no. 2, p. 295-317.

O'Nions, R. K., Hamilton, P. J. and Evensen, N. M., 1977, Variations in $^{143}Nd/^{144}Nd$ and $^{87}Sr/^{86}Sr$ ratios in oceanic basalts: Earth and Planetary Science Letters, v. 34, no. 1, p. 13-22.

Oliver, G. J. H. and Prave, A., 2013, Palaeogeography of Late Triassic red-beds in Singapore and the Indosinian Orogeny: Journal of Asian Earth Sciences, v. 76, p. 214-224.

Oliver, G. J. H., Zaw, K., Hotson, M. D., Meffre, S. and Manka, T., 2014, U–Pb zircon geochronology of Early Permian to Late Triassic rocks from Singapore and Johor: A plate tectonic reinterpretation Gondwana Research, v. 26, no. 1, p. 132-143.

Pankhurst, R. J., Rapela, C. W. and Fanning, C. M., 2000, Age and origin of coeval TTG, I- and S-type granites in the Famatinian arc of NW Argentina: Transactions of the Royal Society of Edinburgh: Earth Sciences, v. 91, no. 1-2, p. 151-168.

Parrish, R. R. and Noble, S. R., 2003, Zircon U-Th-Pb geochronology by isotope dilution - thermal ionization mass spectrometry (ID-TIMS), *in* Hancher, J. M. and Hoskin, P. W. O., eds., Zircon, Volume 53: Washington, D.C., The Mineralogical Society of America, p. 183-212.

Paterson, S. R. and Miller, R. B., 1998, Mid-crustal magmatic sheets in the Cascades Mountains, Washington: Implications for magma ascent: Journal of Structural Geology, v. 20, no. 9-10, p. 1345-1363.

Patiño Douce, A. E., 1999, What do experiments tell us about the relative contributions of crust and mantle to the origin of granitic magma?, *in* Castro, A., Fernandez, C. and Vigneresse, J. L., eds., Understanding Granites: Integrating New and Classical Techniques, Volume 168: London, Geological Society of London, p. 77-94.

Pearce, P. A. and Cann, J. R., 1973, Tectonic setting of basic volcanic rocks determined using trace element analysis: Earth and Planetary Science Letters, v. 19, no. 2, p. 290-300.

Pearce, P. A., Harris, N. B. W. and Tindle, A. G., 1984, Trace element discrimination diagrams for the tectonic interpretation of granitic rocks: Journal of Petrology, v. 25, p. 956-983.

Pedersen, R. B. and Malpas, J. G., 1984, The origin of ocenic plagiogranites from the Karmoy ophiolite, Western Norway: Contribution to Mineralogy and Petrology, v. 88, no. 1-2, p. 36-52.

Peucat, J. J., Jegouzo, P., Vidal, P. and Bernard-Griffiths, J., 1988, Continental crust formation seen through the Sr and Nd isotope systematics of S-type granites in the Hercynian belt of western France: Earth and Planetary Science Letters, v. 88, no. 1-2, p. 60-68.

Pitcher, W. S., 1997, The Nature and Origin of Granite, London, Chapman & Hall, 387 p.:

Prame, W. K. B. N. and Pohl, J., 1994, Geochemistry of pelitic and psammopelitic Precambrian metasediments from southwestern Sri-Lanka: implications for two

contrasting source-terranes and tectonic settings: Precambrian Research, v. 66, no. 1-4, p. 223-244.

Presnall, D. C. and Bateman, P. C., 1973, Fusion relations in the system $NaAlSi_3O_8$-$CaAl_2Si_2O_8$-$KAlSi_3O_8$-SiO_2-H_2O and generation of granitic magmas in the Sierra Nevada batholith: Geological Society of America Bulletin, v. 84, no. 10, p. 3181-3202.

Putthapibian, P. and Gray, C. M., 1983, Age and tin-tungsten mineralisation of the Phuket granites, Thailand, *in* Suensilpong, S., ed., Geology and Mineral Resources of Thailand: Bangkok, DMR, p. 1-10.

Read, H. H., 1948, Granites and granites: Geological Society of America Memoir, v. 28, p. 1-20.

Read, H. H., 1957, The Granite Controversy, London, Thomas Murby & Co., 430 p.:

Robb, L. J., 2005, Introduction to Ore-forming Processes, Malden, Oxford, Victoria, Blackwell Publishing, 373 p.:

Rollinson, H. R., 1993, Using Geochemical Data: Evaluation, Presentation, Interpretation, Harlow, Pearson Education Limited, 352 p.:

Roselee, M. H., Ghani, A. A. and Nyien, K. K., Petrology and Geochemistry of A type igneous rocks from Teluk Ramunia, southeastern Johor [Abstract], *in* Proceedings Proceedings of National Geoscience Conference, Ipoh, 2013, p. 8-9.

Rosenberg, C. L. and Handy, M. R., 2005, Experimental deformation of partially melted granite revisited: implications for the continental crust: Journal of Metamorphic Geology, v. 23, no. 1, p. 19-28.

Sawyer, E. W., 1991, Disequilibrium melting and the rate of melt residuum separation during migmatization of mafic rocks from the Grenville Front, Quebec: Journal of Petrology, v. 32, no. 4, p. 701-738.

Sawyer, E. W., 1994, Melt segregation in the continental crust: Geology, v. 22, no. 11, p. 1019-1022.

Sawyer, E. W., 1998, Formation and evolution of granite magmas during crustal reworking: The significance of diatexites: Journal of Petrology, v. 39, no. 6, p. 1147-1167.

Sawyer, E. W., 2001, Melt segregation in the continental crust: Distribution and movement of melt in anatectic rocks: Journal of Metamorphic Geology, v. 19, no. 3, p. 291-309.

Sawyer, E. W., 2010, Migmatites formed by water-fluxed partial melting of a leucogranodiorite protolith: Microstructures in the residual rocks and source of the fluid: Lithos, v. 116, no. 3-4, p. 273-286.

Schwartz, M. O. and Askury, A. K., 1990, Granite magmatism and tin-tungsten metallogenesis in the Kuantan-Dungun area, Malaysia: Geological Society of Malaysia Bulletin, v. 26, p. 147-179.

Schwartz, M. O., Rajah, S. S., Askury, A. K., Putthapiban, P. and Djaswadi, S., 1995, The Southeast Asian Tin Belt: Earth-Science Reviews, v. 38, no. 2-4, p. 95-293.

Scrivenor, J. B., 1928, The Geology of the Malayan Ore-deposits, London, Macmillan, 216 p.:

Scrivenor, J. B., 1931, The Geology of Malaya, London, Macmillan, 217 p.:

Searle, M. P., Cottle, J. M., Streule, M. J. and Waters, D. J., 2010, Crustal melt granites and migmatites along the Himalaya: melt source, segregation, transport and

granite emplacement mechanisms: Earth and Environmental Transactions of the Royal Society of Edinburgh, v. 100, no. 1-2, p. 219-233.

Searle, M. P., Elliot, J. R., Phillips, R. J. and Chung, S.-L., 2011, Crustal-lithospheric structure and continental extrusion of Tibet: Journal of the Geological Society, v. 168, no. 3, p. 633-672.

Searle, M. P., Whitehouse, M. J., Robb, L. J., Ghani, A. A., Hutchison, C. S., Sone, M., Ng, S. W.-P., Roselee, M. H., Chung, S.-L. and Oliver, G. J. H., 2012, Tectonic evolution of the Sibumasu-Indochina terrane collision zone in Thailand and Malaysia; constraints from new U-Pb zircon chronology of SE Asian tin granitoids: Journal of Geological Society, v. 169, no. 4, p. 489-500.

Şengör, A. M. C., 1984, The Cimmeride orogenic system and the tectonics of Eurasia: Geological Society of America Special Paper, v. 195.

Sevastjanova, I., Clements, B., Hall, R., Belousova, E. A., Griffin, W. L. and Pearson, N. J., 2011, Granitic magmatism, basement ages, and provenance indicators in the Malay Peninsula: Insights from detrital zircon U–Pb and Hf-isotope data: Gondwana Research, v. 19, no. 4, p. 1024-1039.

Shand, S. J., 1943, The Eruptive Rocks, 2nd edn, New York, J. Wiley & Co., 444 p.:

Shi, G. R. and Archbold, N. W., 1995, Permian brachiopod faunal sequence of the Shan-Thai terrane: biostratigraphy, palaeobiogeographical affinities and plate tectonic/palaeoclimatic implications: Journal of Southeast Asian Earth Sciences, v. 11, no. 3, p. 177-187.

Shuib, M. K., 2000, The Mesozoic tectonics of Peninsular Malaysia - An overview, GSM Dynamic Stratigraphy & Tectonics of Peninsular Malaysia - Seminar III. The Mesozoic of Peninsular Malaysia, Volume 26, p. 5.

Shuib, M. K., 2009a, Major faults, *in* Hutchison, C. S. and Tan, D. N.-K., eds., Geology of Peninsular Malaysia: Kuala Lumpur, The University of Malaya, The Geological Society of Malaysia, p. 249-270.

Shuib, M. K., 2009b, Structures and deformation, *in* Hutchison, C. S. and Tan, D. N.-K., eds., Geology of Peninsular Malaysia: Kuala Lumpur, The University of Malaya, The Geological Society of Malaysia, p. 271-308.

Singh, D. S., 1985, Geological map of Peninsular Malaysia: Geological Survey of Malaysia.

Singh, N. and Ghani, A. A., 2000, Sempah Volcanic Complex, Pahang: Proceedings of the Geological Society of Malaysia Annual Geological Conference 2000, p. 67-72.

Snelling, N. J., 1965, Age determination unit. Summary of results from Malaysia, Annual Report Institute Geological Sciences for 1964, 32-33 p.:

Sone, M. and Metcalfe, I., 2008, Parallel Tethyan sutures in mainland Southeast Asia: New insights for the Palaeo-Tethys closure and implications for the Indosinian orogeny: C.R. Geoscience, v. 340, p. 166-179.

Sone, M., Metcalfe, I. and Chaodumrong, P., 2012, The Chanthaburi terrane of southeastern Thailand: Stratigraphic confirmation as a disrupted segment of the Sukhothai Arc: Journal of Asian Earth Sciences, v. 16, p. 16-32.

Stacey, J. S. and Kramers, J. D., 1975, Approximation of terrestrial lead isotope evolution by a 2-stage model: Earth and Planetary Science Letters, v. 26, p. 207-221.

Stauffer, P. H. and Mantajit, N., 1981, Late Paleozoic tilloids of Malaya, Thailand and Burma, *in* Hambrey, M. J. and Harland, W. B., eds., Earth's pre-Pleistocene Glacial Record: Cambridge, Cambridge University Press, p. 331-337.

Steiger, R. H. and Jäger, E., 1977, Subcomission on Geochronology: Convention on the use of decay constants in geo- and cosmochronology: Earth and Planetary Science Letters, v. 36, p. 359-362.

Stevens, G. and Clemens, J. D., 1993, Fluid-absent melting and the roles of fluids in the lithosphere: a slanted summary?: Chemical Geology, v. 108, no. 1-4, p. 1-17.

Streckeisen, A., 1976, To each plutonic rock its proper name: Earth-Science Reviews, v. 12, no. 1, p. 1-33.

Stüwe, K. and Sandiford, M., 1994, Contribution of deviatoric stresses to metamorphic P-T paths - an example appropriate to low-P, high-T metamorphism: Journal of Metamorphic Geology, v. 12, no. 4, p. 445-454.

Stüwe, K., Sandiford, M. and Powell, R., 1993, Episodic metamorphism and deformation in low-pressure, high-temperature terranes: Geology, v. 21, no. 9, p. 829-832.

Tate, R. B., Tan, D. N.-K. and Ng, T. F., 2009, Geological Map of Peninsular Malaysia: The University of Malaya, The Geological Society of Malaysia.

Taylor, H. P., Jr., 1980, The effects of assimilation of country rocks by magmas on $^{18}O/^{16}O$ and $^{87}Sr/^{86}Sr$ systematics in igneous rocks: Earth and Planetary Science Letters, v. 47, no. 2, p. 243-354.

Taylor, R. G., 1979, Geology of tin deposits, Amsterdam, Elsevier Scientific Pub. Co., 543 p.:

Taylor, S. R., 1967, The origin and growth of continents: Tectonophysics, v. 4, no. 1, p. 17-34.

Taylor, S. R. and McLennan, S. M., 1985, The Continental Crust: Its Composition and Evolution, Oxford, Blackwell, 312 p.:

Thomas, R. and Davidson, P., 2012, Water in granite and pegmatite-forming melts: Ore Geology Reviews, v. 46, p. 32-46.

Tija, H. D., 1969, Regional implication of Lebir fault zone: Geological Society of Malaysia Newsletter, v. 19, p. 6-7.

Tija, H. D., 1996, Tectonics of deformed and undeformed Jurassic-Cretaceous strata of Peninsular Malaysia: Geological Society of Malaysia Bulletin, v. 39, p. 131-156.

Tuttle, O. F. and Bowen, N. L., 1958, Origin of granite in the light of experimental studies in the system: $NaAlSi_3O_8$-$KAlSi_3O_8$-SiO_2-H_2O, Geological society of America Memoir, 153 p.:

van Keken, P. E., 2003, The structure and dynamics of the mantle wedge: Earth and Planetary Science Letters, v. 215, no. 3-4, p. 323-338.

Vigneresse, J. L., Tikoff, B. and Ameglio, L., 1999, Modification of the regional stress field by magma intrusion and formation of tabular granitic plutons: Tectonophysics, v. 302, no. 3-4, p. 203-224.

Villaros, A., Buick, I. S. and Stevens, G., 2012, Isotopic variations in S-type granites: An inheritance from a heterogeneous source?: Contribution to Mineralogy and Petrology, v. 163, no. 2, p. 543-561.

Villaseca, C., Barbero, L. and Rogers, G., 1998, Crustal origin of Hercynian peraluminous granitic batholiths of Central Spain: petrological, geochemical and isotopic (Sr, Nd) constraints: Lithos, v. 43, no. 2, p. 55-79.

Walshe, J. L., Solomon, M., Whitford, D. J., Sun, S.-S. and Foden, J. D., 2011, The role of the mantle in the genesis of tin deposits and tin provinces of Eastern Australia: Economic Geology, v. 106, no. 2, p. 297-305.

Wang, K.-L., Chung, S.-L., O'Reilly, S. Y., Sun, S.-S., Shinjo, R. and Chen, C.-H., 2004, Geochemical constraints for the genesis of post-collisional magmatism

and the geodynamic evolution of the northern Taiwan region: Journal of Petrology, v. 45, no. 5, p. 975-1011.

Wang, X., Griffin, W. L., O'Reilly, S. Y. and Li, W.-X., 2007, Three stages of zircon growth in magmatic rocks from the Pingtan Complex, eastern China: Acta Geologica Sinica, v. 81, no. 1, p. 68-80.

Watson, E. B. and Harrison, T. M., 1983, Zircon saturation revisited: temperature and composition effects in a variety of crustal magma types: Earth and Planetary Science Letters, v. 64, no. 2, p. 295-304.

Wen, D.-R., Chung, S.-L., Song, B., Iizuka, Y., Yang, H.-J., Ji, J.-Q., Liu, D.-Y. and Gallet, S., 2008, Late Cretaceous Gangdese intrusions of adakitic geochemical characteristics, SE Tibet: Petrogenesis and tectonic implications: Lithos, v. 105, no. 1-2, p. 1-11.

Whalen, J. B., Currie, K. L. and Chappell, B. W., 1987, A-type granites: geochemical characteristics, discrimination and petrogenesis: Contribution to Mineralogy and Petrology, v. 95, no. 4, p. 407-419.

White, A. J. R., 1979, Sources of granite magmas: Geological Society of America Abstract with Program, v. 11, p. 539.

White, A. J. R. and Chappell, B. W., 1977, Ultrametamorphism and granitoids genesis: Tectonophysics, v. 43, no. 1-2, p. 7-22.

Whitehouse, M. J. and Kamber, B., 2005, Assigning dates to thin gneissic veins in high-grade metamorphic terranes: a cautionary tale from Akilia, southwest Greenland: Journal of Petrology, v. 46, p. 291-318.

Whitehouse, M. J., Kamber, B. and Moorbath, S., 1999, Age significance of U-Th-Pb zircon data from early Archean rocks of west Greenland - a reseessment based

on combined ion-microprobe and imaging studies: Chemical Geology, v. 160, p. 201-224.

Whitney, J. A., 1975, The effects of pressure, temperature, and XH2O on phase assemblage in four synthetic rock compositions: Journal of Geology, v. 83, no. 1, p. 1-31.

Whitney, J. A., 1988, The origin of granite: The role and source of water in the evolution of granitic magmas: Geological Society of America Bulletin, v. 100, no. 12, p. 1886-1897.

Wilson, B. M., 2007, Igneous Petrogenesis: A Global Tectonic Approach, AA Dordrecht, Springer, 466 p.:

Winkler, H. C. F., 1965, Petrogenesis of Metamorphic Rocks, Berlin, Springer-Verlag, 220 p.:

Wu, F.-Y., Jahn, B.-M., Wilde, S. and Sun, D.-Y., 2000, Phanerozoic continental crustal growth: Sr-Nd isotopic evidence from the granites in northeastern China: Tectonophysics, v. 328, no. 1-2, p. 89-113.

Wu, F.-Y., Sun, D.-Y., Li, H.-M., Jahn, B.-M. and Wilde, S., 2002, A-type granites in northeastern China: age and geochemical contraints on their petrogenesis: Chemical Geology, v. 187, no. 1-2, p. 143-173.

Yap, F.-L., 1986, Age determination on the Kuantan granite and dolerite dykes: Geological Society of Malaysia Bulletin, v. 20, p. 415-422.

Yap, F.-L. and Kwan, T.-S., 1984, Age of cassiterite mineralization near Wing Sang Cheong tin mine, Ipoh: Geological Society of Malaysia Bulletin, v. 20, p. 415-422.

Yeap, E.-B., 1993, Tin and gold mineralizations in Peninsular Malaysia and their relationships to the tectonic development: Journal of Southeast Asian Earth Sciences, v. 8, no. 1-4, p. 329-348.

Zen, E.-A., 1986, Aluminium enrichment in silicate melts by fractional crystallization: Some mineralogic and petrographic constraints: Journal of Petrology, v. 27, no. 5, p. 1095-1117.

Zhu, D.-C., Zhao, Z.-D., Niu, Y.-L., Dilek, Y., Wang, Q., Ji, W.-H., Dong, G.-C., Sui, Q.-L., Liu, Y.-S., Yuan, H.-L. and Mo, X.-X., 2012, Cambrian bimodal volcanism in the Lhasa Terrane, southern Tibet: Record of an early Paleozoic Andean-type magmatic arc in the Australian proto-Tethyan margin: Chemical Geology, v. 328, p. 290-308.

Appendix A – Methodology on major and trace element analysis

Samples were crushed and powdered by jaw crusher and corundum mill. The samples were then fused into glass beads. Major elements of samples were given by the **X**-**R**ay **F**luorescence (XRF) analytical results of these glass beads using Rigaku® RIX-2000 spectrometer in the Department of Geosciences, National University of Taiwan. The analytical procedures mentioned in Wang *et al.* (2004) were adopted in this paper, while the **L**oss **O**f **I**gnition (LOI) was determined separately by routine procedures. The glass beads were then crushed, weighed for ~40 mg and digested by HNO_3 (1:1) and super-pure HF in Teflon® beakers at 100 °C for 2 hours. The digested samples were then evaporated to dryness, and then digested by HNO_3 (1:2) at 100 °C again overnight. Internal standard solution of 10 ppb Rh and Bi in 2% HNO_3 was added. The sample solutions were diluted by 2% HNO_3 by 1500 times after all. The sample solutions were then ready for analysis by **I**nductively **C**oupled **P**lasma – **M**ass **S**pectrometry (ICP-MS) technique using an Agilent 7500cx spectrometer also in the Department of Geosciences, National Taiwan University. The precision of the result is generally within ±5% (2σ). The external standard used in the analyses were USGS standards AGV-2, BHVO-2 and BCR-2.

Partition coefficient (Kd) of elements in particular mineral in high silica rhyolite

Kd	Hornblende (Ewart and Griffin, 1994)	Biotite (Mahood and Hildreth, 1983)	Plagioclase (Ewart and Griffin, 1994)	K-feldspar (Ewart and Griffin, 1994)
Ba	4.50	3.70	1.80	2.70
Fe	21.0	59.1	0.12	0.85
Nb	0.76	0.47	0.16	0.21
Rb	0.046	5.30	0.029	0.72
Sr	0.77	7.20	4.04	2.11
Zr	4.20	9.10	0.27	0.16

Recommended values of the USGS andesite standard AGV-2

Element	wt%	±	Oxide	wt %	±
Al	8.95	0.11	Al_2O_3	16.91	0.21
Ca	3.72	0.09	CaO	5.20	0.13
Fe	4.68	0.09	Fe_2O_3	6.69	0.13
K	2.39	0.09	K_2O	2.88	0.11
Mg	1.08	0.02	MgO	1.79	0.03
Na	3.11	0.09	Na_2O	4.19	0.13
P	0.21	0.01	P_2O_5	0.48	0.02
Si	27.7	0.35	SiO_2	59.3	0.7
Ti	0.63	0.13	TiO_2	1.05	0.22

Element	µg/g	±	Element	µg/g	±
Ba	1140	32	Pb	13	1
Be	2.3	0.4	Pr	8.3	0.6
Ce	68	3	Rb	68.6	2.3
Co	16	1	Sc	13	1
Cr	17	2	Sr	658	17
Cu	53	4	Th	6.1	0.6
Dy	3.6	0.2	U	120	5
La	38	1	Y	20	1
Mn	770	20	Yb	1.6	0.2
Nb	15	1	Zn	86	8
Nd	30	2	Zr	230	4
Ni	19	3			

Information values of the USGS andesite standard AGV2

Element	µg/g	±	Element	µg/g	±
Cs	1.16	0.08	Lu	0.25	0.01
Er	1.79	0.11	Sb	0.6	
Eu	1.54	0.10	Sm	5.7	0.3
F	440		Sn	2.3	0.4
Gd	4.69	0.26	Ta	0.89	0.08
Hf	5.08	0.20	Tb	0.64	0.04
Ho	0.71	0.08	Tl	0.27	
Li	11		Tm	0.26	0.02

Recommended values of the USGS basalt (Hawaiian Volcanic Observatory) standard BHVO-2

Element	wt%	±	Oxide	wt %	±
Al	7.16	0.08	Al_2O_3	13.5	0.2
Ca	8.17	0.12	CaO	11.4	0.2
Fe_{tot}	8.63	0.14	Fe_2O_{3tot}	12.3	0.2
K	0.43	0.01	K_2O	0.52	0.01
Mg	4.36	0.07	MgO	7.23	0.12
Na	1.64	0.06	Na_2O	2.22	0.08
P	0.12	0.01	P_2O_5	0.27	0.02
Si	23.3	0.3	SiO_2	49.9	0.6
Ti	1.63	0.2	TiO_2	2.73	0.04

Element	µg/g	±	Element	µg/g	±
Ba	130	13	Nd	25.0	1.8
Ce	38	2	Ni	119	7
Co	45	3	Rb	9.8	1.0
Cr	280	19	Sc	32	1
Cu	127	7	Sr	389	23
Ga	21.7	0.9	V	317	11
Hf	4.1	0.3	Y	26	2
La	15	1	Zn	103	6
Mn	1290	40	Zr	172	11

Information values of the USGS basalt (Hawaiian Volcanic Observatory) standard BHVO-2

Element	µg/g	±	Element	µg/g	±
F	370		Sm	6.2	0.4
Gd	6.3	0.2	Sn	1.9	
Ho	1.04	0.04	Ta	1.4	
Li	5		Tb	0.9	
Lu	0.28	0.01	Th	1.2	0.3
Nb	18	2	Yb	2.0	0.2

Recommended values of the USGS basalt (Columbia River) standard BCR-2

Element	wt%	±	Oxide	wt %	±
Al	7.14	0.10	Al_2O_3	13.5	0.2
Ca	5.09	0.08	CaO	7.12	0.11
Fe_{tot}	9.66	0.15	Fe_2O_{3tot}	13.8	0.2
K	1.49	0.04	K_2O	1.79	0.05
Mg	21.6	0.03	MgO	3.59	0.05
Na	2.34	0.08	Na_2O	3.16	0.11
P	0.15	0.01	P_2O_5	0.35	0.02
Si	25.3	0.4	SiO_2	54.1	0.8
Ti	1.35	0.03	TiO_2	2.26	0.05

Element	µg/g	±	Element	µg/g	±
Ba	683	28	Rb	48	2
Ce	53	2	Sc	33	2
Co	37	3	Sr	346	14
Cr	18	2	Th	6.2	0.7
Eu	2.0	0.1	U	1.69	0.19
Ga	23	2	V	416	14
Gd	6.8	0.3	Y	37	2
La	25	1	Yb	3.5	0.2
Mn	1520	60	Zn	127	9
Mo	248	17	Zr	188	16
Nd	28	2			

Information values of the USGS basalt (Columbia River) standard BCR-2

Element	µg/g	±	Element	µg/g	±
Cs	1.1	0.1	Lu	0.51	0.02
Cu	19	2	Pb	11	2
F	440		Pr	6.8	0.3
Hf	4.8	0.2	Sm	6.7	0.3
Ho	1.33	0.06	Tb	1.07	0.04
Li	9	2	Tm	0.54	

Appendix B – Methodology on Sr-Nd isotope analysis

Powdered samples were weighed for ~80 mg and digested by HNO_3 (1:1) and super-pure HF in 15 mL screw-top Savillex® beakers for 5 days at ~150 °C. The samples were then evaporated to dryness. The samples were then dissolved by 2 mL 4N HCl and 1N HCl, and then put into centrifugal separation. Sr and **R**are **E**arth **E**lements (REE) were isolated from the sample solution and passed through an AG50W-X8 cation-exchange column filled with 100-200 mesh resins produced by Eichrom Industries, Inc, which can selectively extract Sr and REE respectively. Nd fractions were further separated from the REE portion and were purified using LN resin. HCl was used as eluent. Once separated, the Sr and Nd fractions were loaded with a Ta-HF activator on a single W filament and a Re double filament assembly respectively for measurements. The measurements of isotope data rely on **M**ulti-**C**ollector **I**nductively **C**oupled **P**lasma **M**ass **S**pectrometry (MC-ICP-MS), using the Thermo Electron Finnigan™ Naptune in the Department of Geosciences, National Taiwan University. Measured $^{87}Sr/^{86}Sr$ and $^{146}Nd/^{144}Nd$ were then normalized to 0.1194 and 0.7219 respectively for mass fractionation. SRM (NBS) 987 and JNdi-1 were used as Sr and Nd standards during data acquisition. The measured values for $^{87}Sr/^{86}Sr$ and $^{143}Nd/^{144}Nd$ were 0.710287 and 0.512095 respectively.

Recommended values for SRM (NBS) 987 and JNdi-1

Reference	$^{87}Sr/^{86}Sr$	Reference	$^{143}Nd/^{144}Nd$
SRM (NBS) 987	0.710250	JNdi-1	0.512100

Appendix C – Methodology on U-Pb zircon geochronology

U-Pb geochronology is generally considered the most reliable radiometric dating method for dating the crystallization ages of granites due to the long half-life decay (*ca.* 4.5 Ga for ^{238}U and 704 Ma for ^{235}U) and its high precision (0.1 to 1%) (Steiger and Jäger, 1977; Davis *et al.*, 2003; Parrish and Noble, 2003). Compared to ^{40}Ar-^{39}Ar geochronology, which relies on the singular decay of K-Ar, the U-Pb method, on the contrary, relies on two independent chronometers, the ^{238}U-^{206}Pb and the ^{235}U-^{207}Pb systems (Bowring and Schmitz, 2003).

$$^{238}U = {}^{206}Pb + 8{}^{4}He + 6\beta \ (T_{1/2} = 4.4683 \times 10^{9} \text{ years}) \ [11]$$

$$^{235}U = {}^{207}Pb + 7{}^{4}He + 4\beta \ (T_{1/2} = 7.0381 \times 10^{8} \text{ years}) \ [12]$$

These half-lives ($T_{1/2}$) are much longer than the half-lives of their respective intermediate daughters (^{234}Th: 24.10×10^{3} days, ^{231}Th: 255.2 hours). Hence, the Th decays are usually neglected in the systems.

Both ^{206}Pb and ^{207}Pb are long-lived radiogenic isotopes but are observationally stable, while ^{204}Pb is stable isotope used as reference. The total daughter Pb isotope generated by these U decay series in a certain mineral is obtained by the deduction of common Pb (the Pb that present since the formation of mineral) and blank Pb (the Pb that were introduced during analytical processes).

The age of the mineral is given by the following formulae:

$$\frac{^{206}Pb}{^{238}U} = e^{\lambda_{238} t} - 1 [12]$$

$$\frac{^{207}Pb}{^{235}U} = e^{\lambda_{235} t} - 1 [13]$$

Decay constants (λ_{238} = 1.55125 × 10^{-10} $year^{-1}$ and λ_{238} = 9.8485 × 10^{-10} $year^{-1}$) follow the recommendations of Steiger and Jäger (1977).

In granites, accessory mineral zircon is one of the best U-Pb geochronometer. It is because zircon tends to have high U content, and it provides a nearly closed system for both U and Pb (Davis *et al.*, 2003). It is also a robust mineral in the granite magmatic system, which can be stable up to 1690 °C and 4.8 GPa.

High-spatial resolution, high-precision **S**econdary **I**onization **M**ass **S**pectrometry (SIMS) was used to analyze the U-Pb isotopic composition of the extracted zircons. The grains were extracted from rock samples by standard disaggregation, heavy liquid (bromoform) separation and magnetic separation procedures. Handpicked zircons were then mounted in epoxy, polished and imaged using a Robinson **C**athodo**L**uminescence detector, mounted to a Hitachi S4300 **S**canning **E**lectron **M**icroscope (SEM). U-Pb isotope ratios were collected using a Cameca IMS1280 ion microprobe at the NordSIM facility, Swedish Museum of Natural History, Stockholm, following the protocols described by Whitehouse *et al.* (1999) and Whitehouse and Kamber (2005).

Ten or more pooled analyses were obtained from the extracted zircons in each rock sample. More than one analysis may be made on heterogeneous zircons, which were identified in CL images. Each analysis was sputtered by an O_2^- primary beam, with incident energy at 23 kV (-13 kV primary, +10 kV secondary). The primary beam was then operated in aperture illumination (Köhler) mode with spot size at *ca.* 15-20 μm. In each run, procedures including pre-sputtering with a 25 μm raster for 120 seconds, centering of the secondary ion beam in the 3000 μm **F**ield **A**perture (FA), mass

calibration optimization, and optimization of the secondary beam energy distribution, were carried out by the SIMS automatically. $^{90}Zr_2{}^{16}O^+$ species at nominal mass 196 was applied to FA with energy adjustment. All peaks were mass calibrated in the mono-collection sequence and this was carried out at the start of each session. Within each run, only those peaks that yield consistently high signals from the zircon matrix, namely $^{90}Zr_2{}^{16}O^+$, $^{94}Zr_2{}^{16}O^+$ (nominal mass 204), $^{177}HfO_2{}^+$ (nominal mass 209), $^{238}U^+$ and $^{238}U^{16}O_2{}^+$, were scanned with mass calibration optimization, while those intermediate peaks were adjusted by interpolation. To ensure adequate separation of Pb isotope peaks from nearby $HfSi^+$ species, a mass resolution (M/ΔM) of *ca.* 5400 was used. The axial ion-counting electron multiplier was used to detect ion signals. Fully automated chain sequences were applied in each run of sample.

It is assumed the data reduction follows the power law relationship between Pb^+/U^+ and $UO_2{}^+/U^+$ ratios with an empirically derived slope. This is to calculate actual Pb/U ratios with respect to those in the 91500 standard, which provides references for both U concentrations and Th/U ratio. When ^{204}Pb counts exceed average background statistically, common Pb is corrected and it is assumed that the $^{207}Pb/^{206}Pb$ ratio is 0.83 (Stacey and Kramers, 1975). The age interpretations were then done by the Isoplot macros on Excel (Ludwig, 2001). Given the ubiquitous presence of post-crystallization, possibly recent, Pb-loss causing a skewed age dispersion towards apparently younger ages, as well as the presence in some zircons of clear inherited cores, a consistent filtering approach was used to extract the probable crystrallization age. This involved first excluding any obvious older cores, then rejecting the youngest analyses ($^{238}U/^{206}Pb$ age) interpreted on the basis of CL images to belong to the main magmatic crystallization group, which most likely reflect Pb-loss, until the remaining group of

ages yielded a concordia age, *sensu* Ludwig (1998), with a statistically significant low MSWD. In general, concordia ages were obtained from five or more pooled analyses to be robust indicators of the magmatic crystallization age, while those incorporating fewer analyses are given as reference ages that are accorded somewhat lower significance in our interpretation. All ages are presented at 2σ (or, where appropriate, 95% confidence level) including decay constant errors, with the MSWD value representing that of both concordance and equivalence following the recommendation of Ludwig (1998).

Table S1: Ion microprobe U-Th-Pb data of the zircons extracted from Eastern Province granitoids

(1) Based on measured Th and U signals.

(2) f_{206} is the percentage of common Pb estimated from 204Pb counts; in parentheses where these are insignificant;

(3) Ratios after subtraction of common Pb (if detected)

(4) Age based on projecting a line in inverse concordia space from assumed common Pb through the total (uncorrected) ratios onto concordia (Ludwig, 2001)

(5) Grain characteristics based on CL imaging: c = core, r = rim, sp = single phase, r(e) = rim embayment, r(i) = rim inner, oz = oscillatory zoned, uz = unzoned, clb = CL-bright, cld = CL-dark, clm = CL-medium

		Concentration (ppm)							Total (uncorrected) ratio				Radiogenic (corrected) ratio[3]				Calculated age ± s (Ma)		
Sample ID	Characteristics[5]	U	Th	Pb	Th/U_{calc}	Th/U_{meas}[1]	$^{206}Pb/^{204}Pb$	f_{206} (%)[2]	$^{206}Pb/^{238}U$	± s (%)	$^{207}Pb/^{206}Pb$	± s (%)	$^{206}Pb/^{238}U$	± s (%)	$^{207}Pb/^{206}Pb$	± s (%)	$^{207}Pb/^{206}Pb$	$^{206}Pb/^{238}U$	207-corr age[4]
MA33																			
n3964x-21c	sp, uz, cld	32000	26000	470	0.033	0.8	445	4.2	0.0141	10.	0.0841	3.8	0.0135	10.	0.0512	9.2	249 ± 200	253.6 ± 8.8	86.0 ± 8.8
n3964-20	sp, uz, cld	8300	8400	260	0.29	1	38.5	48.6	0.04380	1.1	0.4364	0.74	0.02252	1.3	0.0590	16.	568 ± 316	144 ± 2	141 ± 18
n3964x-07c	sp, oz, clb	1600	1200	53	0.14	0.73	25.8	72.46	0.0962	3.2	0.6233	0.79	0.0265	4.0	0.065	42.	762 ± 695	169 ± 7	162 ± 58
n3964x-32c	sp, oz, clb	4000	2100	130	0.25	0.52	3220	0.58	0.02885	3.0	0.05534	0.42	0.02868	3.0	0.05078	0.65	231 ± 15	182 ± 5	182 ± 5
n3964-33	sp, oz, clb	330	310	13	0.28	0.96	105	17.79	0.03574	0.93	0.1989	1.3	0.02938	0.99	0.0611	15.	644 ± 297	187 ± 2	184 ± 6
n3964-35r	r, uz, cld	22000	2500	720	0.091	0.11	585	3.2	0.03139	1.2	0.07506	0.41	0.03038	1.2	0.04993	1.1	192 ± 25	193 ± 2	193 ± 2
n3964x-18c	sp, uz, clb	600	430	24	0.57	0.72	299	6.26	0.0339	3.0	0.0997	3.7	0.03178	3.1	0.0506	11.	221 ± 241	202 ± 6	202 ± 6
n3964x-29c	c, oz, clb	370	810	20	1.8	2.2	22900	0.08	0.03222	3.0	0.05143	1.1	0.03219	3.0	0.05079	1.1	231 ± 26	204 ± 6	204 ± 6
n3964x-25c	sp, oz, clb	360	270	15	0.73	0.75	1550	1.21	0.03303	3.0	0.0592	2.2	0.03263	3.0	0.0496	3.5	178 ± 79	207 ± 6	207 ± 6
n3964x-15c	sp, oz, clb	320	260	14	0.81	0.82	13400	0.14	0.03271	3.0	0.05084	1.1	0.03267	3.0	0.04975	1.3	183 ± 30	207 ± 6	207 ± 6
n3964x-01c	sp, oz, clb	680	900	30	1.2	1.3	2330	0.8	0.0331	3.0	0.05571	1.5	0.03286	3.0	0.0494	2.7	167 ± 61	208 ± 6	209 ± 6
n3964x-26c	sp, oz, clb	1100	650	43	0.47	0.62	9880	0.19	0.0333	3.0	0.05249	0.60	0.0332	3.0	0.05100	0.72	241 ± 17	211 ± 6	211 ± 6
n3964x-12c	sp, oz, clb	880	280	33	0.25	0.32	10800	0.17	0.0337	3.0	0.05194	0.85	0.0337	3.0	0.05058	0.95	222 ± 22	214 ± 6	213 ± 6
n3964x-34c	sp, oz, clb	950	1500	48	1.3	1.6	9660	0.19	0.0338	3.0	0.05219	0.94	0.0337	3.0	0.05067	1.1	226 ± 25	214 ± 6	214 ± 6
n3964x-06c	sp, uz, cld	7400	1900	280	0.2	0.25	741	2.53	0.0352	3.0	0.06960	0.97	0.0343	3.0	0.04975	1.8	183 ± 42	217 ± 6	218 ± 7
n3964x-36c	sp, oz, clm	930	3000	59	n/d	3.2	239	7.82	0.0367	3.0	0.0997	2.5	0.0338	3.0	0.0372	15.	-541 ± 363	214 ± 6	218 ± 7
n3964-31	sp, oz, clb	660	300	27	0.44	0.46	22200	[0.08]	0.03448	0.91	0.05084	1.6	0.03448	0.91	0.05084	1.6	233 ± 38	219 ± 2	218 ± 2
n3964x-30c	sp, oz, clm	1700	1900	81	n/d	1.1	90.3	20.7	0.0437	3.1	0.2095	2.0	0.0347	3.1	0.0460	15.	-3.1 ± 321.5	220 ± 7	220 ± 10
n3964-24r	sp, oz, cld	890	1300	47	1.4	1.5	1040	1.79	0.03562	0.95	0.0648	1.6	0.03498	0.96	0.0507	3.8	228 ± 87	222 ± 2	222 ± 2
n3964-35c	c, oz, clb	540	380	24	0.93	0.71	>1e6	[0.00]	0.03503	0.93	0.04912	1.8	0.03503	0.93	0.04912	1.8	154 ± 42	222 ± 2	222 ± 2
n3964-24c	sp, oz, clb	630	1200	36	1.6	1.9	6180	0.3	0.03557	0.92	0.05398	1.7	0.03546	0.92	0.0516	2.1	268 ± 48	225 ± 2	224 ± 2
n3964-41	sp, oz, clb	580	1000	33	2	1.8	306	6.12	0.03784	0.97	0.0979	3.1	0.03552	1.0	0.0498	10.	186 ± 226	225 ± 2	225 ± 3
n3964-23	sp, oz, clb	450	460	21	1	1	51800	[0.04]	0.03557	0.91	0.0504	2.0	0.03557	0.91	0.0504	2.0	212 ± 46	225 ± 2	225 ± 2
n3964x-37c	sp, oz, cld	3100	1200	130	0.36	0.39	2070	0.9	0.0365	3.0	0.05759	0.48	0.0362	3.0	0.05051	1.2	219 ± 26	229 ± 7	229 ± 7
n3964x-42c	sp, oz, clm	5100	1000	200	0.16	0.2	689	2.71	0.0374	3.0	0.0720	1.5	0.0363	3.0	0.0507	2.9	228 ± 66	230 ± 7	230 ± 7
n3964-16	sp, oz, clb	1300	620	56	0.54	0.5	4510	0.41	0.03698	0.91	0.05375	1.0	0.03682	0.91	0.05050	1.4	218 ± 33	233 ± 2	233 ± 2
n3964x-13c	sp, oz, clb	1500	590	61	n/d	0.38	168	11.17	0.0413	3.5	0.124	11.	0.0367	3.8	0.034	63.	-772 ± 1,210	232 ± 9	237 ± 10
n3964x-11c	sp, uz, cld	14000	1300	560	0.075	0.092	507	3.69	0.0389	3.9	0.0788	1.3	0.0375	3.9	0.0499	3.1	188 ± 72	237 ± 9	238 ± 9
n3964-03	r(i), uz, cld	13000	930	550	0.075	0.07	1440	1.3	0.03891	0.94	0.06039	0.75	0.03841	0.94	0.05016	1.3	202 ± 30	243 ± 2	243 ± 2
n3964-02	sp, uz, clb	260	140	13	1.1	0.54	71.4	26.19	0.05436	1.6	0.2548	3.9	0.04012	2.3	0.049	43.	130 ± 781	254 ± 6	254 ± 13
MA36																			
n4214-30r	r, uz, clb	380	700	21	2.7	1.9	11100	0.17	0.03431	0.85	0.05045	1.9	0.03425	0.85	0.0491	2.2	154 ± 50	217 ± 2	217 ± 2
n4214-06c	r(i), oz, clb	540	250	23	0.5	0.47	13200	0.14	0.03520	0.84	0.05131	1.7	0.03515	0.84	0.05020	1.8	204 ± 42	223 ± 2	223 ± 2
n4214-25c	sp, oz, clm	410	460	21	0.93	1.1	11300	0.17	0.03595	0.87	0.05311	1.5	0.03589	0.87	0.05181	1.7	277 ± 39	227 ± 2	227 ± 2
n4214-30c	c, oz,clm	1100	610	47	0.63	0.58	1330	1.41	0.03676	0.84	0.06145	0.85	0.03625	0.84	0.05040	2.0	213 ± 45	230 ± 2	230 ± 2
n4214-11c	sp, oz, cld	720	810	37	1.1	1.1	58500	[0.03]	0.03633	0.85	0.05080	1.1	0.03633	0.85	0.05080	1.1	232 ± 25	230 ± 2	230 ± 2
n4214-01c	sp, uz, clm	370	570	21	1.6	1.5	>1e6	[0.00]	0.03654	0.86	0.05034	1.7	0.03654	0.86	0.05034	1.7	211 ± 40	231 ± 2	232 ± 2
n4214-40c	sp, oz, clb	280	310	14	1.3	1.1	13300	[0.14]	0.03699	0.84	0.0500	2.4	0.03699	0.84	0.0500	2.4	197 ± 54	234 ± 2	234 ± 2
n4214-14r	r, uz, clb	1000	110	41	0.13	0.11	2950	0.63	0.03730	0.84	0.05479	0.89	0.03706	0.84	0.04982	1.5	187 ± 34	235 ± 2	235 ± 2
n4214-44r	r, uz, clb	920	120	39	0.13	0.13	219000	[0.01]	0.03908	0.84	0.05169	0.91	0.03908	0.84	0.05169	0.91	272 ± 21	247 ± 2	247 ± 2
n4214-09c	c, uz, cld	900	140	41	0.11	0.16	61800	[0.03]	0.0415	3.7	0.05382	1.7	0.0415	3.7	0.05382	1.7	363 ± 38	262 ± 10	261 ± 10
n4214-14c	c, uz, clb	1500	62	100	0.023	0.042	2810	0.67	0.06311	1.1	0.06854	0.86	0.06269	1.1	0.06339	1.5	721 ± 31	392 ± 4	388 ± 4
n4214-16c	c, uz, clm	440	350	63	0.8	0.79	>1e6	[0.00]	0.10868	0.84	0.06123	0.77	0.10868	0.84	0.06123	0.77	647 ± 17	665 ± 5	665 ± 5
n4214-54r	r, uz, clb	690	120	86	0.067	0.17	62100	0.03	0.11398	0.84	0.06756	0.55	0.11395	0.84	0.06733	0.57	848 ± 12	696 ± 6	691 ± 6
n4214-44c	c, oz, clb	480	190	71	0.44	0.4	98700	[0.02]	0.1185	0.89	0.07050	0.66	0.1185	0.89	0.07050	0.66	943 ± 14	722 ± 6	716 ± 6
n4214-22c	c, uz, cld	540	220	120	0.36	0.41	81200	0.02	0.1560	0.94	0.14605	0.52	0.1559	0.94	0.14589	0.52	2298 ± 9	934 ± 8	844 ± 15
n4214-39c	sp, oz, clb	330	160	60	0.46	0.47	56100	0.03	0.1490	0.84	0.07143	0.68	0.1489	0.84	0.07117	0.70	962 ± 14	895 ± 7	892 ± 7
n4214-42c	c, uz, clm	560	440	120	0.76	0.78	47300	0.04	0.1599	0.84	0.07470	0.52	0.1598	0.84	0.07440	0.53	1052 ± 11	956 ± 7	952 ± 8
n4214-54c	c, uz, clm	560	270	110	0.54	0.49	50400	0.04	0.1603	0.84	0.07546	0.51	0.1603	0.84	0.07518	0.53	1073 ± 11	958 ± 7	953 ± 8
n4214-28c	sp, oz, clb	410	180	98	0.38	0.43	20800	0.09	0.1898	0.90	0.09541	0.65	0.1896	0.90	0.09475	0.69	1523 ± 13	1119 ± 9	1093 ± 10
n4214-24c	sp, oz, clm	89	4.7	34	0.023	0.054	12000	0.16	0.3344	0.85	0.1470	0.86	0.3339	0.85	0.1459	0.89	2299 ± 15	1857 ± 14	1773 ± 21
MA42																			
n3965-37	sp, uz, cld	56000	3900	[795]	n/d	0.069	205	8.08	0.0124	22.	0.1176	5.3	0.0114	22.	0.0545	18.	392 ± 355	214.3 ± 16.2	72.2 ± 16.1
n3965-46	sp, uz, cld	6100	410	160	0.037	0.066	114	18.39	0.02917	2.7	0.196	13.	0.0238	4.7	0.052	85.	271 ± 1,274	152 ± 7	151 ± 8
n3965-20r	r, uz, cld	14000	650	490	0.042	0.046	522	3.58	0.0340	6.9	0.0792	4.6	0.0327	6.8	0.0511	10.	245 ± 221	208 ± 14	207 ± 14

Sample ID	Characteristics[5]	Concentration (ppm)			Th/U_{calc}	Th/U_{meas}[1]	$^{206}Pb/^{204}Pb$	f_{206} (%)[2]	Total (uncorrected) ratio				Radiogenic (corrected) ratio[3]				Calculated age ± s (Ma)		
		U	Th	Pb					$^{206}Pb/^{238}U$	± s (%)	$^{207}Pb/^{206}Pb$	± s (%)	$^{206}Pb/^{238}U$	± s (%)	$^{207}Pb/^{206}Pb$	± s (%)	$^{207}Pb/^{206}Pb$	$^{206}Pb/^{238}U$	207-corr age[4]
n3965-11c	c, uz, clb	520	110	19	0.27	0.21	4870	0.38	0.03280	1.6	0.05169	1.5	0.03267	1.6	0.0487	2.2	132 ± 51	207 ± 3	208 ± 3
n3965-11r	r, oz, clb	2500	220	92	0.11	0.087	2750	0.68	0.03389	1.0	0.05507	0.67	0.03366	1.0	0.04973	1.1	183 ± 26	213 ± 2	214 ± 2
n3965-04	sp, oz, clm	430	390	19	1.1	0.9	69100	[0.03]	0.03380	0.91	0.04937	1.8	0.03380	0.91	0.04937	1.8	165 ± 41	214 ± 2	215 ± 2
n3965-23r	sp, oz, clm	1800	170	68	0.11	0.092	25300	0.07	0.03426	0.93	0.05006	0.85	0.03424	0.93	0.04948	0.96	171 ± 22	217 ± 2	217 ± 2
n3965-07	c, oz, clb	1300	680	56	0.47	0.51	218000	[0.01]	0.03477	1.0	0.05106	0.97	0.03477	1.0	0.05106	0.97	244 ± 22	220 ± 2	220 ± 2
n3965-23c	sp, uz, cld	3900	270	150	0.073	0.07	29200	0.06	0.03502	0.93	0.05055	0.59	0.03500	0.93	0.05005	0.63	197 ± 15	222 ± 2	222 ± 2
n3965-20c	r, uz, cld	1900	1300	86	0.79	0.69	20200	0.09	0.03548	1.1	0.05068	0.79	0.03544	1.1	0.04995	0.88	193 ± 20	225 ± 2	225 ± 2
n3965-25	sp, uz, cld	6800	220	260	0.039	0.032	1010	1.86	0.03714	1.0	0.06280	1.3	0.03645	1.0	0.0482	2.8	108 ± 64	231 ± 2	232 ± 2
n3965-08	sp, uz, clb	450	150	67	0.3	0.32	295000	[0.01]	0.1271	0.91	0.06770	0.78	0.1271	0.91	0.06770	0.78	859 ± 16	771 ± 7	769 ± 7
MA43																			
n3961-10c	sp, oz, clb	580	570	9	0.14	0.99	92.1	20.32	0.01498	1.4	0.214	16.	0.01194	4.3	0.056	110.	438 ± 1,452	83.4 ± 3.3	75.6 ± 5.1
n3961-39	sp, uz, cld	1100	400	15	0.3	0.38	24500	[0.08]	0.01225	1.2	0.0482	2.1	0.01225	1.2	0.0482	2.1	110 ± 48	76.5 ± 0.9	78.4 ± 0.9
n3961-10r	sp, oz, cld	1900	5600	44	n/d	3	2430	0.77	0.01240	2.4	0.05183	1.8	0.01230	2.4	0.0457	2.7	-16 ± 64	78.8 ± 1.9	79.0 ± 1.9
n3961-22	sp, uz, clb	710	1900	17	0.97	2.7	1420	1.31	0.01314	1.2	0.0610	2.2	0.01296	1.2	0.0507	5.4	226 ± 120	83.7 ± 1.0	82.7 ± 1.0
n3961-07	sp, oz, clb	580	2000	16	1.8	3.5	34100	[0.05]	0.01303	1.2	0.0491	2.5	0.01303	1.2	0.0491	2.5	151 ± 58	85.3 ± 1.0	83.3 ± 1.0
n3961-48	c, oz, cld	1200	2300	25	1.2	1.9	21700	[0.09]	0.01303	1.2	0.04859	1.9	0.01303	1.2	0.04859	1.9	128 ± 43	83.0 ± 1.0	83.3 ± 1.0
n3961-11c	sp, oz, clm	490	2000	15	2	4	6460	[0.29]	0.01307	1.2	0.0493	2.8	0.01307	1.2	0.0493	2.8	164 ± 65	84.9 ± 1.0	83.5 ± 1.0
n3961-46	c, uz, cld	1200	1900	24	2.2	1.5	23600	[0.08]	0.01310	1.2	0.04718	1.9	0.01310	1.2	0.04718	1.9	58.2 ± 45.7	84.6 ± 1.0	84.0 ± 1.0
n3961-36	sp, oz, clb	460	1400	12	6.7	3	3310	0.56	0.01328	1.2	0.0512	2.9	0.01321	1.2	0.0467	4.6	35.9 ± 107.2	81.6 ± 1.0	84.7 ± 1.0
n3961-11r	sp, oz, cld	6500	16000	160	2.5	2.5	52700	0.04	0.01333	1.2	0.04803	1.5	0.01332	1.2	0.04775	1.5	86.9 ± 34.7	83.4 ± 1.0	85.3 ± 1.0
n3961-34	c, oz, clb	1400	4400	37	n/d	3.1	997	1.88	0.01351	1.1	0.04824	1.7	0.01326	1.2	0.0332	5.6	-859 ± 155	83.9 ± 1.0	86.4 ± 1.0
MA45																			
n4215-26r	r, oz, clb	730	370	9.9	0.57	0.51	>1e6	[0.00]	0.011194	0.88	0.0473	2.2	0.011194	0.88	0.0473	2.2	66.9 ± 52.0	231.4 ± 0.6	71.8 ± 0.6
n4215-42c	c, uz, clb	790	260	10	0.19	0.33	12100	[0.16]	0.011290	0.86	0.0486	2.2	0.011290	0.86	0.0486	2.2	129 ± 52	222.7 ± 0.6	72.3 ± 0.6
n4215-15c	sp, oz, clm	1600	1100	23	1.9	0.69	18900	0.1	0.011291	0.87	0.04733	1.3	0.011280	0.87	0.04655	1.5	26.2 ± 35.0	261.9 ± 0.6	72.4 ± 0.6
n4215-29r	r, uz, clb	570	270	7.8	1.3	0.48	12700	[0.15]	0.01141	0.89	0.0466	3.1	0.01141	0.89	0.0466	3.1	27.2 ± 71.7	230.0 ± 0.6	73.2 ± 0.7
n4215-45c	sp, oz, cld	1300	510	17	0.2	0.4	33400	[0.06]	0.011461	0.86	0.04912	1.5	0.011461	0.86	0.04912	1.5	154 ± 34	392.0 ± 0.6	73.3 ± 0.6
n4215-12c	sp, oz, clb	500	220	6.8	0.23	0.43	>1e6	[0.00]	0.01148	1.0	0.0488	2.3	0.01148	1.0	0.0488	2.3	138 ± 53	234.6 ± 0.8	73.4 ± 0.8
n4215-05c	sp, oz, cld	1300	700	19	0.43	0.53	21000	[0.09]	0.01150	0.96	0.04787	1.6	0.01150	0.96	0.04787	1.6	92.8 ± 37.5	665.1 ± 0.7	73.7 ± 0.7
n4215-13c	sp, oz, clb	360	570	6.4	n/d	1.6	3390	0.55	0.01149	0.92	0.0466	2.9	0.01143	0.93	0.0423	4.7	-210 ± 114	934.1 ± 0.7	73.7 ± 0.7
n4215-25c	sp, oz, clb	450	460	7	1.1	1	>1e6	[0.00]	0.01151	0.90	0.0474	3.2	0.01151	0.90	0.0474	3.2	68.2 ± 73.4	1857.3 ± 0.7	73.8 ± 0.7
n4215-35r	r, oz, clm	1300	680	18	0.82	0.52	29700	[0.06]	0.011541	0.86	0.04695	1.6	0.011541	0.86	0.04695	1.6	46.9 ± 36.9	227.3 ± 0.6	74.0 ± 0.6
n4215-30c	sp, oz, clb	600	560	9.2	n/d	0.94	14400	[0.13]	0.01155	0.90	0.0457	2.4	0.01155	0.90	0.0457	2.4	-19 ± 57	1119.1 ± 0.7	74.2 ± 0.7
n4215-29c	c, oz, clm	1400	950	21	n/d	0.68	16100	0.12	0.01170	0.86	0.04681	1.8	0.01169	0.86	0.04589	2.0	-8.2 ± 46.7	229.5 ± 0.6	75.1 ± 0.7
n4215-04c	c, uz, clb	620	1000	12	2.9	1.7	13600	[0.14]	0.01176	0.88	0.04692	2.1	0.01176	0.88	0.04692	2.1	45.1 ± 49.1	217.1 ± 0.7	75.4 ± 0.7
n4215-20c	c, oz, clm	1300	720	19	0.64	0.53	>1e6	[0.00]	0.01179	0.85	0.04730	1.4	0.01179	0.85	0.04730	1.4	64.5 ± 33.8	894.9 ± 0.6	75.6 ± 0.6
n4215-26c	c, uz, clb	2300	1100	33	0.78	0.5	7670	0.24	0.01183	0.85	0.04892	1.1	0.01180	0.85	0.04700	1.4	49.2 ± 33.9	234.2 ± 0.6	75.7 ± 0.6
n4215-35c	c, uz, clm	1800	3000	34	2.6	1.7	14700	0.13	0.01204	0.92	0.04804	1.3	0.01203	0.93	0.04703	1.5	50.7 ± 36.0	955.7 ± 0.7	77.1 ± 0.7
n4215-12r	r, oz, clm	2900	1400	42	0.53	0.47	>1e6	[0.00]	0.01217	0.86	0.04743	0.95	0.01217	0.86	0.04743	0.95	70.9 ± 22.4	722.2 ± 0.7	78.0 ± 0.7
n4215-40c	c, uz, cld	2900	6700	67	4.1	2.3	1250	1.5	0.01250	1.2	0.0589	2.6	0.01231	1.2	0.0471	4.2	51.8 ± 97.9	247.1 ± 0.9	78.9 ± 0.9
n4215-45r	r, oz, clm	2200	1000	33	0.56	0.46	21600	0.09	0.01248	0.85	0.04800	1.1	0.01247	0.85	0.04731	1.2	65.0 ± 28.3	958.2 ± 0.7	79.9 ± 0.7
n4215-39c	c, uz, cld	2900	2000	46	1.7	0.67	75000	[0.02]	0.01262	0.85	0.04661	0.98	0.01262	0.85	0.04661	0.98	29.3 ± 23.2	695.6 ± 0.7	80.9 ± 0.7
MA47																			
n3949-12r	sp, uz, cld	9700	4600	410	0.43	0.48	2930	0.64	0.03593	0.97	0.05562	0.50	0.03570	0.97	0.05061	0.70	223 ± 16	226 ± 2	226 ± 2
n3949-12c	sp, uz, clm	1300	590	54	0.32	0.46	808	2.31	0.03732	1.0	0.0693	1.7	0.03646	1.0	0.0512	4.4	248 ± 99	231 ± 2	231 ± 3
n3949-18c	sp, uz, cld	2200	340	94	0.21	0.16	10800	0.17	0.03963	0.95	0.05103	1.0	0.03956	0.95	0.04966	1.2	179 ± 28	250 ± 2	251 ± 2
n3949-04c	sp, uz, cld	2500	680	110	0.25	0.27	30000	0.06	0.04034	0.95	0.05183	0.68	0.04031	0.95	0.05135	0.73	256 ± 17	255 ± 2	255 ± 2
n3949-04r	sp, uz, clm	1300	430	60	0.32	0.34	246000	[0.01]	0.04053	0.95	0.05167	0.98	0.04053	0.95	0.05167	0.98	271 ± 22	256 ± 2	256 ± 2
n3949-31c	c, oz, clb	3400	850	160	0.27	0.25	4920	0.38	0.04068	0.97	0.05429	0.68	0.04053	0.97	0.05131	0.92	255 ± 21	256 ± 2	256 ± 2
n3949-27r	r, oz, clm	1200	440	56	0.44	0.38	64000	[0.03]	0.04065	0.96	0.05098	0.84	0.04065	0.96	0.05098	0.84	240 ± 19	257 ± 2	257 ± 2
n3949-05c	sp, oz, cld	2900	1000	130	0.36	0.35	1870	1	0.04127	0.95	0.05883	0.61	0.04086	0.95	0.05098	1.2	240 ± 27	258 ± 2	258 ± 2
n3949-07c	sp, oz, cld	2000	180	89	0.11	0.086	616	3.04	0.04210	0.95	0.07346	0.90	0.04083	0.95	0.0496	2.6	176 ± 59	258 ± 2	258 ± 3
n3949-17c	c, uz, cld	1500	470	71	0.32	0.31	37800	[0.05]	0.04093	0.96	0.05122	0.94	0.04093	0.96	0.05122	0.94	251 ± 21	259 ± 2	259 ± 2
n3949-27c	c, oz, cld	4000	580	180	0.17	0.14	3380	0.55	0.04139	0.98	0.05465	0.79	0.04116	0.98	0.05031	1.5	209 ± 33	260 ± 3	260 ± 3
n3949-25c	c, uz, cld	2100	730	99	0.36	0.36	43000	[0.04]	0.04125	0.97	0.05135	0.81	0.04125	0.97	0.05135	0.81	257 ± 19	261 ± 2	261 ± 2
MA48																			
n3922-03c	c, uz, clb	190	100	7.7	0.29	0.52	425	4.4	0.03475	1.1	0.0874	3.6	0.03322	1.2	0.0529	11.	326 ± 233	211 ± 2	210 ± 3
n3922x-17c	sp, oz, cld	960	96	41	0.096	0.1	25600	0.07	0.03952	0.86	0.05198	0.86	0.03949	0.86	0.05141	0.91	259 ± 21	250 ± 2	250 ± 2
n3922x-14c	sp, oz, clb	810	25	33	0.034	0.031	170000	[0.01]	0.03879	0.86	0.05115	0.79	0.03879	0.86	0.05115	0.79	248 ± 18	245 ± 2	245 ± 2
n3922x-23c	sp, oz, clb	820	170	40	0.2	0.21	437000	[0.00]	0.04332	0.87	0.05221	0.72	0.04332	0.87	0.05221	0.72	295 ± 16	273 ± 2	273 ± 2
n3922x-21c	sp, oz, clb	320	160	17	0.43	0.49	>1e6	[0.00]	0.04440	0.88	0.05255	1.2	0.04440	0.88	0.05255	1.2	310 ± 26	280 ± 2	280 ± 2
n3922x-20c	sp, oz, clb	420	230	23	0.5	0.55	16000	0.12	0.04406	0.91	0.05325	1.2	0.04401	0.91	0.05234	1.3	300 ± 30	278 ± 2	277 ± 3
n3922-26r	r, oz, clm	660	320	36	0.44	0.48	62500	[0.03]	0.04467	0.94	0.05256	0.76	0.04467	0.94	0.05256	0.76	310 ± 17	282 ± 3	281 ± 3
n3922x-01c	sp, oz, cld	660	360	36	0.61	0.54	83200	[0.02]	0.04423	0.89	0.05130	0.82	0.04423	0.89	0.05130	0.82	254 ± 19	279 ± 2	279 ± 2

Sample ID	Characteristics[5]	Concentration (ppm)			Th/U_{calc}	Th/U_{meas}[1]	$^{206}Pb/^{204}Pb$	f_{206} (%)[2]	Total (uncorrected) ratio				Radiogenic (corrected) ratio[3]				Calculated age ± s (Ma)		
		U	Th	Pb					$^{206}Pb/^{238}U$	± s (%)	$^{207}Pb/^{206}Pb$	± s (%)	$^{206}Pb/^{238}U$	± s (%)	$^{207}Pb/^{206}Pb$	± s (%)	$^{207}Pb/^{206}Pb$	$^{206}Pb/^{238}U$	207-corr age[4]
n3922x-10c	c, uz, cld	1100	520	60	0.55	0.46	8280	0.23	0.04448	0.88	0.05297	0.79	0.04438	0.88	0.05120	1.0	250 ± 24	280 ± 2	280 ± 2
n3922x-22c	sp, uz, cld	1300	1700	85	1.4	1.3	149000	[0.01]	0.04541	0.87	0.05164	0.58	0.04541	0.87	0.05164	0.58	270 ± 13	286 ± 2	286 ± 2
n3922x-05c	sp, oz, cld	780	510	44	0.7	0.66	94200	[0.02]	0.04519	0.87	0.05185	0.74	0.04519	0.87	0.05185	0.74	279 ± 17	285 ± 2	285 ± 2
n3922x-08c	c, uz, clb	370	200	20	0.53	0.53	89900	[0.02]	0.04471	0.86	0.05211	1.1	0.04471	0.86	0.05211	1.1	290 ± 25	282 ± 2	282 ± 2
n3922-19r	r(e), uz, cld	690	490	40	0.72	0.71	97500	[0.02]	0.04516	0.92	0.05208	0.74	0.04516	0.92	0.05208	0.74	289 ± 17	285 ± 3	285 ± 3
n3922x-29c	c, oz, clb	350	180	19	0.45	0.52	34800	[0.05]	0.04466	0.87	0.05314	1.3	0.04466	0.87	0.05314	1.3	335 ± 30	282 ± 2	281 ± 2
n3922x-02c	sp, oz, cld	530	360	30	0.68	0.68	90100	[0.02]	0.04464	1.1	0.05210	0.90	0.04464	1.1	0.05210	0.90	290 ± 20	282 ± 3	281 ± 3
n3922x-06c	sp, oz, clm	640	320	35	0.55	0.51	114000	[0.02]	0.04512	0.86	0.05158	0.82	0.04512	0.86	0.05158	0.82	267 ± 19	285 ± 2	285 ± 2
n3922-27c	sp, oz, clm	390	190	21	0.56	0.49	108000	[0.02]	0.04554	0.91	0.05123	1.1	0.04554	0.91	0.05123	1.1	251 ± 24	287 ± 3	287 ± 3
n3922x-13c	c, uz, clb	360	280	21	0.7	0.78	>1e6	[0.00]	0.04531	0.87	0.05279	1.3	0.04531	0.87	0.05279	1.3	320 ± 29	286 ± 2	285 ± 2
n3922x-15c	sp, oz, cld	1100	1300	72	1.3	1.1	27600	0.07	0.04508	1.1	0.05205	1.1	0.04505	1.1	0.05152	1.1	264 ± 26	284 ± 3	284 ± 3
n3922x-16c	sp, oz, cld	670	130	33	0.18	0.19	>1e6	[0.00]	0.04443	0.90	0.05222	0.80	0.04443	0.90	0.05222	0.80	295 ± 18	280 ± 2	280 ± 2
n3922-03r	r, oz, cld	600	440	35	0.79	0.73	155000	[0.01]	0.04567	0.91	0.05147	0.87	0.04567	0.91	0.05147	0.87	262 ± 20	288 ± 3	288 ± 3
n3922-04c	sp, oz, cld	520	340	30	0.57	0.65	>1e6	[0.00]	0.04585	0.91	0.05291	0.93	0.04585	0.91	0.05291	0.93	325 ± 21	289 ± 3	289 ± 3
n3922-19c	c, oz, cld	840	750	51	1	0.9	122000	[0.02]	0.04619	0.92	0.05132	0.65	0.04619	0.92	0.05132	0.65	255 ± 15	291 ± 3	291 ± 3
n3922x-28c	sp, uz, cld	2300	3600	160	1.9	1.6	6530	0.29	0.04631	0.89	0.05343	0.42	0.04617	0.89	0.05118	0.56	249 ± 13	291 ± 3	291 ± 3
n3922x-18c	c, uz, cld	3100	540	160	0.18	0.17	214000	0.01	0.04588	0.86	0.05200	0.45	0.04588	0.86	0.05193	0.46	282 ± 10	289 ± 2	289 ± 2
n3922-26c	c, uz, cld	490	370	30	0.76	0.75	49100	[0.04]	0.04697	0.92	0.05199	0.83	0.04697	0.92	0.05199	0.83	285 ± 19	296 ± 3	296 ± 3
n3922x-25c	sp, oz, cld	480	290	28	0.64	0.6	61200	[0.03]	0.04758	0.86	0.05175	0.89	0.04758	0.86	0.05175	0.89	274 ± 20	300 ± 3	300 ± 3
n3922-12r	r, oz, cld	1200	56	69	0.041	0.046	63100	0.03	0.05347	0.96	0.05462	0.87	0.05345	0.96	0.05438	0.88	387 ± 20	336 ± 3	335 ± 3
n3922x-07c	sp, uz, cld	710	410	53	0.65	0.57	765	2.44	0.0549	4.1	0.0776	5.0	0.0535	3.9	0.0586	14.	552 ± 288	336 ± 13	334 ± 14
n3922-12c	c, oz, clb	96	68	8.8	0.64	0.71	13700	[0.14]	0.07148	1.1	0.05707	1.7	0.07148	1.1	0.05707	1.7	494 ± 36	445 ± 5	444 ± 5
n3922x-09c	sp, oz, clb	140	110	14	0.83	0.8	13100	[0.14]	0.07488	0.86	0.05602	1.6	0.07488	0.86	0.05602	1.6	453 ± 34	465 ± 4	466 ± 4
n3922-24c	c, uz, clb	390	140	81	0.34	0.35	>1e6	[0.00]	0.1761	0.91	0.07497	0.69	0.1761	0.91	0.07497	0.69	1068 ± 14	1046 ± 9	1045 ± 9
MA50																			
n4216-03c	sp, uz, clb	2200	700	51	0.23	0.32	59.1	31.64	0.03043	0.90	0.2978	2.4	0.02080	0.90	0.049	32.	136 ± 613	133 ± 1	132 ± 8
n4216-02c	sp, oz, clb	1600	780	56	0.22	0.49	164	11.39	0.03295	1.1	0.1435	0.86	0.02920	1.1	0.0546	4.7	394 ± 101	186 ± 2	184 ± 4
n4216-17c	sp, oz, clm	2300	1100	82	0.23	0.49	47.5	39.36	0.04840	0.86	0.3626	1.0	0.02935	1.0	0.0556	16.	435 ± 321	186 ± 2	184 ± 16
n4216-32c	c, uz, clb	1200	570	41	0.16	0.48	689	2.71	0.03083	0.84	0.07529	0.81	0.03000	0.84	0.0541	2.4	375 ± 53	191 ± 2	189 ± 2
n4216-13c	sp, oz, cld	5400	3800	200	0.19	0.71	100	18.67	0.04066	0.84	0.1967	0.64	0.03307	0.87	0.050	6.1	194 ± 135	210 ± 2	209 ± 6
n4216-18c	sp, oz, cld	5000	2500	210	0.29	0.5	65.7	28.45	0.04944	1.5	0.2761	2.9	0.03537	2.0	0.054	29.	357 ± 550	224 ± 4	223 ± 12
n4216-32r	r, uz, cld	4800	1300	190	0.11	0.28	364	5.14	0.03929	0.84	0.09232	0.84	0.03727	0.84	0.0521	2.5	288 ± 57	236 ± 2	235 ± 3
n4216-10c	c, oz, cld	3800	1700	170	0.65	0.45	93.7	19.96	0.04784	0.99	0.2064	2.0	0.03829	1.2	0.0495	15.	172 ± 324	242 ± 3	242 ± 8
n4216-19c	c, oz, clm	680	130	30	0.4	0.19	933	2	0.04146	0.84	0.06356	0.97	0.04063	0.84	0.0478	2.8	87.7 ± 65.3	257 ± 2	258 ± 2
n4216-41c	sp, oz, clb	2300	340	110	0.12	0.15	1170	1.6	0.04284	0.84	0.06467	0.98	0.04215	0.84	0.05214	1.9	292 ± 43	266 ± 2	266 ± 2
n4216-53c	c, oz, clb	790	720	43	0.73	0.91	414	4.52	0.04438	0.84	0.08735	0.78	0.04238	0.85	0.0520	3.2	284 ± 73	268 ± 2	267 ± 3
n4216-31c	c, oz, clb	130	54	6.5	0.45	0.42	>1e6	[0.00]	0.04299	0.84	0.0514	2.4	0.04299	0.84	0.0514	2.4	260 ± 54	271 ± 2	271 ± 2
n4216-33c	c, oz, clm	1500	370	76	0.3	0.25	17500	0.11	0.04465	0.84	0.05174	0.69	0.04460	0.84	0.05090	0.78	236 ± 18	281 ± 2	282 ± 2
n4216-40c	sp, uz, cld	3700	2400	210	0.69	0.65	857	2.18	0.04651	0.84	0.06864	0.84	0.04549	0.84	0.0515	2.0	264 ± 46	287 ± 2	287 ± 3
n4216-19r	r, uz, cld	7000	1100	350	0.13	0.15	1030	1.81	0.04672	0.84	0.06575	0.53	0.04587	0.84	0.05156	1.1	266 ± 24	289 ± 2	289 ± 2
n4216-31r	r, uz, cld	5400	820	270	0.15	0.15	3440	0.54	0.04626	0.84	0.05573	0.46	0.04600	0.84	0.05146	0.63	262 ± 14	290 ± 2	290 ± 2
n4216-53r	r, uz, cld	4600	580	230	0.08	0.13	944	1.98	0.04738	0.84	0.06732	0.79	0.04644	0.84	0.05179	1.3	276 ± 30	293 ± 2	293 ± 3
n4216-49c	sp, oz, cld	6200	580	310	0.075	0.094	1780	1.05	0.04804	0.84	0.05997	1.0	0.04753	0.84	0.05173	1.7	273 ± 37	299 ± 2	300 ± 3
n4216-43c	sp, oz, cld	9300	2200	490	0.14	0.23	618	3.03	0.04961	0.84	0.07505	1.3	0.04811	0.84	0.0513	2.7	255 ± 61	303 ± 2	303 ± 3
n4216-30c	c, oz, clm	1900	780	600	0.42	0.41	2900	0.65	0.2628	0.84	0.09995	0.79	0.2611	0.84	0.0952	1.2	1532 ± 22	1495 ± 11	1492 ± 12
MA51																			
n4219-16r	r, uz, cld	7900	3600	320	0.42	0.45	2200	0.85	0.03483	0.89	0.05682	0.32	0.03453	0.89	0.05014	0.69	201 ± 16	219 ± 2	219 ± 2
n4219-34r	r, oz, clb	690	290	31	0.41	0.42	3470	0.54	0.03799	0.92	0.05523	0.89	0.03779	0.92	0.05100	1.4	241 ± 31	239 ± 2	239 ± 2
n4219-08c	c, uz, clb	430	180	19	0.42	0.42	819	2.28	0.03878	1.1	0.06894	1.4	0.03790	1.0	0.0510	4.7	242 ± 105	240 ± 2	240 ± 3
n4219-35r	r, oz, clb	1000	370	45	0.47	0.37	10300	0.18	0.03799	0.89	0.05146	0.78	0.03792	0.89	0.05003	0.93	196 ± 22	240 ± 2	240 ± 2
n4219-42r	r, oz, clb	780	290	35	0.43	0.37	13000	0.14	0.03832	0.89	0.05153	0.87	0.03827	0.89	0.05039	1.0	213 ± 23	242 ± 2	242 ± 2
n4219-34c	c, oz, clm	780	430	37	0.57	0.55	460	4.07	0.04005	0.90	0.08324	1.2	0.03842	0.89	0.0513	3.3	256 ± 75	243 ± 2	243 ± 3
n4219-27c	sp, uz, clm	760	350	35	0.54	0.46	3150	0.59	0.03863	0.89	0.05495	1.0	0.03840	0.89	0.05029	1.5	208 ± 35	243 ± 2	243 ± 2
n4219-29c	sp, oz, clm	1000	480	48	0.58	0.46	2790	0.67	0.03885	0.89	0.05526	0.72	0.03859	0.89	0.04999	1.2	195 ± 27	244 ± 2	244 ± 2
n4219-08r	r, oz, cld	1800	1200	88	0.81	0.67	1710	1.09	0.03913	0.89	0.05897	0.53	0.03870	0.89	0.05038	1.1	212 ± 25	245 ± 2	245 ± 2
n4219-18c	sp, oz, clm	970	400	45	0.46	0.41	21000	0.09	0.03894	1.1	0.05133	0.73	0.03891	1.1	0.05063	0.80	224 ± 18	246 ± 3	246 ± 3
n4219-02c	sp, oz, clm	1000	480	49	0.46	0.46	60900	0.03	0.03913	0.89	0.05143	0.73	0.03912	0.89	0.05119	0.76	249 ± 17	247 ± 2	247 ± 2
n4219-42c	c, oz, clb	2000	1500	100	0.77	0.73	37900	0.05	0.03916	0.89	0.05126	0.54	0.03914	0.89	0.05087	0.57	235 ± 13	248 ± 2	248 ± 2
n4219-14c	sp, oz, clm	910	360	42	0.42	0.4	35200	0.05	0.03918	0.89	0.05127	0.78	0.03916	0.89	0.05085	0.82	234 ± 19	248 ± 2	248 ± 2
n4219-36c	sp, oz, clm	670	260	31	0.38	0.39	58800	[0.03]	0.03922	0.91	0.05148	1.2	0.03922	0.91	0.05148	1.2	262 ± 27	248 ± 2	248 ± 2
n4219-25c	sp, oz, clb	420	160	19	0.32	0.37	40500	[0.05]	0.03937	0.89	0.05205	1.3	0.03937	0.89	0.05205	1.3	288 ± 30	249 ± 2	249 ± 2
n4219-39c	sp, oz, clm	810	430	39	0.58	0.53	30300	0.06	0.03950	0.96	0.05128	0.96	0.03948	0.96	0.05079	1.0	232 ± 23	250 ± 2	250 ± 2
n4219-43c	sp, oz, clm	530	160	24	0.37	0.3	61000	[0.03]	0.03960	0.91	0.05031	1.0	0.03960	0.91	0.05031	1.0	209 ± 24	250 ± 2	251 ± 2
n4219-35c	c, uz, cld	2200	1600	110	0.86	0.71	1480	1.26	0.04029	0.89	0.0602	1.7	0.03978	0.89	0.0503	3.2	208 ± 73	251 ± 2	252 ± 2

Sample ID	Characteristics[5]	Concentration (ppm)			Th/U_{calc}	Th/U_{meas}[1]	$^{206}Pb/^{204}Pb$	f_{206} (%)[2]	Total (uncorrected) ratio				Radiogenic (corrected) ratio[3]				Calculated age ± s (Ma)		
		U	Th	Pb					$^{206}Pb/^{238}U$	± s (%)	$^{207}Pb/^{206}Pb$	± s (%)	$^{206}Pb/^{238}U$	± s (%)	$^{207}Pb/^{206}Pb$	± s (%)	$^{207}Pb/^{206}Pb$	$^{206}Pb/^{238}U$	207-corr age[4]
n4219-21c	c, uz, clm	1100	460	51	0.46	0.43	96400	[0.02]	0.03997	0.89	0.05108	0.71	0.03997	0.89	0.05108	0.71	244 ± 16	253 ± 2	253 ± 2
n4219-04c	sp, oz, cld	1600	620	76	0.42	0.39	10500	0.18	0.04007	0.89	0.05235	0.59	0.03999	0.89	0.05095	0.71	239 ± 16	253 ± 2	253 ± 2
n4219-16c	c, oz, clb	750	310	36	0.68	0.41	23000	0.08	0.03998	0.89	0.04973	0.86	0.03995	0.89	0.04909	0.96	152 ± 22	253 ± 2	253 ± 2
n4219-30c	sp, oz, clm	940	390	45	0.45	0.42	93000	[0.02]	0.04017	0.93	0.05121	1.1	0.04017	0.93	0.05121	1.1	250 ± 25	254 ± 2	254 ± 2
n4219-03c	sp, oz, clm	870	340	41	0.41	0.39	48500	0.04	0.04025	0.89	0.05145	0.78	0.04024	0.89	0.05115	0.81	248 ± 19	254 ± 2	254 ± 2
n4219-10c	sp, oz, clm	1100	570	54	0.69	0.52	37500	0.05	0.04040	0.92	0.05027	0.70	0.04038	0.92	0.04988	0.74	189 ± 17	255 ± 2	256 ± 2
n4219-13c	sp, oz, clb	550	180	59	0.16	0.33	36200	0.05	0.08815	1.1	0.08926	0.57	0.08811	1.1	0.08888	0.59	1401 ± 11	544 ± 6	523 ± 6
MA52																			
n3950-08c	c, uz, cld	30000	11000	600	0.11	0.38	229	8.18	0.0194	7.6	0.1146	3.0	0.0178	7.5	0.0503	10.	209 ± 227	114 ± 8	113 ± 9
n3950-27c	c, oz, cld	2600	950	110	1.6	0.36	391	4.79	0.03739	0.95	0.0848	2.3	0.03560	0.96	0.0470	6.4	51.7 ± 146.6	226 ± 2	226 ± 3
n3950-06c	sp, oz, cld	1200	380	53	0.36	0.32	35700	[0.05]	0.03851	0.96	0.05054	1.3	0.03851	0.96	0.05054	1.3	220 ± 29	244 ± 2	244 ± 2
n3950-08r	r, oz, clb	670	200	30	0.35	0.3	21400	[0.09]	0.03866	0.96	0.05051	1.5	0.03866	0.96	0.05051	1.5	218 ± 35	245 ± 2	245 ± 2
n3950-02r	sp, oz, clb	740	270	33	0.34	0.36	>1e6	[0.00]	0.03873	0.95	0.05126	1.5	0.03873	0.95	0.05126	1.5	253 ± 34	245 ± 2	245 ± 2
n3950-26c	c, uz, cld	1800	480	79	0.24	0.27	80600	[0.02]	0.03891	0.95	0.05156	0.92	0.03891	0.95	0.05156	0.92	266 ± 21	246 ± 2	246 ± 2
n3950-06r	sp, oz, clb	2000	540	90	0.25	0.27	90700	[0.02]	0.03914	0.95	0.05144	0.92	0.03914	0.95	0.05144	0.92	261 ± 21	247 ± 2	247 ± 2
n3950-02c	sp, oz, cld	890	460	42	0.87	0.52	3380	0.55	0.03938	0.96	0.05327	1.6	0.03916	0.96	0.0489	2.2	144 ± 51	248 ± 2	248 ± 2
n3950-11c	c, oz, cld	2900	850	130	0.26	0.29	112000	[0.02]	0.03975	0.95	0.05163	0.72	0.03975	0.95	0.05163	0.72	269 ± 16	251 ± 2	251 ± 2
n3950-09c	c, uz, cld	2400	870	110	0.3	0.36	2870	0.65	0.04004	0.95	0.05734	0.73	0.03978	0.95	0.05223	1.2	295 ± 27	251 ± 2	251 ± 2
n3950-04c	c, uz, cld	3100	3000	170	0.93	0.95	72200	[0.03]	0.03979	0.95	0.05116	0.85	0.03979	0.95	0.05116	0.85	248 ± 19	252 ± 2	252 ± 2
n3950-28c	c, uz,cld	5700	5800	320	1.1	1	10200	0.18	0.04117	0.95	0.05231	0.58	0.04109	0.95	0.05088	0.71	235 ± 16	260 ± 2	260 ± 2
MA54																			
n3966x-20c	c, uz, clm	530	690	22	n/d	1.3	178	10.52	0.0354	3.0	0.1206	3.6	0.03169	3.1	0.037	30.	-589 ± 661	201 ± 6	204 ± 7
n3966x-44c	sp, uz, clb	200	150	8.6	0.61	0.74	1480	1.26	0.0349	3.0	0.0608	1.9	0.0344	3.0	0.0509	4.2	235 ± 95	218 ± 6	218 ± 7
n3966x-51c	sp, uz, clb	150	110	6.5	0.57	0.76	5180	0.36	0.0348	3.1	0.0539	1.9	0.0347	3.1	0.0511	2.8	244 ± 62	220 ± 7	220 ± 7
n3966-22	sp, uz, clb	380	220	16	n/d	0.58	48.8	38.21	0.0559	3.5	0.347	4.8	0.0345	4.7	0.045	89.	-42 ± 1,371	219 ± 10	219 ± 20
n3966x-31	sp, oz, clb	240	120	10	0.39	0.49	19400	[0.10]	0.03489	1.2	0.05218	1.4	0.03489	1.2	0.05218	1.4	293 ± 32	221 ± 3	221 ± 3
n3966x-27c	sp, uz, clm	210	160	9.2	0.63	0.76	13600	0.14	0.0349	3.0	0.05168	1.7	0.0348	3.0	0.05060	1.9	223 ± 43	221 ± 7	221 ± 7
n3966x-52c	c, uz, clb	210	150	9.1	0.4	0.69	39800	[0.05]	0.0351	3.0	0.05279	1.6	0.0351	3.0	0.05279	1.6	320 ± 36	222 ± 7	222 ± 7
n3966x-32c	sp, oz, clm	180	130	7.8	0.42	0.75	21100	[0.09]	0.0353	3.0	0.05300	1.8	0.0353	3.0	0.05300	1.8	329 ± 40	224 ± 7	223 ± 7
n3966x-17	sp, uz, clb	200	120	8.9	0.54	0.59	16900	[0.11]	0.03548	1.5	0.05120	1.5	0.03548	1.5	0.05120	1.5	250 ± 34	225 ± 3	225 ± 3
n3966x-29c	sp, oz, clm	410	450	19	0.98	1.1	16400	0.11	0.0355	3.1	0.05111	1.2	0.0355	3.1	0.05022	1.3	205 ± 31	225 ± 7	225 ± 7
n3966x-45c	sp, uz, clm	280	230	13	0.55	0.83	6830	0.27	0.0358	3.0	0.0542	2.1	0.0357	3.0	0.0521	2.4	290 ± 55	226 ± 7	226 ± 7
n3966x-42c	sp, uz, clb	140	90	6.3	0.49	0.63	>1e6	[0.00]	0.0357	3.0	0.05096	1.9	0.0357	3.0	0.05096	1.9	239 ± 43	226 ± 7	226 ± 7
n3966x-08c	sp, oz, clm	320	260	14	0.7	0.83	11700	0.16	0.0359	3.0	0.05179	1.4	0.0359	3.0	0.05053	1.7	219 ± 38	227 ± 7	227 ± 7
n3966x-16c	sp, uz, clb	200	170	9.1	0.57	0.87	47800	[0.04]	0.0366	3.0	0.0520	2.2	0.0366	3.0	0.0520	2.2	286 ± 51	232 ± 7	232 ± 7
n3966x-18c	sp, uz, cld	280	310	13	n/d	1.1	682	2.74	0.0371	3.0	0.0559	1.9	0.0360	3.0	0.0339	6.5	-794 ± 176	228 ± 7	233 ± 7
n3966x-15c	sp, uz, cld	820	1000	42	0.92	1.3	1250	1.5	0.0374	3.0	0.0632	2.7	0.0369	3.0	0.0515	4.0	264 ± 89	233 ± 7	233 ± 7
n3966x-36c	sp, uz, clb	210	180	9.9	0.98	0.84	4560	0.41	0.0369	3.0	0.05253	1.6	0.0368	3.0	0.0493	2.5	162 ± 57	233 ± 7	233 ± 7
n3966x-30	sp, oz, clb	130	63	5.6	0.59	0.5	10900	[0.17]	0.03701	1.2	0.0503	2.0	0.03701	1.2	0.0503	2.0	207 ± 46	234 ± 3	234 ± 3
n3966x-33c	sp, oz, clm	160	140	7.5	n/d	0.83	1140	1.64	0.0375	3.0	0.0585	2.7	0.0369	3.0	0.0455	5.3	-30 ± 124	233 ± 7	235 ± 7
n3966x-43c	sp, uz, clm	590	590	29	0.78	0.99	88500	[0.02]	0.0372	3.0	0.05127	0.94	0.0372	3.0	0.05127	0.94	253 ± 21	235 ± 7	235 ± 7
n3966x-35	sp, uz, clb	180	110	8.5	0.5	0.59	53200	[0.04]	0.03738	1.2	0.05212	1.7	0.03738	1.2	0.05212	1.7	290 ± 39	237 ± 3	236 ± 3
n3966x-42x	sp, uz, clm	170	73	7.7	0.44	0.42	39200	[0.05]	0.03757	1.2	0.05079	1.7	0.03757	1.2	0.05079	1.7	231 ± 40	238 ± 3	238 ± 3
n3966-40r	r, uz, clb	290	140	13	1.5	0.5	1060	1.76	0.03834	0.92	0.0613	2.3	0.03767	0.93	0.0474	5.0	68.2 ± 114.6	238 ± 2	239 ± 2
n3966-26	sp, oz, clb	150	63	7	0.23	0.42	5160	[0.36]	0.03829	0.91	0.0587	5.3	0.03829	0.91	0.0587	5.3	555 ± 112	242 ± 2	240 ± 2
n3966-11	sp, uz, clb	290	170	14	0.68	0.59	2600	0.72	0.03874	1.1	0.0562	3.6	0.03846	1.1	0.0506	5.2	222 ± 116	243 ± 3	243 ± 3
n3966-41c	r(i), uz, clb	1200	1100	62	8.4	0.88	373	5.09	0.04092	0.98	0.0867	2.0	0.03884	0.96	0.0465	5.7	26.0 ± 132.0	246 ± 2	247 ± 3
n3966-41r	r(e), uz, clb	330	190	16	0.64	0.58	>1e6	[0.00]	0.03933	0.91	0.0508	2.7	0.03933	0.91	0.0508	2.7	234 ± 61	249 ± 2	249 ± 2
n3966x-12	sp, uz, clm	310	220	16	1.7	0.71	4630	0.4	0.03935	1.2	0.05120	1.2	0.03920	1.2	0.04801	1.9	100 ± 45	248 ± 3	249 ± 3
n3966-31c	sp, uz, clb	200	110	9.7	0.81	0.54	9750	[0.19]	0.03929	0.91	0.0496	2.6	0.03929	0.91	0.0496	2.6	175 ± 60	248 ± 2	249 ± 2
n3966-25	c, uz, cld	380	220	19	0.63	0.58	24100	[0.08]	0.03945	0.91	0.05109	1.8	0.03945	0.91	0.05109	1.8	245 ± 42	249 ± 2	249 ± 2
n3966-38	sp, uz, clm	320	190	16	0.51	0.61	18700	[0.10]	0.03971	0.91	0.0522	1.9	0.03971	0.91	0.0522	1.9	295 ± 44	251 ± 2	251 ± 2
n3966-31r	sp, oz, clb	200	81	9.6	0.49	0.4	>1e6	[0.00]	0.03976	0.91	0.0507	2.7	0.03976	0.91	0.0507	2.7	229 ± 62	251 ± 2	252 ± 2
n3966x-07	sp, uz, clb	190	98	9.2	n/d	0.5	2130	0.88	0.04009	1.2	0.0527	2.2	0.03974	1.2	0.0458	3.6	-13 ± 84	251 ± 3	253 ± 3
n3966-40c	c, uz, clm	320	250	17	1.1	0.76	6200	0.3	0.04007	0.97	0.0522	2.4	0.03995	0.97	0.0498	3.0	186 ± 69	253 ± 2	253 ± 2
n3966-28	sp, oz, clb	190	98	9.2	0.63	0.52	35500	[0.05]	0.04001	0.99	0.0502	2.8	0.04001	0.99	0.0502	2.8	205 ± 64	253 ± 2	253 ± 3
n3966x-47	sp, oz, clb	180	130	14	0.77	0.71	19700	[0.10]	0.05973	1.2	0.05333	1.2	0.05973	1.2	0.05333	1.2	343 ± 26	374 ± 4	374 ± 4
MA55																			
n4220-22r	r, oz, clb	1900	580	83	0.29	0.3	35300	0.05	0.03749	0.89	0.05172	0.60	0.03747	0.89	0.05131	0.65	255 ± 15	237 ± 2	237 ± 2
n4220-44c	c, uz, cld	5700	5400	260	0.48	0.94	13600	0.14	0.03817	0.94	0.05220	0.35	0.03812	0.94	0.05113	0.40	246 ± 9	241 ± 2	241 ± 2
n4220-48c	sp, oz, cld	1900	1300	91	0.59	0.69	780	2.4	0.03958	0.89	0.07079	0.68	0.03863	0.89	0.0520	2.4	286 ± 53	244 ± 2	244 ± 2
n4220-41r	r, uz, clb	830	440	41	0.54	0.54	36600	0.05	0.04094	0.89	0.05176	0.87	0.04092	0.89	0.05135	0.93	257 ± 21	259 ± 2	259 ± 2
n4220-14c	sp, oz, clm	750	260	36	0.36	0.35	17100	0.11	0.04172	0.89	0.05207	0.88	0.04168	0.89	0.05121	0.99	250 ± 23	263 ± 2	263 ± 2
n4220-34c	sp, oz, clb	500	410	28	0.76	0.81	38100	[0.05]	0.04175	0.95	0.05204	1.1	0.04175	0.95	0.05204	1.1	287 ± 24	264 ± 2	263 ± 2

Sample ID	Characteristics[5]	Concentration (ppm)							Total (uncorrected) ratio				Radiogenic (corrected) ratio[3]				Calculated age ± s (Ma)		
		U	Th	Pb	Th/U_{calc}	Th/U_{mean}[1]	$^{206}Pb/^{204}Pb$	f_{206} (%)[2]	$^{206}Pb/^{238}U$	± s (%)	$^{207}Pb/^{206}Pb$	± s (%)	$^{206}Pb/^{238}U$	± s (%)	$^{207}Pb/^{206}Pb$	± s (%)	$^{207}Pb/^{206}Pb$	$^{206}Pb/^{238}U$	207-corr age[4]
n4220-39c	sp, oz, clm	950	560	49	0.6	0.6	29800	0.06	0.04193	0.90	0.05194	0.77	0.04190	0.90	0.05145	0.83	261 ± 19	265 ± 2	265 ± 2
n4220-15c	c, uz, cld	1500	510	74	0.34	0.33	62600	0.03	0.04197	0.89	0.05162	0.62	0.04196	0.89	0.05139	0.64	258 ± 15	265 ± 2	265 ± 2
n4220-11c	sp, oz, cld	1400	730	72	0.52	0.52	116000	[0.02]	0.04217	0.90	0.05154	0.65	0.04217	0.90	0.05154	0.65	265 ± 15	266 ± 2	266 ± 2
n4220-21c	sp, uz, clm	1200	730	61	0.66	0.63	36300	0.05	0.04220	0.90	0.05165	0.82	0.04218	0.90	0.05125	0.86	252 ± 20	266 ± 2	266 ± 2
n4220-07c	sp, uz, cld	2000	570	96	0.31	0.29	69800	0.03	0.04220	0.89	0.05140	0.52	0.04219	0.89	0.05119	0.54	249 ± 12	266 ± 2	267 ± 2
n4220-22c	c, uz, cld	3100	1100	160	0.36	0.36	37700	0.05	0.04251	0.89	0.05199	0.43	0.04249	0.89	0.05161	0.46	268 ± 10	268 ± 2	268 ± 2
n4220-45c	sp, uz, clm	1600	760	80	0.45	0.49	106000	[0.02]	0.04259	0.90	0.05206	0.70	0.04259	0.90	0.05206	0.70	288 ± 16	269 ± 2	269 ± 2
n4220-09c	c, oz, cld	1400	750	74	0.59	0.52	75700	0.02	0.04255	0.89	0.05112	0.86	0.04254	0.89	0.05093	0.87	238 ± 20	269 ± 2	269 ± 2
n4220-41c	c, uz, clm	1400	500	69	0.36	0.36	124000	[0.02]	0.04267	0.89	0.05168	0.64	0.04267	0.89	0.05168	0.64	271 ± 15	269 ± 2	269 ± 2
n4220-06c	sp, uz, cld	2900	850	140	0.31	0.29	63300	0.03	0.04303	0.89	0.05150	0.67	0.04302	0.89	0.05127	0.68	253 ± 16	272 ± 2	272 ± 2
n4220-23c	sp, uz, cld	2900	990	150	0.35	0.34	48400	0.04	0.04314	0.89	0.05181	0.43	0.04312	0.89	0.05150	0.45	263 ± 10	272 ± 2	272 ± 2
n4220-44r	r, oz, clb	1700	710	84	0.39	0.43	32600	0.06	0.04322	0.90	0.05188	0.83	0.04319	0.90	0.05143	0.86	260 ± 20	273 ± 2	273 ± 2
n4220-01c	sp, oz, cld	1200	320	57	0.26	0.28	66000	0.03	0.04327	1.7	0.05259	1.5	0.04325	1.7	0.05237	1.5	302 ± 34	273 ± 4	273 ± 5
n4220-28c	sp, uz, cld	3000	990	150	0.33	0.33	60600	0.03	0.04328	0.89	0.05191	0.43	0.04327	0.89	0.05167	0.44	271 ± 10	273 ± 2	273 ± 2
n4220-38c	sp, oz, clb	430	210	22	0.89	0.49	2990	0.63	0.04355	0.89	0.05387	1.6	0.04328	0.89	0.0489	2.6	145 ± 59	273 ± 2	274 ± 2
n4220-09r	r, oz, clm	1900	850	97	0.48	0.45	83700	0.02	0.04369	0.89	0.05157	0.54	0.04368	0.89	0.05140	0.55	259 ± 13	276 ± 2	276 ± 2
n4220-35c	sp, uz, cld	2000	1200	110	0.66	0.6	18200	0.1	0.04374	0.89	0.05216	0.55	0.04370	0.89	0.05136	0.61	257 ± 14	276 ± 2	276 ± 2
n4220-26c	sp, uz, cld	4100	1500	210	0.4	0.36	97900	0.02	0.04447	0.89	0.05133	0.36	0.04446	0.89	0.05118	0.37	249 ± 9	280 ± 2	281 ± 2
n4220-40c	sp, uz, cld	6800	2900	370	0.48	0.43	42500	0.04	0.04539	0.89	0.05187	0.28	0.04537	0.89	0.05152	0.30	264 ± 7	286 ± 2	286 ± 3
MA66																			
n4563-11c	sp, uz, cld	1900	1000	66	0.26	0.54	2590	0.72	0.03083	2.4	0.0559	2.0	0.03061	2.3	0.0503	2.7	208 ± 61	194 ± 4	194 ± 5
n4563-16c	sp, oz, cld	2100	710	81	0.38	0.33	1850	1.01	0.03343	0.88	0.05765	0.85	0.03309	0.88	0.04970	1.7	181 ± 39	210 ± 2	210 ± 2
n4563-10c	sp, uz, cld	1600	1800	70	1.1	1.1	1960	0.95	0.03360	1.2	0.05696	0.57	0.03328	1.2	0.04947	1.1	170 ± 25	211 ± 3	211 ± 3
n4563-21c	sp, uz, cld	13000	2900	450	0.071	0.23	521	3.59	0.03470	0.88	0.07866	1.1	0.03346	0.88	0.0505	3.0	218 ± 68	212 ± 2	212 ± 2
n4563-36r	r(i), uz, clm	380	260	16	0.7	0.69	3120	0.6	0.03390	1.1	0.05467	0.92	0.03370	1.1	0.04996	1.5	193 ± 34	214 ± 2	214 ± 2
n4563-39c	c, oz, clb	1100	99	39	0.092	0.094	6200	0.3	0.03489	0.93	0.05205	0.53	0.03479	0.93	0.04968	0.88	180 ± 20	220 ± 2	221 ± 2
n4563-19c	sp, oz, cld	2100	2000	98	0.98	0.96	3750	0.5	0.03513	0.90	0.05452	0.58	0.03495	0.90	0.05061	0.74	223 ± 17	221 ± 2	221 ± 2
n4563-33c	c, uz, cld	390	110	15	0.28	0.3	24700	[0.08]	0.03496	0.91	0.05084	0.89	0.03496	0.91	0.05084	0.89	234 ± 20	222 ± 2	221 ± 2
n4563-40c	sp, uz, cld	2200	1100	91	0.46	0.52	10000	0.19	0.03517	0.88	0.05194	0.37	0.03511	0.88	0.05048	0.45	217 ± 10	222 ± 2	222 ± 2
n4563-06c	c, uz, clb	640	180	25	0.19	0.28	2980	0.63	0.03533	0.88	0.0552	3.0	0.03511	0.89	0.0503	4.0	207 ± 91	222 ± 2	223 ± 2
n4563-23c	c, uz, cld	510	120	20	0.25	0.24	23100	[0.08]	0.03557	0.88	0.05076	0.82	0.03557	0.88	0.05076	0.82	230 ± 19	225 ± 2	225 ± 2
n4563-33r	r, oz, cld	620	280	26	0.51	0.45	1330	1.41	0.03611	0.88	0.06118	1.1	0.03560	0.88	0.0501	2.6	201 ± 60	226 ± 2	226 ± 2
n4563-32c	c, uz,cld	650	170	26	0.29	0.26	28500	[0.07]	0.03569	0.89	0.05030	0.69	0.03569	0.89	0.05030	0.69	209 ± 16	226 ± 2	226 ± 2
n4563-41c	sp, oz, clm	490	130	20	0.5	0.27	9150	0.2	0.03571	0.90	0.04999	0.96	0.03564	0.90	0.04839	1.1	118 ± 26	226 ± 2	226 ± 2
MA68																			
n4556-35c	c, oz, clb	910	1000	30	0.84	1.1	1150	1.62	0.02577	1.1	0.06171	0.67	0.02535	1.1	0.04894	1.6	145 ± 36	161 ± 2	161 ± 2
n4556-27c	c, uz, cld	2000	1900	85	0.63	0.92	1550	1.2	0.03202	0.85	0.0609	3.2	0.03164	0.85	0.0514	5.4	260 ± 120	201 ± 2	200 ± 2
n4556-29r	r, oz, clm	1600	510	61	0.3	0.32	2020	0.93	0.03328	1.1	0.05835	0.49	0.03298	1.1	0.05109	1.0	245 ± 23	209 ± 2	209 ± 2
n4556-39c	c, uz, cld	16000	3900	560	0.11	0.25	701	2.67	0.0342	3.2	0.0696	2.5	0.0333	3.1	0.0486	5.9	129 ± 134	211 ± 6	212 ± 7
n4556-26c	c, uz, clb	530	240	22	1.7	0.45	353	5.3	0.03653	0.90	0.0889	5.1	0.03459	0.88	0.0471	15.	56.2 ± 314.2	219 ± 2	220 ± 3
n4556-07c	c, uz, clb	840	220	33	0.21	0.27	4340	0.43	0.03524	1.5	0.05366	0.62	0.03509	1.4	0.05028	0.99	208 ± 23	222 ± 3	222 ± 3
n4556-18c	sp, uz, cld	16000	6400	650	0.24	0.39	2440	0.77	0.03549	1.3	0.05683	0.35	0.03522	1.3	0.05082	0.56	233 ± 13	223 ± 3	223 ± 3
n4556-23c	c, uz, clm	780	560	35	0.73	0.72	46900	0.04	0.03537	0.81	0.05077	0.70	0.03536	0.81	0.05046	0.73	216 ± 17	224 ± 2	224 ± 2
n4556-52c	sp, oz, clb	490	130	20	0.23	0.26	28300	0.07	0.03577	1.0	0.05140	0.80	0.03575	1.0	0.05088	0.85	235 ± 20	226 ± 2	226 ± 2
n4556-44c	sp, uz, clb	640	340	28	0.51	0.52	36600	[0.05]	0.03581	1.2	0.05083	0.73	0.03581	1.2	0.05083	0.73	233 ± 17	227 ± 3	227 ± 3
n4556-19c	sp, oz, clm	1000	660	45	0.76	0.66	40400	0.05	0.03583	0.81	0.05040	0.73	0.03581	0.81	0.05004	0.76	197 ± 18	227 ± 2	227 ± 2
n4556-07r	r, uz, cld	2700	300	100	0.1	0.11	17200	0.11	0.03609	0.99	0.05133	0.35	0.03605	0.99	0.05048	0.39	217 ± 9	228 ± 2	228 ± 2
n4556-29c	c, uz, cld	3200	1600	140	0.64	0.49	2670	0.7	0.03629	0.81	0.05542	1.1	0.03604	0.81	0.04992	1.6	191 ± 37	228 ± 2	228 ± 2
n4556-23r	r, uz, cld	16000	1000	690	0.062	0.064	5570	0.34	0.04063	0.89	0.05231	0.41	0.04049	0.89	0.04967	0.71	180 ± 16	256 ± 2	256 ± 2
n4556-31c	sp, oz, clb	2800	580	120	0.23	0.21	148000	0.01	0.04083	0.95	0.05078	0.45	0.04083	0.95	0.05068	0.45	226 ± 10	258 ± 2	258 ± 2
MA69																			
n4557-23c	c, uz, clb	5600	1500	170	0.062	0.27	71.1	26.3	0.03757	0.85	0.2598	0.84	0.02769	0.81	0.0544	15.	386 ± 302	176 ± 1	175 ± 8
n4557-07c	c, oz, cld	12000	3800	410	0.1	0.31	538	3.48	0.03104	1.5	0.0780	5.6	0.02996	1.4	0.0506	12.	225 ± 264	190 ± 3	190 ± 3
n4557-10c	c, uz, cld	2000	960	71	n/d	0.49	808	2.32	0.03103	1.3	0.06438	1.5	0.03031	1.3	0.0461	2.9	0.0 ± 70.8	193 ± 2	193 ± 3
n4557-15c	c, uz, cld	2300	290	[75]	n/d	0.13	1110	1.68	0.03126	0.81	0.05709	1.4	0.03073	0.81	0.0438	4.9	-122 ± 117	195 ± 2	197 ± 2
n4557-10r	r, oz, cld	1400	590	57	0.41	0.43	60800	0.03	0.03526	1.5	0.05079	0.47	0.03525	1.5	0.05055	0.48	221 ± 11	223 ± 3	223 ± 3
n4557-23r	r, oz, cld	13000	760	460	4800000000	0.061	483	3.87	0.03654	0.89	0.0768	3.8	0.03512	0.88	0.0463	11.	0.0 ± 264.1	223 ± 2	224 ± 2
n4557-33c	sp, oz, cld	3800	1200	160	0.29	0.31	2610	0.72	0.03584	0.98	0.05648	0.75	0.03559	0.97	0.05085	1.1	234 ± 25	225 ± 2	225 ± 2
n4557-17c	c, uz, cld	590	310	26	0.51	0.52	45500	[0.04]	0.03573	0.82	0.05084	0.73	0.03573	0.82	0.05084	0.73	233 ± 17	226 ± 2	226 ± 2
n4557-41c	sp, oz, cld	560	200	24	0.54	0.36	706	2.65	0.03767	0.88	0.0698	3.4	0.03667	0.87	0.0489	7.4	143 ± 166	232 ± 2	233 ± 2
n4557-39c	sp, oz, clb	7200	560	290	0.036	0.078	4500	0.42	0.03763	0.82	0.05363	0.65	0.03748	0.82	0.05036	0.88	212 ± 20	237 ± 2	237 ± 2
n4557-01c	sp, oz, cld	14000	430	590	0.028	0.03	142000	0.01	0.03880	0.84	0.050506	0.15	0.03880	0.84	0.050402	0.15	214 ± 4	245 ± 2	246 ± 2
n4557-54c	sp, oz, cld	8700	2000	370	3E+12	0.23	2380	0.78	0.03931	1.8	0.05253	0.27	0.03900	1.8	0.04634	1.8	0.0 ± 59.4	247 ± 4	248 ± 4
n4557-12c	c, oz, clm	3600	810	160	0.18	0.22	5560	0.34	0.04011	0.86	0.05246	0.49	0.03997	0.86	0.04982	0.78	187 ± 18	253 ± 2	253 ± 2

Sample ID	Characteristics[5]	Concentration (ppm)			Th/U_{calc}	Th/U_{meas}[1]	$^{206}Pb/^{204}Pb$	f_{206} (%)[2]	Total (uncorrected) ratio				Radiogenic (corrected) ratio[3]				Calculated age ± s (Ma)		
		U	Th	Pb					$^{206}Pb/^{238}U$	± s (%)	$^{207}Pb/^{206}Pb$	± s (%)	$^{206}Pb/^{238}U$	± s (%)	$^{207}Pb/^{206}Pb$	± s (%)	$^{207}Pb/^{206}Pb$	$^{206}Pb/^{238}U$	207-corr age[4]
n4557-12r	r, oz, cld	22000	870	970	0.0091	0.04	4030	0.46	0.04201	0.81	0.053282	0.16	0.04181	0.81	0.04963	0.41	178 ± 10	264 ± 2	265 ± 2
n4557-34c	sp, oz, clb	500	88	34	0.24	0.17	25800	0.07	0.05908	0.93	0.05723	0.68	0.05903	0.93	0.05667	0.71	479 ± 16	370 ± 3	368 ± 3
MA73																			
n4558-29c	c, uz, cld	2300	410	38	n/d	0.18	282	6.63	0.01691	1.7	0.0891	6.2	0.01578	1.6	0.036	34.	-627 ± 733	101 ± 2	102 ± 2
n4558-12c	sp, oz, clb	1400	120	26	0.083	0.085	3060	0.61	0.01679	0.81	0.05349	0.84	0.01668	0.81	0.04868	1.3	133 ± 30	107 ± 1	107 ± 1
n4558-37c	c, uz, cld	2500	500	49	0.099	0.2	258	7.24	0.01913	2.2	0.108	12.	0.01774	2.0	0.051	38.	248 ± 699	113 ± 2	113 ± 3
n4558-29r	r, uz, clb	1500	280	31	0.062	0.19	1380	1.36	0.01876	1.5	0.0649	9.3	0.01851	1.5	0.0543	14.	385 ± 291	118 ± 2	117 ± 2
n4558-20c	sp, oz, clb	340	110	11	0.59	0.33	2720	0.69	0.02770	3.1	0.05382	1.1	0.02751	3.1	0.04841	1.9	119 ± 43	175 ± 5	175 ± 5
n4558-22c	sp, oz, cld	1500	1200	69	1.4	0.77	2690	0.7	0.03456	1.3	0.05418	0.92	0.03432	1.3	0.04870	1.3	133 ± 31	218 ± 3	218 ± 3
n4558-41c	sp, oz, clb	650	370	29	0.73	0.57	79200	[0.02]	0.03580	1.1	0.04995	0.69	0.03580	1.1	0.04995	0.69	193 ± 16	227 ± 2	227 ± 2
n4558-13c	sp, oz, clb	320	210	15	0.66	0.66	28700	[0.07]	0.03665	1.0	0.05096	1.0	0.03665	1.0	0.05096	1.0	239 ± 23	232 ± 2	232 ± 2
n4558-09c	sp, oz, cld	220	130	10	0.81	0.58	460	4.07	0.03849	0.94	0.0817	3.5	0.03692	0.92	0.0497	11.	181 ± 232	234 ± 2	234 ± 3
n4558-54c	c, uz, cld	1200	1000	61	0.8	0.82	323	5.79	0.0394	3.0	0.097	25.	0.0371	2.8	0.052	70.	267 ± 1,110	235 ± 7	234 ± 11
n4558-31c	sp, oz, clm	420	260	20	0.71	0.62	20500	0.09	0.03875	0.83	0.05114	1.0	0.03871	0.83	0.05042	1.1	214 ± 25	245 ± 2	245 ± 2
MA76																			
n4559-21c	sp, uz, cld	29000	45000	550	n/d	1.6	252	7.43	0.01648	1.8	0.1029	3.9	0.01526	1.6	0.0441	15.	-104 ± 330	244.0 ± 1.6	98.0 ± 2.1
n4559-38c	c, uz, cld	430	200	18	0.39	0.47	62600	[0.03]	0.03412	0.83	0.05158	0.83	0.03412	0.83	0.05158	0.83	267 ± 19	216 ± 2	216 ± 2
n4559-23c	sp, uz, clm	550	350	24	0.49	0.63	137	13.7	0.03965	2.2	0.160	8.1	0.03422	1.9	0.052	41.	296 ± 740	217 ± 4	216 ± 8
n4559-40c	sp, oz, clb	290	89	11	0.38	0.31	15000	0.12	0.03436	0.81	0.05055	1.0	0.03431	0.81	0.04957	1.2	175 ± 29	217 ± 2	218 ± 2
n4559-28c	sp, oz, clb	710	560	34	0.74	0.8	1540	1.21	0.03751	0.88	0.0608	2.1	0.03705	0.88	0.0513	3.1	254 ± 71	235 ± 2	234 ± 2
n4559-10r	r, oz, clm	680	570	33	0.9	0.84	54000	0.03	0.03719	0.83	0.05088	0.65	0.03717	0.83	0.05060	0.67	223 ± 15	235 ± 2	235 ± 2
n4559-17c	c, uz, cld	920	880	46	1.1	0.95	15400	0.12	0.03730	1.7	0.05133	0.55	0.03726	1.7	0.05037	0.68	212 ± 16	236 ± 4	236 ± 4
n4559-35c	sp, uz, clm	530	320	25	0.6	0.61	46600	[0.04]	0.03764	0.82	0.05113	0.72	0.03764	0.82	0.05113	0.72	247 ± 17	238 ± 2	238 ± 2
n4559-34c	sp, uz, clm	700	440	33	0.6	0.63	28900	0.06	0.03795	0.84	0.05170	0.62	0.03792	0.84	0.05119	0.67	250 ± 15	240 ± 2	240 ± 2
n4559-24c	sp, uz, clm	380	240	18	0.68	0.63	43100	[0.04]	0.03791	0.90	0.05062	0.85	0.03791	0.90	0.05062	0.85	224 ± 20	240 ± 2	240 ± 2
n4559-05c	c, uz, cld	1300	1400	70	1.1	1.1	3710	0.5	0.03827	0.81	0.05463	0.44	0.03808	0.81	0.05068	0.83	226 ± 19	241 ± 2	241 ± 2
n4559-01c	sp, oz, clm	660	360	31	0.66	0.55	10000	0.19	0.03864	0.81	0.05183	0.69	0.03857	0.81	0.05036	0.94	212 ± 22	244 ± 2	244 ± 2
n4559-12c	sp, uz, clb	650	380	31	0.66	0.58	23000	0.08	0.03884	0.81	0.05132	0.83	0.03881	0.81	0.05068	0.88	226 ± 20	245 ± 2	246 ± 2
MA78																			
n4564-07c	sp, oz, cld	5500	2200	11	n/d	0.4	20.2	92.72	0.01765	1.8	0.7771	1.0	0.00129	8.8	0.03	520.	-923 ± 3,762	79.6 ± 0.7	7.7 ± 13.6
n4564-20c	sp, oz, clb	210	110	3	0.15	0.52	2010	0.93	0.01201	0.85	0.0592	3.2	0.01190	0.85	0.0519	5.6	282 ± 124	79.1 ± 0.6	75.8 ± 0.7
n4564-33c	sp, oz, clb	80	88	1.4	0.57	1.1	2920	[0.64]	0.01203	1.1	0.0494	4.6	0.01203	1.1	0.0494	4.6	165 ± 103	79.6 ± 0.8	76.9 ± 0.9
n4564-09c	sp, oz, clb	130	61	1.9	0.088	0.48	41000	[0.05]	0.01232	0.97	0.0555	3.2	0.01232	0.97	0.0555	3.2	434 ± 70	80.2 ± 0.8	78.1 ± 0.8
n4564-09r	sp, oz, clm	84	53	1.3	0.23	0.63	>1e6	[0.00]	0.01234	0.99	0.0505	4.2	0.01234	0.99	0.0505	4.2	216 ± 94	79.6 ± 0.8	78.8 ± 0.8
n4564-11c	sp, oz, clm	67	59	1.1	0.51	0.89	6060	[0.31]	0.01242	1.2	0.0490	5.7	0.01242	1.2	0.0490	5.7	149 ± 128	18.2 ± 0.9	79.4 ± 1.0
n4564-05c	sp, oz, clb	240	150	3.7	0.33	0.64	9490	[0.20]	0.01243	0.87	0.0492	2.6	0.01243	0.87	0.0492	2.6	155 ± 59	76.3 ± 0.7	79.5 ± 0.7
n4564-16c	c, uz, clb	110	140	2	1.1	1.3	3390	[0.55]	0.01243	1.2	0.0479	4.3	0.01243	1.2	0.0479	4.3	92.9 ± 98.4	79.7 ± 0.9	79.6 ± 1.0
n4564-23c	c, uz, clb	310	180	4.7	n/d	0.57	235	7.95	0.01352	0.87	0.1081	3.7	0.01245	0.88	0.0453	16.	-40 ± 344	49.8 ± 0.7	79.9 ± 1.2
n4564-12c	sp, oz, clb	94	120	1.7	0.83	1.2	4820	[0.39]	0.01252	1.3	0.0485	4.0	0.01252	1.3	0.0485	4.0	123 ± 91	80.7 ± 1.1	80.2 ± 1.1
n4564-30c	c, oz, clb	250	110	3.8	0.2	0.45	6470	[0.29]	0.01260	0.85	0.0500	2.4	0.01260	0.85	0.0500	2.4	194 ± 56	89.2 ± 0.7	80.5 ± 0.7
n4564-44c	sp, uz, cld	1600	1900	29	2.3	1.2	29100	[0.06]	0.01265	0.83	0.04688	0.99	0.01265	0.83	0.04688	0.99	43.0 ± 23.6	77.1 ± 0.7	81.1 ± 0.7
n4564-30r	r, oz, cld	2300	380	35	0.29	0.16	1890	0.99	0.01408	1.0	0.05467	0.67	0.01394	1.0	0.04686	1.7	41.9 ± 40.9	81.1 ± 0.9	89.3 ± 0.9
MA90																			
n4565-26c	sp, oz, clm	1400	1100	19	n/d	0.73	289	6.47	0.011470	0.86	0.0947	1.2	0.010729	0.85	0.0435	5.6	-138 ± 134	79.1 ± 0.6	69.1 ± 0.8
n4565-08c	sp, oz, clb	110	200	2.3	1.1	1.8	8740	[0.21]	0.01234	0.97	0.0487	4.4	0.01234	0.97	0.0487	4.4	135 ± 101	59.6 ± 0.8	78.9 ± 0.8
n4565-21c	sp, oz, clb	59	83	1.1	0.57	1.4	2300	[0.81]	0.01243	1.2	0.0500	5.2	0.01243	1.2	0.0500	5.2	196 ± 117	88.0 ± 1.0	79.4 ± 1.0
n4565-17c	c, uz, clb	720	1100	10	n/d	1.5	530	3.53	0.01295	0.86	0.0725	1.5	0.01250	0.85	0.0446	5.5	-76 ± 129	80.1 ± 0.7	80.3 ± 0.8
n4565-48c	sp, uz, clm	150	240	2.6	n/d	1.6	347	5.39	0.01303	1.0	0.0752	4.0	0.01232	0.98	0.0318	21.	-980 ± 532	199.9 ± 0.8	80.5 ± 1.0
n4565-51c	c, uz, clm	320	960	8	n/d	3	4240	0.44	0.01267	0.86	0.0472	3.2	0.01262	0.86	0.0437	4.4	-127 ± 106	79.6 ± 0.7	81.2 ± 0.7
n4565-55c	c, uz, clb	77	130	1.5	n/d	1.6	1220	1.53	0.01292	1.1	0.0554	4.9	0.01272	1.1	0.0432	10.	-154 ± 237	68.8 ± 0.9	82.0 ± 1.0
n4565-12c	sp, uz, cld	85000	180000	1600	0.88	2.1	190000	0.01	0.01375	0.91	0.048004	0.15	0.01375	0.91	0.047926	0.16	95.6 ± 3.7	105.0 ± 0.8	88.0 ± 0.8
n4565-40c	sp, oz, clb	1900	1100	32	0.31	0.58	1560	1.2	0.01414	0.97	0.0579	3.1	0.01397	0.97	0.0485	4.5	123 ± 102	95.6 ± 0.9	89.3 ± 0.9
n4565-28r	r, oz, cld	23000	5900	390	0.14	0.25	1130	1.65	0.01519	0.95	0.06143	1.2	0.01493	0.94	0.04842	1.9	120 ± 45	89.4 ± 0.9	95.5 ± 0.9
n4565-28c	c, oz, clm	8600	3300	160	0.3	0.38	4610	0.41	0.01649	1.0	0.05107	0.46	0.01642	1.0	0.04787	0.61	92.8 ± 14.5	105 ± 1	105 ± 1
n4565-42c	sp, uz, cld	9700	4600	190	0.57	0.47	1220	1.53	0.01692	0.83	0.0598	4.1	0.01666	0.83	0.0477	7.1	85.6 ± 159.6	106 ± 1	107 ± 1
n4565-03c	sp, uz, clm	320	400	13	11	1.3	543	3.44	0.02665	0.84	0.0737	2.9	0.02573	0.85	0.0465	8.8	24.3 ± 198.8	164 ± 1	164 ± 2
n4565-18c	sp, uz, clm	270	200	11	0.68	0.74	26600	[0.07]	0.03150	0.83	0.05058	1.5	0.03150	0.83	0.05058	1.5	222 ± 34	200 ± 2	200 ± 2
MA91																			
n4566-03c	c, uz, clm	230	82	3.3	0.17	0.36	8580	[0.22]	0.01252	0.87	0.0496	2.6	0.01252	0.87	0.0496	2.6	175 ± 58	2569.3 ± 0.7	80.0 ± 0.7
n4566-14c	sp, uz, clb	570	230	8.5	0.37	0.41	25200	[0.07]	0.01264	0.90	0.04785	1.7	0.01264	0.90	0.04785	1.7	91.8 ± 40.3	265.9 ± 0.7	81.0 ± 0.7
n4566-12c	sp, oz, cld	800	460	13	0.49	0.58	16600	[0.11]	0.01273	0.96	0.04793	1.4	0.01273	0.96	0.04793	1.4	95.8 ± 32.8	4828.6 ± 0.8	81.5 ± 0.8
n4566-13c	c, uz, clm	500	240	7.6	0.33	0.48	19000	[0.10]	0.01274	1.0	0.04842	1.8	0.01274	1.0	0.04842	1.8	120 ± 41	83.2 ± 0.8	81.5 ± 0.8
n4566-11c	c, uz, clm	340	130	5.4	0.065	0.37	257	7.26	0.01409	0.86	0.1158	1.6	0.01307	0.84	0.0594	8.6	581 ± 177	84.6 ± 0.7	82.4 ± 1.2
n4566-07c	sp, uz, clm	830	380	13	0.41	0.45	53200	[0.04]	0.01298	0.88	0.04787	1.5	0.01298	0.88	0.04787	1.5	92.9 ± 34.3	243.1 ± 0.7	83.1 ± 0.7

Sample ID	Characteristics[5]	Concentration (ppm)			Th/U_{calc}	Th/U_{meas}[1]	$^{206}Pb/^{204}Pb$	f_{206} (%)[2]	Total (uncorrected) ratio				Radiogenic (corrected) ratio[3]				Calculated age ± s (Ma)		
		U	Th	Pb					$^{206}Pb/^{238}U$	± s (%)	$^{207}Pb/^{206}Pb$	± s (%)	$^{206}Pb/^{238}U$	± s (%)	$^{207}Pb/^{206}Pb$	± s (%)	$^{207}Pb/^{206}Pb$	$^{206}Pb/^{238}U$	207-corr age[4]
n4566-17c	r(e), uz, clm	490	210	7.7	n/d	0.42	4560	0.41	0.01324	0.85	0.0496	2.4	0.01318	0.85	0.0463	3.3	0.0 ± 91.8	83.7 ± 0.7	84.6 ± 0.7
n4566-08c	sp, oz, clb	980	540	16	0.59	0.56	15600	[0.12]	0.01321	0.85	0.04766	1.3	0.01321	0.85	0.04766	1.3	82.5 ± 31.6	81.6 ± 0.7	84.6 ± 0.7
n4566-16c	sp, uz, clb	300	160	12	0.45	0.52	29600	[0.06]	0.03392	0.89	0.05110	1.7	0.03392	0.89	0.05110	1.7	245 ± 39	215 ± 2	215 ± 2
n4566-10c	sp, oz, cld	2700	370	110	0.18	0.14	7530	0.25	0.03852	0.86	0.05152	0.54	0.03843	0.86	0.04957	0.73	175 ± 17	243 ± 2	244 ± 2
n4566-04c	c, uz, clb	250	89	12	0.34	0.35	15400	[0.12]	0.04212	0.83	0.05176	1.3	0.04212	0.83	0.05176	1.3	275 ± 30	266 ± 2	266 ± 2
n4566-01c	sp, oz, clb	540	400	360	0.73	0.74	335000	0.01	0.4897	0.83	0.17671	0.46	0.4897	0.83	0.17667	0.46	2622 ± 8	2569 ± 18	2543 ± 27
n4566-05c	sp, uz, cld	14000	28000	[31463]	n/d	1.9	21.4	87.35	8.810	2.0	0.8112	0.68	1.1	160.	0.642	7.9	4607 ± 109	4829 ± 12332	1295 ± 6525
MA97																			
n4567-47c	c, oz, clm	140	100	2.2	0.62	0.73	10700	[0.17]	0.01216	0.93	0.0480	3.6	0.01216	0.93	0.0480	3.6	101 ± 84	372.0 ± 0.7	77.8 ± 0.7
n4567-49c	sp, oz, clb	740	1400	15	5.6	1.9	1820	1.03	0.01239	1.5	0.05466	1.7	0.01226	1.5	0.0466	4.8	26.7 ± 110.5	73.6 ± 1.1	78.7 ± 1.2
n4567-36c	sp, oz, clm	270	230	4.3	0.45	0.86	11200	[0.17]	0.01237	0.99	0.0490	2.6	0.01237	0.99	0.0490	2.6	148 ± 60	84.7 ± 0.8	79.1 ± 0.8
n4567-50c	sp, oz, clb	190	170	3.2	0.61	0.87	7470	[0.25]	0.01243	0.88	0.0484	3.1	0.01243	0.88	0.0484	3.1	119 ± 72	82.4 ± 0.7	79.6 ± 0.7
n4567-31c	c, uz, clb	140	77	2.1	n/d	0.55	7630	[0.25]	0.01247	0.98	0.0455	3.5	0.01247	0.98	0.0455	3.5	-27 ± 82	83.8 ± 0.8	80.1 ± 0.8
n4567-21c	sp, oz, cld	120	120	2.1	n/d	0.94	3640	[0.51]	0.01255	0.96	0.0445	3.7	0.01255	0.96	0.0445	3.7	-82 ± 82	82.6 ± 0.8	80.7 ± 0.8
n4567-38c	sp, oz, cld	280	440	5.5	n/d	1.5	3520	0.53	0.01285	0.84	0.0502	3.2	0.01278	0.83	0.0460	4.4	-1.5 ± 102.8	80.4 ± 0.7	82.0 ± 0.7
n4567-14c	c, uz, clb	220	170	3.7	n/d	0.78	832	2.25	0.01319	0.87	0.0619	3.4	0.01289	0.87	0.0441	8.6	-105 ± 199	79.9 ± 0.7	83.0 ± 0.8
n4567-04r	r, oz, clb	270	230	4.4	n/d	0.86	723	2.59	0.01320	0.87	0.0583	2.6	0.01286	0.86	0.0377	10.	-507 ± 254	79.3 ± 0.7	83.4 ± 0.8
n4567-03c	c, oz, clb	280	310	4.8	n/d	1.1	293	6.38	0.01380	6.0	0.089	22.	0.01292	5.6	0.038	100.	-453 ± 1,616	99.4 ± 4.6	83.7 ± 5.5
n4567-12c	c, oz, clb	220	280	4.2	0.97	1.3	>1e6	[0.00]	0.01309	0.95	0.0483	2.8	0.01309	0.95	0.0483	2.8	113 ± 65	77.9 ± 0.8	83.8 ± 0.8
n4567-04c	c, uz, cld	1000	1200	20	1.2	1.1	22400	[0.08]	0.01323	0.93	0.04765	1.6	0.01323	0.93	0.04765	1.6	81.7 ± 38.2	78.6 ± 0.8	84.7 ± 0.8
n4567-39c	sp, oz, clb	180	200	3.8	0.091	1.1	>1e6	[0.00]	0.01554	1.0	0.0738	2.2	0.01554	1.0	0.0738	2.2	1035 ± 44	79.7 ± 1.0	96.2 ± 1.1
n4567-01c	sp, uz, cld	810	510	60	0.6	0.63	58800	0.03	0.05942	0.83	0.05462	0.61	0.05940	0.83	0.05437	0.63	387 ± 14	372 ± 3	372 ± 3
MA100																			
n4568-14c	c, oz, clm	150	140	2.5	n/d	0.92	1820	1.03	0.01250	0.96	0.0515	3.0	0.01237	0.95	0.0434	6.4	-147 ± 147	81.6 ± 0.8	79.7 ± 0.8
n4568-35c	c, uz, clm	120	100	2	0.38	0.85	7610	[0.25]	0.01250	0.90	0.0496	3.6	0.01250	0.90	0.0496	3.6	178 ± 81	80.9 ± 0.7	79.9 ± 0.7
n4568-44c	c, uz, cld	190	180	3.3	n/d	0.92	1950	0.96	0.01263	0.83	0.0533	2.8	0.01251	0.82	0.0457	6.1	-20 ± 140	81.2 ± 0.7	80.3 ± 0.7
n4568-35r	r, oz, cld	110	66	1.6	n/d	0.58	392	4.77	0.01288	0.89	0.0657	3.2	0.01227	0.86	0.0272	24.	-1474 ± 669	79.3 ± 0.7	80.6 ± 0.8
n4568-08c	sp, uz, cld	290	220	4.7	0.4	0.75	9950	[0.19]	0.01264	0.80	0.0492	2.2	0.01264	0.80	0.0492	2.2	155 ± 50	83.0 ± 0.6	80.8 ± 0.7
n4568-21c	sp, uz, cld	98	58	1.5	0.21	0.59	4420	[0.42]	0.01267	0.94	0.0510	3.7	0.01267	0.94	0.0510	3.7	240 ± 83	81.2 ± 0.8	80.8 ± 0.8
n4568-01c	sp, oz, clb	220	240	4	0.22	1.1	219	8.55	0.01392	1.5	0.1216	7.4	0.01273	1.4	0.055	24.	403 ± 470	232.1 ± 1.1	80.8 ± 1.9
n4568-29c	c, uz, clb	280	220	4.6	n/d	0.79	12300	[0.15]	0.012579	0.77	0.0447	2.3	0.012579	0.77	0.0447	2.3	-71 ± 56	80.6 ± 0.6	80.9 ± 0.6
n4568-50r	c, oz, clb	290	240	4.9	0.41	0.8	15900	[0.12]	0.01267	0.81	0.0493	2.3	0.01267	0.81	0.0493	2.3	163 ± 52	81.8 ± 0.7	81.0 ± 0.7
n4568-07c	c, uz, clb	160	150	2.8	0.48	0.89	2960	[0.63]	0.01267	0.82	0.0492	3.7	0.01267	0.82	0.0492	3.7	158 ± 85	80.1 ± 0.7	81.0 ± 0.7
n4568-50c	c, uz, clb	290	310	5.2	0.9	1.1	10400	[0.18]	0.012656	0.77	0.0480	2.2	0.012656	0.77	0.0480	2.2	98.1 ± 51.3	78.6 ± 0.6	81.0 ± 0.6
n4568-32c	sp, oz, clb	780	700	13	n/d	0.9	1740	1.08	0.012913	0.77	0.05489	1.4	0.012774	0.76	0.0464	3.1	0.0 ± 90.9	80.1 ± 0.6	81.9 ± 0.6
n4568-15c	sp, oz, clb	840	1000	16	0.9	1.2	1940	0.97	0.013080	0.68	0.05598	1.4	0.012953	0.68	0.0484	2.9	118 ± 66	81.1 ± 0.6	82.9 ± 0.6
n4568-22c	sp, oz, clm	1700	620	72	0.65	0.37	787	2.38	0.03756	0.65	0.06731	0.49	0.03667	0.65	0.04861	1.8	129 ± 43	232 ± 1	233 ± 2
MA104																			
n4569-42c	sp, uz, cld	7100	6200	200	0.41	0.87	1290	1.45	0.02328	1.2	0.06190	0.41	0.02294	1.2	0.05054	0.96	220 ± 22	146 ± 2	146 ± 2
n4569-07c	sp, oz, cld	2300	2100	81	0.49	0.9	209	8.95	0.02920	0.72	0.1221	1.6	0.02658	0.70	0.0520	6.1	283 ± 133	169 ± 1	168 ± 3
n4569-03c	sp, uz, cld	4300	790	140	0.13	0.19	2430	0.77	0.02883	1.1	0.05754	0.77	0.02861	1.1	0.05152	1.3	264 ± 29	182 ± 2	181 ± 2
n4569-01c	c, uz, cld	1600	530	59	0.28	0.33	8800	0.21	0.03133	0.67	0.05291	0.58	0.03126	0.67	0.05124	0.72	252 ± 16	198 ± 1	198 ± 1
n4569-26r	sp, oz, cld	3700	1300	140	n/d	0.35	240	7.78	0.03580	2.0	0.1012	1.8	0.03302	1.8	0.0393	9.0	-400 ± 221	209 ± 4	212 ± 5
n4569-26c	sp, oz, cld	1000	440	42	0.48	0.42	600	3.12	0.03542	0.68	0.07426	0.87	0.03431	0.68	0.0497	2.4	183 ± 56	217 ± 1	218 ± 2
n4569-47r	r, uz, cld	2400	790	100	0.3	0.32	158	11.87	0.04085	0.67	0.1454	1.6	0.03600	0.66	0.0524	7.7	303 ± 167	228 ± 1	227 ± 4
n4569-52c	sp, oz, cld	3600	1400	150	0.37	0.4	444	4.21	0.03806	0.66	0.08366	1.1	0.03646	0.66	0.0506	2.9	222 ± 66	231 ± 1	231 ± 2
n4569-01r	r, oz, cld	7200	1800	300	0.3	0.24	623	3	0.03781	0.65	0.07435	0.37	0.03668	0.65	0.05080	0.95	232 ± 22	232 ± 1	232 ± 2
n4569-47c	c, uz, cld	10000	9900	500	0.49	0.98	141	13.26	0.04400	1.8	0.1576	2.1	0.03816	1.2	0.0539	9.5	368 ± 200	241 ± 3	240 ± 6
n4569-33c	sp, oz, cld	880	710	44	0.74	0.8	805	2.32	0.03928	0.68	0.0698	2.3	0.03837	0.67	0.0516	4.1	267 ± 91	243 ± 2	243 ± 2
n4569-31c	sp, oz, cld	890	570	43	0.73	0.64	6230	0.3	0.03878	0.66	0.05292	0.70	0.03867	0.66	0.05056	0.94	221 ± 22	245 ± 2	245 ± 2
n4569-11c	sp, uz, cld	3200	620	140	0.22	0.2	88300	0.02	0.03897	0.66	0.05075	0.47	0.03896	0.66	0.05059	0.47	222 ± 11	246 ± 2	247 ± 2
n4569-36c	sp, oz, cld	700	400	33	0.68	0.58	66800	[0.03]	0.03901	0.66	0.05026	0.80	0.03901	0.66	0.05026	0.80	207 ± 18	247 ± 2	247 ± 2
n4569-30c	sp, uz, cld	6900	2900	340	0.54	0.42	2230	0.84	0.04127	0.66	0.05682	0.24	0.04093	0.66	0.05024	0.48	206 ± 11	259 ± 2	259 ± 2
MA109																			
n4570-19r	r, uz, clb	320	79	12	n/d	0.24	1710	1.09	0.03542	0.68	0.05399	1.3	0.03503	0.68	0.0454	2.7	-37 ± 65	222 ± 1	223 ± 2
n4570-38r	r, uz, clb	440	97	17	0.37	0.22	6110	0.31	0.03542	0.69	0.05107	1.2	0.03531	0.69	0.04866	1.8	131 ± 42	224 ± 2	224 ± 2
n4570-35r	sp, uz, cld	710	170	29	0.25	0.25	82200	[0.02]	0.03572	0.68	0.05070	0.83	0.03572	0.68	0.05070	0.83	227 ± 19	226 ± 2	226 ± 2
n4570-35c	sp, uz, clm	690	100	27	0.16	0.15	116000	[0.02]	0.03574	0.66	0.05035	0.84	0.03574	0.66	0.05035	0.84	211 ± 19	226 ± 1	226 ± 1
n4570-02r	r, oz, clb	510	110	21	0.27	0.21	>1e6	[0.00]	0.03588	0.67	0.05008	1.1	0.03588	0.67	0.05008	1.1	199 ± 26	227 ± 2	227 ± 2
n4570-43r	r, oz, clm	920	170	37	0.2	0.18	64900	[0.03]	0.03637	0.66	0.05034	0.77	0.03637	0.66	0.05034	0.77	211 ± 18	230 ± 1	230 ± 2
n4570-15r	r, oz, clm	680	120	29	0.22	0.18	63400	[0.03]	0.03825	0.66	0.05103	0.83	0.03825	0.66	0.05103	0.83	242 ± 19	242 ± 2	242 ± 2
n4570-43c	c, uz, cld	1700	110	74	0.049	0.067	4960	0.38	0.04103	0.66	0.05510	0.91	0.04087	0.66	0.05214	1.3	292 ± 31	258 ± 2	258 ± 2
n4570-15c	c, uz, clb	1300	180	58	0.21	0.14	6240	0.3	0.04168	0.69	0.05390	1.4	0.04156	0.69	0.0515	2.1	265 ± 47	262 ± 2	262 ± 2
n4570-51c	c, uz, clb	1300	30	57	0.028	0.023	53800	0.03	0.04221	0.69	0.05286	0.87	0.04219	0.69	0.05258	0.89	311 ± 20	266 ± 2	266 ± 2

Sample ID	Characteristics[5]	Concentration (ppm)			Th/U_{calc}	Th/U_{meas}[1]	$^{206}Pb/^{204}Pb$	f_{206} (%)[2]	Total (uncorrected) ratio				Radiogenic (corrected) ratio[3]				Calculated age ± s (Ma)		
		U	Th	Pb					$^{206}Pb/^{238}U$	± s (%)	$^{207}Pb/^{206}Pb$	± s (%)	$^{206}Pb/^{238}U$	± s (%)	$^{207}Pb/^{206}Pb$	± s (%)	$^{207}Pb/^{206}Pb$	$^{206}Pb/^{238}U$	207-corr age[4]
n4570-30c	c, uz, cld	1700	99	88	0.067	0.058	22700	0.08	0.04762	0.66	0.05411	0.48	0.04759	0.66	0.05346	0.52	348 ± 12	300 ± 2	299 ± 2
n4570-38c	c, oz, cld	1600	550	110	0.38	0.34	76800	0.02	0.06018	0.68	0.05499	0.41	0.06016	0.68	0.05480	0.42	404 ± 9	377 ± 3	376 ± 3
n4570-02c	c, uz, clb	280	42	20	0.17	0.15	17100	0.11	0.06145	0.70	0.06911	0.89	0.06139	0.70	0.06827	0.97	877 ± 20	384 ± 3	377 ± 3
n4570-06c	sp, oz, clb	410	160	30	0.4	0.39	65800	[0.03]	0.06150	0.66	0.05538	0.87	0.06150	0.66	0.05538	0.87	428 ± 19	385 ± 2	384 ± 3
n4570-19c	c, uz, cld	680	86	120	0.049	0.13	24600	0.08	0.1518	0.86	0.1105	0.91	0.1516	0.86	0.110	0.92	1799 ± 17	910 ± 7	863 ± 10

Table S2: Ion microprobe U-Th-Pb data of the zircons extracted from Main Range Province granitoids

(1) Based on measured Th and U signals.

(2) f_{206} is the percentage of common Pb estimated from 204Pb counts; in parentheses where these are insignificant;

(3) Ratios after subtraction of common Pb (if detected)

(4) Age based on projecting a line in inverse concordia space from assumed common Pb through the total (uncorrected) ratios onto concordia (Ludwig, 2001)

(5) Grain characteristics based on CL imaging: c = core, r = rim, sp = single phase, r(e) = rim embayment, r(i) = rim inner, oz = oscillatory zoned, uz = unzoned, clb = CL-bright, cld = CL-dark, clm = CL-medium

		Concentration (ppm)							Total (uncorrected) ratio				Radiogenic (corrected) ratio[3]				Calculated age ± s (Ma)		
Sample ID	**Characteristics[5]**	**U**	**Th**	**Pb**	**Th/U_{calc}**	**Th/U_{meas}[1]**	**$^{206}Pb/^{204}Pb$**	**f_{206} (%)[2]**	**$^{206}Pb/^{238}U$**	**± s (%)**	**$^{207}Pb/^{206}Pb$**	**± s (%)**	**$^{206}Pb/^{238}U$**	**± s (%)**	**$^{207}Pb/^{206}Pb$**	**± s (%)**	**$^{207}Pb/^{206}Pb$**	**$^{206}Pb/^{238}U$**	**207-corr age[4]**
MA06																			
n3962-07c	c, oz, clb	1700	1300	29	0.16	0.75	172	10.9	0.01481	0.85	0.1398	2.3	0.01319	0.87	0.0547	9.1	399 ± 192	227.8 ± 0.7	83.7 ± 1.6
n3962-10c	c, oz, clm	5100	1600	130	0.096	0.32	77.5	24.13	0.02918	0.85	0.2450	2.6	0.02214	1.2	0.057	23.	497 ± 437	141 ± 2	139 ± 6
n3962x-14c	sp, oz, cld	3700	930	110	0.14	0.25	62.3	30.01	0.03659	1.3	0.2909	2.3	0.02561	1.3	0.057	21.	504 ± 398	163 ± 2	161 ± 10
n3962-07r	r, oz, cld	47000	5600	1400	0.066	0.12	4750	0.39	0.02704	2.3	0.05372	0.69	0.02693	2.3	0.05063	0.97	224 ± 22	171 ± 4	171 ± 4
n3962x-12c	sp, oz, cld	9600	1900	310	0.08	0.19	127	14.68	0.03338	1.8	0.170	6.9	0.02848	1.4	0.055	32.	427 ± 595	181 ± 3	180 ± 6
n3962x-02c	sp, oz, cld	4000	960	130	0.19	0.24	575	3.25	0.02942	1.3	0.07613	1.2	0.02847	1.3	0.0506	2.9	223 ± 66	181 ± 2	181 ± 2
n3962-16c	sp,oz, cld	16000	4600	530	0.27	0.28	85.1	21.98	0.03652	1.4	0.2225	3.7	0.02849	1.8	0.050	30.	186 ± 575	181 ± 3	181 ± 7
n3962x-22c	sp, oz, clm	2100	1800	83	0.55	0.87	445	4.21	0.03055	1.3	0.0861	1.8	0.02926	1.3	0.0532	4.0	337 ± 87	186 ± 2	185 ± 3
n3962-26c	c, oz, clm	1100	290	38	0.22	0.26	684	2.73	0.03074	0.92	0.0719	1.6	0.02990	0.94	0.0504	4.4	214 ± 100	190 ± 2	190 ± 2
n3962-05c	sp, oz, clm	1200	350	42	0.13	0.3	264	7.07	0.03286	0.87	0.1121	3.3	0.03054	0.85	0.0570	8.4	493 ± 175	194 ± 2	192 ± 3
n3962x-01c	c, uz, cld	9500	1800	320	0.13	0.19	138	13.51	0.03527	1.8	0.1574	3.2	0.03051	1.6	0.0515	16.	262 ± 325	194 ± 3	193 ± 5
n3962-04c	c, oz, cld	5700	950	200	0.75	0.17	137	13.39	0.03661	0.86	0.1541	5.2	0.03170	0.86	0.047	29.	28.0 ± 579.4	201 ± 2	201 ± 5
n3962x-31c	sp, uz, cld	5100	3500	200	0.5	0.68	782	2.39	0.03294	1.3	0.0698	1.7	0.03216	1.3	0.0511	3.7	244 ± 83	204 ± 3	204 ± 3
n3962-26r	r, oz, cld	9500	2500	350	0.18	0.26	219	8.55	0.03527	1.1	0.1193	2.5	0.03225	0.99	0.0523	8.4	298 ± 182	205 ± 2	204 ± 3
n3962x-15c	sp, oz, cld	3300	2300	140	0.66	0.7	1690	1.1	0.03388	1.3	0.05918	1.6	0.03350	1.3	0.0505	2.4	219 ± 55	212 ± 3	212 ± 3
n3962-30c	sp, oz, clb	330	140	13	0.59	0.42	3910	0.03	0.03426	0.87	0.0494	2.2	0.03425	0.88	0.0492	3.3	156 ± 77	217 ± 2	217 ± 2
n3962-04r	r, oz, clm	1100	400	46	0.38	0.35	8930	0.21	0.03476	0.86	0.05158	1.0	0.03469	0.86	0.04994	1.3	192 ± 30	220 ± 2	220 ± 2
n3962-03r	r, oz, clb	560	310	23	0.73	0.56	8260	0.23	0.03479	0.87	0.05080	1.4	0.03471	0.87	0.04902	1.8	149 ± 41	220 ± 2	220 ± 2
n3962-13c	sp, oz, clm	800	55	30	0.077	0.068	17900	0.1	0.03532	0.84	0.05083	1.3	0.03528	0.84	0.05001	1.5	195 ± 35	224 ± 2	224 ± 2
n3962-11c	sp, oz, cld	5800	770	220	0.14	0.13	785	2.38	0.03643	0.93	0.0679	4.6	0.03556	0.86	0.0491	11.	154 ± 239	225 ± 2	226 ± 2
n3962-03c	c, oz, cld	3600	900	150	0.24	0.25	1630	1.15	0.03639	0.84	0.05987	0.55	0.03597	0.84	0.05087	1.1	235 ± 26	228 ± 2	228 ± 2
n3962-10r	r, oz, cld	14000	980	550	0.066	0.071	4430	0.18	0.03701	0.87	0.05266	0.31	0.03694	0.87	0.05127	0.40	253 ± 9	234 ± 2	234 ± 2
n3962x-28c	sp, oz, cld	9300	1900	410	0.2	0.2	403	4.64	0.04135	1.3	0.0878	1.6	0.03943	1.3	0.0514	4.0	257 ± 90	249 ± 3	249 ± 4
n3962x-17c	sp, oz, clb	1400	200	75	0.059	0.14	129	14.53	0.05476	1.3	0.1772	0.95	0.04681	1.3	0.0653	4.6	784 ± 93	295 ± 4	290 ± 8
MA07																			
n4211-19c	sp, uz, cld	9100	2300	300	0.4	0.26	345	5.42	0.03127	0.83	0.09099	0.95	0.02958	0.83	0.0483	3.7	114 ± 84	188 ± 2	188 ± 2
n4211-08r	r, oz, cld	5400	1300	180	0.32	0.25	196	9.55	0.03360	0.83	0.12398	0.64	0.03039	0.83	0.0489	3.5	141 ± 79	193 ± 2	193 ± 3
n4211-09r	r, oz, cld	19000	4800	660	0.18	0.25	549	3.41	0.03240	0.83	0.07626	0.88	0.03130	0.83	0.0495	2.4	171 ± 55	199 ± 2	199 ± 2
n4211-35c	sp, uz, cld	10000	4900	370	0.25	0.48	495	3.78	0.03269	0.83	0.0801	1.8	0.03145	0.83	0.0504	4.5	213 ± 102	200 ± 2	200 ± 2
n4211-51c	sp, oz, clm	3200	3200	140	1.2	0.99	611	3.06	0.03430	0.83	0.0734	1.4	0.03325	0.83	0.0493	3.3	160 ± 74	211 ± 2	211 ± 2
n4211-37c	sp, oz, cld	7900	3200	310	0.36	0.4	743	2.52	0.03446	0.83	0.07044	0.58	0.03360	0.83	0.05067	1.2	226 ± 28	213 ± 2	213 ± 2
n4211-02c	sp, oz, clm	2300	440	87	0.14	0.19	986	1.9	0.03439	0.83	0.06586	0.56	0.03374	0.83	0.05097	1.4	240 ± 31	214 ± 2	214 ± 2
n4211-36c	sp, oz, clm	1800	1100	77	0.56	0.63	3300	0.57	0.03404	0.83	0.05546	0.83	0.03385	0.83	0.05101	1.3	241 ± 29	215 ± 2	214 ± 2
n4211-09c	c, oz, clb	790	520	33	1	0.66	2820	0.66	0.03410	0.85	0.05386	1.0	0.03387	0.85	0.04863	1.9	130 ± 44	215 ± 2	215 ± 2
n4211-15c	sp, oz, clb	1300	780	55	0.9	0.59	13600	0.14	0.03395	0.83	0.04988	0.85	0.03390	0.83	0.04880	0.99	138 ± 23	215 ± 2	215 ± 2
n4211-15r	sp, oz, cld	8500	3000	340	0.34	0.35	847	2.21	0.03498	0.83	0.06750	0.57	0.03421	0.84	0.05016	1.1	202 ± 25	217 ± 2	217 ± 2
n4211-43c	sp, oz, clm	1700	2000	84	1.2	1.2	47300	0.04	0.03452	0.83	0.05083	0.75	0.03451	0.83	0.05052	0.79	219 ± 18	219 ± 2	219 ± 2
n4211-04c	sp, oz, clm	6300	2000	250	0.42	0.32	634	2.95	0.03561	0.83	0.0720	3.6	0.03456	0.83	0.0488	7.9	139 ± 175	219 ± 2	219 ± 2
n4211-17c	sp, uz, cld	6800	2500	270	0.32	0.37	677	2.76	0.03562	0.83	0.07220	0.32	0.03464	0.83	0.05051	1.0	219 ± 24	220 ± 2	219 ± 2
n4211-43r	sp, oz, cld	1600	1500	74	1.1	0.91	24200	0.08	0.03472	0.83	0.05050	1.0	0.03469	0.83	0.04989	1.1	190 ± 25	220 ± 2	220 ± 2
n4211-06c	sp, oz, cld	5500	6200	250	0.89	1.1	320	5.85	0.03702	1.1	0.09631	0.72	0.03486	1.1	0.0504	2.5	214 ± 56	221 ± 2	221 ± 3
n4211-08c	c, uz, clb	1400	730	58	0.51	0.52	17200	0.11	0.03504	0.83	0.05130	0.83	0.03500	0.83	0.05045	0.91	216 ± 21	222 ± 2	222 ± 2
n4211-12c	sp, oz, cld	8400	4300	350	0.54	0.5	940	1.99	0.03624	0.83	0.06520	0.86	0.03551	0.83	0.04956	1.9	174 ± 43	225 ± 2	225 ± 2
n4211-16c	sp, oz, cld	4300	3000	190	0.71	0.69	657	2.85	0.03676	0.85	0.0726	5.2	0.03572	0.94	0.0503	11.	208 ± 235	226 ± 2	226 ± 2
n4211-02r	r, oz, cld	3300	1100	140	0.39	0.33	955	1.96	0.03741	0.86	0.06491	1.2	0.03668	0.86	0.0495	2.1	172 ± 47	232 ± 2	233 ± 2
MA13																			
n3923x-25c	sp, oz, cld	670	390	26	0.85	0.59	1620	1.16	0.03136	1.1	0.0581	3.3	0.03100	1.1	0.0490	5.8	147 ± 131	197 ± 2	197 ± 2
n3923x-29r	r, uz, cld	1400	160	48	0.13	0.12	140	13.37	0.03727	1.1	0.1556	6.2	0.03228	1.7	0.051	33.	223 ± 622	205 ± 3	204 ± 5
n3923-13c	sp, uz, clb	360	110	15	0.32	0.3	55300	[0.03]	0.03536	0.91	0.05045	1.3	0.03536	0.91	0.05045	1.3	216 ± 29	224 ± 2	224 ± 2
n3923x-05r	sp, oz, cld	920	350	38	0.34	0.38	63900	[0.03]	0.03550	0.87	0.05136	0.92	0.03550	0.87	0.05136	0.92	257 ± 21	225 ± 2	225 ± 2
n3923x-16c	sp, oz, clb	470	140	19	0.19	0.3	40900	[0.05]	0.03526	0.86	0.05363	1.1	0.03526	0.86	0.05363	1.1	356 ± 24	223 ± 2	223 ± 2
n3923x-01r	sp, oz, cld	860	210	34	0.28	0.25	23200	0.08	0.03503	0.86	0.05065	0.79	0.0350	0.86	0.05001	0.87	196 ± 20	222 ± 2	222 ± 2
n3923-27c	sp, oz, clb	730	690	35	1	0.95	42200	[0.04]	0.03574	0.95	0.05014	0.92	0.03574	0.95	0.05014	0.92	202 ± 21	226 ± 2	227 ± 2
n3923-08c	sp, oz, clb	260	130	11	0.51	0.51	24600	[0.08]	0.03584	0.92	0.05068	1.3	0.03584	0.92	0.05068	1.3	226 ± 31	227 ± 2	227 ± 2
n3923x-05c	sp, oz, clb	410	140	17	0.43	0.35	22400	[0.08]	0.03537	0.86	0.04976	1.2	0.03537	0.86	0.04976	1.2	184 ± 27	224 ± 2	224 ± 2
n3923x-15c	c, uz, cld	3300	2300	150	0.75	0.7	40300	0.05	0.03594	0.86	0.05083	0.42	0.03593	0.86	0.05047	0.44	217 ± 10	228 ± 2	228 ± 2
n3923x-12c	sp, oz, clb	830	520	37	0.66	0.63	863	2.17	0.03604	0.91	0.0677	2.2	0.03526	0.92	0.0507	4.2	226 ± 94	223 ± 2	223 ± 2
n3923x-10c	sp, oz, clb	490	210	20	0.48	0.44	57300	[0.03]	0.03509	0.87	0.05019	1.1	0.03509	0.87	0.05019	1.1	204 ± 25	222 ± 2	222 ± 2

Sample ID	Characteristics[5]	Concentration (ppm)			Th/U_{calc}	Th/U_{meas}[1]	$^{206}Pb/^{204}Pb$	f_{206} (%)[2]	Total (uncorrected) ratio				Radiogenic (corrected) ratio[3]				Calculated age ± s (Ma)		
		U	Th	Pb					$^{206}Pb/^{238}U$	± s (%)	$^{207}Pb/^{206}Pb$	± s (%)	$^{206}Pb/^{238}U$	± s (%)	$^{207}Pb/^{206}Pb$	± s (%)	$^{207}Pb/^{206}Pb$	$^{206}Pb/^{238}U$	207-corr age[4]
n3923-04c	sp, oz, clb	420	320	19	0.71	0.76	33400	[0.06]	0.03607	0.93	0.05102	1.1	0.03607	0.93	0.05102	1.1	242 ± 26	228 ± 2	228 ± 2
n3923-20r	sp, oz, cld	1200	230	46	0.17	0.2	1680	1.12	0.03651	0.91	0.05990	0.76	0.03610	0.91	0.05116	1.3	248 ± 30	229 ± 2	228 ± 2
n3923-07c	r, oz, clb	330	140	14	0.36	0.43	37900	[0.05]	0.03615	0.93	0.05170	1.2	0.03615	0.93	0.05170	1.2	272 ± 28	229 ± 2	229 ± 2
n3923x-21c	sp, oz, clb	860	240	35	0.26	0.27	26300	0.07	0.03554	0.87	0.05160	0.82	0.03551	0.87	0.05104	0.89	242 ± 20	225 ± 2	225 ± 2
n3923x-06c	sp, oz, clb	780	380	33	0.53	0.49	94900	[0.02]	0.03554	0.87	0.05030	0.86	0.03554	0.87	0.05030	0.86	209 ± 20	225 ± 2	225 ± 2
n3923x-01c	sp, oz, cld	1900	1200	86	0.71	0.63	67800	0.03	0.03604	0.87	0.05040	0.54	0.03603	0.87	0.05018	0.56	203 ± 13	228 ± 2	228 ± 2
n3923x-30r	r, oz, cld	1100	190	44	0.2	0.16	2880	0.65	0.03587	0.86	0.05485	0.96	0.03563	0.86	0.04975	1.4	183 ± 33	226 ± 2	226 ± 2
n3923-07r	r, uz, cld	840	49	33	0.055	0.058	121000	[0.02]	0.03663	0.92	0.05123	0.88	0.03663	0.92	0.05123	0.88	251 ± 20	232 ± 2	232 ± 2
n3923x-03c	sp, oz, clb	1400	280	57	0.24	0.2	131000	[0.01]	0.03651	0.86	0.05016	0.63	0.03651	0.86	0.05016	0.63	202 ± 15	231 ± 2	231 ± 2
n3923-09c	sp, uz, cld	4000	700	160	0.19	0.17	19700	0.09	0.03698	0.93	0.05088	0.34	0.03695	0.93	0.05014	0.40	201 ± 9	234 ± 2	234 ± 2
n3923x-19c	sp, oz, clb	630	73	25	0.11	0.12	30700	0.06	0.03645	0.86	0.05230	0.94	0.03643	0.86	0.05182	1.0	277 ± 23	231 ± 2	230 ± 2
n3923-20c	sp, oz, cld	1000	130	41	0.15	0.12	31800	0.06	0.03706	0.92	0.05016	0.66	0.03703	0.92	0.04970	0.71	181 ± 16	234 ± 2	235 ± 2
n3923x-24c	sp, oz, cld	1000	540	46	0.37	0.53	10400	[0.18]	0.03656	0.86	0.0534	3.4	0.03656	0.86	0.0534	3.4	346 ± 75	231 ± 2	231 ± 2
n3923x-15r	r, sp, cld	3400	310	130	0.099	0.092	2970	0.63	0.03695	0.86	0.05545	0.68	0.03672	0.86	0.05050	0.96	218 ± 22	232 ± 2	233 ± 2
n3923-17r	r, sp, cld	2400	130	97	0.062	0.055	61400	0.03	0.03823	1.0	0.05029	0.51	0.03822	1.0	0.05005	0.54	197 ± 13	242 ± 2	242 ± 2
n3923x-22c	sp, oz, cld	3800	4000	200	1.3	1.1	15400	0.12	0.03823	0.86	0.05118	0.40	0.03818	0.86	0.05023	0.46	206 ± 11	242 ± 2	242 ± 2
n3923x-23c	sp, oz,clm	1300	340	60	0.29	0.27	32000	0.06	0.04118	0.87	0.05279	0.62	0.04115	0.87	0.05233	0.66	300 ± 15	260 ± 2	260 ± 2
n3923x-29c	c, uz, clb	1400	150	66	0.087	0.1	124000	[0.02]	0.04222	0.86	0.05373	0.56	0.04222	0.86	0.05373	0.56	360 ± 13	267 ± 2	266 ± 2
n3923-30c	c, oz, clb	410	130	21	0.34	0.32	96200	[0.02]	0.04420	1.1	0.05318	1.1	0.04420	1.1	0.05318	1.1	336 ± 25	279 ± 3	278 ± 3
n3923-17c	c, oz, clb	400	260	27	0.64	0.65	106000	[0.02]	0.05326	0.97	0.05393	0.83	0.05326	0.97	0.05393	0.83	368 ± 19	335 ± 3	334 ± 3
n3923x-18c	c, oz, clb	460	250	31	0.54	0.55	4000	0.47	0.05412	0.99	0.05872	0.92	0.05387	0.99	0.05507	1.3	415 ± 29	338 ± 3	337 ± 3
n3923x-31c	sp, uz, clb	250	77	21	0.31	0.3	24300	0.08	0.07327	0.89	0.05675	1.3	0.07321	0.89	0.05615	1.3	458 ± 29	455 ± 4	455 ± 4
n3923x-26c	sp, oz, clb	290	100	25	0.37	0.36	>1e6	[0.00]	0.07317	0.86	0.05626	0.94	0.07317	0.86	0.05626	0.94	462 ± 21	455 ± 4	455 ± 4
n3923x-28c	sp, oz, cld	2400	1100	220	0.47	0.45	223000	0.01	0.07658	0.88	0.05643	0.32	0.07657	0.88	0.05636	0.32	467 ± 7	476 ± 4	476 ± 4
n3923x-02c	c, oz, clb	370	58	43	0.06	0.16	38500	0.05	0.1050	2.6	0.0723	3.1	0.1049	2.6	0.0719	3.1	983 ± 62	643 ± 16	634 ± 16
n3923x-11c	c, uz, clm	330	30	41	0.072	0.092	75900	[0.02]	0.1137	1.8	0.06582	0.85	0.1137	1.8	0.06582	0.85	801 ± 18	694 ± 12	691 ± 12
MA14																			
n3943-18c	sp, oz, clm	550	320	23	0.72	0.57	36900	[0.05]	0.03327	2.2	0.04954	1.6	0.03327	2.2	0.04954	1.6	174 ± 37	211 ± 5	211 ± 5
n3943-13c	sp, oz, clm	570	290	23	0.51	0.51	8200	0.23	0.03371	2.2	0.05236	1.5	0.03364	2.2	0.0506	2.1	221 ± 48	213 ± 5	213 ± 5
n3943-04c	sp, oz, clb	640	350	27	0.67	0.54	>1e6	[0.00]	0.03362	2.2	0.04970	1.4	0.03362	2.2	0.04970	1.4	181 ± 33	213 ± 5	213 ± 5
n3943-04r	sp, oz, clm	1500	460	59	0.33	0.31	39300	0.05	0.03392	2.2	0.05062	0.94	0.03391	2.2	0.05024	0.99	206 ± 23	215 ± 5	215 ± 5
n3943-25xc	sp, uz, clb	470	320	20	0.59	0.69	>1e6	[0.00]	0.03429	1.4	0.05133	1.8	0.03429	1.4	0.05133	1.8	256 ± 42	217 ± 3	217 ± 3
n3943-29c	sp, oz, clb	1100	200	44	0.18	0.18	18000	0.1	0.03451	1.4	0.05084	1.3	0.03447	1.4	0.05002	1.5	196 ± 34	218 ± 3	219 ± 3
n3943-21c	sp, oz, clm	690	25	26	0.053	0.036	>1e6	[0.00]	0.03475	1.4	0.04909	1.5	0.03475	1.4	0.04909	1.5	152 ± 35	220 ± 3	221 ± 3
n3943-25c	sp, uz, clb	490	410	22	0.51	0.83	>1e6	[0.00]	0.03502	2.2	0.0522	3.1	0.03502	2.2	0.0522	3.1	294 ± 69	222 ± 5	221 ± 5
n3943-20r	r, oz, clm	650	200	26	0.27	0.3	19500	[0.10]	0.03541	1.4	0.05105	1.7	0.03541	1.4	0.05105	1.7	243 ± 38	224 ± 3	224 ± 3
n3943-30c	sp, uz, clm	850	100	33	0.18	0.12	>1e6	[0.00]	0.03578	1.4	0.04898	1.4	0.03578	1.4	0.04898	1.4	147 ± 33	227 ± 3	227 ± 3
n3943-20c	c, oz, cld	250	170	51	0.71	0.69	>1e6	[0.00]	0.1602	1.5	0.07161	1.3	0.1602	1.5	0.07161	1.3	975 ± 26	958 ± 14	957 ± 14
MA15																			
n4212-38c	sp, uz, cld	5300	2700	180	0.52	0.5	181	10.34	0.03223	0.83	0.1297	2.9	0.02889	0.98	0.0483	14.	112 ± 295	184 ± 2	184 ± 3
n4212-32c	sp, oz, clb	240	340	12	4.8	1.4	1170	1.6	0.03361	0.84	0.0599	2.2	0.03307	0.85	0.0473	5.1	64.3 ± 117.3	210 ± 2	211 ± 2
n4212-40c	sp, oz, clb	1300	270	48	0.19	0.21	28300	0.07	0.03398	0.83	0.05145	1.3	0.03396	0.83	0.05093	1.4	238 ± 32	215 ± 2	215 ± 2
n4212-53c	sp, oz, clb	410	470	19	1.5	1.2	9010	0.21	0.03415	0.83	0.05081	1.5	0.03408	0.83	0.04918	1.9	156 ± 45	216 ± 2	216 ± 2
n4212-14c	sp, oz, clb	280	160	12	0.46	0.58	12800	[0.15]	0.03435	0.85	0.0515	2.2	0.03435	0.85	0.0515	2.2	264 ± 51	218 ± 2	217 ± 2
n4212-08c	sp, oz, cld	1900	520	75	0.25	0.27	4060	0.46	0.03453	0.87	0.05448	0.94	0.03437	0.87	0.05086	1.3	234 ± 30	218 ± 2	218 ± 2
n4212-08r	sp, oz, clb	510	220	21	0.35	0.43	>1e6	[0.00]	0.03440	0.83	0.05132	1.4	0.03440	0.83	0.05132	1.4	255 ± 31	218 ± 2	218 ± 2
n4212-45c	sp, uz, clb	320	200	14	0.73	0.65	>1e6	[0.00]	0.03451	0.87	0.05005	2.0	0.03451	0.87	0.05005	2.0	197 ± 45	219 ± 2	219 ± 2
n4212-48c	sp, oz, clb	710	120	27	0.18	0.17	36500	[0.05]	0.03462	0.83	0.05042	1.2	0.03462	0.83	0.05042	1.2	215 ± 27	219 ± 2	219 ± 2
n4212-07c	sp, oz, cld	1400	970	62	0.6	0.68	73900	[0.03]	0.03467	0.83	0.05117	0.82	0.03467	0.83	0.05117	0.82	248 ± 19	220 ± 2	220 ± 2
n4212-47c	sp, oz, clm	1800	1800	83	1.1	1	1810	1.04	0.03500	0.83	0.05816	1.2	0.03464	0.83	0.05002	1.8	196 ± 42	220 ± 2	220 ± 2
n4212-19c	sp, oz, clm	780	160	30	0.23	0.2	59500	[0.03]	0.03481	0.83	0.04994	1.1	0.03481	0.83	0.04994	1.1	192 ± 26	221 ± 2	221 ± 2
n4212-46r	sp, oz, clm	920	260	37	0.24	0.29	>1e6	[0.00]	0.03488	0.83	0.05122	1.4	0.03488	0.83	0.05122	1.4	251 ± 32	221 ± 2	221 ± 2
n4212-10c	sp, oz, cld	1300	590	55	0.42	0.45	21200	0.09	0.03497	0.83	0.05144	0.86	0.03494	0.83	0.05075	0.94	229 ± 22	221 ± 2	221 ± 2
n4212-07r	sp, oz, cld	3000	400	110	0.14	0.13	12000	0.16	0.03501	0.83	0.05147	0.73	0.03496	0.83	0.05025	0.86	207 ± 20	222 ± 2	222 ± 2
n4212-46c	sp, oz, clb	540	270	23	0.63	0.5	28700	[0.07]	0.03496	0.84	0.04965	1.3	0.03496	0.84	0.04965	1.3	179 ± 31	222 ± 2	222 ± 2
n4212-28r	sp, oz, cld	2000	360	76	0.19	0.18	58700	0.03	0.03524	0.83	0.05072	0.71	0.03523	0.83	0.05047	0.73	216 ± 17	223 ± 2	223 ± 2
n4212-06c	sp, uz, clb	1300	1600	66	2.3	1.2	1780	1.05	0.03590	0.83	0.05652	1.5	0.03552	0.83	0.0482	2.6	111 ± 60	225 ± 2	226 ± 2
n4212-28c	sp, oz, clb	290	440	16	n/d	1.5	75.4	24.82	0.04754	1.9	0.242	6.4	0.03574	2.8	0.046	60.	-7.5 ± 1037.4	226 ± 6	227 ± 12
n4212-43c	c, uz, clb	310	130	36	0.34	0.44	90200	[0.02]	0.0948	1.8	0.06638	0.99	0.0948	1.8	0.06638	0.99	818 ± 21	584 ± 10	579 ± 10
MA16																			
n4213-12c	sp, oz, clb	630	410	24	0.85	0.66	1020	1.84	0.02985	0.86	0.0637	1.9	0.02930	0.87	0.0493	3.7	162 ± 84	186 ± 2	186 ± 2
n4213-36r	sp, oz, clm	1100	470	40	0.67	0.43	6080	0.31	0.03146	0.83	0.05083	1.1	0.03137	0.83	0.04840	1.5	119 ± 35	199 ± 2	200 ± 2
n4213-36c	sp, oz, cld	6500	8400	290	0.99	1.3	2000	0.93	0.03197	0.90	0.05815	0.57	0.03167	0.90	0.05082	1.2	233 ± 26	201 ± 2	201 ± 2
n4213-51c	sp, oz, clm	1700	1000	66	0.68	0.61	1720	1.08	0.03288	0.83	0.05783	0.85	0.03252	0.83	0.04931	1.6	162 ± 37	206 ± 2	207 ± 2
n4213-43c	sp, oz, clb	580	870	30	2.6	1.5	3940	0.47	0.03339	0.83	0.05232	1.7	0.03323	0.83	0.0486	4.1	128 ± 95	211 ± 2	211 ± 2
n4213-23c	sp, uz, clb	480	390	21	0.88	0.81	26400	[0.07]	0.03360	0.83	0.05010	1.6	0.03360	0.83	0.05010	1.6	200 ± 36	213 ± 2	213 ± 2
n4213-21c	sp, uz, clm	1300	140	47	0.095	0.11	17500	0.11	0.03373	0.83	0.05147	0.87	0.03369	0.83	0.05063	1.0	224 ± 23	214 ± 2	214 ± 2
n4213-29r	sp, oz, cld	1700	400	65	0.29	0.24	17900	0.1	0.03403	0.83	0.05022	0.80	0.03400	0.83	0.04940	0.90	167 ± 21	216 ± 2	216 ± 2

Sample ID	Characteristics[5]	Concentration (ppm)							Total (uncorrected) ratio				Radiogenic (corrected) ratio[3]				Calculated age ± s (Ma)		
		U	Th	Pb	Th/U_{calc}	Th/U_{meas}[1]	$^{206}Pb/^{204}Pb$	f_{206} (%)[2]	$^{206}Pb/^{238}U$	± s (%)	$^{207}Pb/^{206}Pb$	± s (%)	$^{206}Pb/^{238}U$	± s (%)	$^{207}Pb/^{206}Pb$	± s (%)	$^{207}Pb/^{206}Pb$	$^{206}Pb/^{238}U$	207-corr age[4]
n4213-10c	sp, oz, clm	1000	630	44	0.54	0.61	2390	0.78	0.03438	0.85	0.05730	1.1	0.03411	0.85	0.05117	1.8	249 ± 40	216 ± 2	216 ± 2
n4213-50c	sp, oz, clb	1800	2100	89	1.2	1.2	17200	0.11	0.03442	0.83	0.05139	0.71	0.03438	0.83	0.05053	0.81	220 ± 19	218 ± 2	218 ± 2
n4213-29c	sp, oz, clb	900	120	33	0.61	0.14	144	12.98	0.03933	1.7	0.149	9.2	0.03423	2.6	0.047	49.	44.6 ± 876.7	217 ± 5	218 ± 7
n4213-47c	sp, oz, clb	630	280	25	0.66	0.44	16300	0.11	0.03442	0.83	0.04972	1.4	0.03438	0.83	0.04882	1.7	139 ± 39	218 ± 2	218 ± 2
n4213-46c	sp, oz, clb	930	670	41	0.85	0.72	39000	[0.05]	0.03443	0.83	0.04987	1.0	0.03443	0.83	0.04987	1.0	189 ± 24	218 ± 2	218 ± 2
n4213-22r	sp, oz, cld	3400	940	130	0.34	0.28	27900	0.07	0.03461	0.85	0.05030	0.58	0.03458	0.85	0.04978	0.63	185 ± 15	219 ± 2	219 ± 2
n4213-25c	sp, uz, clb	420	440	20	1.4	1	8890	0.21	0.03488	0.83	0.05105	1.5	0.03481	0.83	0.04940	1.8	167 ± 42	221 ± 2	221 ± 2
n4213-50r	sp, oz, cld	1500	740	63	0.59	0.5	29500	0.06	0.03486	0.83	0.05024	1.0	0.03484	0.83	0.04974	1.0	183 ± 24	221 ± 2	221 ± 2
n4213-22c	sp, oz, cld	4200	1500	170	0.36	0.36	22600	0.08	0.03524	0.83	0.05105	0.48	0.03521	0.83	0.05040	0.52	213 ± 12	223 ± 2	223 ± 2
n4213-05c	sp, oz, cld	3900	2400	170	0.64	0.61	37800	0.05	0.03525	0.88	0.05069	0.52	0.03523	0.88	0.05030	0.57	209 ± 13	223 ± 2	223 ± 2
n4213-09c	sp, uz, cld	2200	2300	110	1.2	1.1	1570	1.19	0.03626	0.86	0.05950	0.73	0.03583	0.86	0.05017	1.6	203 ± 38	227 ± 2	227 ± 2
n4213-32c	sp, oz, clb	550	380	38	0.35	0.7	13000	0.14	0.05276	0.83	0.06390	0.95	0.05268	0.83	0.06279	1.1	701 ± 23	331 ± 3	327 ± 3
MA19																			
n3944-12c	sp, oz, clb	350	250	15	0.46	0.71	12800	[0.15]	0.03333	1.4	0.0529	2.3	0.03333	1.4	0.0529	2.3	324 ± 51	211 ± 3	211 ± 3
n3944-26c	sp, oz, clb	240	150	10	0.64	0.61	9080	[0.21]	0.03352	1.4	0.0502	2.8	0.03352	1.4	0.0502	2.8	203 ± 64	213 ± 3	213 ± 3
n3944-25c	sp, oz, clb	640	230	25	0.31	0.36	29800	[0.06]	0.03366	1.4	0.05117	1.8	0.03366	1.4	0.05117	1.8	249 ± 42	213 ± 3	213 ± 3
n3944-02r	r, uz, clb	430	97	16	0.26	0.23	20900	[0.09]	0.03363	1.4	0.05025	1.9	0.03363	1.4	0.05025	1.9	207 ± 43	213 ± 3	213 ± 3
n3944-20c	sp, oz, clb	370	210	15	1.5	0.57	8480	0.22	0.03384	1.4	0.0494	2.3	0.03377	1.4	0.0476	2.9	80.3 ± 67.1	214 ± 3	215 ± 3
n3944-09c	c, uz, cld	3600	3200	160	1.4	0.88	1230	1.53	0.03439	1.4	0.06075	1.0	0.03386	1.4	0.04874	1.8	135 ± 43	215 ± 3	215 ± 3
n3944-32c	sp, oz, clb	1400	850	61	0.53	0.59	44300	[0.04]	0.03409	1.4	0.05103	1.2	0.03409	1.4	0.05103	1.2	242 ± 27	216 ± 3	216 ± 3
n3944-09r	r, oz, cld	5500	730	220	0.18	0.13	5180	0.36	0.03712	1.4	0.05218	0.53	0.03699	1.4	0.04933	0.92	164 ± 21	234 ± 3	235 ± 3
n3944-04cx	sp, oz, clm	290	180	27	0.65	0.63	21500	0.09	0.0755	1.4	0.05731	1.4	0.0755	1.4	0.05664	1.4	477 ± 32	469 ± 6	469 ± 7
n3944-04c	sp, oz, clm	310	230	30	0.62	0.76	5910	0.32	0.0762	1.3	0.0603	2.3	0.0760	1.3	0.0579	2.9	525 ± 63	472 ± 6	471 ± 6
n3944-02c	c, oz, clb	400	300	42	0.72	0.75	136000	[0.01]	0.0795	1.4	0.05821	1.1	0.0795	1.4	0.05821	1.1	538 ± 25	493 ± 7	493 ± 7
MA20																			
n3945-28c	c, uz, cld	3800	2100	82	2.9	0.54	67	27.91	0.02455	1.4	0.267	6.4	0.01770	2.0	0.046	75.	19.5 ± 1204.9	113 ± 2	113 ± 7
n3945-17c	r, oz, clm	1100	610	33	0.2	0.57	42.8	43.66	0.03678	1.4	0.4028	1.0	0.02072	1.3	0.067	22.	853 ± 396	132 ± 2	128 ± 14
n3945-23r	r, oz, cld	6500	1500	270	0.86	0.23	85	22.01	0.04202	1.4	0.2227	0.64	0.03277	1.5	0.0497	6.9	180 ± 153	208 ± 3	208 ± 8
n3945-30c	sp, oz, clm	1100	450	44	0.4	0.41	4760	0.39	0.03371	1.4	0.05326	1.3	0.03358	1.4	0.05017	2.0	203 ± 45	213 ± 3	213 ± 3
n3945-06c	sp, oz, clb	780	310	31	0.42	0.4	22900	[0.08]	0.03399	1.4	0.05029	1.5	0.03399	1.4	0.05029	1.5	209 ± 35	215 ± 3	215 ± 3
n3945-28r	r, oz, clb	1000	400	41	0.37	0.4	21900	0.09	0.03426	1.4	0.05144	1.4	0.03423	1.4	0.05077	1.5	230 ± 35	217 ± 3	217 ± 3
n3945-25c	sp, oz, clm	1500	780	60	0.6	0.54	46300	[0.04]	0.03428	1.4	0.04984	1.2	0.03428	1.4	0.04984	1.2	187 ± 27	217 ± 3	217 ± 3
n3945-26c	sp, uz, clm	1500	770	64	0.7	0.5	28300	0.07	0.03452	1.4	0.04974	1.1	0.03449	1.4	0.04922	1.2	158 ± 29	219 ± 3	219 ± 3
n3945-12c	sp, uz, cld	4800	2400	200	0.58	0.51	4990	0.37	0.03479	1.4	0.05238	0.79	0.03466	1.4	0.04944	1.1	169 ± 25	220 ± 3	220 ± 3
n3945-23c	c, oz, clm	1600	290	130	0.029	0.18	3560	0.53	0.0785	1.4	0.06970	0.64	0.0781	1.4	0.06565	1.5	795 ± 31	485 ± 7	479 ± 7
MA23																			
n3946-32c	sp, oz, clb	520	380	22	0.66	0.73	6010	0.31	0.03269	1.4	0.0532	2.2	0.03259	1.4	0.0507	3.0	228 ± 67	207 ± 3	207 ± 3
n3946-39c	sp, oz, clb	110	75	4.7	0.51	0.66	3680	[0.51]	0.03283	1.4	0.0515	4.5	0.03283	1.4	0.0515	4.5	261 ± 99	208 ± 3	208 ± 3
n3946-14c	sp, oz, clb	330	160	13	0.32	0.48	>1e6	[0.00]	0.03339	1.4	0.0529	2.5	0.03339	1.4	0.0529	2.5	325 ± 55	212 ± 3	211 ± 3
n3946-28c	sp, oz, clb	240	78	9.2	0.25	0.33	8080	[0.23]	0.03346	1.4	0.0525	2.9	0.03346	1.4	0.0525	2.9	306 ± 66	212 ± 3	212 ± 3
n3946-25c	sp, oz, clb	750	370	30	0.67	0.5	17800	0.11	0.03343	1.3	0.04970	1.5	0.03340	1.3	0.04887	1.6	142 ± 38	212 ± 3	212 ± 3
n3946-03c	sp, oz, clb	320	110	12	0.88	0.36	5860	0.32	0.03383	1.4	0.0502	2.9	0.03372	1.4	0.0477	3.7	85.0 ± 84.5	214 ± 3	215 ± 3
n3946-39r	sp, oz, cld	800	200	31	0.58	0.25	20000	0.09	0.03385	1.4	0.04859	2.0	0.03381	1.4	0.0479	2.2	91.9 ± 50.7	214 ± 3	215 ± 3
n3946-25r	sp, oz, cld	950	520	40	0.55	0.54	17800	0.11	0.03418	1.4	0.05108	1.5	0.03414	1.4	0.05025	1.6	207 ± 38	216 ± 3	216 ± 3
n3946-30c	c, oz, clb	360	150	21	0.34	0.43	17300	[0.11]	0.0475	2.6	0.0558	1.9	0.0475	2.6	0.0558	1.9	446 ± 42	299 ± 8	298 ± 8
n3946-37c	sp, oz, clb	550	460	120	0.84	0.84	5750	0.33	0.1650	1.4	0.07606	0.73	0.1644	1.4	0.07358	0.98	1030 ± 20	981 ± 13	979 ± 13
MA26																			
n3947-14c	c, oz, clb	800	490	32	n/d	0.61	1090	1.72	0.03319	0.95	0.05947	1.2	0.03262	0.95	0.0459	3.2	-9.2 ± 74.9	207 ± 2	208 ± 2
n3947-22c	sp, oz, clb	440	600	22	2.1	1.4	1330	1.41	0.03387	0.96	0.0598	2.1	0.03339	0.98	0.0487	4.8	135 ± 110	212 ± 2	212 ± 2
n3947-15r	sp, oz, clb	160	160	7.4	1	0.98	3830	[0.49]	0.03354	1.0	0.0502	3.0	0.03354	1.0	0.0502	3.0	206 ± 68	213 ± 2	213 ± 2
n3947-02c	sp, oz, clb	360	75	13	0.19	0.21	9170	[0.20]	0.03371	0.96	0.05106	1.9	0.03371	0.96	0.05106	1.9	244 ± 42	214 ± 2	214 ± 2
n3947-30c	sp, oz, clb	280	77	11	0.37	0.28	6250	[0.30]	0.03396	0.98	0.0492	2.5	0.03396	0.98	0.0492	2.5	157 ± 58	215 ± 2	216 ± 2
n3947-21c	sp, oz, clb	600	80	23	0.11	0.13	10500	[0.18]	0.03456	0.95	0.05163	1.6	0.03456	0.95	0.05163	1.6	269 ± 36	219 ± 2	219 ± 2
n3947-15c	sp, oz, cld	720	240	29	0.58	0.33	9190	0.2	0.03464	1.0	0.05013	1.5	0.03457	1.0	0.04853	1.8	125 ± 41	219 ± 2	220 ± 2
n3947-12c	sp, oz, clm	1400	430	55	0.41	0.31	14400	0.13	0.03526	0.98	0.05039	0.97	0.03522	0.98	0.04937	1.1	166 ± 26	223 ± 2	223 ± 2
n3947-11r	r, oz, cld	4500	330	170	0.085	0.075	24000	0.08	0.03586	0.99	0.05031	0.59	0.03583	0.99	0.04970	0.66	181 ± 15	227 ± 2	227 ± 2
n3947-14r	r, oz, cld	3400	360	130	0.14	0.11	13700	0.14	0.03599	0.97	0.05039	0.79	0.03594	0.97	0.04931	0.89	163 ± 21	228 ± 2	228 ± 2
n3947-04c	sp, oz, clb	490	120	40	0.15	0.25	3840	0.49	0.0712	7.2	0.06738	1.3	0.0709	7.2	0.0636	2.0	729 ± 41	441 ± 31	437 ± 31
n3947-11c	c, oz, clb	660	600	66	0.91	0.91	25800	0.07	0.07510	0.95	0.05678	0.87	0.07504	0.95	0.05622	0.94	461 ± 21	466 ± 4	467 ± 4
MA29																			
n3963x-03c	c, uz, cld	400	110	12	n/d	0.27	49.9	37.47	0.0451	3.8	0.3329	1.7	0.02823	3.2	0.032	53.	-1007 ± 1,124	179 ± 6	183 ± 15
n3963x-01c	c, oz, clm	2700	190	87	0.067	0.071	985	1.9	0.03083	1.3	0.06463	1.2	0.03024	1.3	0.0497	2.5	181 ± 58	192 ± 2	192 ± 2
n3963-02c	c, oz, clb	440	260	16	0.7	0.6	2210	0.84	0.03079	0.87	0.0560	1.9	0.03053	0.88	0.0494	4.0	167 ± 90	194 ± 2	194 ± 2
n3963-16c	c, oz, clb	110	47	4.1	0.26	0.42	2330	0.8	0.03128	0.93	0.0578	3.5	0.03103	0.95	0.0515	6.1	264 ± 134	197 ± 2	197 ± 2
n3963x-18c	sp, uz, clm	500	200	18	0.55	0.41	2650	0.71	0.03158	1.3	0.0544	1.9	0.03136	1.3	0.0488	3.1	139 ± 72	199 ± 3	199 ± 3
n3963-27r	sp, oz, clm	1500	180	52	0.11	0.12	1470	1.27	0.03182	0.90	0.05902	1.4	0.03141	0.89	0.0490	2.6	149 ± 60	199 ± 2	200 ± 2
n3963-27c	sp, oz, clb	740	150	26	0.34	0.21	3850	0.49	0.03183	0.85	0.05152	1.4	0.03168	0.85	0.0477	2.1	84.4 ± 50.1	201 ± 2	202 ± 2
n3963x-26c	sp, oz, clm	1400	250	48	0.48	0.19	243	7.7	0.03515	1.3	0.1079	1.3	0.03245	1.3	0.0472	5.4	56.9 ± 124.4	206 ± 3	207 ± 3

Sample ID	Characteristics[5]	Concentration (ppm)							Total (uncorrected) ratio				Radiogenic (corrected) ratio[3]				Calculated age ± s (Ma)		
		U	Th	Pb	Th/U_{calc}	Th/U_{meas}[1]	$^{206}Pb/^{204}Pb$	f_{206} (%)[2]	$^{206}Pb/^{238}U$	± s (%)	$^{207}Pb/^{206}Pb$	± s (%)	$^{206}Pb/^{238}U$	± s (%)	$^{207}Pb/^{206}Pb$	± s (%)	$^{207}Pb/^{206}Pb$	$^{206}Pb/^{238}U$	207-corr age[4]
n3963-09r	r, oz, clm	4000	99	140	0.02	0.025	15900	0.12	0.03302	0.85	0.05093	0.94	0.03298	0.85	0.05001	1.0	196 ± 23	209 ± 2	209 ± 2
n3963-21c	sp, oz, clm	540	180	20	0.35	0.33	3880	0.48	0.03319	0.90	0.05326	1.6	0.03303	0.90	0.0495	2.3	170 ± 54	209 ± 2	210 ± 2
n3963x-11c	sp, oz, cld	1800	490	68	0.3	0.27	7610	0.25	0.03356	1.3	0.05209	0.57	0.03347	1.3	0.05016	0.85	203 ± 20	212 ± 3	212 ± 3
n3963-30c	sp, oz, clb	280	360	14	1.5	1.3	>1e6	[0.00]	0.03427	0.86	0.0498	2.3	0.03427	0.86	0.0498	2.3	186 ± 52	217 ± 2	217 ± 2
n3963-09c	c, uz, clb	350	230	15	0.98	0.64	17300	[0.11]	0.03469	0.96	0.0489	2.3	0.03469	0.96	0.0489	2.3	143 ± 52	220 ± 2	220 ± 2
n3963-15r	r, oz, clb	990	240	38	0.45	0.25	16400	0.11	0.03482	0.84	0.04914	1.4	0.03478	0.84	0.04825	1.6	111 ± 37	220 ± 2	221 ± 2
n3963-16r	r, oz, cld	2500	170	96	0.083	0.066	14500	0.13	0.03547	0.86	0.05018	0.77	0.03543	0.86	0.04916	0.88	155 ± 21	224 ± 2	225 ± 2
n3963-02r	r, oz, clm	2800	220	110	0.091	0.078	17900	0.1	0.03607	0.85	0.05032	0.70	0.03603	0.85	0.04950	0.78	171 ± 18	228 ± 2	229 ± 2
n3963-15c	c, oz, clm	1800	170	70	0.12	0.092	13500	0.14	0.03615	0.86	0.05063	0.89	0.03610	0.86	0.04953	1.0	173 ± 24	229 ± 2	229 ± 2
n3963-23c	c, oz, clm	890	320	40	0.16	0.36	59.8	31.27	0.05406	0.91	0.3047	1.1	0.03716	1.1	0.0632	13.	715 ± 254	235 ± 3	231 ± 14
n3963x-24c	sp, oz, cld	2000	240	79	0.16	0.12	646	2.89	0.03799	1.3	0.0728	1.6	0.03689	1.3	0.0500	3.4	197 ± 78	234 ± 3	234 ± 3
n3963-05c	sp, uz, clb	330	100	54	0.25	0.3	61200	[0.03]	0.1377	1.2	0.0722	1.7	0.1377	1.2	0.0722	1.7	992 ± 34	831 ± 10	826 ± 10
n3963-25c	sp, uz, clb	380	28	62	0.062	0.074	49000	0.04	0.1478	0.86	0.06927	0.79	0.1477	0.86	0.06898	0.81	898 ± 17	888 ± 7	888 ± 7
n3963x-06c	sp, oz, clb	430	200	84	0.46	0.46	125000	0.01	0.1602	1.3	0.07250	0.40	0.1602	1.3	0.07238	0.40	997 ± 8	958 ± 11	956 ± 12
n3963x-17c	sp, oz, clb	350	180	90	0.49	0.52	74200	0.03	0.1988	1.3	0.09536	0.37	0.1987	1.3	0.09517	0.38	1531 ± 7	1168 ± 14	1144 ± 15
MA30																			
n3948-08c	c, oz, clb	790	160	28	0.36	0.2	1310	0.74	0.03253	0.95	0.0540	2.3	0.03229	0.95	0.0483	3.8	112 ± 87	205 ± 2	205 ± 2
n3948-04r	sp, oz, cld	840	170	30	1.7E+12	0.21	2690	0.7	0.03341	0.97	0.05176	1.7	0.03317	0.98	0.0463	3.1	0.0 ± 84.6	210 ± 2	211 ± 2
n3948-22r	sp, oz, clb	390	230	16	0.53	0.58	6610	0.03	0.03387	0.97	0.05110	1.9	0.03386	0.97	0.0508	3.5	234 ± 79	215 ± 2	215 ± 2
n3948-31c	c, uz, clb	170	87	7	0.47	0.52	5520	0.09	0.03396	1.1	0.0515	3.6	0.03393	1.1	0.0509	5.4	235 ± 120	215 ± 2	215 ± 2
n3948-09c	sp, oz, clb	340	88	13	0.16	0.26	1480	0.18	0.03413	0.95	0.0547	2.5	0.03407	0.96	0.0534	3.6	345 ± 80	216 ± 2	215 ± 2
n3948-04c	sp, oz, clb	660	360	27	0.65	0.56	5960	0.31	0.03403	0.98	0.05173	1.6	0.03393	0.97	0.04927	2.0	160 ± 47	215 ± 2	215 ± 2
n3948-17c	sp, oz, clb	210	140	9.1	0.98	0.68	10100	[0.19]	0.03424	1.0	0.0491	2.8	0.03424	1.0	0.0491	2.8	153 ± 64	217 ± 2	217 ± 2
n3948-30c	sp, oz, clb	390	97	15	0.25	0.25	3360	0.07	0.03436	0.96	0.05106	1.9	0.03433	0.97	0.0505	2.8	218 ± 64	218 ± 2	218 ± 2
n3948-22c	sp, oz, cld	360	190	15	n/d	0.53	4670	0.4	0.03440	0.96	0.04872	2.0	0.03427	0.96	0.0456	3.0	-26 ± 70	217 ± 2	219 ± 2
n3948-08r	r, oz, cld	2300	210	87	0.16	0.09	7480	0.25	0.03508	0.97	0.04989	0.87	0.03499	0.97	0.04792	1.3	95.2 ± 30.7	222 ± 2	222 ± 2
n3948-12c	sp, oz, clb	360	100	44	0.22	0.28	14200	0.36	0.1071	1.4	0.06879	1.3	0.1067	1.4	0.0660	1.6	807 ± 34	654 ± 9	650 ± 9
MA31																			
n4218-19c	sp, oz, clb	230	100	9.2	0.28	0.44	37000	[0.05]	0.03335	1.1	0.0530	2.2	0.03335	1.1	0.0530	2.2	330 ± 50	212 ± 2	211 ± 2
n4218-13c	sp, oz, clb	410	120	16	0.26	0.29	14500	0.13	0.03370	0.93	0.05204	1.6	0.03366	0.93	0.05103	1.8	242 ± 41	213 ± 2	213 ± 2
n4218-42c	sp, oz, clm	1100	710	46	0.83	0.67	5650	0.33	0.03453	0.95	0.05212	1.1	0.03441	0.95	0.04952	1.6	173 ± 37	218 ± 2	218 ± 2
n4218-18r	r, oz, cld	2100	360	81	0.17	0.17	22500	0.08	0.03451	0.95	0.05072	1.0	0.03448	0.95	0.05006	1.1	198 ± 24	219 ± 2	219 ± 2
n4218-52c	sp, oz, clb	770	720	36	0.9	0.94	20600	0.09	0.03488	0.94	0.05147	1.1	0.03485	0.94	0.05076	1.3	230 ± 29	221 ± 2	221 ± 2
n4218-02c	sp, oz, clm	1200	200	45	0.15	0.18	51400	0.04	0.03490	0.93	0.05118	0.98	0.03489	0.93	0.05090	1.0	236 ± 23	221 ± 2	221 ± 2
n4218-04c	sp, oz, clb	550	220	23	0.37	0.4	13400	0.14	0.03506	0.94	0.05195	1.7	0.03501	0.94	0.05086	1.9	235 ± 43	222 ± 2	222 ± 2
n4218-21c	sp, oz, clb	590	290	25	0.73	0.49	3100	0.6	0.03529	0.97	0.0537	2.5	0.03508	0.97	0.0489	4.5	144 ± 102	222 ± 2	223 ± 2
n4218-01c	sp, oz, cld	970	96	37	0.11	0.098	29700	0.06	0.03533	0.93	0.05057	1.0	0.03531	0.93	0.05008	1.1	199 ± 25	224 ± 2	224 ± 2
n4218-16c	sp, oz, clm	870	490	38	0.74	0.56	87300	[0.02]	0.03552	0.94	0.04954	1.1	0.03552	0.94	0.04954	1.1	173 ± 26	225 ± 2	225 ± 2
n4218-36r	r, oz, cld	2600	290	100	0.16	0.11	25500	0.07	0.03560	0.93	0.04971	0.72	0.03557	0.93	0.04913	0.79	154 ± 19	225 ± 2	226 ± 2
n4218-35c	sp, oz, clb	780	350	33	0.4	0.45	>1e6	[0.00]	0.03597	0.96	0.05100	1.1	0.03597	0.96	0.05100	1.1	241 ± 26	228 ± 2	228 ± 2
n4218-28c	sp, oz, clb	430	100	17	0.36	0.25	17700	0.11	0.03596	0.94	0.04994	1.6	0.03592	0.94	0.04911	1.8	153 ± 41	227 ± 2	228 ± 2
n4218-14c	sp, oz, cld	1700	1000	75	0.59	0.63	63800	[0.03]	0.03605	0.93	0.05087	0.79	0.03605	0.93	0.05087	0.79	235 ± 18	228 ± 2	228 ± 2
n4218-10r	r, oz, cld	1100	190	43	0.17	0.17	21900	0.09	0.03610	0.93	0.05107	0.94	0.03607	0.93	0.05040	1.0	214 ± 24	228 ± 2	229 ± 2
n4218-38c	sp, oz, cld	3900	1600	170	0.43	0.42	29900	0.06	0.03664	0.93	0.05060	0.52	0.03662	0.93	0.05011	0.56	200 ± 13	232 ± 2	232 ± 2
n4218-31c	c, oz, clm	1600	1100	76	1.1	0.68	8650	0.22	0.03700	0.93	0.05048	0.78	0.03692	0.93	0.04877	0.98	137 ± 23	234 ± 2	234 ± 2
n4218-05r	r, oz, cld	1700	130	72	0.034	0.076	26400	0.07	0.03877	0.97	0.06738	1.4	0.03874	0.97	0.06684	1.5	833 ± 30	245 ± 2	240 ± 2
n4218-31r	r, oz, cld	6200	850	260	0.15	0.14	5700	0.33	0.03895	0.94	0.05255	0.80	0.03882	0.94	0.04997	1.3	194 ± 29	245 ± 2	246 ± 2
n4218-41c	c, uz, clb	310	190	23	0.51	0.6	22700	0.08	0.06021	0.94	0.05651	1.3	0.06016	0.94	0.05587	1.4	447 ± 31	377 ± 3	376 ± 3
n4218-12c	c, uz, clb	500	140	45	0.24	0.28	13100	0.14	0.07268	0.97	0.07229	0.85	0.07258	0.97	0.07120	0.93	963 ± 19	452 ± 4	443 ± 4
n4218-18c	c, uz, clb	110	83	10	0.97	0.72	14700	[0.13]	0.07115	0.93	0.0531	2.1	0.07115	0.93	0.0531	2.1	335 ± 46	443 ± 4	445 ± 4
n4218-05c	c, oz, clb	270	140	43	0.13	0.51	50000	0.04	0.1239	1.6	0.1623	1.2	0.1238	1.6	0.1621	1.2	2478 ± 20	753 ± 11	659 ± 16
n4218-36c	c, uz, clb	470	270	89	0.56	0.56	95900	0.02	0.1513	1.0	0.07083	0.61	0.1513	1.0	0.07068	0.62	948 ± 13	908 ± 9	907 ± 9
n4218-10c	c, uz, cld	3100	1500	600	0.51	0.51	140000	0.01	0.1596	0.93	0.07150	0.24	0.1596	0.93	0.07140	0.24	969 ± 5	955 ± 8	954 ± 9
MA62																			
n4562-41c	sp, oz, clm	440	350	20	0.7	0.79	44600	[0.04]	0.03377	0.67	0.05130	0.77	0.03377	0.67	0.05130	0.77	254 ± 18	214 ± 1	214 ± 1
n4562-39r	sp, oz, cld	720	130	27	0.17	0.19	71900	[0.03]	0.03401	0.71	0.05116	0.61	0.03401	0.71	0.05116	0.61	248 ± 14	216 ± 2	215 ± 2
n4562-29c	sp, uz, clb	480	380	21	0.87	0.8	64300	[0.03]	0.03397	0.68	0.05020	0.74	0.03397	0.68	0.05020	0.74	204 ± 17	215 ± 1	215 ± 1
n4562-25c	sp, oz, clm	470	400	21	0.77	0.84	33600	[0.06]	0.03404	0.67	0.05109	0.76	0.03404	0.67	0.05109	0.76	245 ± 17	216 ± 1	216 ± 1
n4562-39c	sp, uz, clb	720	640	33	0.84	0.9	50100	[0.04]	0.03419	0.67	0.05101	0.79	0.03419	0.67	0.05101	0.79	241 ± 18	217 ± 1	217 ± 1
n4562-10c	sp, oz, cld	1000	470	42	0.45	0.46	81500	[0.02]	0.03433	0.77	0.05074	0.53	0.03433	0.77	0.05074	0.53	229 ± 12	218 ± 2	218 ± 2
n4562-02c	sp, uz, cld	1600	1400	73	0.79	0.87	88200	[0.02]	0.03436	0.69	0.05109	0.41	0.03436	0.69	0.05109	0.41	245 ± 9	218 ± 1	218 ± 1
n4562-36c	sp, oz, cld	780	440	33	0.56	0.57	18700	0.1	0.03454	0.67	0.05155	0.80	0.03450	0.67	0.05077	0.96	230 ± 22	219 ± 1	219 ± 1
n4562-02r	sp, oz, cld	1100	460	45	n/d	0.41	1800	1.04	0.03466	0.77	0.05289	0.80	0.03430	0.77	0.04468	1.9	-73 ± 47	217 ± 2	219 ± 2
n4562-31c	sp, uz, clm	370	200	16	0.53	0.54	37400	[0.05]	0.03469	0.68	0.05077	0.85	0.03469	0.68	0.05077	0.85	230 ± 19	220 ± 1	220 ± 1
n4562-21c	sp, oz, cld	1000	370	42	0.45	0.36	10100	0.18	0.03520	0.71	0.05119	0.56	0.03514	0.71	0.04973	0.72	183 ± 17	223 ± 2	223 ± 2
n4562-03c	sp, uz, cld	3000	1300	140	0.68	0.44	1300	1.44	0.03903	0.67	0.06045	0.43	0.03847	0.67	0.04914	1.1	155 ± 26	243 ± 2	244 ± 2
n4562-14c	sp, oz, clb	680	46	50	0.028	0.067	75700	[0.02]	0.0677	2.1	0.06262	1.1	0.0677	2.1	0.06262	1.1	696 ± 24	422 ± 9	418 ± 9
n4562-19c	sp, oz, clb	650	120	270	0.089	0.19	242000	0.01	0.3248	0.73	0.2231	0.97	0.3248	0.73	0.2231	0.97	3003 ± 15	1813 ± 12	1532 ± 45

Sample ID	Characteristics[5]	Concentration (ppm)							Total (uncorrected) ratio				Radiogenic (corrected) ratio[3]				Calculated age ± s (Ma)		
		U	Th	Pb	Th/U_{calc}	Th/U_{meas}[1]	$^{206}Pb/^{204}Pb$	f_{206} (%)[2]	$^{206}Pb/^{238}U$	± s (%)	$^{207}Pb/^{206}Pb$	± s (%)	$^{206}Pb/^{238}U$	± s (%)	$^{207}Pb/^{206}Pb$	± s (%)	$^{207}Pb/^{206}Pb$	$^{206}Pb/^{238}U$	207-corr age[4]
MA110																			
n4571-35c	c, oz, cld	2400	240	85	0.082	0.1	180	10.42	0.03617	0.65	0.1362	2.4	0.03240	0.66	0.0549	9.9	408 ± 207	206 ± 1	204 ± 4
n4571-09c	sp, uz, cld	3200	2200	140	1.2	0.71	332	5.63	0.03703	0.70	0.0926	2.7	0.03494	0.69	0.0482	7.1	111 ± 160	221 ± 2	222 ± 2
n4571-03c	sp, oz, cld	950	650	43	0.68	0.68	24800	0.08	0.03533	0.66	0.05133	0.77	0.03530	0.66	0.05074	0.83	229 ± 19	224 ± 1	224 ± 1
n4571-16r	r, oz, cld	650	250	27	0.41	0.38	77300	[0.02]	0.03556	0.66	0.05039	0.88	0.03556	0.66	0.05039	0.88	213 ± 20	225 ± 1	225 ± 1
n4571-24r	r, oz, clb	310	130	13	0.34	0.41	3480	0.54	0.03596	0.69	0.0567	2.9	0.03577	0.69	0.0525	3.5	308 ± 79	227 ± 2	226 ± 2
n4571-43c	sp, oz, cld	900	230	36	0.36	0.26	1410	1.33	0.03613	0.66	0.05949	0.69	0.03565	0.66	0.04906	1.6	150 ± 36	226 ± 1	226 ± 2
n4571-25c	sp, oz, cld	810	360	34	0.45	0.44	43600	[0.04]	0.03580	0.66	0.05049	0.79	0.03580	0.66	0.05049	0.79	217 ± 18	227 ± 1	227 ± 1
n4571-35r	r, oz, cld	1400	250	55	0.22	0.19	12400	0.15	0.03604	0.66	0.05131	0.68	0.03599	0.66	0.05012	0.80	201 ± 19	228 ± 1	228 ± 1
n4571-48c	sp, uz, cld	1500	820	65	0.64	0.56	10600	0.18	0.03614	0.66	0.05153	1.0	0.03607	0.66	0.05015	1.3	202 ± 30	228 ± 1	229 ± 2
n4571-16c	c, uz, cld	1100	610	50	0.68	0.55	61400	0.03	0.03676	0.75	0.05015	0.67	0.03675	0.75	0.04991	0.69	191 ± 16	233 ± 2	233 ± 2
n4571-51r	r, oz, cld	2500	290	100	0.12	0.11	17400	0.11	0.03700	0.65	0.05149	0.47	0.03696	0.65	0.05064	0.55	225 ± 13	234 ± 2	234 ± 2
n4571-28c	sp, uz, clm	4700	2800	220	0.68	0.6	6200	0.3	0.03786	0.65	0.05278	0.31	0.03775	0.65	0.05041	0.45	214 ± 10	239 ± 2	239 ± 2
n4571-40c	c, uz, clb	600	170	28	0.27	0.29	31300	0.06	0.03998	0.68	0.05258	1.2	0.03996	0.68	0.05211	1.3	290 ± 29	253 ± 2	252 ± 2
n4571-51c	c, uz, clb	320	120	52	0.38	0.38	122000	[0.02]	0.1321	2.2	0.07847	0.76	0.1321	2.2	0.07847	0.76	1159 ± 15	800 ± 17	787 ± 17